Daniel Dilg

The Role of HIRA in Cardiovascular Development

PhD Thesis

University College London

Thesis submitted for the award of

Doctor of Philosophy

Supervisors:

Ariane Chapgier

Peter Scambler

ACKNOWLEDGEMENTS

I would firstly like to say a huge thank you to Ariane and Pete, my two supervisors without whom this PhD would have never happened. Big thanks to Ariane for putting up with my impatience and teaching me so many lab techniques. I will always remember that EGS has loooong arms. Your scientific inputs with keywords such as “check!”, “you were supposed to” and “on va y arriver” will resonate in my mind forever. Thanks Pete for your complex insights, unprecedented level of sarcasm and the occasional age-old French stereotypical jokes. We surely had a lovely time during the numerous HIRA meetings. Special thanks to Rasha for cheerfully joining the HIRA team, getting fantastic ChIP results and turning a dynamic duo into a terrific trio. Thank you Yoann for being part of the HIRA team and sharing the dissection of some embryos.

In Pete’s lab, special thanks to Amelie for answering all my in situ and heart anatomy questions. Same goes for Cath, aka “Scary”, who always had a kind word of wisdom and Sarah for efficiency 101. Of course the younger crew, Sophie, Matt, Joel, Nelo and Jen were a massive support for daily experiments, the well needed lunch breaks and overall scientific input! I will always be grateful for Matt’s powerful Hi-Fi which gave an artistic touch to my PhD and helped ploughing away through endless genotyping, Q-PCR and microtoming. Sophie, you set the standards of a PhD student and definitely helped steering me in the right direction. Joel, your random questions (What is new in the world of classical music?) were bizarre and challenging, and Nelo and Jen, you both made the lab an awesome place to work in!

From my office, thanks Elisa, Victor, Mira, Maria, Sonia and Toby for feedback on my slides or posters, and putting up with my sporadic rant over a failed experiment.

Big thanks so much to Jess for supporting me during the hardest part of the PhD: where nothing worked and the road ahead looked impossible. Your moral support, constant optimism and pro-academic coaching were vital! Best of luck with your PhD, I am sure it will be a breeze!

Cian, what would I have done without our regular tennis, bomberman and exemplary cycling (ahem racing...) sessions across London? I’ll never forget about CNVs, Q-Q plots, PCAs

and sequencing artefacts. More importantly, flatsharing with you made this whole PhD a much more enjoyable experience!

Special thanks to Bertrand Vernay for outstanding microscopy and imaging support, as well as the excellent Angela d'Esposito, who also was, coincidently, a great friend and tennis partner.

The UCL Genomics Service were remarkable, thank you so much to Tony Brooks for RNAseq and ChIPseq. Thank you to Chela James for genomic conversions. The animal house staff were very nice, approachable and kept my mice happy. Thanks Rowan for our many science chats and for your magic food drawer as well as Mahalia for your read through and office hyacinths.

Obviously, my family and my friends were the most supportive in difficult times. My parents provided me with love, food and shelter and were kind enough to listen to the frustrations of a stressed PhD student. Big thanks to my aunt and my cousin for checking up on me regularly! Also, there are many friends which made it possible: Fix for feeding me and hosting me in the very last stages, Ting ting and Matt for being good listeners in the last few months in the cherished Shadwell flat and Judith and the French class for getting my mind off science 2 hours a week.

Massive thanks to Sakshi for putting up with me, feeding me, always encouraging me relentlessly and taking me on romantic strolls in Switzerland. I'm sure your fish will behave and you will be the first one to witness the effect of maternal predation in Cichlids. I cannot wait to finally spend a whole day with you without mentioning HIRA, figures or manuscripts ☺ .

I, Daniel Dilg, confirm that the work presented in this thesis is my own. Where information has been derived from other sources, I confirm that this has been indicated in the thesis.

This thesis is dedicated to my wonderful parents

ABSTRACT

HIRA was originally identified in the group of Peter Scambler as a candidate gene for DiGeorge syndrome and was later identified to deposit the histone variant H3.3. Constitutively null *Hira* embryos all die between embryonic day (E) 6.5 and 10.5, with some mutants presenting with heart defects. A conditional allele was therefore employed to examine the role of HIRA during heart development. Conditional ablation in the cardiogenic mesoderm (*Mesp1Cre*) led to surface oedema, ventricular septum defects (VSD) and embryonic lethality. More specific *Cre* drivers have shown that HIRA is essential in cardiomyocytes (*Nkx2.5Cre*) but is not in endothelial cells (*Tie2Cre*).

RNAseq analysis and *in situ* hybridization were used to detect an upregulation of the troponins *Tnni2* and *Tnnt3* and a decreased expression of *Epha3*, a gene necessary for fusion of the interventricular septum with the endocardial cushions. In addition, immunostaining of Troponin C (TnC) emphasised a disorganisation of the contracting meshwork of myofibril. ChIPseq experiment revealed that HIRA binds to GAGA rich DNA sequence in the embryonic heart and is enriched at the common enhancer of *Tnni2/Tnnt3 (TLT).* Furthermore, *in vitro* and *in vivo* co-immunoprecipitations revealed that HIRA interacts with WHSC1 a protein thought to play a major role in Wolf-Hirschhorn syndrome, as well as BRG1, a chromatin remodelling complex required for cardiogenesis. WHSC1 also interacts with NKX2.5, a major cardiac transcription factor that binds the same regulatory *TLT* site as HIRA. Altogether, this work gives evidence for a specific requirement of HIRA in mesodermal cardiac progenitors during heart development. HIRA influences contractility, troponins expression and the endothelial to mesenchymal transition in the cardiac cushions.

TABLE OF CONTENT

ABBREVIATIONS

ASD Atrial Septal Defect

bp base pair

AVC Atrioventricular cushions

AVSD Atrioventricular septal defect

BABB Benzyl alcohol benzyl benzoate

β-gal Beta galactosidase

cDNA complementary DNA

ChIP Chromatin immunoprecipitation

ChIPseq ChIP with massively parallel DNA sequencing

DGS DiGeorge syndrome

E Embryonic stage mouse

EGS Ethelene Glycol-bis-succinimidyl Succinate

ESC Embryonic stem cell

EC Endothelial cells

EMT Endothelial to mesenchymal transition

FACT Facilitates chromatin transcription

FHF First heart field

GO Gene ontology

H&E Haematoxylin and Eosin

HDAC Histone deactetylase

HMTase Histone methyltransferase

HUCA HIRA/UBN1/CABIN1/ASF1a complex

ISH *In situ* hybridization

LA Left atrium

LV Left ventricle

cNCC Cardiac neural crest cell

OFT Outflow tract

OPT Optical projection tomography

PBS Phosphate buffer saline

PCR Polymerase chain reaction

qRT-PCR Quantitative real-time PCR

RA Right atrium

RNAseq RNA sequencing

RV Right ventricle

SAHF senescence associated heterochromatin foci

SHF Second heart field

TSS transcription start site

TF Transcription factor

TLT site *Tnni2/Lsp1/Tnnt3*

VSD Ventricular septum defect

WHSC1 Wolf-Hirschhorn syndrome candidate 1

LIST OF FIGURES

LIST OF TABLES

Chapter 1 INTRODUCTION

1.1) Heart development and cell lineages contributing to the heart

Being the first organ to be formed in the embryo, the heart plays a pivotal role during embryogenesis and is necessary for survival past midgestation. Cardiogenesis involves tightly-regulated morphological changes orchestrated by many different lineages each contributing to a specific cardiac structure. An overview is given here on the temporal development and tissue contributions of some cardiac progenitors.

1.1.1) Cardiogenic mesoderm

In the murine model, the heart first arises from mesodermal cells in the primitive streak at embryonic day (E)6 (Buckingham et al., 2005). As gastrulation proceeds, mesodermal multipotent cardiac progenitors (MCPs) migrate to the splanchnic mesoderm forming the cardiac crescent which is constituted of both first heart field and second heart field (FHF and SHF) cells (Buckingham et al., 2005) (Figure 1-1).

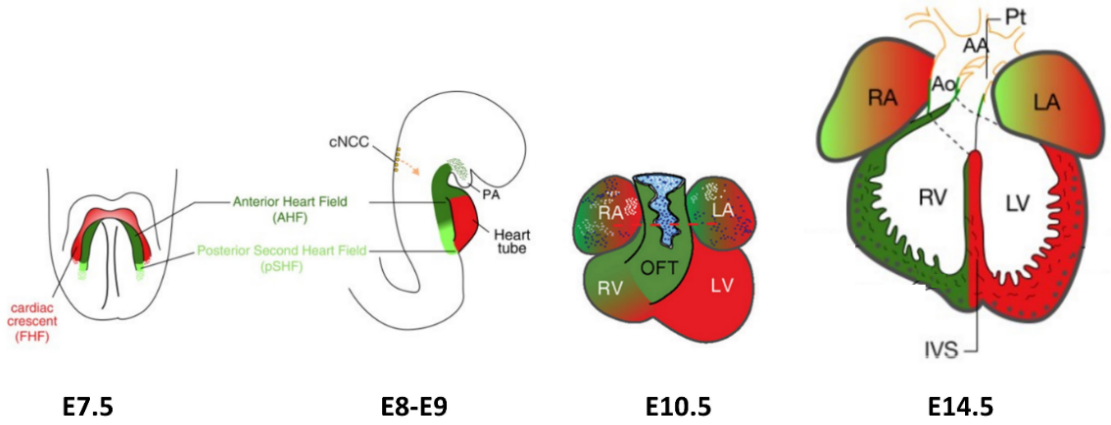

Figure 1-1 Two lineages contribute to the formation of the heart

At E7.5 the cardiac crest forms, composed of the FHF (red) and lying medial to it, the SHF (green). The SHF is divided into the anterior (aSHF) and posterior regions (pSHF). Between E8 and E9, the cardiac crescent fuses at the midline to form the primitive heart tube. The cardiac neural crest cells (cNCC) migrate from the neural tube to colonise the pharyngeal arch arches and eventually the OFT. At E10.5 the heart is composed of primitive chambers which will undergo septation until E14.5-E15.5. RV/LV: Right/Left ventricle. RA/LA: Right/Left atrium. OFT: Outflow tract. IVS: Interventricular septum. Ao: aorta. AA: arch arteries. Pt: Pulmonary trunk. Adapted from (Zaffran et al., 2014) and (Buckingham et al., 2005)

The primitive heart tube then forms at E8 as the population of cells referred to as the FHF merges in the midline (Vincent and Buckingham, 2010). Those cardiogenic mesodermal cells of FHF serve as a scaffold for a second wave of myocardial cells, referred to as the SHF (Dyer and Kirby, 2009). This population of undifferentiated MCPs comes from the pharyngeal mesoderm

and lie medial to the FHF (Buckingham et al., 2005). The FHF will then contribute exclusively to the left ventricle whilst the SHF cells will form the outflow tract, and a mix of both heart fields will participate in the formation of the right ventricle (RV) and both atria (Figure 1-1).

1.1.2) Heart looping and formation of the chambers

The heart tube at E8 is formed by endocardial cells coming from both sides of the embryo and the neural crest cells. As these endocardial cells form a lumen, they are enveloped by myocardial cells (Moorman et al., 2003). The inflow tract sits posteriorly to the heart tube, whilst the outflow tract (OFT) is located anteriorly. As the SHF cells extend the heart tube by making a significant contribution to the cranial pole, the connection between the primitive left ventricle and the mediastinum (central component of the thorax) is disrupted and the now free tube starts looping in the rightward direction at E8.5-E9, which is a necessary event for the formation of the primitive chambers (Moorman et al., 2003).

At E10.5 the heart displays the following anatomical features: the ventricle, the atrioventricular canal (AVC), the atrium and the OFT with an inner endocardial lining and an outer myocardial layer. The heart can be described as partially partitioned by the primitive atrial septum, inter-ventricular septum (IVS) and atrioventricular cushions (AV cushions). Between E10.5 and E15.5, those prototypic four chambers will be become fully separated. The IVS starts to grow from the apex of the heart to separate the ventricular chamber into left and right ventricles, eventually connecting with the OFT to separate ventricular outlets (Anderson et al., 2014). Between the endocardial lining and an outer myocardial layer, the endocardial cushions arise through the accumulation of cardiac jelly (i.e. extracellular matrix). These local tissue swellings are rapidly invaded by mesenchymal cells resulting from the epithelial to mesenchymal transition (EMT) (Lin et al., 2012). In the heart this process is often referred to as endothelial to mesenchymal (EndMT) since the cells involved are endothelial (Kovacic et al., 2012). However, the distinction between EMT and EndMT remains unclear in the current literature, since both terms encompass endothelial cells. EndMT is crucial to the growth and correct establishment of the semilunar valves, the atrioventricular septum, the mitral and tricuspid valves and the membranous part of the IVS, which is derived from the atrioventricular cushions (Person et al., 2005) (Figure 1-2). Many soluble growth factors such as TGF-β, EGF-related growth factors, and VEGF have been shown to govern endocardial cushion transformation shaping (Person et al., 2005, Barnett and Desgrosellier, 2003). However EPH receptor family and its ephrin ligands, which are of particular interest in this thesis (see p75), have also attracted the attention. Originally found to be axonal guidance cues (Moorman and Christoffels, 2003), this family of receptors and ligands regulate an important aspect of the heart morphogenesis. Lethal valve and cushion malformations have been

identified in mouse embryonic mutants for *Ephrin-A1* (Frieden et al., 2010), *Ephrin-B2* (Cowan et al., 2004) ligands and *EphA3* receptor (Stephen et al., 2007).

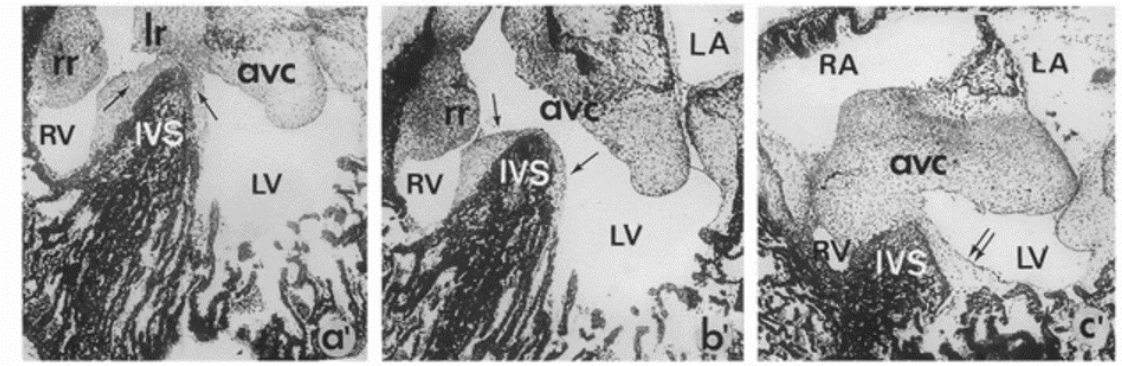

Figure 1-2 Mesenchymal cells contribute to the formation of the AVC and the IVS

Endothelial to mesenchymal (EndMT) leading to local tissue swellings gives rise to endocardial cushions. Here, transverse section of the heart in chicken embryos at stage 28 show the participation of the mesenchymal tissue derived from the atrioventricular cushions (AVC) on the interventricular septum (IVS) (arrows). RV/LV: Right/Left ventricle. RA/LA: Right/Left atrium. Adapted from (Strauss et al., 1987).

1.1.3) Septation of the OFT into pulmonary trunk and aorta

After heart looping, the common OFT needs to be septated in order to form the aorta (Ao) and the pulmonary trunk (PT). The walls of the OFT are made of myocardium whilst the lumen is lined with cardiac jelly, containing mesenchymal cells originating from the endocardium (proximal) the neural crest (distal). These cardiac neural crest cells (cNCC) delaminate from the dorsal neural tube and migrate through the pharyngeal arches to colonise the OFT. As the pharyngeal region is being remodelled, the aorto-pulmonary septum starts the distal septation of the OFT (Webb et al., 2003). This septum is comprised of proliferating mesenchymal cells which arise from an EMT on both sides of the vessel. Once the endothelium fuses, the septal bridge is formed and SHF-derived smooth muscle cells as well as myocardium further separates the OFT into two distinct vessels (Plein et al., 2015). Eventually, the “zipper like” fusion of the cushions attach to the IVS, thus fusing the base of the aorta to the left ventricle and the PT to the right ventricle (van den Hoff et al., 1999).

1.1.4) Lineages contributing to the heart

As mentioned above, MCPs arise from the differentiation of a common progenitor. Through labelling of cardiac precursors in different regions of the mouse heart during development (Meilhac et al., 2004), it is possible to identify molecular markers for cardiac progenitors. There are many known core genes which are part of the regulatory network for early cardiac development determining First and Second Heart Fields (Herrmann et al., 2012). Below is the description of those genes which have been better characterised and which have been used to drive *Cre* expression and thereby the ablation of *Hira* in various conditional contexts.

1.1.4.1) Mesp1

In 1999, Saga *et al* were the first to demonstrate that *Mesp1* is the earliest cardiac progenitor and is "activated at first in the extraembryonic mesoderm and then in the common precursor cells of myocardium, endocardium, and the vascular system" (Saga et al., 1999). It belongs to a basic helix-loop-helix (bHLH) transcription factor family and is first detected at E6.5 (Figure 1-3) in a certain part of the mesoderm which has ingressed through the primitive streak. Defined as a cardiogenic mesodermal marker, *Mesp1* is a potent tool to use for conditional knockout. All cells that constitute the heart come from *Mesp1*-expressing cells, except for a small population of cardiac neural crest cells (see p7). However, the skull vault and its connective tissues in the craniofacial mesenchyme also have some *Mesp1* positive cells (Yoshida et al., 2008). Recently, *Mesp1* lineage was found come from two temporally distinct pools of cells restricted to either the FHF or SHF (Lescroart et al., 2014). In contrast to the model in which *Mesp1* is expressed in the earliest multipotent cardiovascular progenitors common to the FHF and SHF, single cell recombination event in *Rosa–Confetti* mice demonstrated that *Mesp1* actually marks distinct classes of cardiovascular progenitors which are restricted to specific lineages during gastrulation (**Error! Reference source not found.**).

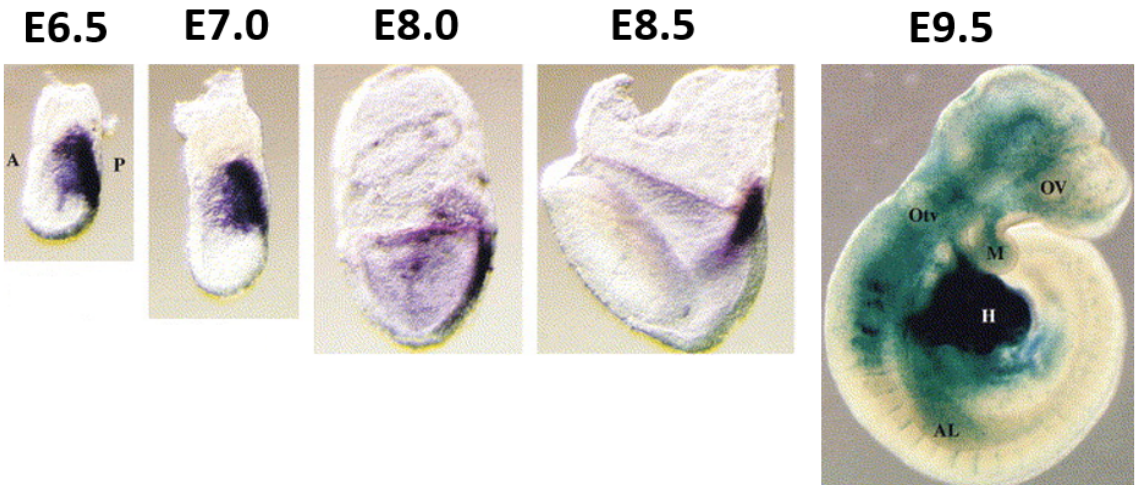

Figure 1-3 Mesp1 is an early regulator of cardiovascular progenitors

Studies have demonstrated that *Mesp1* represents the earliest marker of cardiovascular progenitors. *Mesp1* expression is shown here by *in situ* hybridization from E6.5 to E8.5. The activity of the *Mesp1Cre* recombinase at E9.5 is done by crossing a knock-in *Mesp1Cre* mouse to a transgenic mouse line carrying the reporter gene construct CAG-CAT-Z which directs expression a lacZ gene upon Cre-mediated excision of the loxP-flanked chloramphenicol acetyltransferase (CAT) gene located between the CAG promoter and the lacZ gene. This lineage trace shows the strongest expression of *Mesp1* in the heart (H), some in Otic Vesicle (Otv), in the optic vesicle (OV), in the mandibular arch (M) and in the anterior limb (AL). A/P: Anterior/Posterior. Taken from (Saga et al., 2000)

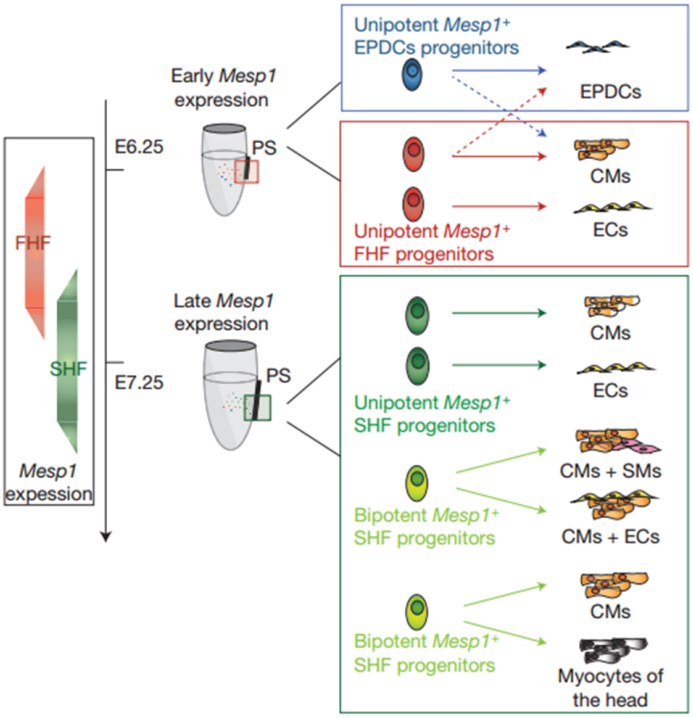

Figure 1-4 Mesp1 expressing cells consist of distinct pools of FHF or SHF progenitors

Clonal analysis of prospective cardiovascular progenitors revealed that *Mesp1* progenitors consist of two temporally distinct pools. The model presented here show cardiovascular progenitors which are committed to a particular lineage, depending of their temporal expression of *Mesp1* between E6.25 and E7.5. FHF is shown in red and SHF in green. The two populations have an overlapping expression at E6.75. PS: primitive streak EPDC: epicardial derived cells CM: cardiomyocytes EC: endothelial cell SM: smooth muscle cell. Adapted from (Lescroart et al., 2014)

1.1.4.2) Nkx2.5

Nkx2.5 is highly expressed in the early heart progenitor cells in both the FHF and SHF during murine embryogenesis from E7.5 (Biben and Harvey, 1997). It is the homologue of *Tinman* (drosophila) which is a master cardiac regulator (Bodmer, 1993). In contrast to *Mesp1* which is switched off around E10.5, it continues to be expressed at a high level in the heart through adulthood (Kasahara et al., 1998). *Nkx2.5* progenitors are expressed in cardiac endothelium and smooth muscle, in addition to virtually all cardiomyocytes of all four chambers of the heart (Figure 1-5) (Ma et al., 2008). NKX2.5 cooperates, amongst other, with MEF2C for determining ventricular identity.

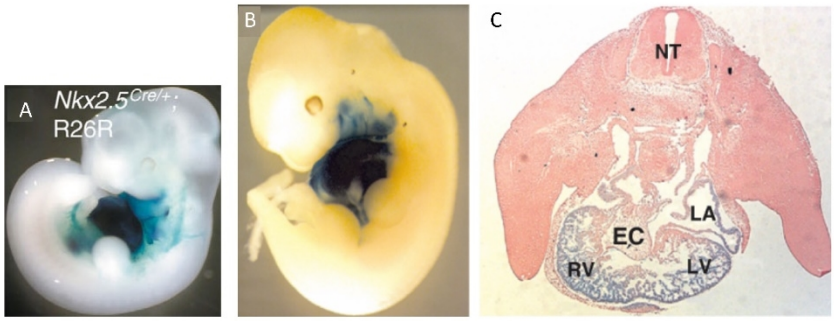

Figure 1-5 Cardiomyocytes express *Nkx2.5* from E7.5 during heart development

Nkx2.5 is a transcription factor expressed 24 hours after *Mesp1* in heart progenitor cells in both the FHF and SHF. *Nkx2*.5 expression is shown here using a knock-in *Nkx2.5Cre* construct. When crossed to ROSA26 (R26R), activity of the *Nkx2.5Cre* recombinase allele is detected here by β-gal at E9.5 (A) and at E11.5 (B-C). Lateral view (B) and transverse section (C). Both stages reveal an expression restricted to cardiac tissues. Right/Left ventricle (RV/LV), Endocardial cushions (EC), Left atrium (LA). Adapted from (Moses et al., 2001).

1.1.4.3) Mef2c

Mef2c is partly controlled by *Nkx2.5* and therefore expressed slightly later at around E7.75 (Lin et al., 1997). *Mef2c* null embryos fail to develop cardiac structures which derive from the anterior heart field (AHF) (Lin et al., 1997). The SHF regions can be split into the anterior and posterior, each transcriptionally distinct (Zaffran et al., 2004) (Figure 1-6). The AHF includes the splanchnic and pharyngeal mesodermal regions that encompass the arterial pole of the primary heart tube. Using a *Mef2cCre* transgenic allele (used in this PhD project) crossed to a *Cre*-dependent *LacZ* reporter mice, the expression of *Mef2c* was traced to the right ventricle and ventricular septum, and the endothelial and myocardial cells of the OFT. However, no staining was observed in cells from the atria, the epicardium nor the coronary vessels (Verzi et al., 2005) (Figure 1-7).

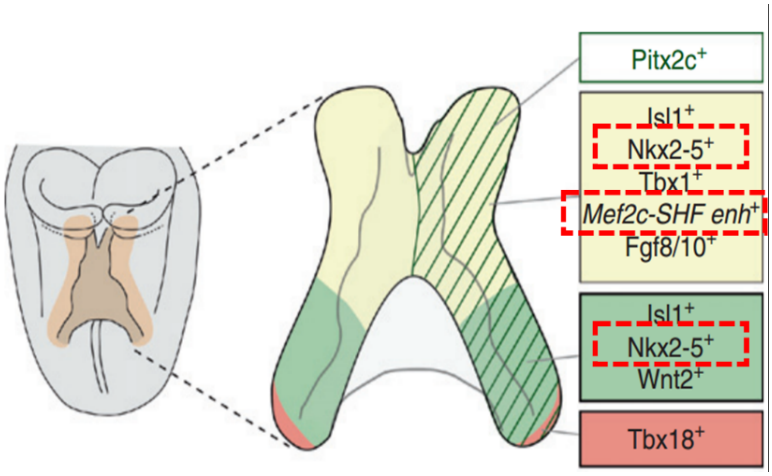

Figure 1-6 The SHF is made of an anterior and posterior part

The SHF has two transcriptionally distinct regions. The schematic represents the heart tube at E8.0. *Nkx2.5* is expressed in both the posterior (green) and anterior (yellow) parts of the SHF, whilst *Mef2c* is restricted to the anterior region. Adapted from (Vincent and Buckingham, 2010).

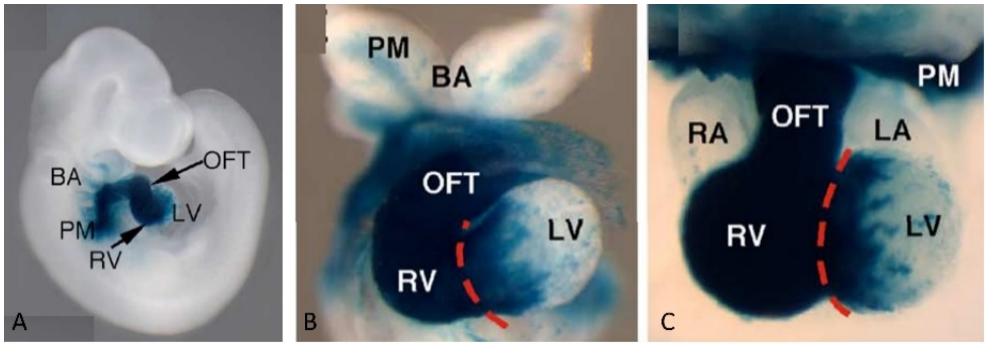

Figure 1-7 Mef2c is expressed in the SHF

Mef2c is cardiac transcription factor which is a key regulator of the SHF. The expression of the *Mef2cCre* transgene allele is displayed here in the cardiac lineage as seen in the lateral view at E9.5 (A). Cre activity can be detected with as early as E7.75 in the cardiac crescent by the same method to the one described above with *Nkx2.5Cre* (6). Expression is detected here in the right ventricle (RV), outflow tract (OFT), in the pharyngeal mesoderm (PM) and in the branchial arches at E9.5 (A). Expression in absent from common arterial chamber and most of the left ventricle (heart at E9.5 (B) and at E12.5 (C). Adapted from (Verzi et al., 2005).

1.1.4.4) Wnt1

Wnt1's vital role in the development of the central nervous system (CNS) was apparent when mutant embryos showed a complete loss of the entire mid/hindbrain region (McMahon and Bradley, 1990). A lineage study using transgenic *Wnt1Cre* mice crossed with R26R conditional reporter allele revealed that NCC are highly migratory (Jiang et al., 2000). NCCs which derive from the dorsal aspect of the neural tube are expressed in dorsal root ganglia, peripheral nervous system, melanocytes, adrenal medulla and craniofacial mesenchyme (Jiang et al., 2000). Early experiments which used a combination vital dye labelling and *exo utero* embryological injections revealed that the NCCs populate the pharyngeal arches (Serbedzija et al., 1992) (Figure 1-8). *Wnt1* was found to be expressed in the mesenchymal component of the pharyngeal arches at E9.5 (Jiang et al., 2000). At E12, during the asymmetric reorganisation of the great vessels, NCCs actively participate in the remodelling and septation of the OFT. It should be noted that NCCs are also involved in the formation of atrioventricular valves (Nakamura et al., 2006), their supporting sinuses, the coronary arteries and cardiac neural ganglia, as well as the parasympathetic and the sympathetic innervation of the venous pole of the heart (Hildreth et al., 2008).

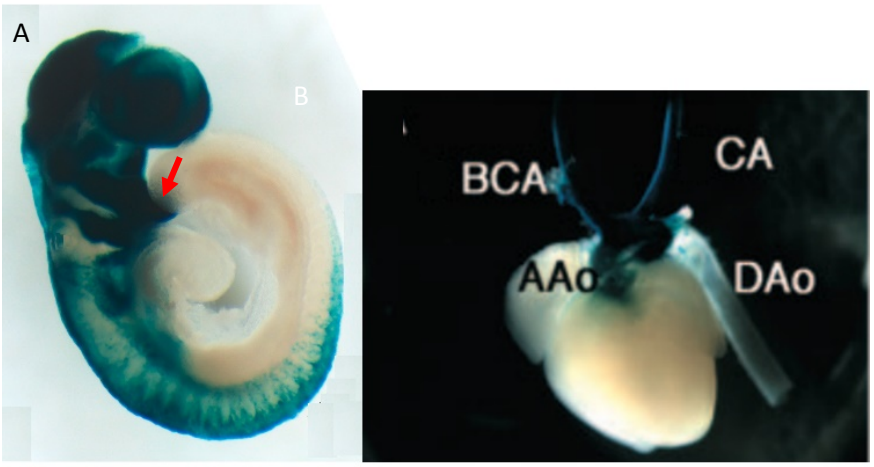

Figure 1-8 Wnt1 is expressed in neural crest cells which contribute to the formation of the heart

A subpopulation of NCCs migrate along the pharyngeal arches and are necessary for the remodelling and septation of the OFT. The expression of *Wnt1Cre* is shown here, using a R26R-lacZ transgene, and can be detected in the NCCs from E7.5. At E9.5, the expression is visible in fore- and midbrain and in the mesenchymal component of the pharyngeal arches (red arrow) (A). Migratory neural crest cells colonise the brachiocephalic artery (BCA), the carotid artery (CA) and parts of the ascending/descending aorta (A/DAo) (B) at E14.5. Adapted (Jacques-Fricke et al.)(A) and (Nakamura et al., 2006)(B).

1.1.4.5) Tie2

Tie2 was originally shown to target reporter gene expression (LacZ) in virtually all vascular endothelial cells during embryogenesis and in postnatal life (Schlaeger et al., 1997). Both *Tie2-lacZ* transgenic mice (Schlaeger et al., 1997) and *Tie2-Cre* transgenic crossed with CAG-CAT-Z (Kisanuki et al., 2001) (in which *LacZ* expression is activated by Cre-mediated recombination) show a strong β-galactosidase activity in every ECs of blood vessels by E11.5 (Figure 1-9). Using the *Tie2Cre* allele, an early expression was noticed at E7.5 in some mesodermal cells and extraembryonic tissue. By E8.5, a fraction of the ECs in the aorta and the endocardium were labelled. From E9.5 though, the expression of *Tie2* was ubiquitous in the developing endocardium and ECs present in cardiac tissue, including mesenchymal cells resulting from the endothelial to mesenchymal transition in the endocardial cushions (Kisanuki et al., 2001). Although *Tie2* is not expressed in the haematopoietic lineage, some circulating endothelial progenitor cells have been detected, which originate from the bone marrow (Zhang et al., 2002).

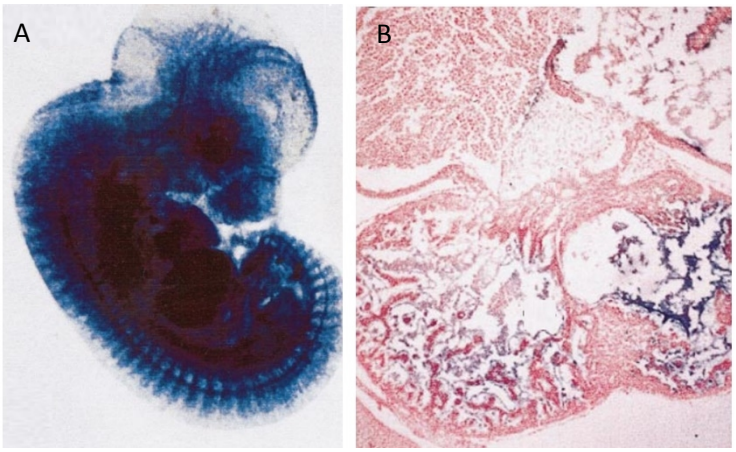

Figure 1-9 Tie2Cre labels endothelial cells throughout the organism

The endothelial specific promoter/enhancer *Tie2* was used to create a *Tie2Cre* transgenic mice which has a Cre recombinase activity in the endothelial lineage. Here, the transgene *Tie2Cre* activity is visualised via a CAG-CAT-Z reporter. All blood vessels reveal a Cre activity, as seen in the lateral view at E11.5 (A). The endocardium shows expression of *Tie2cre* in this transverse section (B). Both images are from an E11.5 embryo and adapted from Kisanuki (Kisanuki et al., 2001)

1.1.5) Heart contractility governed by troponins

After cardiac looping at E10.5, the heart becomes increasingly essential for the rest of the embryo to receive enough blood to proceed with development. Cardiac and skeletal muscle progenitors are both derived from mesoderm and differentiate into striated muscle fibres, which have a comparable structure. Muscle fibres contain tubular myofibrils, composed of numerous sarcomeres. The two boundaries of a sarcomere are called Z discs, to which actin molecules are bound. Parallel to the actin thin filaments lies the myosin heads of the thick filaments (Figure 1-10). The myosin heads bind to and exert force onto the actin molecule thus forcing the two filaments to slide along one another and shorten the sarcomere and initiate global muscle contraction. The actin thin filament consists of 3 troponin subunits: TnC, TnI, and TnT, to which Ca^{2+} can bind. Calcium ions generate the interaction force between actin and myosin, whilst local ATP hydrolysis promotes the high energy configuration of the myosin head and drives muscle contraction (Lehman et al., 1994). The thin filament is helically arranged with tropomyosin, a long flexible molecule, which together with troponins, are attached to actin (Figure 1-10). When Ca^{2+} bind specifically to TnC, TnC-TnI interaction is strengthen whilst the interaction between TnI and actin weakens. This enables Tropomyosin to "rock and roll" dynamically to modify the strength with which myosin head binds to actin (Gordon et al., 2001). The organisation of the contracting meshwork of myofibril and the regulation of cross-bridge actin-myosin interactions is highly dynamic and vital during heart development, and reduced cardiac output can arrest development or lead to pericardial oedema at E14.5 (Peng et al., 2008). Contractility in embryonic hearts was quantified using

maximum Ca^{2+}-activated isometric force normalized to the cross-sectional area (F_{CSA}). Between E10.5 and E19.5, contractility increases by 5-fold (Siedner et al., 2003).

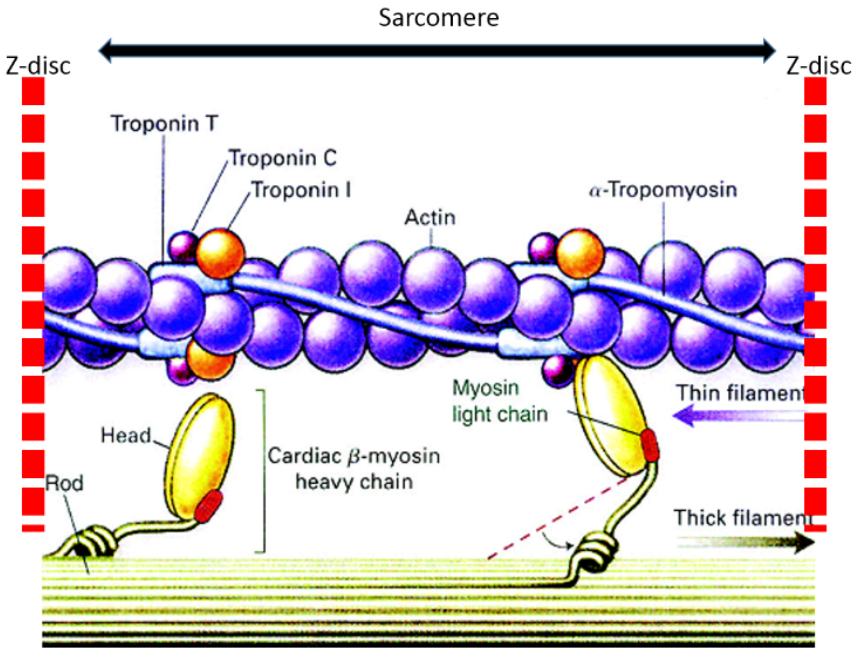

Figure 1-10 Sarcomeres drive muscle contraction

Muscle fibres contain many tubular myofibrils, arranged parallel to each other and composed of numerous sarcomeres. The schematic representation of a sarcomere is shown here, with the two opposite conformations of the myosin head: released (left) and anchored (right) to the actin filament. An actin filament consists of 3 troponin subunits (TnC, TnI, and TnT) which govern the release of Ca^{2+} and the local hydrolysis of ATP.

1.2) Chromatin structure and regulation of transcription

1.2.1) Chromatin structure

The DNA of the entire genome is compacted in most cells, as it needs to be packaged tightly in the nucleus whilst remaining accessible to the molecular machinery. Chromatin serves various purposes: compacting DNA into the nucleus, protecting it from damage caused by reactive oxygen species (Mansoor and Ali, 2007) or ultra violet light (Durante et al., 2013), controlling gene expression (Felsenfeld et al., 1996), DNA replication (Alabert and Groth, 2012) and DNA repair (Price and D'Andrea). Two main global states define chromatin; heterochromatin where the chromatin is highly condensed, and as a consequence where gene expression is usually silent, and euchromatin where the chromatin is more open, and as a consequence where genes are more accessible by the transcription machinery. The scaffold of chromatin is essentially made of nucleosomes, which are responsible for the chromatin conformation and contain eight histone proteins with 145-147 nucleotides wrapped around them (Figure 1-11). There are five types of histones: H1, H2A, H2B, H3 and H4 (Annunziato, 2008). Apart from the linker H1 all histones assemble in pairs which together form an octamer

(Figure 1-12). The H1 linker histone supports unwrapped DNA which varies in length between 10 to 50 bp. It has been shown that 75 to 90% of genomic DNA is wrapped around nucleosomes (Segal et al., 2006). This structure is highly stable as a result of the negatively charged deoxyribose-phosphate DNA backbone and the positively charged histones (Blank and Becker, 1996). DNA sequences, which have a variable capacity to bend (Widom, 2001), can affect the position of nucleosomes (Segal et al., 2006) and to a certain extent impact transcription. Studies of the DNA deformability sequence pattern have all converged to the sequence motif "CGRAAATTTYCG", where R= A or G (purines) and Y = C or T (pyrimidines) (Trifonov, 2011), which would favour the wrapping around a histone octamer. However such a sequence is highly degenerate and much controversy surrounds the field of nucleosome positioning (Kaplan et al., 2010). Linear DNA wrapped around nucleosomes is compacted 30 to 40 times, by bending it at an atomic level, but also on a larger gene scale by forming higher-order helices (Van Holde et al., 1974). These higher order tertiary structures are the result of complex interactions between chains of nucleosomes and are dynamically adjusted in part by histone modification patterns. Via the modification of histones, nucleosomes recruit other proteins and this can drastically affect transcription. The patterns of histone post-translational modifications which correlates with chromosomal state and indirectly, transcriptional levels is sometimes referred to as the "histone code" hypothesis (Jenuwein and Allis, 2001). The term "code" refers to the numerous possible combinations that, for example, a single H3 can have. There are 10 lysines which can adopt 4 methylations: mono-, di-, and tri- or unmethylated. There are therefore, in theory, over a million (4^10=1,048,576) possible states, hence the term "histone code".

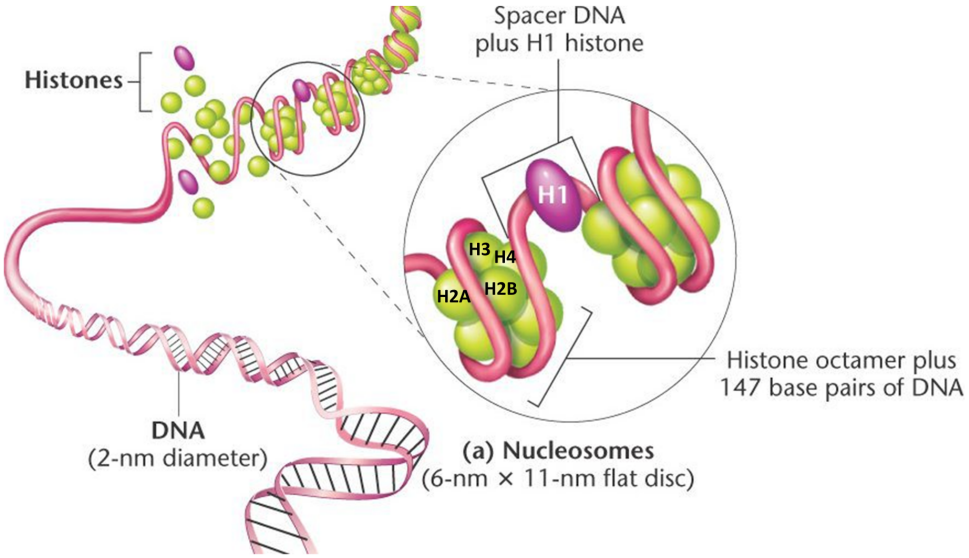

Figure 1-11 DNA wraps around nucleosomes which are constituted of a histone octamer

The diagram represents the eukaryotic chromosomal structure and compaction, in which 147 nucleotides of linear DNA are wrapped around a histone octamer and between 10 to 50 nucleotides are bound to the H1 linker histone. Adapted from Namrata Chhabra (2015).

In eukaryotes, highly compacted DNA cannot host the basal transcriptional machinery and needs to be modified (Struhl, 1999) by three main mechanisms: either through methylation of CpG dinucleotides, or via ATP-dependent chromatin remodelling, or by histone modifications (Agalioti et al., 2000). The latter include methylation, acetylation, phosphorylation, ubiquitination and sumoylation (Bannister and Kouzarides, 2011), some examples of which will be discussed in more detail below.

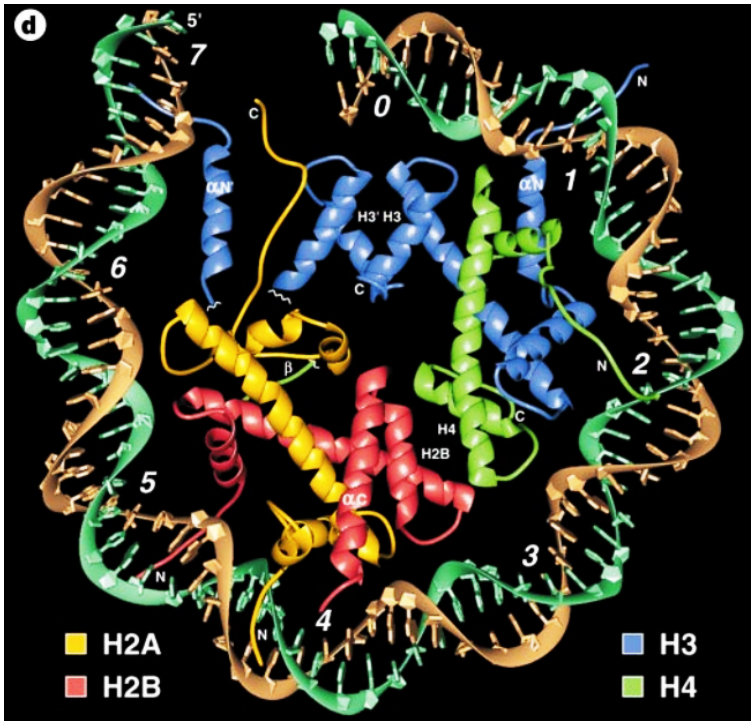

Figure 1-12 Crystal structure of a nucleosome reveals the interaction between histones

The X-ray crystal structure of the nucleosome core presented here shows the 146-bp DNA phosphodiester backbones (brown and turquoise) in a superhelix conformation with the eight histone protein forming the nucleosome (blue: H3; green: H4; yellow: H2A; red: H2B). The 2.8 angstrom resolution of the crystal gave an overview of histone-histone interactions. For example, the two H3 bind through their C-terminal domain which forms a 4-helix bundle. From (Luger et al., 1997).

1.2.2) DNA methylation

Whilst the regulation of gene expression during development is primarily encoded in the DNA sequence itself, epigenetic information which lies in the methylation status of the fifth position in the cytosine 6-atom ring (Smith and Meissner, 2013), also has a general impact on the transcriptome. First discovered in the early 1980s (Haigh et al., 1982), evidence was given for the upregulation of unmethylated genes in the chicken β-globin locus. The methylation is mainly governed by three highly conserved enzymes: DNA methyltransferase 1 (DNMT1), DNMT3A and DNMT3B (Okano et al., 1999). Methylation can take place during the semi-conservative replication of DNA, copying the methylation from a parental DNA strand to its new partner after replication but also *de novo*. To maintain the expression of a gene, the DNMTs keep CpGs at promoters unmethylated and are vital for the expression of housekeeping genes. DNA methylation tends to be more stable than histone methylation in somatic cells, although the diversity of the latter has recently attracted a lot of attention.

1.2.3) Histone modification

The roles of histone acetylation and methylation in “nuclear function” were first described by Vincent Allfrey (Allfrey et al., 1964) in the 1960s, who discovered that acetylated histone increased RNA synthesis compared to arginine rich histones. Experiments which used electron microscopy and analytical ultracentrifugation (sedimentation velocity) showed that

acetylated oligonucleosomes remained in an extended conformation (Garcia-Ramirez et al., 1995) compared to controls, thus further supporting the idea that chromatin condensation is reduced by histone acetylation. Histone dimers H2A-H2B and tetramers H3-H4, the latter ultimately driving the assembly of the nucleosome (Talbert and Henikoff, 2010), are all made of a globular domain and a NH_2 terminus, called the "tail". This tail can be modified post-translationally. In addition to altering chromatin structure, histone acetylation can regulate transcription by recruiting chromatin remodelling enzymes (Agalioti et al., 2000) (see p20). Histone tail modifications are regulated by many proteins such as histone acetyltransferase (HAT) and histone deacetylases (HDAC)(Figure 1-13). They govern acetylation of the ε-amino group via catalysis of an acetyl group from acetyl-CoA onto a lysine residue at multiple sites, thus weakening the binding strength between DNA and histones.

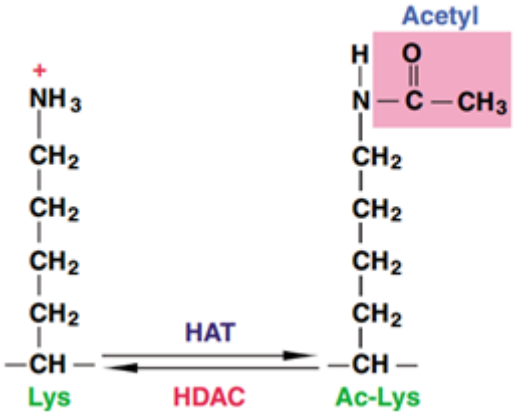

Figure 1-13 Lysine is reversibly acetylated

Histones have a globular domain and a NH_2 terminus, which can be acetylated by a histone acetyltransferase (HAT) or deacetylated by a histone deacetylase (HDAC). The representation here shows both nonacetylated (left) and acetylated lysine residues (right). Adapted from (Yang and Seto, 2007)

There are three main groups of HATs: GNAT ((Gcn5)-related N-acetyltransferases), MYST and CBP/p300 (adenoviral E1A-associated protein of 300 kDa) (Bordoli et al., 2001). Using high temporal fluorescence microscopy, evidence demonstrated that histone H3 lysine-27 acetylation (H3K27Ac) influenced transcription within minutes of its incorporation in nucleosomes, in two distinct steps: first the acetylation facilitated the binding of transcriptional activators to the chromatin and second, RNA PolII complex rapidly switched from initiation to elongation state (Stasevich et al., 2014). The effect of the accumulation of various methylation and acetylation modifications of histone lysine residues is discussed below.

The inheritance of histone modification during cell division remains unclear. In a semi conservative model of replication, the transmission of DNA methylation has been well characterised: DNMT1 specifically targets hemi-methylated sites to replicate methylation

patterns (Jin et al., 2011). One theory named “piggy-back model” suggests that the cell uses DNA methylation pathways to replicate histone modifications (Martin and Zhang, 2007). In mouse fibroblast cells, the methyl-CpG-binding protein MeCP2 can deposit H3K9 monomethylation (Fuks et al., 2003). Evidence for “reading” and “writing” modifications from the old H3/H4 to the new one, thereby transferring the modifications to the *de novo* synthesized strand, is provided by WDR5 and HP1 proteins (Wysocka et al., 2005) in *X.laevis*, which recruit methyltransferases. A similar mechanism in yeast suggested that the old histones from the bulk chromatin segregated randomly to both daughter strands during DNA replication, with Swi6, a H3K9 “reader”, triggering methyltransferase activity on adjacent nucleosomes (Hall et al., 2002). However, addition players involved in epigenetic inheritance have also been identified. A cofactor of DNA polymerases, PCNA (Proliferating cell nuclear antigen), which binds to both the leading and lagging strands during DNA replication (Moldovan et al.) was found to recruit HDACs (Milutinovic et al., 2002), chromatin remodellers (Poot et al., 2004), methyltransferase (Huen et al., 2008) and histone chaperone CAF1 (Quivy et al., 2008). These chromatin-binding proteins or chromatin modifiers have been involved in copying DNA methylation and specific histone modifications from mother to daughter cells (Probst et al., 2009).

1.2.4) Epigenetic modification regulating transcription

There are many examples in which the environment impacts epigenetic marks. Neural plasticity, for example, is durably changed by cocaine via HDACs. This was seen by the acetylation of H3K9/14 and H4K5/8/12/16, markers of transcriptional activation, in the promoter region of cocaine responsive genes (Rogge and Wood, 2013). Interestingly in hearts where hypertrophy has been induced, the promoters of a set of NFκB target genes were found to be overacetylated thus suggesting a mechanism for potential cardioprotection by inhibition of HDAC activity (Ooi et al., 2015, Kang et al., 2015). Some lysine acetylation can also reside in the histone core itself, rather than in the “tail”, such as H3K56 (Bannister and Kouzarides, 2011). Enrichment of H3K56Ac at the *Vegfr1* promoter was found to be vital for the upregulation of this gene in endothelial cells (Dutta et al., 2010), and since this residue is located towards the major groove of the entry-exit site of the DNA super helix, it is more likely to affect the DNA/histone interaction (Masumoto et al., 2005). There are many different HDACs and they have a low substrate specificity, thus allowing one enzyme to deacetylate multiple residues. HDACs can be classified into four families: HDAC1, -2, -3 and -8 (class I); HDAC4, -5, -6, -7, -9 and -10 (class II) and HDAC11 (class IV) which all require Zn^{2+} for deacetylase activity and the sirtuin family (class III) which require NAD^{+} as a cofactor (Yang and Seto, 2007). HDACs are often part of a large multiprotein complexes as exemplified by HDAC1 and HDAC2 which are part of the NuRD, Sin3a and Co-REST complex. However, it has been shown that HDAC1 can act independently to control embryonic stem (ES) cell differentiation

(Dovey et al., 2010). An increase of H3K56Ac in ES cells lacking HDAC1 led to an overexpression of cardiomyocyte-, muscle-, and neuronal-specific markers (Dovey et al., 2010). HATs have often been implicated in cardiac muscle development. The HAT P300 for instance is expressed from E7.5 in the mouse, and *P300*-null embryos die between E9.5 and E11.5 as a result of thin myocardium and diminished trabeculation (Yao et al., 1998).

Histone tails can be methylated on arginines or lysines. SUV39H1 was the first protein to be identified as a histone methyltransferase (Rea et al., 2000) (HMTase), after it was found to be responsible for position effect variegation in drosophila (Tschiersch et al., 1994). SUV39H1, acting through H3K9 methylation, recruits HP1 to juxtapose euchromatin with heterochromatin (Elgin and Reuter, 2013, Stewart et al., 2005). Many other HMTases have been identified and all present with a highly conserved SET domain. Depending on their intrinsic properties, they can modify specific lysine residues to a certain degree. For instance, the phenylalanine in DIM5 allows tri-methylation of a lysine (Zhang et al., 2003), whilst the tyrosine in SET7/9 in the equivalent catalytic domain only deposits mono-methyls (Xiao et al., 2003). Specific methylation patterns have been found to have strong connections to gene expression (Sims and Reinberg, 2006, Wamstad et al., 2012). H3K4me1 is usually found on active/poised enhancers, H3K4me3 on active/poised promoters and H3K36me3 on actively transcribed regions (Hon et al., 2009). H3K27ac has a similar enrichment pattern to H3K4me1 (Table 1-1) but can also predict active versus poised enhancers (Creyghton et al., 2010). H3K27me3, on the other hand, is associated with inactive promoters (Wamstad et al., 2012). Differentiation of mesodermal progenitors to cardiomyocyte requires EZH2, the major histone methyltransferase of the Polycomb repressor complex 2 (PRC2), which deposits H3K27me3 to repress foetal genes like *Nppa, Nppb* and *Myh7* (Delgado-Olguin et al., 2012). Thus, post-translational modification of histones play a key role in gene regulation, however the incorporation of core histone variants can also govern gene expression.

Table 1-1 H3K4me1 and H3K27Ac enhancer marks strongly overlap in the developing heart (mouse genome)

E11.5 H3K4me1 peaks	146 000
E11.5 H3K27Ac peaks	77 000
Overlapping regions (E11.5)	58 000
E13.5 H3K4me1 peaks	260 000
E13.5 H3K27ac peaks	116 000
Overlapping regions (E13.5)	110 900

Genome wide regions enriched for the histone marks for enhancers in the embryonic heart were downloaded from ENCODE project (Encyclopedia of DNA Elements, encode database ENCSR663VWL) (Shen et al., 2012)

1.2.5) Histone variants

Nucleosomal histones were previously thought to be highly stable and static once incorporated within the chromatin of non-dividing cells. However, separately encoded forms of canonical histones, or variant histones, can also be deposited as the replication fork carries out DNA synthesis (replication dependent) or as it is often the case, independent of replication (Maze et al., 2014). Canonical histones are defined by their expression which peaks during the S phase of replication, unlike variant histones (Szenker et al., 2011). Histone variants are deposited via a replication independent manner (Henikoff and Ahmad, 2005), as opposed to canonical histones, which are translated only during the replication phase (Hardy and Robert, 2010). Some histone variants are nonallelic variants of the canonical form and present distinct biophysical characteristics which can alter nucleosome stability (Kamakaka and Biggins, 2005). Furthermore, unlike canonical histones, variant histone gene contain introns and are polyadenylated, which allows them to be post-transcriptionally modified (Old and Woodland, 1984). Among the core histones, H2A has the most variants: H2A.Z, MacroH2A, H2A-Bbd, H2AvD, and H2A.X. They differ both in size of their C-terminal tails and their sequence (Figure 1-14). H2B known variants are TSH2B, H2BFWT, H2BE. H3 has H3.1, H3.2, H3.3, H3.4 (also known as H3.1t and H3t) and H3.5 (H3.3C). H4 does not seem to have any variant. Genome wide studies have demonstrated that various genome regions sometime present a higher proportion of certain histone variant (Yukawa et al., 2014). Two well studied variants are discussed below: H2A.Z and H3.3.

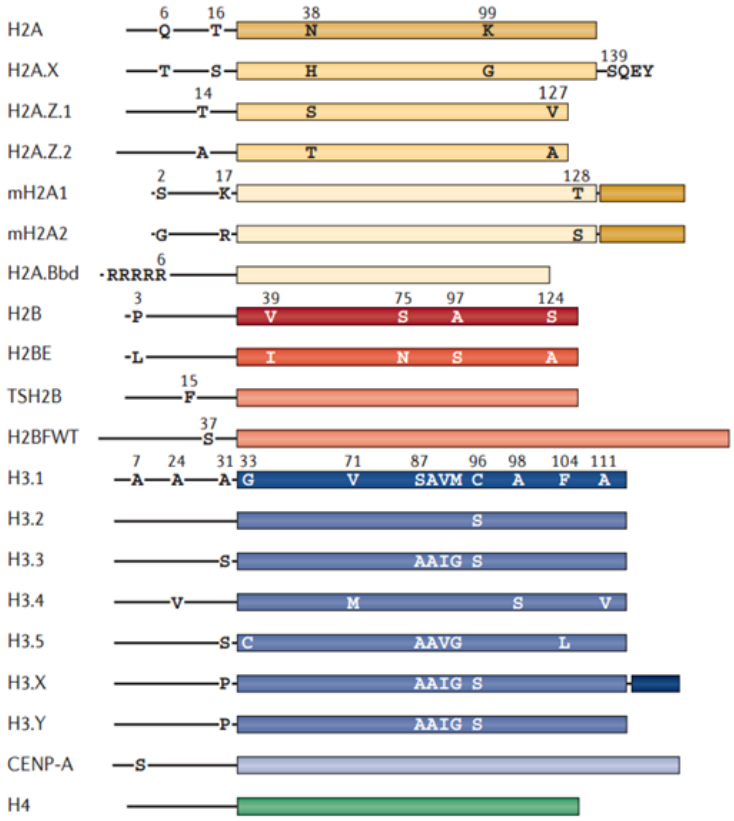

Figure 1-14 H2A, H2B and H3 have variants in human

Graphical representations of H2A (yellow), H2B (red), H3 (blue) variants are displayed here. H4 (green) is the most conserved histone which acts as an anchoring site for the other histones and does not have variants. Key amino changes and position number are displayed. Black line represent unstructured histone tails.

H2A.Z is constitutively expressed but is predominantly located in intergenic regions of the genome (Rangasamy et al., 2003, Kamakaka and Biggins, 2005). Experiments in promyelocytic cell line HL60 have shown that H2A.Z serves a dual purpose: it associates with promoters to demarcate active genes and maintain transcriptionally poised status, and its incorporation in coding region represses transcription by increasing nucleosomal stability (Farris et al., 2005). Similarly in the plant *Arabidopsis thaliania*, H2A.Z's occupancy changes with temperature in order to either physically block the progression of RNA Pol II (since DNA will be wrapped more tightly around nucleosomes) or occlude cis-elements from activating transcription factors (Kumar and Wigge, 2010). In human T lymphocytes, a genome wide study showed that H2A.Z is deposited at the promoter region, upstream and downstream of the transcription start site (TSS). This deposition was positively correlated with the level of gene expression (Barski et al., 2007) (Figure 1-15).

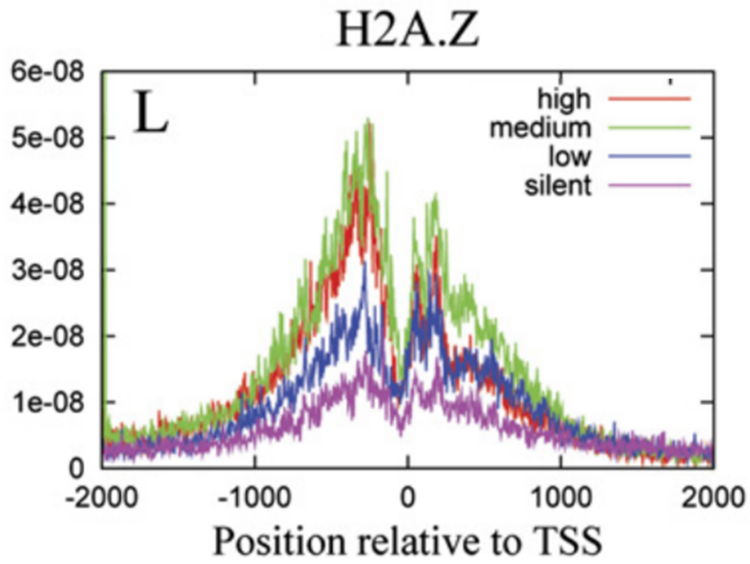

Figure 1-15 H2A.Z is enriched around the TSS in human cells

Binding levels of the H2A variant H2A.Z are shown here. An enrichment was observed in the promoter region, upstream and downstream of the transcription start site (TSS). In addition, the deposition of H2A.Z was found to correlate with level of gene expression in human CD4+ T cells. Y-axis: normalised counts. X-axis: base pairs upstream (-) and downstream (+) of the TSS. Each groups represent 1000 genes ranked according to their levels of expression. Adapted from (Barski et al., 2007)

H3.3 can be deposited during and outside of replication in drosophila (Ahmad and Henikoff, 2002). This variant histone has the particularity of having two separate coding genes: *H3.3a* and *H3.3b* which, in mouse, human and *Drosophila*, have a different DNA sequence (distinct untranslated region), and sometimes pattern of expression (Bramlage et al., 1997), but both translating to the same chain of amino acid (Bramlage et al., 1997, Szenker et al., 2011). H3.3 differs by only four amino acids from the canonical form of H3 in the fly (A->S31, S->A87, V->I89 and M->G90), and five in human and mouse (an additional V->C96), on its α2 helix, and yet it has a major impact on chromatin conformation. In *Drosophila melanogaster,* a single mutation of H3.1 or "canonical H3" towards H3.3 is sufficient for replication independent deposition (Ahmad and Henikoff, 2002). The functional properties of H3.3 are diverse: for example the phosphorylation of serine on position 31 (S31P) of H3.3 at the metaphase potentially protects the spread of heterochromatin onto euchromatin, thus keeping H3.3 chromatin in an open conformation (Hake et al., 2005). In HeLa cells, H3.3 disturbs higher order chromatin folding, protects from H2A.Z-mediated compaction and promotes gene expression (Chen et al., 2013). Many looked at H3.3 in the context of epigenetic memory (Ng and Gurdon, 2008). In *X.laevis* embryos, nuclear transfer experiments demonstrated the capacity of H3.3 enrichment to maintain genes in an active state, for up to 24 cell division (Ng and Gurdon, 2008). In development, H3.3 has been associated with transcriptional activity. For example in X.*laevis,* H3.3 incorporation is associated with gene activation at enriched sites (Ng and Gurdon, 2008). H3.3 enrichment has also been observed in

silent chromatin loci at telomeres and centromeres in ES cells and mouse embryonic fibroblasts (Goldberg et al., 2010, Wong et al., 2009, Santenard et al., 2010). The TTAGGG sequence repeated in telomeres was found to be significantly enriched in H3.3 (Goldberg et al., 2010), which carried the H3K9me3 mark thus revealing a function of H3.3 in maintaining constitutive heterochromatin (Udugama et al., 2015). In ES cells, H3.3 enrichment was found in gene rich regions of the genome and overlapped with markers of transcription such as phosphorylated RNA polymerase II (RNAPII), H3K4me3, H3K36me3, H3K4me1 (Goldberg et al., 2010) as well as transcription factor binding sites. H3.3 was found to be enriched around the TSS of both active and repressed genes which have a high CpG content in ES cells, but not on the TSS itself, probably due to the CpG residues locally depleting nucleosomes (Fenouil et al., 2012, Goldberg et al., 2010). In addition, H3.3 deposition at the gene body was only observed on active genes and not on repressed genes (Goldberg et al., 2010).

Similarly in HeLa cells, H3.3 is selectively enriched at TSSs of active genes (Jin et al., 2009). Bivalent genes bear both the activating H3K4me3 and repressing H3K27me3 histone modifications and are thought to be poised for activation during differentiation (Mikkelsen et al., 2007). In ESCs, a strong enrichment of H3.3 was observed at the TSS of bivalent genes, which was abolished by mutations towards H3.2 or H3.1 (Banaszynski et al., 2013).

In conclusion, H3.3 deposition has a pleiotropic role across different regions of the genome and at different times during development. Interestingly, studies on the combination of histone variants (eg: H2A.Z and H3.3) on nucleosome core particles in HeLa cells revealed that H3.3 enrichment at the TSS often co-locates with H2A.Z, which suggests H3.3 could play a role on DNA accessibility and gene regulation. The distribution of these unstable double variants (H3.3/H2A.Z) is different from nucleosomes with H2A.Z and H3.3 alone, and are thought to play a central part in the activation of promoters and the formation of “nucleosome-free regions” (Jin et al., 2009).

1.2.6) Examples of chromatin remodelling proteins in the heart

ATP dependent chromatin-remodelling enzyme seem to have evolved to accommodate the growing complexity of chromatin as eukaryotic unicellar life evolved into complex organisms. Using techniques such as chromatin immunoprecipitation serial analysis of gene expression (ChIP-SAGE) and ChIP-seq (Schones and Zhao, 2008), four classes of ATP dependent chromatin-remodelling enzyme have been identified: SWI/SNF, ISWI, CHD and INO80 complexes, which are encoded by a total of 30 subunits. These enzymes are crucial for the assembly and the dissolution of chromatin structures and they all share one function: to increase nucleosome mobility. However, new functions are still being discovered such as maintaining higher order structure of chromosome, regulating telomeres structure and maintenance (Yu et al., 2007), segregating chromosomes or serving as DNA replication

checkpoints. In the SWI/SNF complex, there are many subunits, including BRG1 and BRM. Officially named "SWI/SNF-related, matrix-associated, actin-dependent regulator of chromatin" (SMARC), this complex is more often referred to as Brg1/Brm-Associated Factors (BAF). BRG1 (Brahma-related gene 1) has been associated with transcription factor of the pluripotency network in ES cells, such as *Oct4*, *Sox2* and *Nanog* (Ho et al., 2009) and when mutated, can cause tumours (Jones et al., 2012, Love et al., 2012). BRG1 attracted much attention for its role in heart development and maintenance. In zebrafish, DPF3 is part of the BAF complex and is required for cardiac looping and contractility (Lange et al., 2008). *Brg1* myocardium conditional mutants are embryonic lethal as a result of thin compact myocardium and complete lack of interventricular septum (IVS) (Hang et al., 2010). BRG1 directly bind to and regulates α-MHC and β-MHC to preserve the α/β –MHC ratio in the foetal heart myocardium (Hang et al., 2010). *In vitro* experiments showed that the α-MHC repression by BRG1 was dependant on HDACs (Hang et al., 2010). Similarly, BAF60c, which recruits BRG1 to heart-specific enhancers (*Tbx5, Nkx2.5* and *Gata4)* is required for cardiogenesis (Lickert et al., 2004). Furthermore, *Tbx5, Tbx20* and *Nkx2.*5 all share an essential allelic balance with *Brg1,* supporting the dosage sensitive model of the BAF complex during heart development (Takeuchi et al., 2011). A trans differentiation experiment using mesodermal cells differentiating to cardiomyocyte gave evidence for the critical role of Baf60c in the cardiac lineage (Takeuchi and Bruneau, 2009). Ablation of *Brg1* by *Tie2Cre* in the endocardium led to hypotrabeculation (Stankunas et al., 2008) . BRG1 normally binds the promoter area to negatively regulated ADAMTS1 protein, a secreted matrix metalloproteinase, which shape the extracellular matrix (cardiac jelly) to form the trabeculae.

The chromatin remodelling BRG1 has various roles during cardiogenesis, which implicates multiple pathways.

1.2.7) WHSC1: an example of a Histone methyltransferase playing a role during heart development

The HMTase Wolf–Hirschhorn syndrome candidate 1 (WHSC1, also known as NSD2 or MMSET) specifically trimethylates H3K36. Intriguingly, *Whsc1*$^{-/-}$ embryos, which have a global reduction of H3K36me3 across the genome, show upregulation of genes implicated in heart development (Nimura et al., 2009) (*Pdgfra, Igfbp5, Bmp2,* and *Isl1*) but a downregulation of bone development-related genes (Lee et al., 2014) (*Opn, Col1a1*). The discrepancy between the two phenotypes can be explained by multiple factors. First WHSC1 deposits H3K36me3 which acts as a "repressor of overactivation of transcription in active genes" (Lee et al., 2014) but this methyltransferase also associates with co-factors that may influence gene expression themselves, such as transcription factors. In the developing murine heart for instance, the WHSC1-NKX2.5 complex mainly acts through H3K36me3 deposition which negatively regulates transcription, whilst in the osteoprogenitors, the WHSC1-p300-RUNX2 complex drives the

deposition of H4Ac (Lee et al., 2014) (marker of activation) which has a superior impact on gene expression than H3K36me3 deposition. Methylation of histone tail can also be modified dynamically during the differentiation process. For instance, certain domain structures in the PRC2 complex such as the Tudor domain and PHD finger domain have the capacity to bind or read histone tail modifications. It was shown that in mouse ES cell differentiation, PHF19 and No66 (a demethylase) bind to H3K36me3 on hitherto activated genes, recruit the PRC2 complex, and drive a switch from H3K36me3 to H3K27me3, which ultimately leads to transcriptional repression (Brien et al., 2012).

1.3) Known role of HIRA

HIRA (HIR histone cell cycle regulation defective homolog A or Histone chaperone histone regulator A) is a large protein of 1017 amino acid residues first discovered in the yeast *Saccharomyces cerevisiae* (Sherwood et al., 1993). In the yeast, there are two proteins Hir1p and Hir2p which interact. Their names derive from the fact that they are transcriptional corepressors of six of the eight histone genes (HTA1-HTB1, HHT1-HHF1, and HHT2-HHF2) (Spector et al., 1997, Osley, 1991). When the DiGeorge critical region (see below) was cloned from human DNA, the 1017 amino acids sequence, which contained the 766 amino acids previously known as TUPLE1, was identified as HIRA, the human homologue of Yeast Hir1p and Hir2p (Lamour et al., 1995). Northern blots identified *HIRA* transcripts in all foetal organs, including the heart (Lamour et al., 1995). Research on cell cycle regulators through cyclin-dependent kinases (cdks) in a human osteosarcoma cell line revealed that HIRA is a cyclin cdk2 substrate phosphorylated during S phase. Its overexpression led to an arrest in S-phase (Hall et al., 2001). Its role has since been identified in *Xenopus laevis* (Ray-Gallet et al., 2002) and *Drosophila melanogaster* (Loppin et al., 2005) as a histone chaperone which deposits core histones and has been studied to gain some insight into the mechanism of epigenetic regulation.

1.3.1) Disputed candidate for DiGeorge syndrome

Our group was originally researching HIRA since it was a candidate genes for DiGeorge syndrome (Halford et al., 1993, Farrell et al., 1999, Scambler, 2000, Lamour et al., 1995) (DGS). First characterised by Angelo DiGeorge in 1965 (Cooper et al., 1965), this condition is often caused by a well characterised deletion of chromosome 22q11 (de la Chapelle et al., 1981), with 1 in 4000 live births affected (Scambler, 2000). Many birth defects have been associated with this deletion, which leads to various abnormalities such as facial dysmorphism, hypoplastic thymus gland and learning difficulty. The main cause of mortality in those patients, however, are congenital heart defects. They vary between persistent outflow tract abnormalities (truncus arteriosus, interrupted aortic arch type B), ventricular septal defect

(VSD) and tetralogy of Fallot (ToF). A high resolution analysis of this region helped chromosome 22 to be the first fully sequenced human chromosome (Kirsch et al., 2000), which maps to chromosome 16 in the mouse (Lund et al., 1999). Mapping the deletion revealed that most patient had a 3 Mb deletion, covering 35 genes (Scambler, 2000), including *TBX1* and *HIRA* (Figure 1-16).

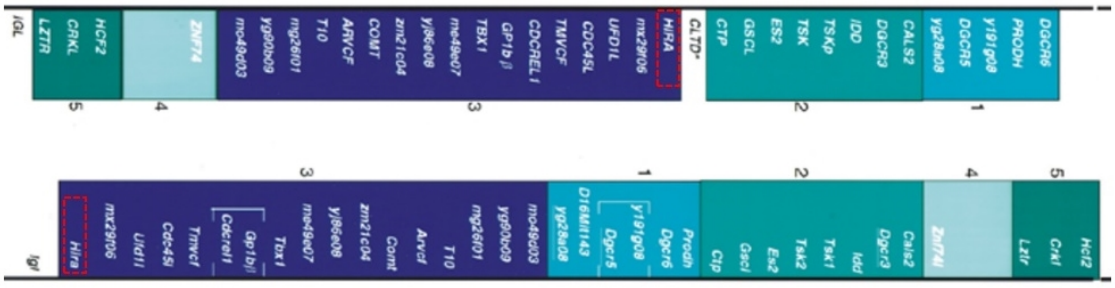

Figure 1-16 Hira is located within the 22q11 deletion region in human and mouse

Schematic representation of the genes of the 22q11 deletion located in the human genome (top) and their homologue in the mouse genome (bottom) on chromosome 16. *HIRA* (framed in red) in the centre in human and on the edge of an engineered deletion in the mouse. Taken from Scambler (2000) (Scambler, 2000).

In an Israeli cohort of DGS patients, the 22q11.2 deletion was detected in 109 of 140 subjects (77.8%) by fluorescent *in situ* hybridization (FISH) using a HIRA probe (Michaelovsky et al., 2012). In another cohort of 350 patients with traits typical of DGS/VCFS (Velo-cardio-Facial syndrome, another name for DGS (Shprintzen, 2008)), a typical 22q11 deletion was reported in 78% of cases using the available FISH probes (Rauch et al., 2005). The 20% unaccounted for might be due to a poorly defined etiology, or misdiagnosed patients showing common symptoms which together phenocopy DGS. By using a PCR based technique called multiplex ligation-dependent probe amplification (MLPA), sensitivity was increased and allowed for the detection of deletions either proximal or distal to the FISH probes (Stachon et al., 2007), although between 10 and 20% of patients remained negative for HIRA FISH and/or MLPA testing. These patients might display microdeletions, variant breakpoints or atypical deletions which challenges the use of HIRA as the best candidate loci for DGS. A mouse model which has a heterozygous deletion (Df(16)) encompassing around 1 Mb of the homologous region on chromosome 16 displays cardiovascular abnormalities characteristic of DGS (Lindsay et al., 1999). This phenotype was rescued when a P1-bacteriophage artificial chromosome containing *Tbx1* was expressed in transgenic embryos. Furthermore, haploinsufficiency (the result of a decreased gene dosage) of *Tbx1* reproduces many features of DiGeorge in mouse embryos (Lindsay et al., 2001, Paylor et al., 2006, Calmont et al., 2009). *Hira* heterozygous mutants, on the other hand, do not show any abnormality and are viable (Roberts et al., 2002). Therefore, *TBX1* seems to be the most critical candidate (Restivo et al., 2006, Calmont et al., 2009) for

DGS. In addition, human *TBX1* missense mutations have been associated with the major features of DGS (Zweier et al., 2007).

1.3.2) HIRA is part of multiprotein complex

Soon after its discovery, evidence was given for the capacity of HIRA to bind histones (Lorain et al., 1998). In the developing nervous system, HIRA was found to interact with the transcription factor PAX3 (Magnaghi et al., 1998). In HeLa cells transfected with H3.3 tagged HIRA, immuno-affinity purification experiments identified that HIRA was part of a multiprotein complex which includes UBN1, CABIN1 (Rai et al., 2011) and ASF1a (Tagami et al., 2004).

Ubinuclein (UBN1) was first known for being a ubiquitously expressed nuclear protein which binds various transcription factors (Aho et al., 2000) such as *C-jun.* UBN1 binds to HIRA through its WD40 domain and is required for HIRA mediated formation of senescent associated heterochromatin foci (SAHF) (Banumathy et al., 2009). SAHFs are domains of facultative heterochromatin which have the ability to silence genes necessary for proliferation during senescence (Aird and Zhang, 2013)

Recently, a novel UBN1 domain (Hpc2-related) was identified, which gives the HIRA complex its H3.3 binding specificity (Daniel Ricketts et al., 2015).

CABIN1, also known as CAIN, is the mammalian homologue of Hir3 in yeast. It is a known repressor of the transcription factor MEF2 which is done via the recruitment of both histone deacetylases and a histone methyltransferase (Jang et al., 2007). In the U2OS bone osteosarcoma cell line, CABIN1 directly interacts with HIRA and UBN1 (Rai et al., 2011). Further evidence for a functional role of CABIN1 came from a knockdown (KD) experiment followed by transcriptome analysis: in both HIRA KD and CABIN1 KD, the resulting set of dysregulated genes in HeLa cells was almost identical (Rai et al., 2011).

ASF1 (Anti-silencing function 1) was originally recognised as a gene that de-represses silenced loci when it was overexpressed in the yeast (Le et al., 1997) and its function as a mediator of chromatin assembly after DNA replication was then established in the fly (Tyler et al., 1999). ASF1 is known to directly interact with histones through its hydrophobic beta sheet motif (English et al.). Its role during DNA replication is vital since in the absence of ASF1, DNA unwinding necessary to establish the replication fork is greatly reduced, probably due to an altered displacement of nucleosomes (Groth et al., 2007). The maintenance protein complex (MCM) interacts with ASF1a and the histone chaperone FACT (facilitates chromatin transcription) via histones H3 and H4 (Groth et al., 2007). Interestingly, FACT interacts with HIRA and together participate in H3.3 replacement (Nakayama et al., 2007). In this large

quaternary HIRA/UBN1/CABIN1/ASF1a complex sometimes referred to as HUCA, HIRA is thought to act as a scaffold (Rai et al., 2011).

1.3.3) Known roles *in vitro*

In a model of embryonic stem cell differentiation*, Hira* null cells were found to have an accelerated rate of differentiation (Meshorer et al., 2006). Embryonic bodies developed as soon as 24h in the mutant cells as opposed to 72h in WT control cells. It was suggested that this rapid differentiation correlates with a reduced incorporation of H3.3 thereby promoting the change of euchromatin into heterochromatin thus contributing to the loss of stemness. These data reveal the importance of HIRA in the early differentiation steps of ES cells to control the major rearrangements of the chromatin. However, HIRA has a moderate effect on gene expression in undifferentiated ESC (Goldberg et al., 2010). Similarly in HeLa cells, HIRA or CABIN1 knockdown only "modestly" affected gene expression (Rai et al., 2011). HIRA controls H3.3 enrichment at active and repressed high-CpG-density promoters (HCP) genes in undifferentiated cells. More precisely, HIRA deposits H3.3 at, and around the gene's TSS (Goldberg et al., 2010). In HeLa cells, HIRA collaborates with histone binding protein ASF1a to deposit H3.3 at active promoters and at active/weak poised enhancers (Pchelintsev et al., 2013b). Four clusters involving HIRA have been defined, each with a different coregulator composition and associated with a different nucleosome deposition pattern. For example, in the cluster in which HIRA is associated with active enhancers, there was an enrichment of H3K4me1, H3K4me3 and p300 whereas in the cluster marking promoters of actively transcribed genes, there were CpG islands and a similar methylation/acetylation pattern except for the absence of H3K4me1 (Pchelintsev et al., 2013a).

Using a C2C12 myoblast cell line, it was shown that HIRA is required for differentiation into multinucleated myotubes (Yang et al., 2011). The deposition of H3.3 was detected at the core enhancer region (CER), the distal regulatory region (DRR) and the proximal regulatory region (PRR) of *MyoD* which is expressed during myogenic differentiation (Yang et al., 2011). Similarly, transdifferentiation experiments using C2C12 revealed a transient requirement for HIRA/ASF1a during osteogenesis (Song et al., 2012).

In vitro research on angiogenesis using yolk sac endothelial cells (YSECs) revealed an important role for HIRA in regulating the response of endothelial cells to angiogenic signals. When stimulated with fibroblast growth factor FGF2 and epidermal growth factor EGF, the upregulation of *Vegfr1* seems to be mainly associated with histone H3 becoming acetylated at Lysine 56 (H3AcK56) at the *Vegfr1* loci. This process happens via an exchange of nonacetylated histone H3 with H3AcK56, rather than direct acetylation of the Lysine 56 at the chromatin. Knockdown of HIRA prevented both upregulation of *Vegfr1* and drastically reduced levels of H3AcK56 (Dutta et al., 2010).

1.3.4) Known roles *in vivo*

In *Drosophila*, *Hira* has been linked to male infertility. In the fly, the sperm nucleus is lacking all 4 core histones, replaced by the chromosomal proteins protamines. Upon fertilization, the nucleosome particles are assembled from maternal histones which are deposited in the male pronucleus. In *sesame* mutated eggs which have a homozygous mutation in *Hira* (Llevadot et al., 1998), this process fails and the haploid (maternal only) embryos die before hatching (Loppin et al., 2000). HIRA is therefore required to form DNA replication competent male pronuclei. Further investigation revealed the existence of multiple chromatin assembly machineries since in *Hira* mutant embryos, H3.3 deposition remains intact in all somatic and germline nuclei, except for late spermatid and sperm nuclei (Bonnefoy et al., 2007).

HIRA-dependent H3.3 deposition is required for the late stage of gastrulation in the *Xenopus Laevis* embryo. *Hira* morphants and *H3.3* morphants showed very similar phenotypes (Szenker et al., 2012). Both mutants had almost identical levels of H3.3 in total chromatin and a comparable sensitivity to micrococcal nuclease assay, a tool used to assess the conformation and condensation of chromatin.

In the chick, *Hira'*s role was investigated in the neural crest cells (see p7). Total ablation of this cell population in the developing chick embryo leads to phenotypes similar to the ones observed in DGS patients (Kirby and Waldo, 1995). *cHira* antisense treatment (used for gene attenuation before the development of siRNA) in the premigratory neural crest cells also resulted in cardiovascular features of DGS (Farrell et al., 1999), such as persistent truncus arteriosus. This condition happens when the common truncus arteriosus fails to septate thus not giving rise to the pulmonary trunk and aorta. Neural crest cells normally contribute to the aorticopulmonary septum separating the arterial trunk and prevent the formation of other anatomical defect such as VSDs.

In the mouse, maternal HIRA is present and required for mouse development past the zygote stage (Lin et al., 2014). *Hira* starts to be expressed in the blastula stage from E4.5 (Ariane Chapgier personal communication). Described by our group in 2002, the *Hira* null mice are early embryonic lethal. No embryos survived past E11 with all mutants displaying growth retardation and some displaying severely disorganised tissues as early as E6.5. Early cardiac markers myosin heavy chain 2a and 2v (MCL2a/2v) were either severely downregulated or absent at around E10. Therefore, HIRA is thought to be required in the mesendoderm from the beginning of gastrulation (Roberts et al., 2002).

These results demonstrate the importance of HIRA during cellular differentiation in various species and tissues.

1.3.5) HIRA in DNA repair and cellular senescence

Genome stability is critical to preserve cell functions. Histone variants and histone signature patterns are crucial in establishing that robustness (Talbert and Henikoff, 2010). In yeast, hormesis, also known as “cross-tolerance”, is the phenomenon by which cells exposed to mild stress activate certain core environmental stress response (CESR) genes. There is evidence for HIRA in increasing the accessibility of RNA pol II to the required genes during heat stress and oxidative stress response by nucleosome eviction (Chujo et al., 2012b). This was shown to be dependant of Slm9, one of the fission yeast homologue of HIRA, which was enriched at the promoters of *ctt1, gpx1*, and *hsp9* (CESRs) in a stress-dependent manner (Chujo et al., 2012b).

Senescence is a vital response acquired by the cell after the activation of oncogenes. This proliferation arrest is necessary to control and confine nascent tumours (Collado and Serrano, 2010). The mechanisms by which pre-malignant tumours enter senescence are complex. However, a remarkable phenomenon is the appearance of SAHFs (Cruickshanks et al., 2013). This local remodelling of chromatin structure requires the incorporation of Heterochromatin protein 1 (HP1) and the histone H2A variant macroH2A. In human fibroblasts, HIRA and ASF1a (members of the HUCA complex) regulate the formation of SAHFs (Zhang et al., 2005), thus driving cell cycle exit. In addition of SAHFs, general chromatin changes are likely to contribute to senescence. For instance, DNA methylomes revealed that methylation changes in senescence resemble those in cancer (Cruickshanks et al., 2013), further supporting the notion of a fine balance separating premalignant senescent cells from malignant tumours. The epigenetic landscape of senescent cells is therefore more dynamic than previously thought. HIRA has been shown to be one of the critical regulators of chromatin required for efficient suppression of oncogene induced neoplasia (Rai et al., 2014). H4K16Ac is highly enriched in the promoters of genes active during senescence. HIRA governs the Incorporation and maintenance of H4K16ac and H3.3 into chromatin to suppress tumorigenesis and induce senescence (Rai et al., 2014).

During cellular life, chromatin alteration due to cell stress can result in DNA damage, which can impact both the genome and the epigenome. Research on DNA damage-induced chromatin plasticity in response to UV radiation has shown that histone chaperones are important for restoring the structure and the function of chromatin. In the “access–repair–restore” model (Figure 1-17), damaged chromatin is loosened to facilitate the access of repair machineries, before being reorganized once DNA repair has been completed (Adam et al., 2014). HIRA has been identified as a promoter of transcription “restart” after severe genotoxic stress in both tumour cells and primary fibroblasts, through the deposition of newly synthesized H3.3 at genomic sites where UV irradiation was directed using a micropore filter

(Adam et al., 2013). In addition, the acetyltransferase HAT1 which incorporates H4K5/K12Ac-H3.3 at sites of double-strand breaks and associates with other homologous repair proteins such as RAD50/51 was found to interact with HIRA. This histone turnover activity at the site of DNA lesions was found to be HIRA dependant (Yang et al., 2013).

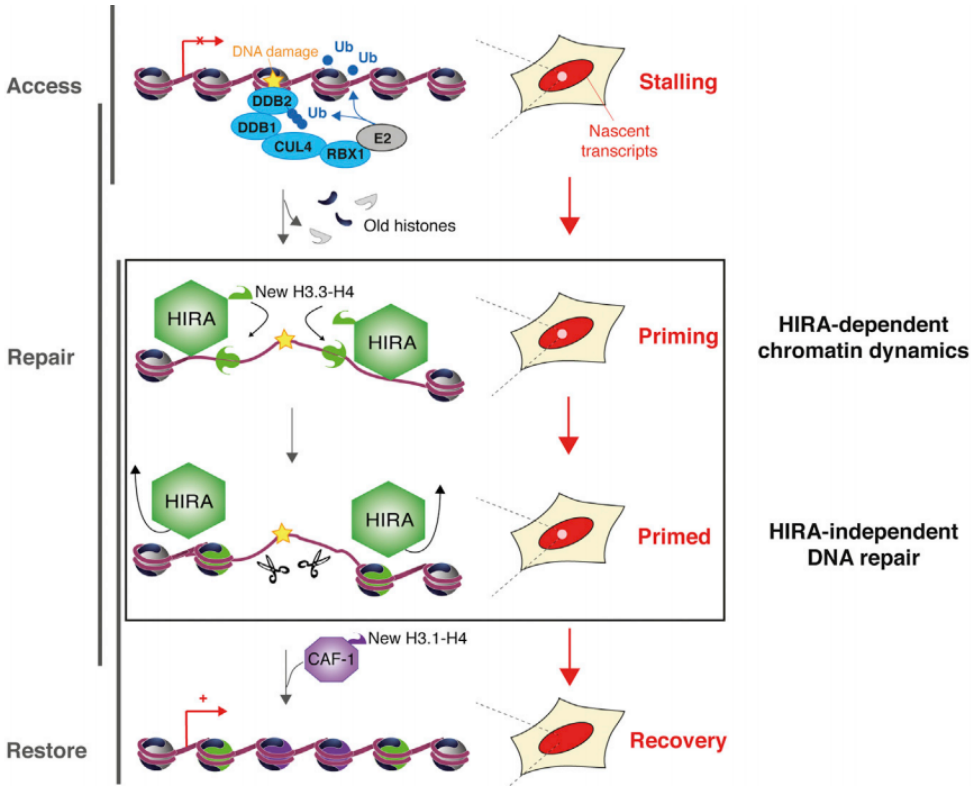

Figure 1-17 HIRA is recruited at DNA damage sites to participate in chromatin bookmarking

DNA damage such as UV radiation can be partly repaired by histone chaperones, which can restore the structure and the function of chromatin. Here, this schematic representation shows the recruitment of HIRA at sites of DNA damage. HIRA deposits new H3.3 histones to promote chromatin reorganisation such as CAF1 mediated canonical histone H3.1 deposition. Adapted from (Adam et al., 2013)

1.3.6) H3.3 mutations and its consequences

H3.3 mutations can affect development. For example in zebrafish H3.3 mutants, only tissue cranial neural crest (CNC) cell population was affected. A mutation in H3f3a, one of five zebrafish variant H3.3 genes, demonstrated that one of the roles of H3.3 is to prevent the formation of aberrant H3 homodimers. H3.3 mutants died by 7 days post fertilization (dpf) from CNC-derived cartilage, bone and teeth malformations preventing the fish from eating (Cox et al., 2012). Using timelapse immunofluorescence on live embryos, a lack of mutated H3.3 was only observed in the chromatin during metaphase/anaphase, rather than at all times during the cell cycle. This shows that H3.3 is present but is not integrated to the nucleosome. Further investigation of the nucleosome showed that mutated H3.3 “overbinds” WT H3.3, thus preventing normal formation of WT H3.3-H4 heterodimers (Cox et al., 2012). The replication independent property of H3.3 deposition proved to be crucial to CNC development since the

same mutation in replication dependant H3.2 did not lead to any defects. The authors propose a model in which the unique developmental pattern of ectomesenchyme makes this CNC lineage particularly sensitive to H3.3 incorporation compared to lineages with simpler differentiation pathways (Cox et al., 2012).

In the mouse, *ex vivo* research has shown that H3.3 is required early during development. Morpholinos injection targeted against both H3.3A and H3.3B in zygotes at the two cell stage led to arrest at the morula stage (Lin et al., 2013). In contrast to *Drosophila* where H3.3 mutants are viable but sterile (Sakai et al., 2009), H3.3 seems to be crucial during mouse development (Lin et al., 2013). The arrest at the morula stage was not cause by dysregulation of genes related to lineage commitment (*Oct4, Nanog* or *Sox2*) but was due to over-condensation and mis-segregation of chromosomes due to a specific decrease of H3.3K36me2 and H4K16ac. During early development, the chromatin needs to stay condensed to achieve faithful chromosome segregation and developmental competence. H3.3 and H1 have an antagonistic epistatic relationship, which explains the over incorporation of linker H1 to the chromatin in H3.3 mutants (Lin et al., 2014) and the resulting chromosome over-condensation.

In human, heterozygous mutations in H3.3 were found to be responsible for the lethal brain tumour Glioblastoma Multiforme(GBM) (Schwartzentruber et al., 2012). In almost a third of the affected children, a single nucleotide variant (SNV) was found in *H3F3A*, one of the two genes coding for H3.3. The switch from glycine to arginine or valine on the 34th amino acid of H3.3 (G34R/V) or a change from lysine 27 to methionine (K27M) is sufficient to cause GBM. 44% of these paediatric GBM patients also had mutations in either ATRX (a-thalassaemia/mental retardation syndrome X-linked) and/or DAXX (death-domain associated protein), which are H3.3 histone chaperones active in the telomeres (Figure 1-18). However, recent research on ATRX-dependent deposition of H3.3 has unveiled that this chaperone is not entirely restricted to pericentric heterochromatin and telomeres but also occurs at heterochromatic sites throughout the genome, especially at sites carrying H3K9me3, a modification associated with silenced imprinted alleles (Voon et al., 2015). The rest of the tumours were largely explained by mutations in the tumour suppressor *TP53.* Mutations in *H3.3* genes are highly prevalent in GBM, only one patient suffering from myelodysplastic syndrome (MDS) out of 77 had a mutated *H3F3A* gene in bone marrow cells (Attieh et al., 2013).

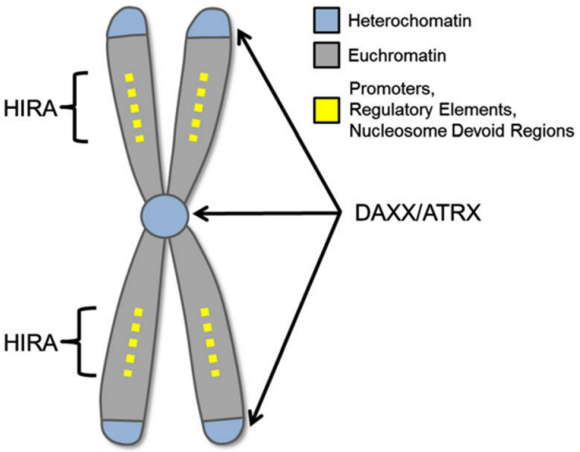

Figure 1-18 DAXX deposits H3.3 at the telomeres and centromeres

DAXX is a H3.3 histone chaperone that targets subtelomeric and pericentromeric regions of the chromosome, whilst HIRA deposits H3.3 in transiently nucleosome-free gene rich regions. From (Kallappagoudar et al., 2015).

In a cohort of patients suffering from chondroblastoma and giant cell tumour of bone, a unique "signature" was identified in the genes coding for H3.3. The same mutation, a p.Lys36Met, was identified in *H3F3B* in all patient with chondroblastoma, whilst the vast majority (49 out 53) of patients with giant cell tumour of bone had a p.Gly34Trp alteration in *H3F3A.*

1.4) HIRA conditional allele

1.4.1) Hira null embryos are lethal early in development

As discussed above, *Hira* was not the strongest candidate amongst the 35 genes deleted in the typical DGS. However HIRA is a well characterised histone chaperone depositing the variant histone H3.3 within chromatin which has been implicated in a multitude of biological processes from fertilization, through nuclear reprogramming, maintenance of stemness, cell cycle regulator and cellular senescence.

Hira null embryos display a range of developmental defects during and subsequent to gastrulation (Roberts et al., 2002) and a small proportion of these mutants which survived to E10.5 showed abnormal heart looping and substantial pericardial oedema.

1.4.2) Hira conditional allele

In order to bypass the early lethality of *Hira* null embryos, a *Hira* conditional allele (*Hira*$^{fl/fl}$) was designed by the Sanger institute (Figure 3-1,p*48*). This allele contains a Beta-galactosidase cassette surrounded by FRT (flippase recognition target) sites which can be targeted by the flippase recombinase. It is analogous to Cre-lox recombination. Once flippase is applied, the Beta-galactosidase cassette is lost and the allele becomes functional. Further recombination by CRE recombinase, which targets LoxP sites, ablates exon 4 which creates a non-functional copy of *Hira.*

1.4.3) Rationale

Hira has never been examined in the heart before. The global aim of this thesis was to dissect the potential role of *Hira* during heart development. To this aim, the following genetic tools were used: a floxed *Hira* allele, a *Hira* null allele and various *Cre* recombinase expressed in cardiovascular precursor cells.

The following questions were addressed:

- Is HIRA expressed in the heart?
- What phenotype results from the ablation of *Hira* in cardiogenic mesoderm (*Mesp1Cre*)?
- What phenotype results from the ablation of *Hira* in other lineages contributing to the formation of the heart?
- Does ablation of *Hira* in adult cardiomyocyte affect normal heart function?
- Does HIRA interact with transcription factors or chromatin remodeling protein?
- What are the downstream transcriptional effects resulting from the ablation of *Hira?*
- Is there evidence for specific HIRA binding sites across the genome that might directly affect transcription?

Chapter 2 Materials and methods

2.1) Animal breeding

2.1.1) Mouse lines and breeding

Animal maintenance, husbandry and procedures were carried out in accordance with British Home Office regulations. All lines were maintained on a CD1-ICR background. Pups resulting from various breeding pairs were ear-clipped between 11 and 13 days old identify and genotype them. Offspring were weaned at 21 days of age. The following lines were used:

Hiratm1a (MGI:4431679)
Mesp1Cre (MGI:2176467)
Mef2CCre (MGI:3639735)
Wnt1Cre (MGI:2386570)
Nkx2.5Cre (MGI:2654594)
Tie2Cre (MGI: 2450311)
Tcf/Lef GFP reporter (MGI: 4881498T)
Myh6MerCreMer (MGI:3050453)

Whilst all *Cre* are constitutively active, the *Myh6MerCreMer*, also referred to as *alphaMHC-Cre-Mer-Cre* needs tamoxifen injection to be activated. Tamoxifen was prepared in sesame oil (Sigma-Aldrich) and was administered by intraperitoneal injections (0.05 mg/g body weight), every day for three consecutive days.

2.1.2) Embryo collection

Sexually mature mice (6 weeks old female and 8 weeks old male) were paired and overnight mating was verified by vaginal plug in the morning, which translated to half a day of gestation (E0.5). Pregnant females were sacrificed at the relevant stage (E10.5 - E18.5) by cervical dislocation. Collected embryos were briefly stored in cold phosphate buffered saline (PBS) before being dissected. E18.5 embryos were stored overnight in PBS at 4C or killed directly by decapitation before dissection.

2.1.3) DNA extraction and polymerase chain reaction for genotyping

DNA was extracted using the yolk sac for embryos younger than E11.5, tail tips for embryos older than E11.5 and ear clips for postnatal and adult mice. The tissues were digested in adequate volume of Tail Lysis Buffer (below) containing 400ug/ml proteinase K (Sigma) overnight at 56°C. The same volume of 100% isopropanol was then used to precipitate the DNA, which was washed using 70% ethanol, before air drying and resuspension in 100 to 200 µl of distilled H_2O.

Tail Lysis buffer

Stock content	Final Concentration
1M Tris pH8.8	100mM
0.5M EDTA	5mM
10% SDS	0.20%
5M NaCl	200mM

Genotyping for mutant, heterozygous and wild-type animals carrying the Sanger allele was done with a BIOTAQ^{TM} DNA Polymerase kit using the following primers (table below).The PCR product was run on a 2% agarose gel to differentiate between the two amplimers (wild type, and the construct containing loxP sites). Furthermore, the presence of Cre activity was confirmed in embryos by detection of a third "rec" product following recombination (see p50).

List or primers used for genotyping

Cre-F	GTTCGCAAGAACCTGATGGACA
Cre-R	CTAGAGCCTGTTTTGCACGTTC
HIRA-KO-F	TGCAACTCTGAGAGGTCATTCTGGC
HIRA-KO-R	GGGACTGGCTGCTATTGGGC
FRT-F (red arrow)	CCTCTCAGTGTCACTGGG
FRT-R (red arrow)	CCCAGCCCTGATTCAGAT

PCR reaction mix

Components for 1 reaction	Total volume 25µl
Buffer 10X	2.5µl
MgCl2	0.75µl
dNTPs (25mM)	0.2µl
Forward and Reverse Primers (10µM)	1µl
Taq Pol	0.2µl
Genomic DNA	1µl
H20	17.35µl

PCR cycling conditions

94°	3 min
94°	30s
60° (all PCR except Cre) **Cre:64°**	30s
72°	1min
Repeat steps 2→4 40 times	
72°	10min

2.2) Imaging methods to phenotype mutants and assess HIRA expression

2.2.1) Dissecting microscope for macro histology

Embryos were dissected and captured using a dissecting microscope (Zeiss AxioCam HRc). An ultra-violet lamp was used to detect GFP expression if needed.

2.2.2) Optical projection tomography

First presented in a Science paper in 2002 (Sharpe et al., 2002), OPT offers the possibility to image various tissues using different wavelengths thus allowing the use of probe/antibody based immunofluorescence. Samples are cleared using 2 parts benzyl alcohol to 1 part benzyl benzoate (BABB). This step is crucial since the parallel light beams going through the specimen will not diffract or scatter extensively, thus increasing the final resolution. The sample contained in agarose rotates and is imaged every 0.45°. The acquisition is done by projection onto a CCD sensor (Figure 2-1).

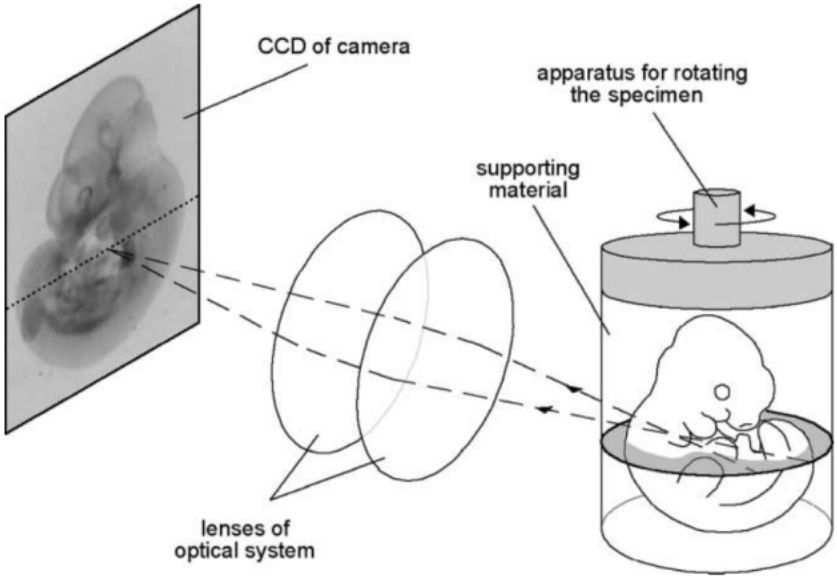

Figure 2-1 Optical Projection Tomography allows 3D visualisation of whole embryos

Optical projection tomography (OPT) allows the imaging of large biological samples. Here, this schematic shows a cleared sample lit by a source of light. The resulting image of the projection is captured by a CCD sensor. That process is repeated after the sample rotates by 0.45° to obtain a total of 800 images. Taken from (Sharpe et al., 2002).

Once the scan is complete, a back-projection algorithm and a 3D reconstruction step are applied to obtain the final useable data. The resolution (9µm) exceeds more often used techniques such as MRI and is roughly equivalent to µCT although it does not reach cellular level. More importantly in this context, OPT data gives the possibility of viewing the sample in any plane orientation, by "virtual reslicing" (Figure 2-2). This feature has proven very useful for the detection of VSDs.

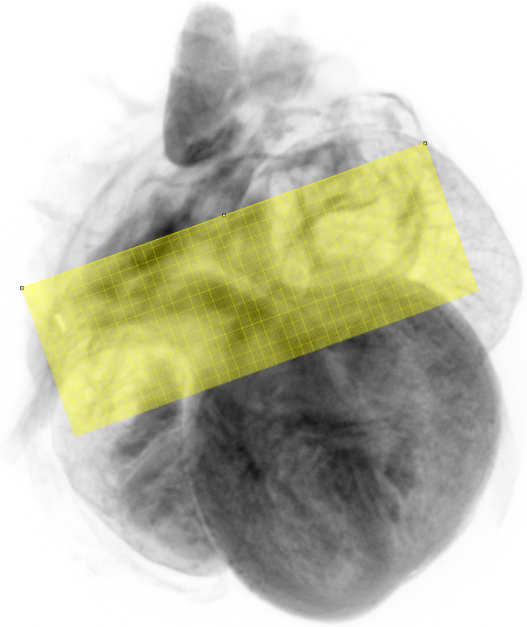

Figure 2-2 Image J is used to perform virtual reslicing of OPT acquired image stacks

An OPT scan can result in a slightly tilted sample as seen in this image J screenshot of a 3D reconstruction of an embryonic heart (in grey/black) at E15.5. It is necessary to virtually "reslice" the heart for the identification of certain cardiac defects, such as a VSD or valve malformations. Image J can correct the angle as seen by the stacks (yellow) which have a 15° tilt compared with a horizontal line.

Embryos were fixed overnight in 4% PFA/PBS and mounted in low-melting agarose (Life Technologies). Up to E14.5, whole embryos were processed. At E15.5, the trunks were opened and cartilage from the rib cage was discarded to help with the subsequent scanning since cartilage does not clear completely. Samples were then trimmed to remove the excess of agarose and washed in 100% methanol followed by clearing in BABB. Scanning was undertaken using a Bioptonics OPT Scanner 3001M (MRC Technology, Edinburgh, UK). NRecon software (Skyscan NV) was used for image reconstruction from projections using a back-projection algorithm. FIJI (Image J) and Volocity were used for image analysis and 3D reconstruction.

2.2.3) Image J and Volocity for 3D visualisation

FIJI (Fiji Is Just ImageJ) (1.46r) was used to visualise the long axis sections reconstructed by OPT. "Sliding" along the antero-posterior axis allowed for the correct identification of vessels. The pulmonary trunk (PT) was traced by semi-automatically filling out the vessel for approximately 150 slices, starting from the OFT and finishing in the lungs.

The extracted 3D vessel was loaded in Volocity® 3D Image Analysis Software, along with the original OPT reconstructed scan. Volocity, unlike FIJI, has a set of transparency and black level fine tuning functions which, combined with 3D visualization of samples, allows the full restoration of specific subparts of the captured image. The channels were set as followed:

red for PT and green for the heart. Way points were set up for 360 degree rotation and zoom (see supplementary video).

2.2.4) Ultrasound scan for heart function

The heart function of adult (~6 months) *Myh6MerCreMer;Hira*$^{fl/-}$ and *Myh6MerCreMer;Hira*$^{fl/+}$ controls were measured using a Visualsonics Vevo 2100 ultrasound system prior to *Cre* induction. Echocardiography M-mode recordings were used to measure chamber dimensions. Using left ventricular systolic and diastolic chamber dimensions, the ejection fraction was calculated by the software. During the following 3 days, the mice were injected every day with tamoxifen (Sigma-Aldrich) which was prepared in sesame oil (Sigma-Aldrich) using 0.1 mg/g body weight by intraperitoneal injection. The mice were subjected to echocardiography analysis 2 and 8 weeks after the injection period.

2.2.5) Paraffin embedding and Haemotoxylin and Eosin staining

Dissected embryos were fixed overnight in 4% paraformaldehyde (PFA) in PBS and then dehydrated by increasing concentration of ethanol (30% to 100%). They were then cleared using histoclear (National Diagnostics) for one hour, and embedded in paraffin overnight after several wax washes at 60°C. A microtome was used to section embryos to 10-12µm thickness and sections were transferred onto SuperFrost®PLUS microscope slides (VWR) for overnight drying. Most sections presented in this thesis will be following the long axis of the heart, unless stated otherwise. For morphological examination, sections were warmed to 60°C to dewax, then rehydrated through a decreasing concentration of ethanol (100% to 30%) and finally H_20. Slides were stained using freshly-filtered Mayer's Haematoxylin solution (Sigma-Aldrich) followed by aqueous Eosin solution (Sigma- Aldrich) and rinsed further in H_2O. Slides were mounted with glass coverslips using DPX solution (Merck).

2.2.6) Alcian Blue staining for Cartilage visualisation

Due to the extremely fine balance between KOH mediated tissue digestion and keeping the skeleton in one piece, the traditional approach for alcian blue cartilage described by McLeod (McLeod, 1980) was abandoned, following many failures. The observed embryos were young (E12.5-E13.5) and presented mostly fragile cartilage. Therefore the following alternative protocol adapted from (Nagy et al., 2009) was used.

Embryos were fixed in Bouin's solution overnight at 4°. The next day they were washed in a solution of 70% ethanol plus 0.1% NH4OH for 24 hours until the embryos appear white with no remaining yellow colour. Then they were equilibrated in 5% acetic acid (two changes, each for at least one hour) before being stained with 0.05% alcian blue in 5% acetic acid for 2-4 hours. 4 hours tended to yield a nicer stain. The embryos were sequentially washed twice with 5% acetic acid for 1 hour each. Finally the embryos were washed in methanol (two times 1 hour) and then cleared in BABB.

2.2.7) Beta Galactosidase to trace HIRA expression

X-gal staining is a convenient way to detect β-galactosidase enzyme activity. In bacteria, β-Galactosidase catalyzes β-galactosides into monosaccharides. Here X-gal (5-bromo-4-chloro-3-indolyl-beta- D-galactopyranoside) was used as a substrate which is cleaved into galactose and 5-bromo-4-chloro-3-hydroxyindole. The latter is dark blue which is easily detected under white light.

E10.5 embryos were dissected in cold PBS and fixed in 4%PFA at room temperature for 2 hours. Subsequently, they were washed 3 times for 20 min in detergent at RT: (0.1M Na_2HPO_4 pH 7.3, 0.1 M NaH_2PO_4 pH 7.3, 2 mM $MgCl_2$, 0.1% sodium deoxycholate, 0.02% Nonidet P-40, 0.05% bovine serum albumin (BSA), in ddH_2O.). X-gal (Thermo) is added (0.3mg/ml) last minute to the stain solution (2 mM NaCl, 5 mM $K_3Fe(CN)_6$, 5 mM $K_4Fe(CN)_6$, in detergent wash). E10.5 embryos were placed in stain solution for up to an hour, E13.5 for up to 4 hours and E15.5, around 12 hours. They were wrapped in foil to conceal from light and placed in a 37 degrees incubator. For older embryos (E13.5 – E15.5), the penetration of the stain solution was incomplete so embryos were sectioned prior to staining.

2.2.8) In situ hybridisation

Plasmids for synthesising antisense RNA probes were kindly given by Tim Mohun (*Tnni2,* Image clone 1448494 cut with EcoRI and RNA synthesized with T3 RNA polymerase) and by Jeffrey Bush (*Epha3* cut with XhoI and synthesized with T7 polymerase). Plasmids were linearised using the appropriate restriction enzymes for generating antisense probes, and extracted from a 1% agarose gel using the QIAquick Gel Extraction Kit (Qiagen). 1µg of linearised plasmid was used for in vitro transcription of probes using a DIG RNA labelling kit (Roche). Probes were precipitated by addition of 2µl 0.5M EDTA (pH 8), 5µl 4M LiCl and 150µl ethanol to the reaction and extracted by centrifugation.

Paraffin sections were prepared as previously described in milliQ water treated with RNAse-A. Slides were rehydrated then incubated in 20µg/ml Proteinase K (Sigma-Aldrich) for 8 minutes, washed in 2mg/ml glycine then PBS, and fixed in 4% PFA/PBS for 20 minutes. Following further PBS washes they were incubated for 1 hour at 70°C in a humidified chamber in hybridisation buffer (50% formamide, 5xSSC pH 4.5, 50µg/ml yeast RNA, 1% SDS, 50µg/ml heparin) followed by overnight incubation in hybridisation buffer containing between 1 and 2µg/ml of antisense RNA probe. Slides were then rinsed twice in 2x SSC buffer pH4.5, followed by three washes at 65°C in Solution I (50% formamide, 5x SSC pH4.5, 1% SDS), two washes in Solution II (50% formamide, 2x SSC pH4.5) and finally two washes at room temperature in MABT (0.1M maleic acid, 0.15M NaCl, 0.01% Tween-20, 2mM Levamisole (Sigma-Aldrich), pH7.5). Slides were then incubated in blocking solution (2% Boehringer Blocking Reagent

(Roche), 10% sheep serum in MABT) for 1 hour followed by overnight incubation at 4°C with an alkaline-phosphatase (AP) conjugated anti-DIG antibody (Roche) diluted 1:2000 in blocking buffer. Following further washes in MABT and AP buffer (100mM Tris, pH 9.5, 50mM MgCl2, 100mM NaCl, 0.1% Tween-20, 2mM Levamisol), AP activity was detected using BM Purple (Roche) for at least 24 hours. Signal took up to 4 days to appear but was highly specific.

2.3) Quantifying gene expression in the heart

2.3.1) RNA extraction

2.3.1.1) Trizol

Total RNA from embryonic hearts was first extracted with Trizol (Invitrogen 15596-018) following the manufacturer's instructions. Briefly, E12.5 hearts with the relevant phenotype which had been stored at -80°C were dissolved in 350µl Trizol reagent using a needle and syringe. Samples were incubated at room temperature (RT) for at least five minutes. 60µl chloroform was then added and tubes shaken vigorously and centrifuged at RT for 15 minutes. The upper aqueous layer was transferred to a fresh tube and 150µl isopropanol added to precipitate the RNA. Samples were centrifuged for 10 minutes at 4°C and RNA pellets were washed in 70% EtOH, air dried and resuspended in 30µl RNase-free H2O. Nanodrop1000 was used to quantify and assess sample quality. The A260/A280 ratio should be above 1.6, and although it was around 1.8, the nanodrop measurements displayed an isopropanol contamination (Figure 2-3). Subsequent washes with 70% ethanol helped purify the RNA, but the quality was never good enough for RNAseq.

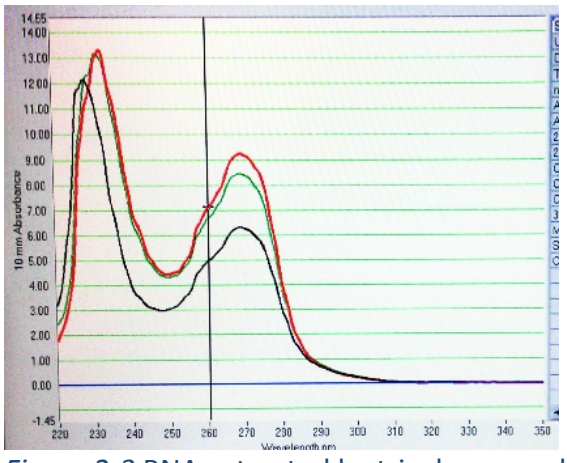

Figure 2-3 RNA extracted by trizol can result in chloroform or isopropanol contamination

The absorbance (or optical density (OD)) measured by the nanodrop is used to check the purity of the nucleic acid extraction. A peak is normally expected at 260nm for nucleic acids. The OD ratio A260/A280 and the A260/A230 have to be greater than 2 to ensure an optimal quality of RNA/DNA. This shift seen here may be caused by residual chloroform or isopropanol, used during Trizol extraction.

2.3.1.2) Qiagen column

Total RNA was isolated using RNeasy Mini kits (Qiagen) according to manufacturer's instructions, including the optional on column DNase digestion step, and eluted into 30µl RNase-free H_2O. The extractions resulted in a more consistent yield (around 100ng/µl) and higher purity (Figure 2-4).

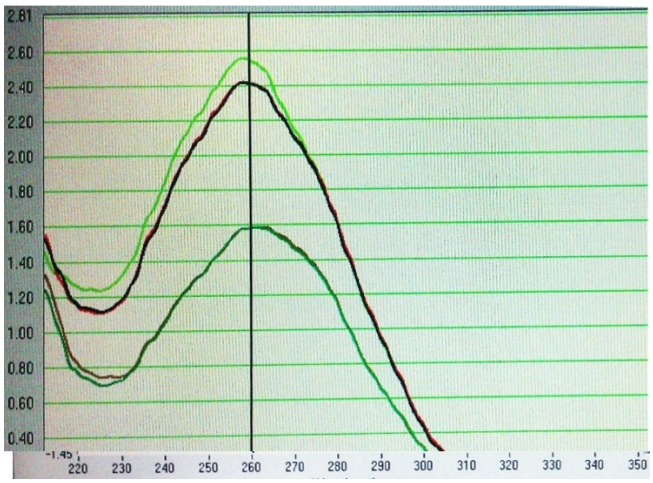

Figure 2-4 RNA extracted by Qiagen columns is consistently clean

The nanodrop absorbance profile here shows A260/A230 ratio equal or greater than 2.

2.3.2) Reverse transcription

The High-Capacity RNA-to-cDNA™ Kit (Thermo fisher 4387406) was used to obtain cDNA for the qRT-PCR experiments, according to the manufacturer's instructions. Briefly, up to 2 µg of RNA in 9µl was added to the 10 µl of 2x RT Buffer and 1µl of 20x RT Enzyme for a total of 20µl. The reaction mix was placed at 37°C for an hour and at 95°C for 5 min.

2.3.3) Designing primers using primer blast

Primers for qRT-PCR were designed using primer-blast (http://www.ncbi.nlm.nih.gov/tools/primer-blast/) with the following option: primers must span an exon-exon junction, thus ensuring amplification of cDNA *only* since contamination by genomic DNA remains possible. Furthermore, pair of primers were tested against a database of mRNA possible off-targets. Finally the PCR product size was set to be between 80 and 160 bp (Figure 2-5).

Figure 2-5 Example of primers spanning exon-exon junctions

Table 2-1 Primers used for qRT-PCR

Atp1b1-F	TCTCAGATGTGTCCGTTCTTCT
Atp1b1-R	TGGAAAGAGAGTGAAAGGCAAG
Epha3-F	GGACCCTCCCAGGATGTACT
Epha3-R	AGCACACTTAGCAGCACCAT
F11-F	GAAAGCCGGGAGGAAACTGT
F11-R	CCTGGACGTCAGATTGAGCA
Gata5-F	GGACCAGCTTCGTACCTGAC
Gata5-R	TGGCAGTATGGCAGTTGGAG
Igfbpl1-F	TCTACTCCTCAGTTCCGGGT
Igfbpl1-R	CATCTACAGGCAGTCTCCCC
Lyve1-F	CAGCACACTAGCCTGGTGTTA
Lyve1-R	CGCCCATGATTCTGCATGTAGA
Prox1-F	AGAAGGGTTGACATTGGAGTGA
Prox1-R	TGCGTGTTGCACCACAGAATA
Scn7a-F	TGTCTCCTCTAAACTCCCTCAG
Scn7a-R	TGCGTAAATCCCAAGCAAAGT
Nrp2-F	TTTGCAGGTGAGGATTTTAAAGTGG
Nrp2-R	CACCAGCCCCTGAGGTAGAG
Ramp1-F	GACGCTATGGTGTGACTGGG
Ramp1-R	AGAAACAGCCAATCGTGTGC
Tbx3-F	AGATCCGGTTATCCCTGGGAC
Tbx3-R	CAGCAGCCCCCACTAACTG
Isl1-F	ATGATGGTGGTTTACAGGCTAAC
Isl-R	TCGATGCTACTTCACTGCCAG
Nppb-F	GAGGTCACTCCTATCCTCTGG
Nppb-R	CCATTTCCTCCGACTTTTCTC
Pdgfra-F	TGCCTTGAAAGCAACGTCAG
Pdgfra-R	TTGTTTCTCACTTCTCCAGGGTA
Slc4a1-F	CGGTCAGGTCTATGTGGAGC
Slc4a1-R	TTCCTCCAGCCCTATCCAGT
Tnni2-F	CCGCCGAGAATCTGAGAAGG
Tnni2-R	TGCAGAGTTCCTGCACTTCA
Tnnt3-F	ATTGACCAAGCCCAGAAGCA
Tnnt3-R	AGAAGTCCAGGAGGAAGCCC
Tnnt1-F	GCAGAGAGAGCTGAGCAACA
Tnnt1-R	AGGTAGCCCCCAAAATGAGC
Casq1-F	CTTCGCTACCTTCGACAGCA
Casq1-R	GGGTTGATCTCCTGTGCTCC
Acta1-F	TGAAGCCTCACTTCCTACCCT
Acta1-R	CGTGTGGCTCAGTAGGAGAG
Krt8-F	CCATGAAGAGGAGATCCGTGA
KRt8-R	CTCGTACTGGGCACGAACTT
Krt19-F	ATTACTGCCCTGAGGAGCCA
Krt19-R	TTCAGCTCCTCAATCCGAGC

2.3.4) SYBR green Real-time PCR: absolute quantification

Absolute quantification was performed using SYBR green to determine the amount of original transcripts in the total RNA. This method uses the standard curve method, which establishes a quantity for an unknown sample based on a serial dilution of a known quantity. Standard curves were established by pooling all the samples together and diluting subsequently or in series 10 times, twice, to obtain 1, 0.1 and 0.01 quantities of cDNA templates. There are two main reasons for using this technique as opposed to the more traditional ΔΔCT method: The efficiency of the primers is analysed using the standard curve and is taken into account when measuring unknown samples every time but mainly we do not need to spend time optimising the efficiency so it fits GADPH's. Second, there is no need for using a housekeeping gene control more than once, if running multiple plates. The CFX96

Touch™ Real-Time PCR Detection System was used. Following the reaction, samples were run on an agarose gel to verify the amplimer size.

2.3.5) RNAseq: analysis with Strand NGS

RNA extraction was done in triplicate from *Mesp1Cre;Hira*$^{-/fl}$ and *Mesp1Cre;Hira*$^{+/fl}$ embryonic hearts at E11.5 and E12.5 using the QIAGEN RNeasy mini kit (74104). RNAseq was processed by the ICH genomics facility, which used an Illumina NextSeq 500, and paired ends reads were produced. Reads were aligned and normalised using BOWTIE and DEseq R package. Strand NGS 2.5 software was used which uses the DEseq algorithm, was used to incorporate additional downstream analysis such as Gene Ontology and to re-analyse the aligned files (.bam). By applying the Mann Whitney unpaired test, Benjamini Hochberg False discovery rate (FDR) and filtering the genes using adjusted p-value ≤ 0.05 and absolute fold change ≥ 1.5, 95 % of the results were identical to the DEseq package used by the UCL Genomics facility. The main advantage provided by strand NGS is the ability to perform a gene ontology (GO) analysis and generate heatmaps of various groups of genes.

2.4) Investigating HIRA's binding partners: Co-immunoprecipitation

Immunoprecipitation (IP) is a commonly used method for antigen detection: it involves the capturing of an immune complex using antibodies bound to a heavier molecule (i.e., beads) which can be retrieved by centrifugal force or magnets. Co-Immunoprecipitation is an extension of IP: it allows the purification of the primary target (i.e., the antigen) as well as other macromolecules which are bound to the original target. After elution of this large complex from the beads, the samples are analysed by sodium dodecyl sulfate-polyacrylamide gel electrophoresis (SDS-PAGE), followed by Western blot detection to verify the identity of the antigen.

Around 20 embryonic hearts at E14.5 and 30 hearts at E12.5 from WT embryos were dissected in cold PBS and flash frozen in liquid nitrogen before being digested using a syringe with gradually smaller needles (19G, 23G, 25G) in RIPA buffer (50mM Tris pH 7.4, 150mM NaCl, 1% NP-40, 1mM EDTA, 50mM NaF, 0.5% Deoxycholic acid, sodium orthovanate 20nMm, anti-protease cocktail 1X, 1mM PMSF). In parallel, magnetic beads coated with sheep anti-mouse IgG (AB 11201D) and the supernatant recovered from HIRA hybridomas (prepared by Dr Chapgier) were mixed and left rolling overnight at 4°. The mouse IgG (mouse IgG1 k monoclonal isotype control AB 18447, lot GR 53099-6) and the beads were mixed in a separate tube. The beads were washed with RIPA buffer the next day using magnets. After the final wash, the protein lysate was mixed mix with the beads overnight rolling at 4°. 100µl was saved and stored at -80° to load as the input. The next day the beads which have immunoprecipitated HIRA were washed in RIPA and resuspended in Laemli buffer (3X Laemli:

120mM Tris pH6.8, 3% SDS, 5% Glycerol, 0.01% Bromophenol, 1.5% β-Mercaptoethanol) and boiled at 100° for 15min to separate the beads from the antibodies and proteins. After a 1min cooling on ice, the magnet was used to collect the beads. The lysate is then stored at -80° before being loaded on the polyacrylamide gel.

Separating gel: 8% acrylamide: 18.5ml H_20, 10.7ml acrylamide 30%, 10ml Tris 1.5M pH8.8, 400µl SDS 10%, 400µl APS 10%, 24µl Temed. Stacking gel: 5% acrylamide, 6.8ml H_20, 1.7ml acrylamide 30%, 1.25ml Tris 1M pH 6.8, 100µl SDS 10%, 100µl APS 10%, 10ul Temed. Run buffer (10x): 30.25g Tris, 144g Glycine, 100ml SDS 10%. Up to 1 L of H_20. Transfer buffer (10X): 30.25g Tris, 144g glycine, Up tp 1 L of H_20. For 1X, use 20% methanol.

Pre-cast gradient gels (Mini-PROTEAN TGX 4%-15%, Biorad 456-1083) were also used. 30µl were loaded per well. The gels were then transferred onto a PVDF membrane (Biorad 162-0177) using a semidry or wet technique. The membrane was blocked with 5% milk-TBST 1X for 1h at RT, washed 3 times with TBST then incubated with Hira antibody (supernatant from WC119 hybridoma) in 1% milk- TBST 1X overnight at 4°C. Next the membrane was washed 3 times with TBST, incubated with a secondary antibody (Amersham NA93310V) for 45 min at RT then washed 3 times with TBST and finally revealed with ECL (Amersham RPN2209, 28906837) with the appropriate secondary (Amersham NA93340V or NA93310V).

Table 2-2 List of commercial antibodies

GAPDH	Millipore MAB374
BRG1	Millipore 07-478
WHSC1	Atlas HPA015801
HDAC1	Millipore 05-100
HDAC2	Millipore 05-814
CAIN	Abcam ab3349

2.5) Chromatin immunoprecipitation (ChIP)

As mentioned in chapter one, the biological significance of the location of the interactions between proteins and DNA can have an important impact on the understanding of gene expression regulation, differentiation and disease. Chromatin immunoprecipitation (ChIP) is the precipitation of a protein of interest from a chromatin preparation (usually fragments with a size of 500 to 1000bp) to determine the DNA sequences associated with it (Figure 2-6). The main issue with ChIP is that given the broad diversity of tissue and cell types, types of chromatin bound proteins or modifications being assayed, it is difficiult to define one single guide to perform this experiment (Furey, 2012). The ChIP protocol used for HIRA is described below.

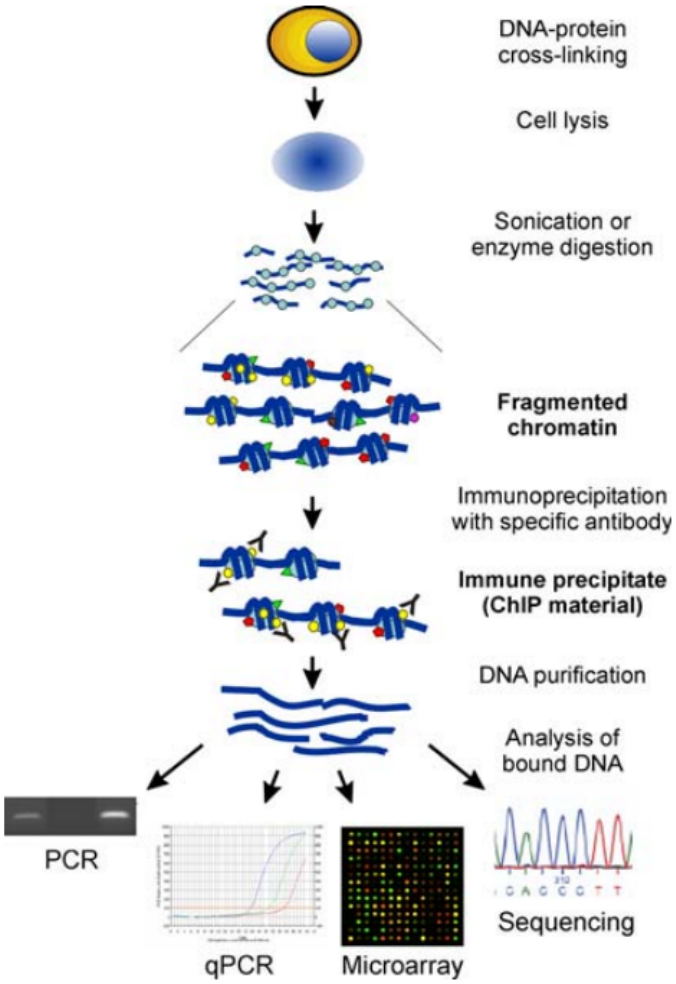

Figure 2-6 Main steps involved in ChIP and methods of analysis

Schematic of the steps necessary to carry out chromatin immunoprecipitation (ChIP) assay with the associated methods commonly used for downstream analysis. Taken from (Collas, 2010)

2.5.1) Dual Fixation

The first step of ChIP relies on the cross-linking of proteins to DNA. The fixation reagent used most commonly is formaldehyde (HCHO). However, this molecule has relatively short spacer arm. There is an ongoing debate whether HIRA directly binds to DNA or rather, like a transcriptional coactivators, it is in close proximity to the DNA. The HIRA ChIP protocol developed by Dr Chapgier was used which involves a combination of HCHO and EGS, a large molecule with long spacer arms (Zeng et al., 2006).

30 to 40 E12.5 hearts were pooled (equivalent to 10 million cells for ESC experiments), washed in PBS and cross-linked for 45 min with 1.5mM of EGS (Sigma, E3257), followed by 15min of 1% formaldehyde (from a freshly made filtered stock at 18.5%) at 37°C. The reaction was quenched by the addition of 125mM of Glycine, left for 15min at RT. Hearts/cells were lysed in 50mM Hepes-KOH pH 7.5, 140mM NaCl, 1mM EDTA, 10% glycerol, 0.5% NP-40, 0.25% Triton, 1X anti-protease cocktail (Roche, 04693132001), 1mM PMSF for 10 min at 4°C (LB1). The hearts/cells were briefly spun down resuspended in 10mM Tris-HCL pH 8.0, 200mM NaCl,

1mM EDTA, 0.5mM EGTA, 1X anti-protease cocktail, 1mM PMSF for 10 min at 4°C (LB2). Finally the hearts/cells were resuspended in10mM Tris-HCL pH 8.0, 100mM NaCl, 1mM EDTA, 0.5mM EGTA, 0.1% DOC, 0.5% N-Lauroylsarcosine, 1X anti-protease cocktail and 1mM PMSF rolling o/n at 4°C (LB3).

2.5.2) Sonication

Fixed and lysed chromatin needs to be broken into small fragments before being immuno-precipitated. A fine balance is required in this step. Having too large fragments reduces the resolution of the protein of interest binding sites and having fragments too small might fail to provide the necessary template for PCR amplification. HIRA ChIP requires a total combined time of 1 hour of sonication at 5µA with Soniprep 150 MS, with at least the equivalent time resting on ice to prevent the chromatin solution from overheating.

2.5.3) Immunoprecipitation and purification of DNA

In parallel to the sonication step, antibodies were coupled to magnetic beads (dynabeads InVitrogen, 112.03D, 112.01D) for at least 4 hours and washed 3 times in LB3. 10% of input was taken and protein–DNA complexes were selectively immunoprecipitated using WC15 antibody against HIRA, rolling overnight. Beads were then washed once with 20mM tris pH 8.0, 150mM NaCl, 0.1% SDS, 1% Triton, 2mM EDTA (WB1), once with 20mM Tris pH 8.0, 500mM NaCl, 0.1% SDS, 1% Triton, 2mM EDTA (WB2), once with 10mM Tris pH 8.0, 150mM LiCl, 1% NP-40, 1% DOC, 1mM EDTA, then TE 10:1, 50mM NaCl (WB3), and finally in TE 10:1. Samples were treated overnight with 50mM Tris pH 8.0, 10mM EDTA and 1% SDS at 65°C (elution buffer), to reverse cross-linking, then with RNAse (Qiagen, 19101) for an hour at 25°C and with PK for 2h at 56°C. DNA was purified with QIAGEN's PCR purification kit (28104).

2.5.4) Designing genomic primers using IGV

Integrative genome viewer (IGV), created by the Broad Institute, is a software in which enrichment of a given protein across the genome can be viewed easily (Figure 2-7). For example, ChIP-seq for a specific histone trace allows the user to browse genomic regions enriched (usually gene rich) or depleted (usually intergenic). Once the sequences are extracted, they can be loaded in a program such as primer blast to design primers (see p39).

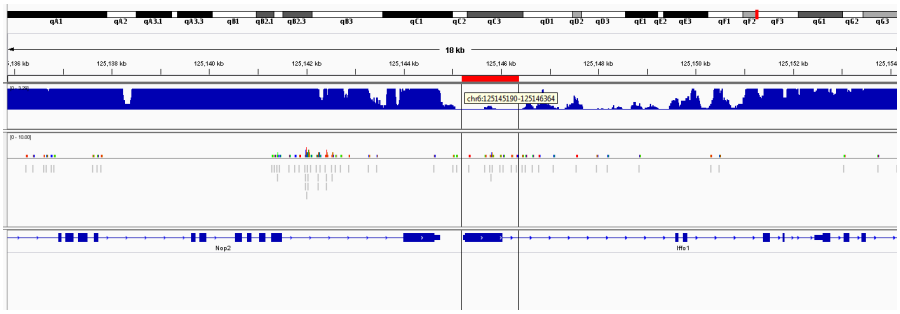

Figure 2-7 IGV screenshot displaying two tracks

Integrative genome viewer displaying here two different types of genome wide data: a “wig” file (for wiggle) on top, and a “bam” file in the middle, which displays individual reads from a massive parallel sequencing platform. The lower trace is the mouse reference genome. DNA sequence can be retrieved, here shown in red over the TSS of *Iffo1*.

2.5.5) Q-ChIP

In the last step of ChIP, purified DNA is quantified by quantitative PCR, using the purified input chromatin as a positive control. As a first quality control, the Ct values obtained from the input (genomic DNA) for any target loci should be almost identical, unless the region presents high copy number variants (CNVs). ChIP enrichment was calculated using the percent Input Method. Signals obtained from the ChIP were divided by signals obtained from the input. This input sample represents the amount of total chromatin used in the ChIP, here 10% was used. See the example below:

z= 2^-(Ct_ChIP – Ct_Input) * 100 * (b/a) * (d/c)

z= enrichment to Input (=100%)
a=Volume of sample used for IP
b=Volume of sample saved for Input
c=Amount of DNA ChIP used for Q-PCR
d=Amount of DNA Input used for Q-PCR

Using 10% input and taking the same amount from ChIP and input for the PCR:
z= 2^-(Ct_ChIP – Ct_Input) * 100 * (10/100)

Table 2-3 Primers used for qChIP

Lsp1F 180bp upstream of TSS	TGCTACTCTTGGGGCTGACT
Lsp1R 180bp upstream of TSS	CAGGACCTCAAATCCAGCAG
Lsp1F 160bp upstream of TSS	TGGCTGGAATGCACCGATAA
Lsp1R 160bp upstream of TSS	ATGCATTTGGCAGGTGACAG
Gata5F upstream of TSS	AAGCCTGGCAGCTACAAGAA
Gata5R upstream of TSS	AAGGAACTAAGCCCCTGCTG
Gata5F2 upstream of TSS	GATAGGCCTGGTCTGGTTGG
Gata5R2 upstream of TSS	GGACACCAGCTAACAGGGAG
Ctrl neg X6 -F	CCCCTTTCTGAAGCACTCTG
Ctrl neg X6 –R	TAAGGCGTCATTTCCCAAAG
Ctrl neg X8 -F	AAGGGGCCTCTGCTTAAAAA
Ctrl neg X8 -R	AGAGCTCCATGGCAGGTAGA
Tbx3 exon5 - F	CTCAGTCCCAGTCCCTTGAC
Tbx3 exon5 - R	CACCCTGCTGAGGGTCAATA

2.5.6) ChIPseq and analysis

Current state-of-the-art technologies allows for genome-wide sequencing of ChIPed DNA. ChIPseq provides fewer artefacts and greater coverage compare to ChIP-chip (Park, 2009). This process first involves the amplification of the immunoprecipitated chromatin (input) to construct a library. Depending on the “expected” outcome of a ChIPseq, different peak callers can be applied. Experiments can be ranked in the following 3 categories: point source (highly localized signals, such as for transcription factors), broad source (signals that span large domains; for example a histone modification) and mixed source (signals that have elements of both, such as for RNA polymerase II) (Furey, 2012). The required sequencing depth was difficult to assess since the types of peak were uncertain. A histone chaperone is more likely to generate broad peaks (or not “discrete” peaks), therefore the maximum number of reads were selected: 120 million. This would allow the detection of lower levels of enrichment over the genomic background. Finally ChIPseq can be used for “footprinting”, which allows the identification of DNA binding motifs. Most motifs are already present in databases, such as JASPAR (Neph et al., 2012) (Figure 2-8).

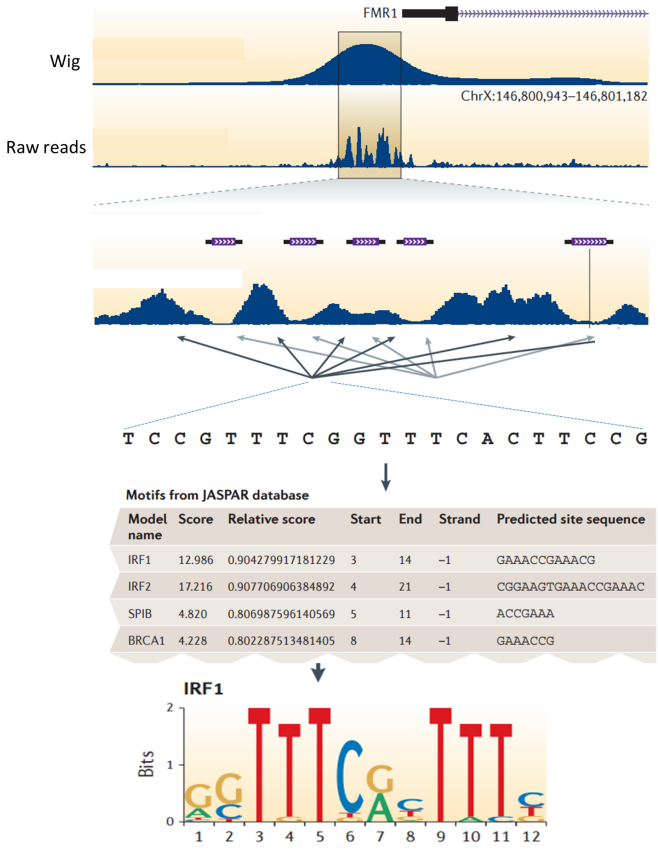

Figure 2-8 Illustration of a ChIPseq workflow

Diagram displaying the steps necessary to obtain a binding motif from ChIPseq data. The sequence retrieved from peaks (or binding sites) are aligned to the Jaspar database (a transcription factor binding profile database derived from published collections of experimentally tested DNA binding proteins).

Libraries were prepped using the NEB DNA Ultra kit, with a selection of fragments size of ~200bp. They were sequenced on the Illumina NextSeq 500, v2 chemistry. Alignment was done using bowtie2. Peak detection and consensus sequence discovery was done using Strand NGS software 2.5, which includes the algorithm of MACS1.4 ($p \leq 10^{-4}$)(Model-based Analysis for ChIP-Seq), after removal of sequences with poor- quality bases and removal of duplicate sequences. List of genes within +/- 5Kb was generated using Strand NGS. Bedtools intersect tools was used (code was ran by Dr Chapgier and included with her permission) to define the overlaps between different BED files. (Code used: intersectBed -a NKX2-5Chipseqe11-5MM10.bed -b Peaks_detected_by_MACS-4.bed > overlap2.bed). CEAS-Package-1.0.2 analysis of cis-regulatory elements was used for genome wide enrichment patterns of HIRA ChIPseq. IN addition, PAPST (Peak Assignment and Profile Search Tool) software was used to overlap regions of interest (Bible et al., 2015).

Chapter 3 HIRA is required in the cardiogenic mesoderm

The development of the cardiovascular system is regulated by sequential, time controlled pathways. Transcription in the heart is partly regulated by the conformation of chromatin, which is likely to be dependent on histone variant deposition. HIRA has never been studied previously in the context of heart development. To adress its potential role during cardiovascular development, its expression was first traced using the β-galactosidase cassette of the transgenic mouse strain *Hiratm1a* (Figure 3-1).

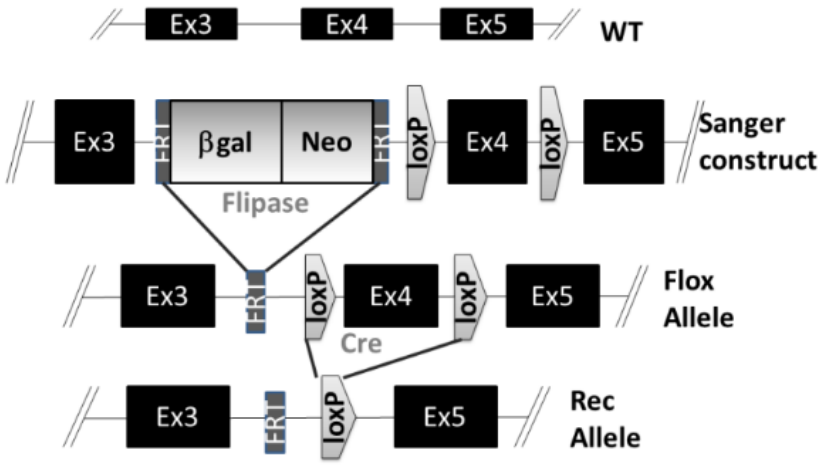

Figure 3-1 Hira pre-conditional allele was generated by the Wellcome Trust Sanger Institute

Hiratm1a(EUCOMM)Wtsi, MGI:4431679 construct used for *Hira* reporter before Flippase was applied to revert it to a WT allele ("Flox allele"). Cre recombinase subsequently splices out exon 4 ("rec allele").

The pattern of expression of *Hira* during embryonic development are presented below as well as the various phenotypes observed when ablating *Hira* from the cardiogenic mesoderm.

3.1) Expression of *Hira* at E10.5 and E13.5 and in the adult

Described in the previous chapter, this method consists of identifying cells expressing the β-galactosidase-neomycin cassette, here located between exon 3 and exon 4 of *Hira*. By crossing $Hira^{\beta Gal/+}$ with $Hira^{+/+}$ mice, $Hira^{\beta Gal/+}$ and $Hira^{+/+}$ embryos were recovered with a ratio of 1:1. The assay was conducted on whole embryos between E10.5 and E15.5. However, past E12.5, the penetration of the X-gal became problematic (data not shown), so cryosections were analysed after this stage. As shown by a long axis cross section of the heart at E13.5, all cardiac tissue were found to be *Hira* positive (Figure 3-2). At E8.5, *Hira* was expressed ubiquitously (personal communication from Dr Chapgier).

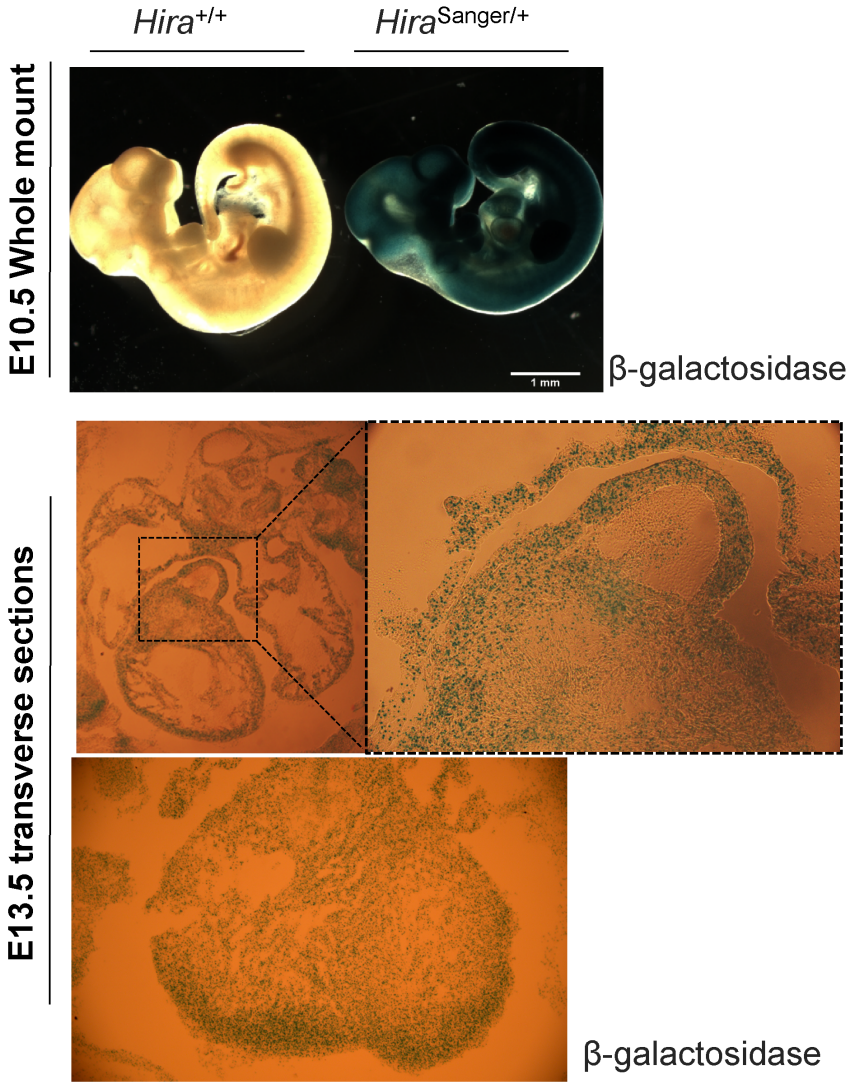

Figure 3-2 Hira is ubiquitously expressed in the heart at E13.5
β-galactosiade knockin reporter showed that HIRA is ubiquitously expressed throughout the embryo at E10.5 (top panel). At E13.5 cardiac expression was verified by long axis section, prior to staining (bottom panel).

Although not checked at the embryonic stage, HIRA protein expression was identified in the adult (Figure 3-3) by western blot analysis, from total protein extracts from dissected hearts.

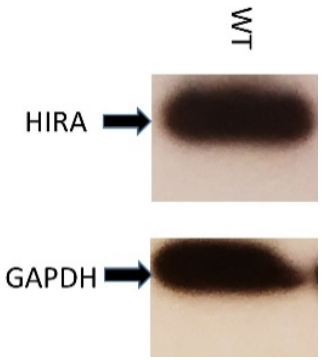

Figure 3-3 HIRA is expressed in the adult heart

Western blot analysis from a heart biopsy of a 8 month old adult mouse revealed that HIRA is expressed in the heart postnatally. Western blot shown is representative of three biological replicates

3.2) Conditional mutagenesis of *Hira* with *Mesp1Cre*

3.2.1) PCR

The anterior limb of *Mesp1Cre;Hira*$^{fl/-}$ embryos was used for DNA extraction . Genotyping was done by detecting the presence of *Cre* and *Hira* null allele by PCR (data not shown). *Cre* activity was further confirmed by PCR amplification using primers outside the loxP sites (Figure 3-4).

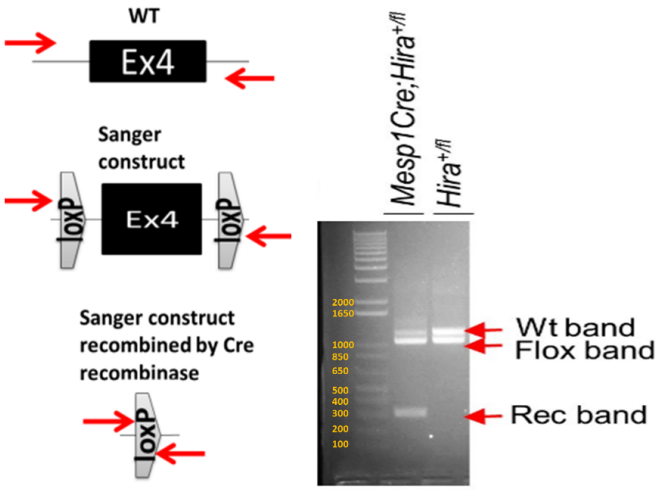

Figure 3-4 Recombination of *Hira* conditional allele is visualised by PCR

Recombination of the floxed allele by *Mesp1* driven CRE recombinase was assessed by PCR (red arrows represent forward and reverse primers) using DNA from the anterior limb which contains *Mesp1* positive cells, detection of the various alleles is shown.

3.2.2) RNA-seq

In addition to genomic DNA recombination, *Cre* activity was also confirmed in total RNA extracted from hearts by RNAseq. Reduced number of reads were observed at the exon 4 of *Hira* (Figure 3-5). Transcriptome analysis will be covered in the next chapter.

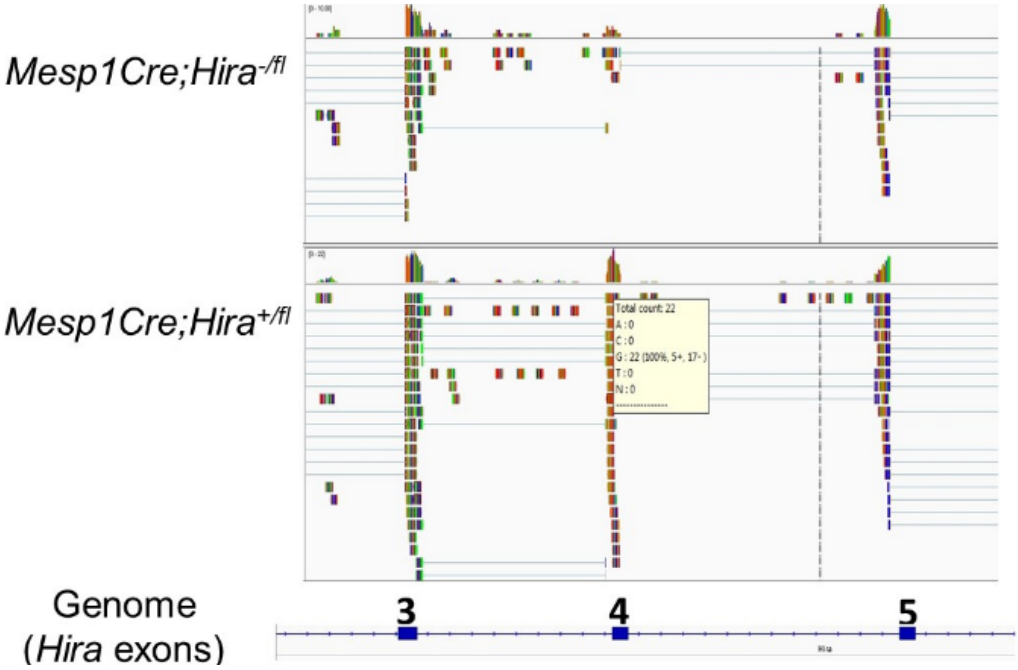

Figure 3-5 RNAseq gives evidence of recombination of the *Hira* conditional allele

Recombination was also demonstrated at the mRNA level by the reduced number of reads in RNAseq (22 in control and 3 in mutant).

3.3) HIRA is required in the *Mesp1* lineage

The *Hira* conditional allele was first tested by Dr Chapgier using *ActinCre* and *TCre* to validate the allele in vivo. *Brachyury* (*T*) is expressed early in development and marks progenitor cells arising from the primitive streak and tail bud, thus generating mesoderm and endoderm during gastrulation (Perantoni et al., 2005). Generation of *TCre;Hira*$^{-/fl}$ embryos resulted in a similar phenotype to *Hira*$^{-/-}$ embryos (Ariane Chapgier, personal communication).

3.3.1) *Mesp1Cre;Hira*$^{-/fl}$ is embryonic lethal.

Mesp1Cre;Hira$^{-/+}$ were crossed to *Hira*$^{fl/fl}$ mice to generate conditionally null embryos. Viability was assessed first. No mutants (*Mesp1Cre;Hira*$^{-/fl}$) were recovered at P10, out of 4 litters observed (Table 3-1).

Table 3-1 Embryonic phenotype resulting from the conditional ablation of Hira

	Mesp1Cre;Hira$^{-/fl}$				***Nkx2.5Cre;Hira$^{-/fl}$***	***Mef2cCre;Hira$^{-/fl}$***	***Tie2Cre;Hira$^{-/fl}$***	***Wnt1Cre;Hira$^{-/fl}$***
STAGE	**E10.5**	**E12.5**	**E13.5**	**E15.5**	**E15.5**	**ADULT**	**E15.5**	**E18.5**
VSD	N/O	N/O	N/O	12/12	5/9	N/O	0/5	0/10
ASD	N/O	N/O	N/O	10/12	4/9	N/O	0/5	0/10
Thin ventricular wall	0/4	0/9	0/12	3/12	0/9	N/O	0/5	0/10
Constricted PT	0/4	0/9	0/12	1/12	3/9	N/O	0/5	0/10
Oedema	0/4	0/9	3/12	12/12	0/9	N/O	0/5	0/10
Haemorrhage	0/4	2/9	6/12	12/12	0/9	N/O	0/5	0/10
Exencephaly	0/4	1/9	0/12	0/12	0/9	N/O	0/5	0/10
VIABLE by P10	**NO (0/12)**				**YES (1/9)**	**YES (4/4)**	**YES (6/6)**	**NO (0/40)**

Number of embryos observed for the indicated phenotype at the indicated stage related to the total number of embryos collected. N/O indicates none observed. The number of collected and thus viable embryos are also indicated at 10 days post-birth (P10) related to the number of expected embryos.

3.3.2) *Mesp1Cre;Hira$^{-/fl}$* display fully penetrant oedema at E15.5

The morphology of embryos was examined at E15.5, for which a Mendelian ratio of mutants was recovered (Table 3-1). This implied that most embryos were dying between E15.5 and birth (around E20). At E15.5, all *Mesp1Cre;Hira$^{-/fl}$* embryos presented with a severe oedema, sometimes accompanied by haemorrhage (Figure 3-6).

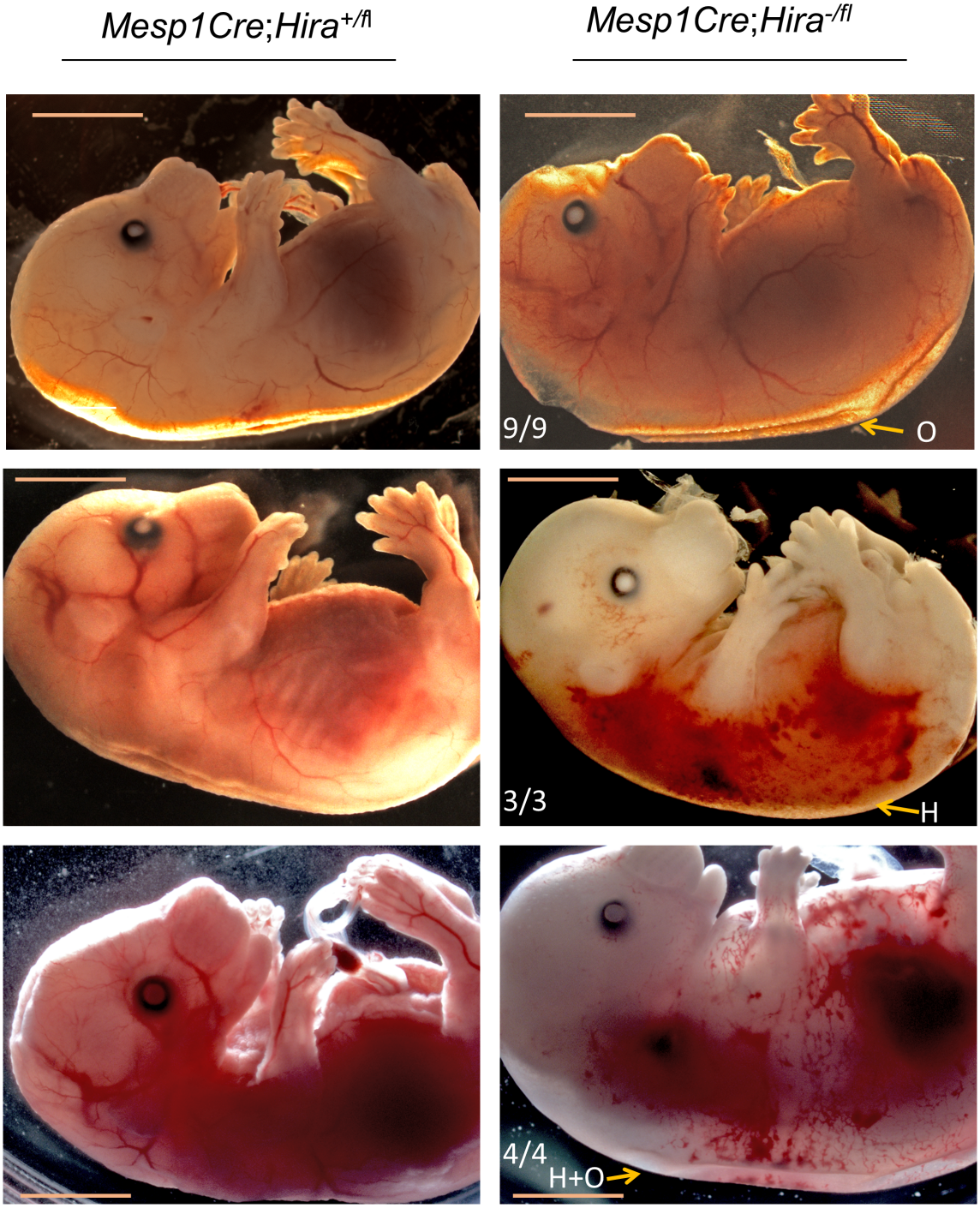

Figure 3-6 Mesp1Cre;Hira$^{-/fl}$ embryos display oedema and haemorrage at E15.5

The *Hira* conditional allele was used in conjunction with the cardiac specific cre driver *Mesp1Cre.* Here the lateral view of littermate embryos with the indicated genotype show that at E15.5, all mutants displayed a severe oedema (O) and haemorrhage (H) as indicated. *Scale bar represents 2mm*

3.3.3) E15.5 *Mesp1Cre;Hira$^{-/fl}$* embryos display a fully penetrant Ventricular Septum Defect (VSD) and partially penetrant Atrial Septal Defect (ASD)

By Optical Projection Tomography (OPT), whole embryonic trunks were scanned at E15.5. The ribs were removed to enhance the quality of the image capture. A fully penetrant VSD was observed in the mutant hearts (n=12). The interventricular septum has completely separated the two ventricles in WT embryos at E15.5, as expected (Figure 3-7). 83% of mutants also had

an ASD whilst none was observed in their WT littermates (n=10).

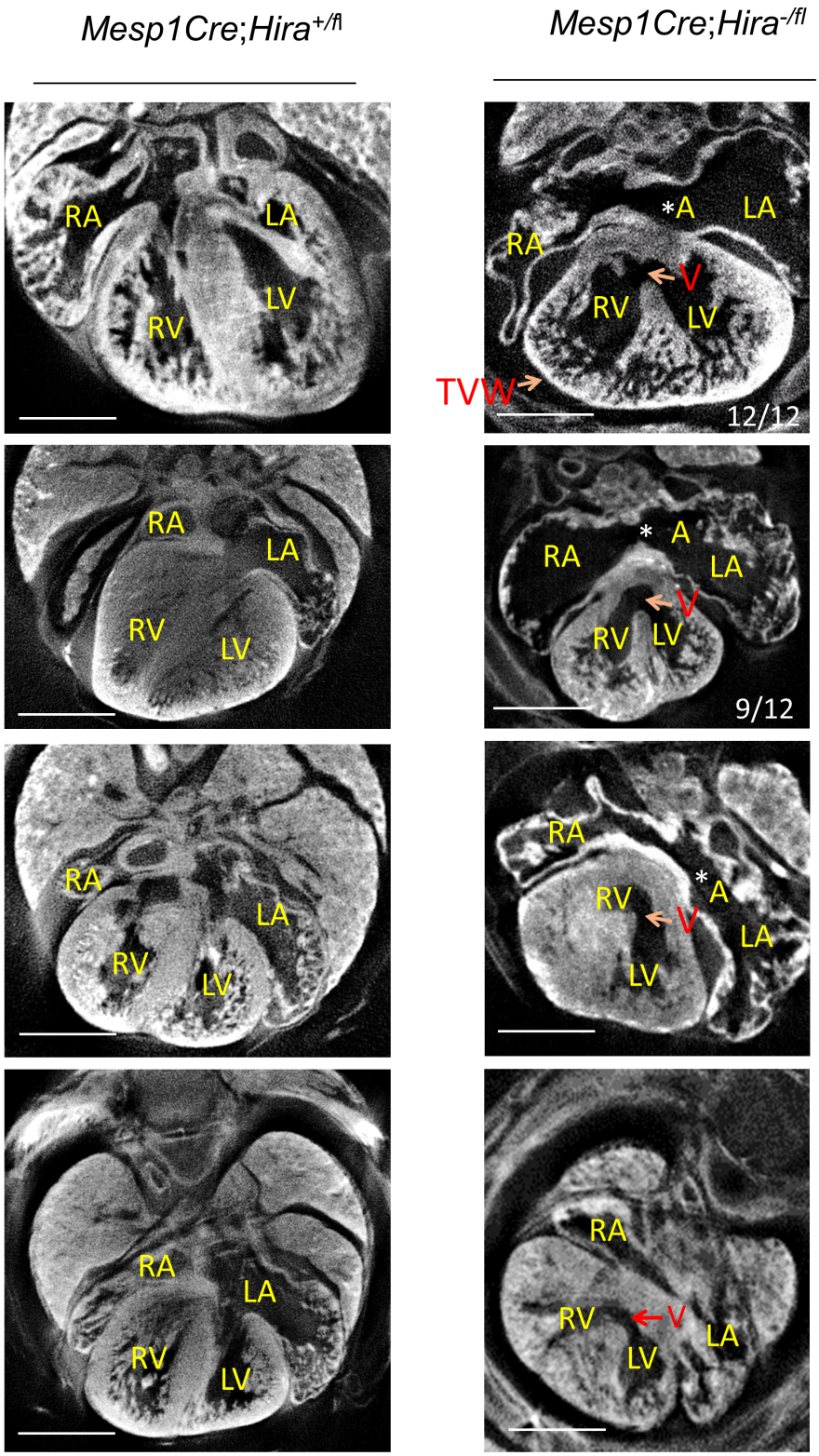

Figure 3-7 Mesp1Cre;Hira$^{-/fl}$ embryos display a VSD at E15.5

Optical Projection Tomography was used to scan whole embryonic trunks of *Mesp1Cre;Hira$^{-/fl}$ and Mesp1Cre;Hira$^{+/fl}$* at E15.5. Long axis view of the heart revealed that a VSD (V) was systematically present at this stage in the mutants. An ASD (A) was observed in 9 out of 12 embryos. Thin ventricular wall (TVW) was observed in 3 out of 12 embryos. Right/left ventricle: RV/LV. Right/left atrium: RA/LA. *Scale bars represents 0.5mm*

3.3.4) Disruption of fusion between endocardial cushion and membranous portion of the ventricular septum at E12.5

The earliest defect observed in *Mesp1Cre* conditional *Hira* mutants were at E12.5. In a small proportion (11%) of mutants, exencephaly and haemorrhage were observed (Figure 3-8). Interestingly, H&E staining on long axis sections revealed that some E12.5 *Mesp1Cre;Hira*$^{-/fl}$ embryos displayed abnormally shaped endocardial cushions (Figure 3-9). The rightward tubercles of the atrioventricular cushions form the membranous septum (Anderson et al., 2015). A deficiency of the muscular part of the ventricular septum was observed, since the point of contact between the septum and the atrioventricular cushions (or endocardial cushions (EC)) was mispositioned in the mutants compared to the control (Figure 3-9).

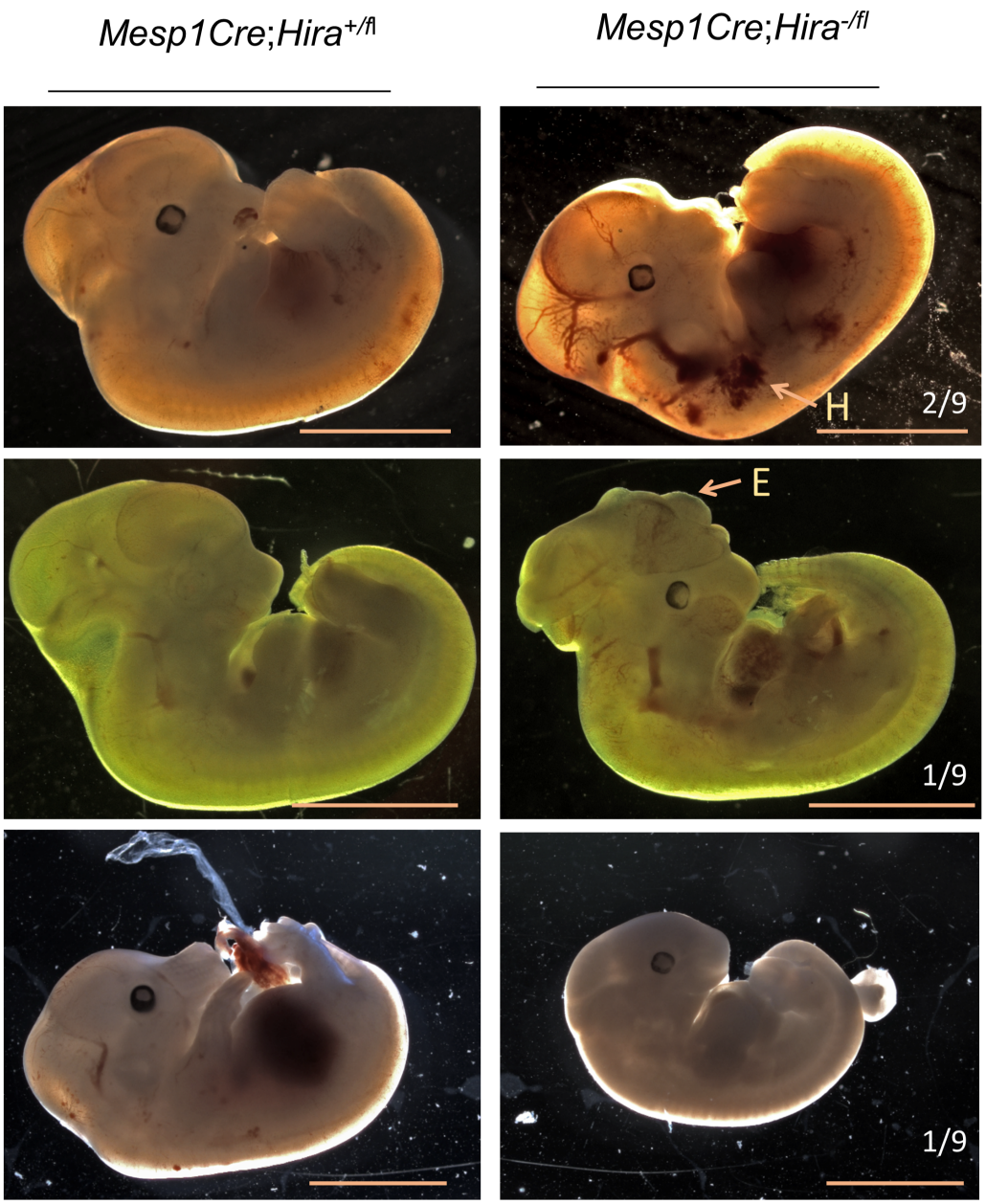

Figure 3-8 Mesp1Cre;Hira$^{-/fl}$ embryos have a partially penetrant phenotype at E12.5
Malformations in *Mesp1Cre* conditional *Hira* mutants were first detected at E12.5. Here a lateral view of littermate embryos is presented with the indicated genotype. A small proportion of *Mesp1Cre;Hira*$^{-/fl}$ embryos presented with exencephaly (E) and haemorrhage (H). *Scale bars represent 2mm.*

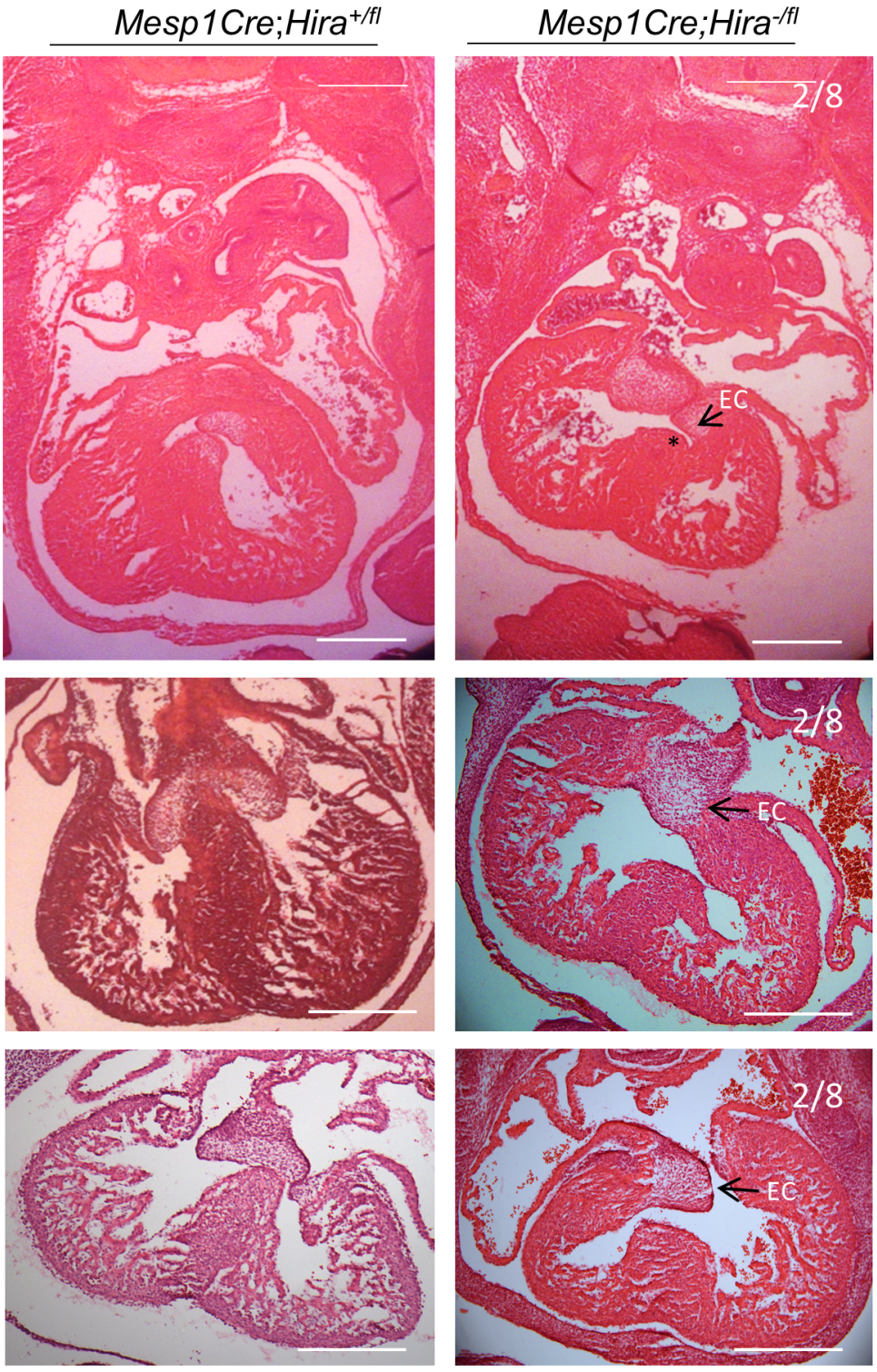

Figure 3-9 Mesp1Cre conditional *Hira* mutants have a disrupted fusion between the endocardial cushion and the ventricular septum at E12.5

At E12.5, some *Mesp1Cre;Hira*$^{-/fl}$ embryos displayed abnormally shaped endocardial cushions. The H&E staining on long axis sections presented here revealed a disruption of the endocardial cushion (EC) fusion (two controls and two littermate mutants shown). The muscular septum is deficient (*, top) and the relatively flat rather than crescentic cushion shape in the mutant are indicated (arrows). *Scale bars represent 0.5mm*

3.4) *Nkx2.5* driven ablation of *Hira*

As mentioned above, cardiogenic mesodermal ablation of *Hira* leads to embryonic lethality, likely due to cardiac malformations. The *Nkx2.5Cre* allele allows the ablation of *Hira* in cardiomyocytes, amongst other cell types, of the FHF and SHF, from E7.5 (see p5). This subset of cells is mostly directly derived from *Mesp1* expressing progenitors (see discussion p64). Therefore, to further dissect the role of *Hira* in the cardiac lineage, *Nkx2.5Cre;Hira*$^{+/-}$ were crossed to *Hira*$^{fl/fl}$ mice.

3.4.1) *Nkx2.5Cre;Hira*$^{-/fl}$ embryos present with a partially penetrant VSD at E15.5

The morphology of the heart of *Nkx2.5Cre;Hira*$^{fl/-}$ embryos was observed at E15.5. 54% of mutants presented with a VSD (n=5). Unlike the *Mesp1* conditional mutants, none of the mutants here displayed oedema.

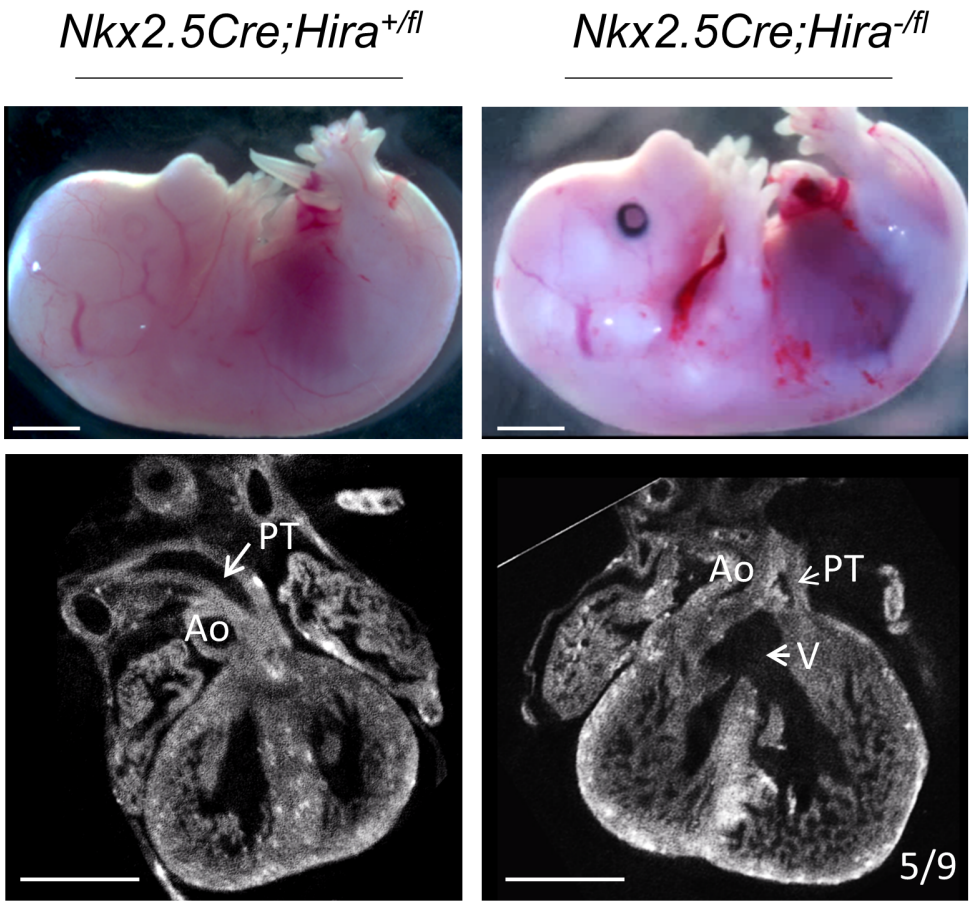

Figure 3-10 Nkx2.5Cre conditional *Hira* mutants display a VSD at E15.5

Ablation of *Hira* in cardiomyocytes was done using a *Nkx2.5Cre* allele. Here, the lateral view of *Nkx2.5Cre;Hira*$^{-/fl}$ mutants revealed a normal external appearance (top panel). OPT long axis section revealed a VSD (V) and an overriding of the aortic root of the muscular septum (bottom panel). The aorta (Ao) and the pulmonary trunk (PT) are indicated. *Scale bars represent 2mm in whole embryo and 0.5mm in long axis sections.*

3.4.2) *Nkx2.5Cre*;Hira$^{-/fl}$ embryos display a constriction of the pulmonary trunk

33% of *Nkx2.5Cre;Hira*$^{-/fl}$ embryos had a hypoplastic pulmonary trunk (PT) (or constricted PT) at E15.5 by using OPT followed by 3D reconstruction of the vessel (Figure 3-11).

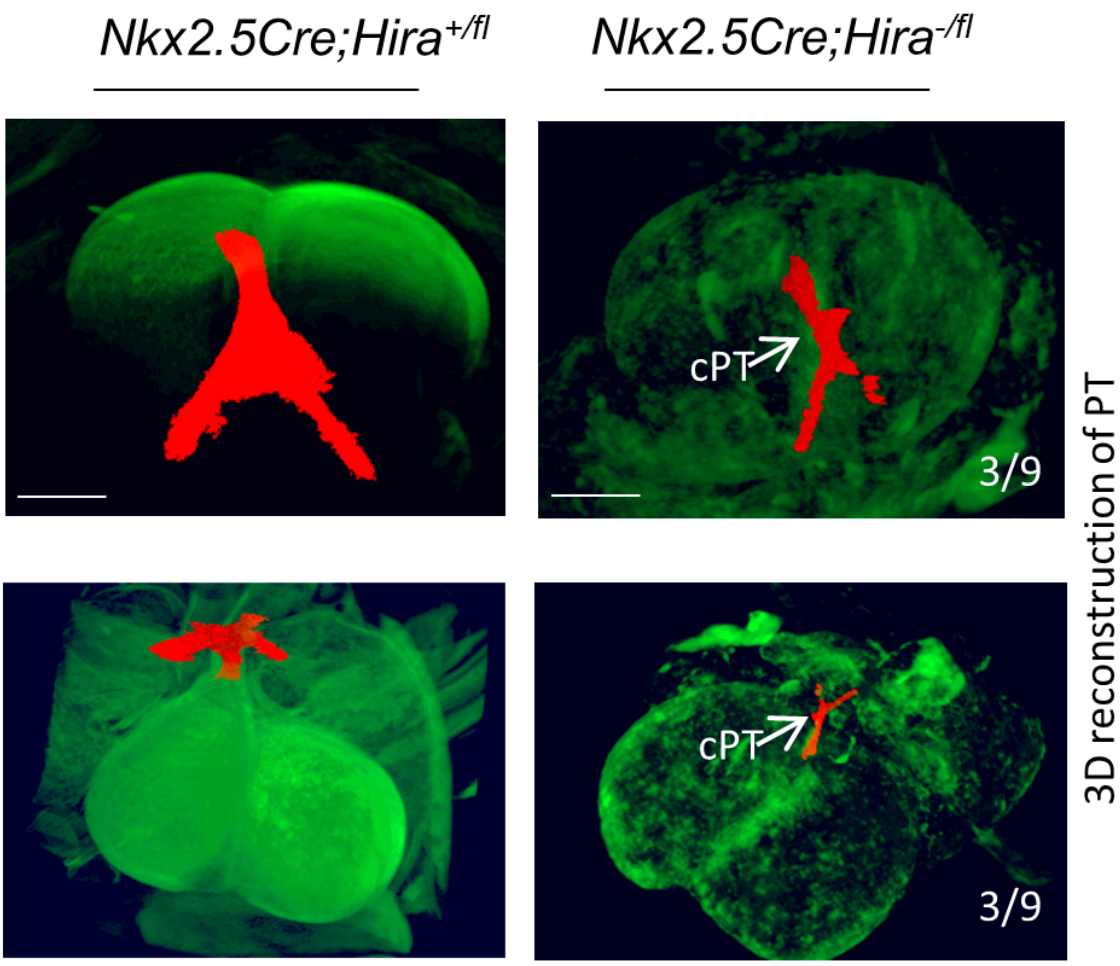

Figure 3-11 Nkx2.5Cre conditional *Hira* mutants have a constricted pulmonary trunk

Ablation of *Hira* by *Nkx2.5Cre* led to a constricted pulmonary trunk (cPT) at E15.5. Here, the 3D reconstruction of *Nkx2.5Cre;Hira*$^{-/fl}$ embryonic hearts shows the cPT in red. *Scale bars represent 0.5mm.*

3.5) *Hira* is not required in the SHF for heart formation and post-natal survival

Using a *Mef2cCre* driver, the effect of *Hira* ablation was characterised in the SHF (see p6). Generation of *Mef2cCre;Hira*$^{-/fl}$ animals led to a recovery of the expected mendelian ratio of mutants at the weaning stage (P21) (Table 3-1). The animals were observed until the age of 6 months when they were culled and their hearts was analysed by OPT. As the adult hearts were much thicker than embryonic ones, the clearing process had to be extended and the clearing agent renewed multiple times. In addition, the OPT scanning settings had to be

tweaked to acquire the images with a longer wavelength which gave higher imaging depth for a slight loss of resolution. No cardiac malformations were observed (n=4) (Figure 3-12).

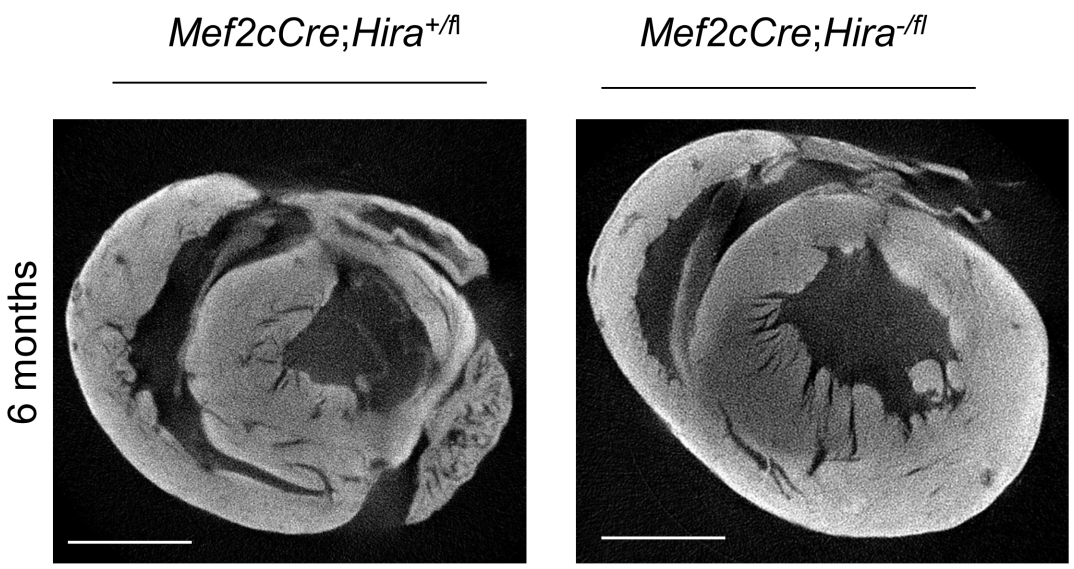

Figure 3-12 Mef2cCre conditional *Hira* mutants present no cardiac defects

Ablation of *Hira* in the SHF was done using the *Mef2cCre* driver. No embryonic lethality was observed. Here, the OPT scan shows a short axis section of the heart of a 6 months old *Mef2cCre;Hira*$^{-/fl}$ (right/left ventricle: RV/LV). This OPT scan is representative of all the hearts observed (n=4). *Scale bars represent 2mm.*

3.6) *Wnt1Cre;Hira*$^{-/fl}$ embryos suggest a non-cardiac role for HIRA in the neural crest cell population

Since a requirement for *Hira* has been described in neural crest cell in chick (Farrell et al., 1999), the role of *Hira* was tested in this lineage using *Wnt1Cre*.

3.6.1) Perinatal lethality of *Wnt1Cre;Hira*$^{-/fl}$

The litters resulting from crossing *Wnt1Cre;Hira*$^{-/+}$ to *Hira*$^{fl/fl}$ mice were first surveyed at P10. No mutants were observed (**Error! Reference source not found.**).

3.6.2) No heart or great vessel abnormalities at E18.5

Surprisingly, a Mendelian ratio of *Wnt1Cre;Hira*$^{-/fl}$ embryos was recovered at E18.5. The mutants had a normal external appearance and no OFT or great vessel malformations (Figure 3-13). The mutant hearts were dissected and analysed by OPT. No OFT, valves or septation malformations were identified (Figure 3-13).

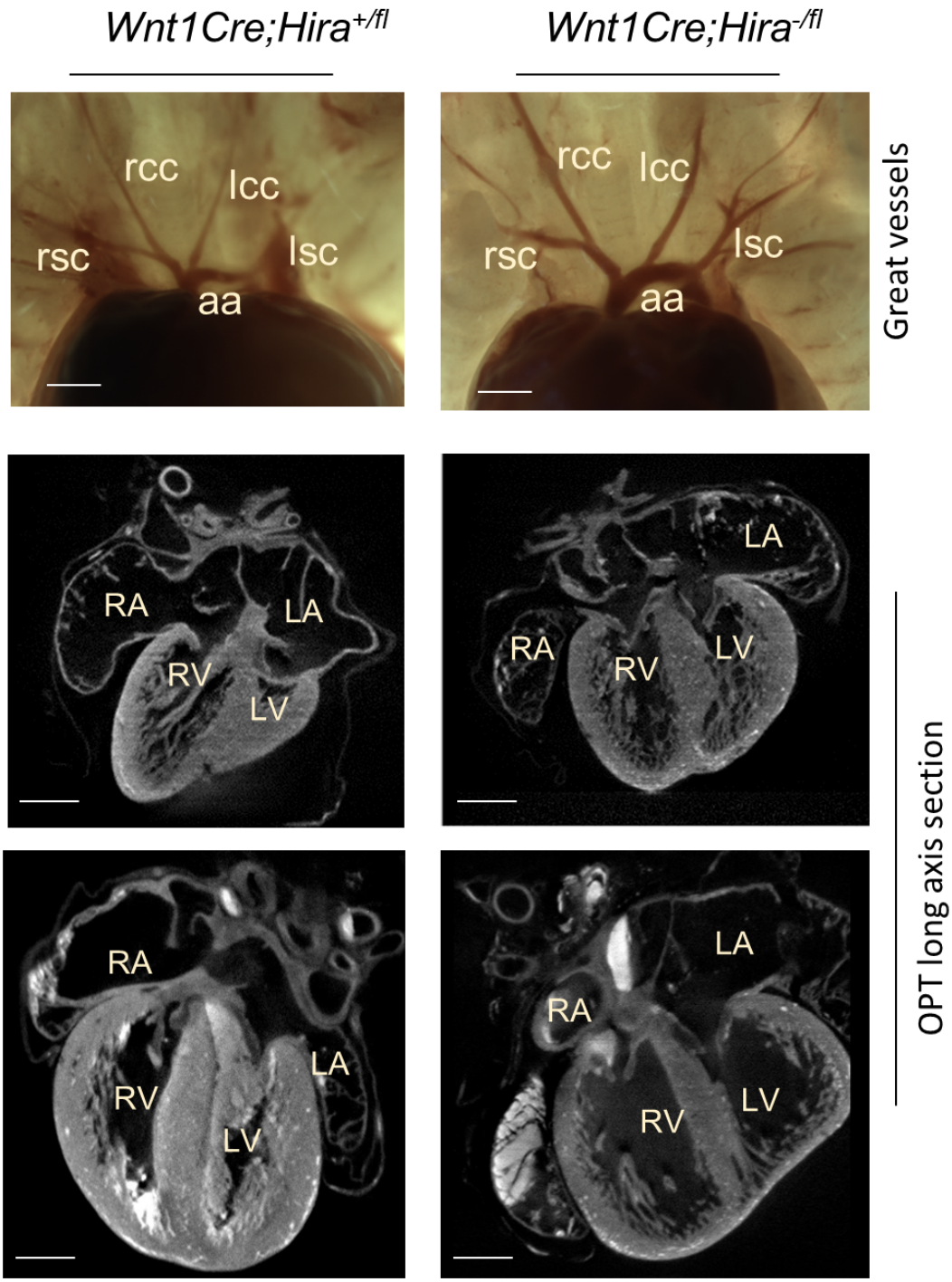

Figure 3-13 Wnt1Cre conditional Hira mutants do not present with any cardiac phenotype

Driving ablation of *Hira* in the neural crest cell population led to postnatal death but no cardiovascular malformations were detected at the embryonic stage. Here, the great vessel structure (top panel) and OPT long axis section (bottom panel) are presented in E18.5 *Wnt1Cre*;*Hira*$^{-/fl}$ hearts and their control. No heart defects were observed in these mutants. This OPT scan is representative of all the hearts observed (n=10). rsc: right subclavian artery, rcc: right common carotid, lsc: left subclavian, lcc: left common carotid, aa: aortic arch. RV/LV: Right/left ventricle. RA/LA: Right/left atrium. *Scale bars represent 0.5mm in long axis sections. Work carried out in collaboration with Yoann Rose and Ariane Chapgier*

3.7) *Tie2Cre;Hira$^{-/fl}$* embryos are viable but adults show a growth defect

A requirement for *Hira* has been previously described in endothelial cells. An *in vitro* system revealed a HIRA-dependant upregulation of *Vegfr1* in response to angiogenic signals (Dutta et al., 2010) (see p25). *Tie2Cre;Hira$^{fl/-}$* mutants only suffered from a partially penetrant proportionate growth reduction at the weaning stage (data not shown). At 6 weeks of age, the mutant animals remained smaller but behaved normally. At E15.5, embryonic trunks were analysed by OPT and no vessel nor endocardial tissue malformations were observed (Figure 3-14). Hearts collected from growth retarded adults were smaller compared to their WT littermates (Figure 3-14) but only in proportion to their reduced body size and did not have any structural malformation.

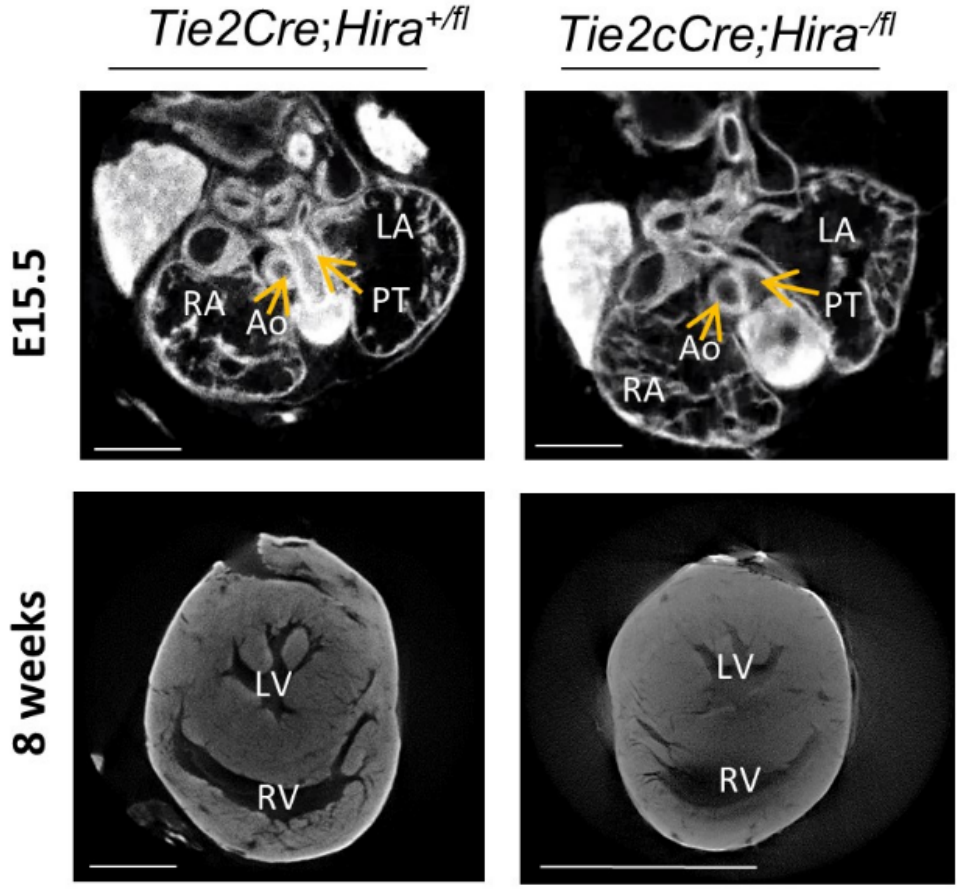

Figure 3-14 Tie2Cre conditional *Hira* mutants are viable

Driving ablation of *Hira* in the endothelial lineage did not lead to embryonic lethality or malformations. Here, *Tie2Cre;Hira$^{-/fl}$* long axis sections are shown at E15.5 and in the adult (8 weeks) by OPT. Mutant embryos did not show any defects and their adult heart only showed proportional size reduction to the body size. This OPT scan is representative of all the hearts observed (n=5). The Aorta (Ao), the PT, the right and left atrium (RA/LA) and the right and left ventricle (RV/LV) are indicated. *Scale bars represent 0.5mm in top panel and 2mm lower panel*

3.8) *Myh6MerCreMer;Hira$^{-/fl}$*: A pilot study investigating the role of HIRA in adult cardiomyocytes

Given the fact that HIRA is a replication independent histone chaperone, it was postulated that HIRA might be playing a role in post-mitotic cardiomyocytes. To test this

hypothesis, a *Cre* driver was used (*Myh6MerCreMer*) which induces recombination in cardiac muscle cells upon injection of tamoxifen (Sohal et al., 2001). It is important to note that this inducible *Cre* driver is also known to provoke DNA damage once activated by tamoxifen, probably due to DNA breaks at non-loxP sites (Bersell et al., 2013). HIRA has been shown to be implicated in the DNA damage response (Adam et al., 2013) (see p27). The Visualsonics Vevo 2100 ultrasound machine which measures heart function was used to measure the potential impact by the ablation of *Hira* on cardiomyocytes. The total ejection fraction was measured by quantifying the heart volume in triplicates at diastolic and systolic stages, prior to tamoxifen injection and 2 weeks and 8 weeks after (Figure 3-15).

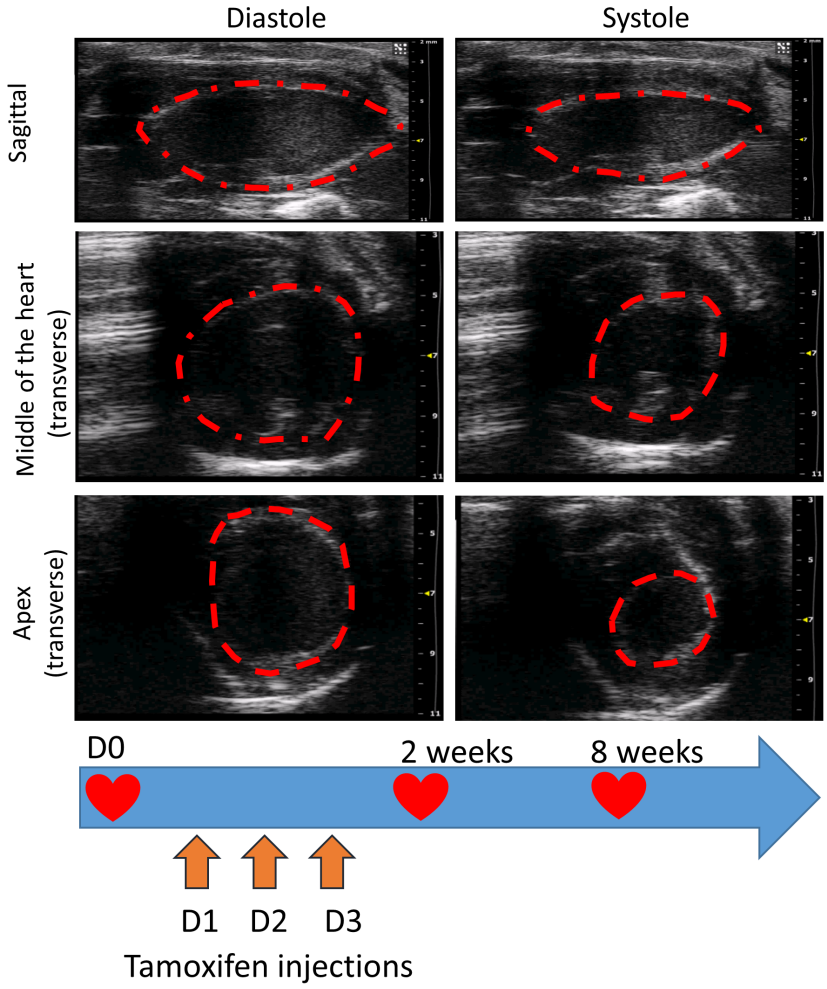

Figure 3-15 Experimental design to assess the effect on heart function of the ablation of *Hira* in post-mitotic cardiomyocytes: a pilot study

Ablation of *Hira* in post-mitotic cardiomyocytes was carried out using a *Myh6MerCreMer* allele. The potential effect on heart function was done using an ultrasound machine. Here, stills from ultrasound image are shown with frames where the heart is in full diastole and systole with the indicated imaging planes (top panel). Below is a schematic representing the timeline used to analyse the long term effect of the ablation of *Hira* ablation.

The results (data not shown) showed a too great variability between each animal to draw any conclusion. The knockdown of HIRA was confirmed post-mortem by sampling ventricular wall tissue and detecting HIRA protein levels by western blot (Figure 3-16).

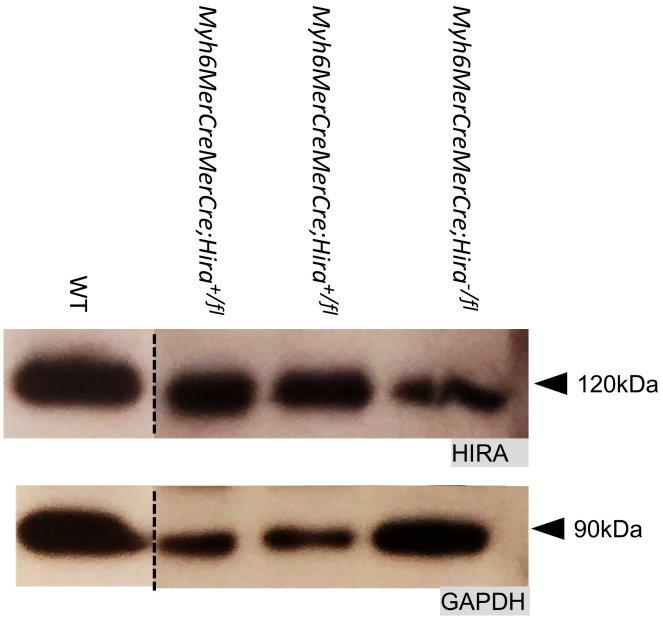

Figure 3-16 Western blot analysis of HIRA knockdown in *MyhMerCreMer* conditional mutants

Western blot of total protein extract from a heart biopsy postmortem are shown. HIRA level is diminished in the mutant compared to *Cre* control and WT. Western blot shown is representative of three hearts.

3.9) Discussion

3.9.1) HIRA is required autonomously in the FHF

The *Mesp1Cre* conditional Hira mutants all have cardiac defects and generalised oedema. The variability observed between mutants could be the result of the patchy level of efficiency of *Mesp1Cre* within a litter. Moreover, *Hira* phenotypes can be variable since *Hira*-null embryos displayed a spectrum of phenotypes, from mildly affected to severe (Roberts et al., 2002). Some *Mesp1Cre* conditional *Hira* mutants collected at E12.5 were degenerating whilst some at E13.5 or E14.5 had a normal appearance.

The data presented in this chapter shows that HIRA is required in the cardiogenic mesoderm for normal development after E10.5. As discussed earlier (see p4), *Mesp1* is mainly expressed in the FHF and SHF, but is also partly expressed in muscles of the face, the

embryonic liver and some foetal haematopoietic stem cells. Therefore, non-cardiac tissue could potentially contribute to the overall phenotype. *Nkx2.5Cre* conditional *Hira* mutants were used to test for that possibility. As mentioned earlier, *Nkx2*.5's expression is principally restricted to cardiomyocytes of the FHF and SHF (see p5) although the SHF expression has been shown to be variable and highly dependent on genetic background (Moses et al., 2001, Ramsbottom et al., 2014). *Nkx2.5Cre;Hira*$^{fl/-}$ mice were mostly embryonic lethal and displayed a similar phenotype to the *Mesp1Cre;Hira*$^{fl/-}$ animals, even if no mutant embryos presented with oedema. On the other hand, when *Hira* was ablated from a region of the SHF referred to as the anterior heart field, no effect on development or postnatal growth was detected. This lack of phenotype in *Mef2cCre;Hira*$^{fl/-}$ animals suggests that HIRA is not required in the anterior SHF for heart development to proceed normally. Taken together, this implies that HIRA is required in the FHF rather than in the SHF although absence of HIRA from the SHF could potentially act to exacerbate the phenotype of FHF mutants. Despite the known cooperation between the transcription factors *Nkx2.5* and *Mef2c* during cardiogenesis (Vincentz et al., 2008), the phenotypes resulting from the conditional *Nkx2.5Cre* and *Mef2cCre Hira* mutants differ significantly. The mild phenotype observed in *Nkx2.5Cre Hira* mutants and the absence of phenotype in *Mef2cCre Hira* mutants, compared to the severe phenotype observed in *Mef2cCre;Nkx2.5*$^{f/f}$ (embryonic lethality at E9.5) (Cambier et al., 2014) might indicate that some transcription factors (NKX2.5) can have a stronger and more rapid impact on gene expression during development, compared a histone chaperone such as HIRA.

3.9.2) Pulmonary stenosis specific to *Nkx2.5Cre;Hira*$^{-/fl}$ embryos

A constriction of the pulmonary trunk (PT) was seldom found in *Mesp1* conditional mutants (1/12) but was more prevalent in Nkx2.5Cre;Hira$^{-/fl}$ embryos (3/9). Sometimes referred to as pulmonary Infundibular stenosis, this feature is one of the characteristics features of tetralogy of Fallot (ToF), a congenital heart defect. In ToF, the narrowing of the PT increases the pressure inside the right ventricle after birth which leads to ventricular hypertrophy. ToF patients also present with a VSD and an overriding aorta, which were also detected in some *Nkx2.5Cre;Hira*$^{-/fl}$ embryos at E15.5 (5/9). The single surviving *Nkx2.5Cre* conditional *Hira,* although much smaller compare to its littermate control (see p57), did not show any cardiac malformations by OPT (data not shown).

Contrary to what was previously thought, pharyngeal arch arteries (PAAs) have been recently found to have an *Nkx2.5*-linage contribution. Endothelial cells from PAAs 3, 4 and 6, which give rise to postnatal carotid arteries, right subclavian artery and aorta, and pulmonary arteries, respectively, express *Nkx2.5* at E10.5 and E11.5 (Paffett-Lugassy et al., 2013). In contrast to *Mesp1*'s expression which is strictly mesodermal, the expression of *Nkx2.5* in pharyngeal endodermal cells underlying the SHF (Zhang et al., 2014b) could partially explain our phenotype.

Finally, it is worth nothing that some patients with ToF have a mutated copy of *NKX2.5 (McElhinney et al., 2003).* The *Nkx2.5Cre* used here is a knock-in allele and thus there is the potential for interaction between hemizygous levels of NKX2.5 and absence of HIRA. While no phenotypes were observed in *Nkx2.5Cre;Hira*$^{+/fl}$ embryos (n=6) such a genetic interaction remains a possibility. However, to our knowledge, no mutations of *HIRA* have been described in exome sequencing analyses of patients with congenital heart defect, although one study of a Chinese cohort associated a variant in the 3' UTR region of HIRA to the diagnosis of ToF (Wang et al., 2014).

Taken together, these results suggest that *Hira* might be involved in certain cases of ToF and could play a role in the CPF and in the PAAs. It is important to note that although the higher-level organization regulatory networks are conserved between mice and humans (Stergachis et al., 2014), an ENCODE project review stated how 50% of murine TF binding sites in regulatory elements are absent in humans, and 25% have migrated to different genomic locations (Carninci, 2014). Mutations can therefore be species specific and one has to be cautious in translating results across species.

3.9.3) Requirement of Hira in endothelial cells: in vitro vs in vivo results

The low penetrant growth reduction phenotype observed in *Tie2Cre* conditional mutants did not seem to be due to cardiac malformations, according to the reconstruction of the adult hearts by OPT. However, since vascularisation is important for a proper bone formation (Portal-Nunez et al., 2012), it is possible that HIRA could be required for angiogenesis during skeletal development which would explain the growth retardation of *Tie2Cre;Hira*$^{fl/-}$ adults (n=3). Since no embryonic or postnatal lethality was observed and only a reduction of size was observed in some adult mutants, it suggests that the role of HIRA in postnatal angiogenesis is not as critical as the endothelial network formation on matrigel had originally predicted (Dutta et al., 2010). Taken together, these somehow contradicting data on the role of HIRA in endothelial cells highlight the differences between *in vitro* and *in vivo* systems. The later encompasses a significant amount of both angiogenic and angiostatic factors (Distler et al., 2003) (VEGFs, FGFs, angiopoietins, PDGF, angiogenin), which could compensate for the lack of *Hira* during angiogenesis. A requirement for HIRA in the endothelial cell population might be more evident in a repair or regeneration situation. For example, hypoxia-induced angiogenesis (Krock et al., 2011) could be used (during development or after birth) to see if *Tie2Cre;Hira*$^{fl/-}$ mice display a similar endothelial cell proliferation, sprouting, migration and adhesion compared to controls. In addition, a tumour-transplantation experiment, which is often used to survey angiogenesis in cancer (Eklund et al., 2013), could be carried out in this context to test the angiogenic capacity of *Tie2Cre;Hira*$^{fl/-}$ mice. Subsequently,

the expression of *Vegfr1* could be quantified to measure the impact of the ablation of HIRA in proliferating ECs, as predicted by (Dutta et al., 2010).

3.9.4) Possible causes of lethality of the *Wnt1Cre;Hira$^{-/fl}$* newborns

The absence of cardiac and great vessel phenotypes in the *Wnt1Cre;Hira$^{-/fl}$* embryos up to E18.5 argues against a requirement of HIRA in cNCCs during cardiovascular development. This was contradictory to the results found in chick, in which a knockdown of *Hira* in premigratory neural crest cells resulted in failure of outflow tract septation (Farrell et al., 1999) (see p26). The perinatal death that was observed in *Wnt1Cre;Hira$^{-/fl}$* mutants could rather be the result of a neurological problem or a cleft palate defect interfering with swallowing (Trainor, 2010) since *Wnt1Cre* is expressed in craniofacial NCCs. It is worth noting that a review has recently pointed out the discrepancies often found in loss-of-function phenotypes between non-mammalian and mouse models (Barriga et al., 2015). For example the migration of neural crest cell is dependent on non-canonical WNT signalling in Xenopus, zebrafish and chick, but that is not the case in the mouse. Future experiments could involve examining neurological structures in *Wnt1Cre;Hira$^{-/fl}$* mutants for possible malformations. The innervation of the heart could also be affected (Hildreth et al., 2008), which could be tested by immunostaining with neurofilament-66 (Payne et al., 2015). The neuronal axons of the sympathetic/parasympathetic system, if affected, could causes arrhythmias.

3.9.5) HIRA is not required in normal conditions in post mitotic cardiomyocytes

The pilot experiment to investigate the potential role of HIRA in post mitotic cardiomyocytes suggests that HIRA is not required for normal heart function. After 3 consecutive days of tamoxifen injection, the animals were monitored for 8 weeks. The behaviour and cardiac output both mutants, *Cre* controls and WT animals remained unaltered. However, there are many aspects of this pilot experiment which have not been investigated. For example, it remains a possibility that a diminished expression of *Hira* could impact on the DNA repair mechanism, which would have been solicited after the deleterious *Cre* expression (see p61). A quantification of total DNA lesions could have addressed this question. DNA damage rarely impacts rapidly on cell function and rather has long term effect, such as premature ageing (de Boer et al., 2002). A long term ageing study of conditional *Hira* mutants could potentially shed some light on the role of HIRA in cardiac ageing. Furthermore, HIRA has already been shown to play an important part during the formation of SAHFs (see p27) which could further impact the rate of cells entering senescence. Future work involving immunofluorescence on heart sections to observe cell morphology or markers of senescence such as senescence associated beta-galactosidase (SA-βgal) activity or $p16^{INK4a}$ tumor suppressor protein (Debacq-Chainiaux et al., 2009).

Another means of testing the requirement of HIRA in the adult heart would be after cardiac stress. Dobutamine, which stimulates the β1-adrenoceptors of the heart (Calligaris et al., 2013) and increases contractility and cardiac output could be used to see whether the hearts respond as well once *Hira* has been ablated. Gene activation after myocardial infarct (MI) has been well characterised (Haubner et al., 2012). It would be interesting to perform a RNAseq after MI or cryoinjury to analyse the role of HIRA in regulating key genes involved in cardiac recovery.

In summary, this chapter has shown that HIRA is not required for homeostasis in adult cardiomyocytes. However, the external phenotype, embryonic lethality and cardiac malformations caused by the ablation of *Hira* in cardiogenic mesoderm during development indicate a crucial role of HIRA in myocardial precursors. The following chapter will examine the downstream transcriptional changes following *Hira* ablation.

Chapter 4 Genome wide analysis of genes dysregulated in the absence of *Hira*

4.1) RNAseq analysis of *Mesp1Cre*;*Hira*$^{-/fl}$ hearts at E11.5 and E12.5

Ablation of *Hira* in the cardiogenic mesoderm (*Mesp1Cre*) led to the most drastic and penetrant phenotypes with a 100% penetrant oedema and VSD at E15.5. In order to investigate the transcriptional changes responsible for these defects, a RNAseq was performed on total RNA from embryonic hearts at E11.5, as the heart have just completed looping and prior to the appearance of the malformation of the atrioventricular cushions at E12.5. Since the majority of defects were only observed much later and that the cushion defects at E12.5 were only partially penetrant, the E12.5 stage was selected as well.

4.1.1) List of genes significantly changed at E11.5 vs E12.5

Mesp1Cre;*Hira*$^{fl/-}$ transcripts were compared to *Mesp1Cre*;*Hira*$^{fl/+}$ by RNAseq. This genome-wide analysis was performed using total RNA extracted from embryonic hearts. 360 coding transcripts were changed in the mutant hearts (MannWhitney unpaired test, Benjamini Hochberg FDR, $p \leq 0.05$, FC ≥ 1.5) at E12.5, and 159 at E11.5 (Figure 4-1).

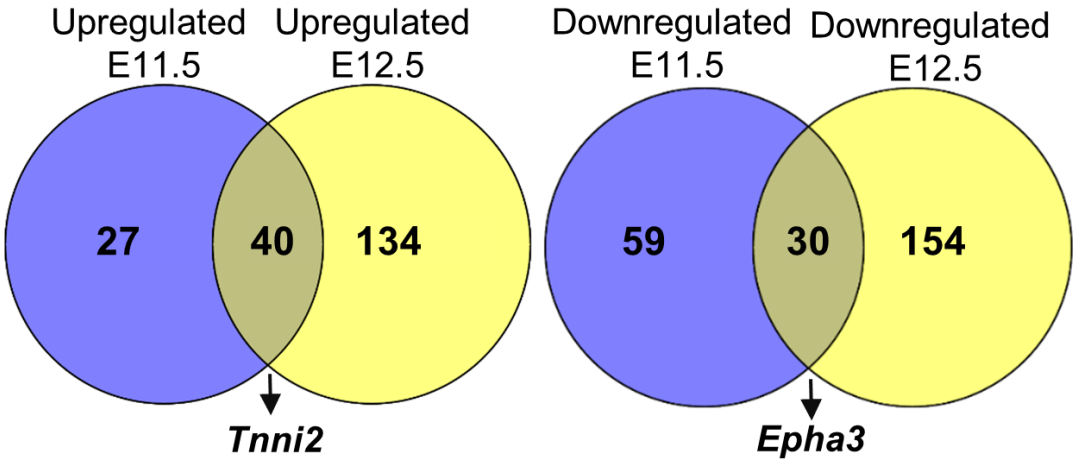

Figure 4-1 A higher number of genes are dysregulated at E12.5 compared to E11.5 in *Mesp1Cre* conditional *Hira* mutants

Venn diagram indicating the number of genes whose expression is up or downregulated in *Mesp1Cre*;*Hira*$^{-/fl}$ compared to *Mesp1Cre*;*Hira*$^{+/fl}$ hearts at E11.5 and E12.5. RNA extraction and sequencing was done in triplicate from *Mesp1Cre*;*Hira*$^{-/fl}$ and *Mesp1Cre*;*Hira*$^{+/fl}$ embryonic hearts at E11.5 and E12.5.

The E12.5 batch was mainly used for downstream analysis since there were 2.5 times more transcripts significantly affected at that stage, compared to E11.5 (Figure 4-1). This rational presents the risk of observing additionally dysregulated genes which would mainly reflect secondary events rather than genuine HIRA controlled genes, however the level of up or downregulation of genes observed at E11.5 was often too low to detect HIRA targets (Table 4-1).

Table 4-1 Gene dysregulation in *Mesp1Cre;Hira*$^{-/fl}$ hearts is more important at E12.5 compared to E11.5

	E11.5	Abs FC	E12.5	Abs FC
Epha3	**DOWN**	**2.4**	**DOWN**	**2.4**
Lyve1	DOWN	2.5	DOWN	5.1
Ramp1	DOWN	1.5	DOWN	2
Tbx3	DOWN	1.2	DOWN	1.5
Isl1	DOWN	2.9	DOWN	1.4
Pdgfra	DOWN	1.28	DOWN	1.2
Tnni2	**UP**	**3.4**	**UP**	**5.7**
Tnnt3	**UP**	**2.4**	**UP**	**3.1**
Tnnt1	DOWN	1.7	DOWN	1.8
Casq1	UP	1.7	UP	2
Acta1	UP	1.7	UP	1.7
KRt8	UP	1.2	UP	2.6
Krt19	UP	1.5	UP	2

The list of genes presented here is a subset of genes relevant for cardiac development, which have been extracted from the RNAseq list of genes dysregulated in both stages. The genes underlined are studied in greater depth in this thesis and have been partly selected for their early (E11.5) dysregulation.

At E12.5, the RNAseq analysis demonstrated the absence of trend towards up or downregulation in the list of significantly dysregulated genes (48.8% down vs 51.2% up) (Figure 4-2). Genes of interest were identified based on their known roles during heart development, their level of fold change and their adjusted *p*-values.

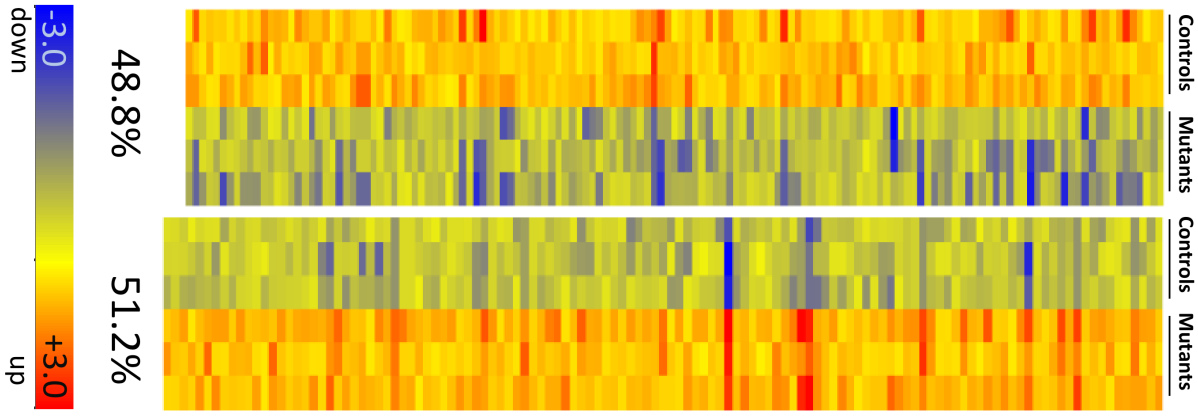

Figure 4-2 The ablation of *Hira* results in both up and downregulation of a set of genes

RNAseq comparing *Mesp1Cre;Hira*$^{-/fl}$ heart transcripts with *Mesp1Cre;Hira*$^{+/fl}$ hearts at E12.5 resulted in gene down- and up-regulation. Here the heatmap format is used to visualise the differential gene expression in the heart of mutants (*Mesp1Cre;Hira*$^{-/fl}$) vs controls (*Mesp1Cre;Hira*$^{+/fl}$) in triplicates at E12.5

4.1.2) Gene ontology analysis: myofibril/sarcomere

Since long lists of genes can be challenging to examine, a gene ontology (GO) analysis on the list of differentially expressed genes ($p \leq 0.05$, $FC \geq 1.5$) was carried out in an effort to group genes into defined functional groups which might be part of important processes relevant for cardiac development. There are now many databases contributing to the GO consortium. They include, amongst others, the Mouse Genome Informatics (MGI), UniProt-Gene Ontology Annotation and the University College London-based annotation group. From the list of 46 GO terms obtained, 7 overlapping ones were of particular interest (Table 4-2) since they covered genes encoding proteins directly involved with muscle contractility.

Table 4-2 List of GO terms

GO number	GO term	p-value	Number of genes
GO:0005488	binding	1.03E-05	152
GO:0032501|GO:0050874	multicellular organismal process	4.55E-06	81
GO:0044707	single-multicellular organism process	7.83E-07	79
GO:0044444	cytoplasmic part	2.83E-05	76
GO:0032502	developmental process	1.80E-08	67
GO:0044767	single-organism developmental process	1.58E-08	67
GO:0048856	anatomical structure development	6.47E-10	65
GO:0007275	multicellular organismal development	5.38E-08	61
GO:0048731	system development	7.64E-10	59
GO:0065008	regulation of biological quality	2.94E-08	42
GO:0048513	organ development	4.03E-06	41
GO:0005576	extracellular region	4.76E-08	41
GO:0048869	cellular developmental process	7.05E-05	40
GO:0030154	cell differentiation	2.12E-05	40
GO:0002376	immune system process	5.16E-07	28
GO:0044421	extracellular region part	3.08E-06	26
GO:0042592	homeostatic process	7.58E-06	22
GO:0005615	extracellular space	1.40E-04	19
GO:0097458	neuron part	1.38E-04	19
GO:0002520	immune system development	1.98E-06	16
GO:0048534	hematopoietic or lymphoid organ development	9.92E-07	16
GO:0030097	hemopoiesis	6.45E-06	14
GO:0031012	extracellular matrix	8.83E-05	13
GO:0048872	homeostasis of number of cells	8.48E-08	11
GO:0030099	myeloid cell differentiation	9.08E-08	11
GO:0030424	axon	7.66E-05	11
GO:0015669	gas transport	3.90E-14	9
GO:0002262	myeloid cell homeostasis	4.27E-08	9
GO:0034101	erythrocyte homeostasis	6.97E-09	9
GO:0030016	myofibril	1.16E-05	9
GO:0030218	erythrocyte differentiation	3.43E-09	9
GO:0043292	contractile fiber	1.98E-05	9
GO:0005833	hemoglobin complex	1.33E-15	8
GO:0044449	contractile fiber part	5.22E-05	8
GO:0044445	cytosolic part	9.81E-05	8
GO:0015671	oxygen transport	8.62E-14	8
GO:0030017	sarcomere	2.72E-05	8
GO:0005344|GO:0015033	oxygen transporter activity	3.72E-14	8
GO:0019825	oxygen binding	8.65E-12	8
GO:0020037	heme binding	1.67E-04	8
GO:0048821	erythrocyte development	3.69E-05	4
GO:0061515	myeloid cell development	7.34E-05	4
GO:0005865	striated muscle thin filament	1.24E-05	4
GO:0036379	myofilament	2.00E-05	4
GO:0005861	troponin complex	3.59E-05	3

GO analysis of the genes significantly dysregulated in *Mesp1Cre;Hira*$^{-/fl}$ embryonic hearts that have an over-representation of one or more GO terms that pass the cut-off p-value of 10^{-4}. Terms relating to contractility and myofibril structure are highlighted in orange.

A list of 8 genes was obtained from the GO terms “myofibril” and “striated muscle thin filament” (Figure 4-3) which are important in establishing and regulating cardiac contractility. A trend for upregulation was detected, except for *Tnni1 and Slc4a1* which were downregulated by 2 and 3 fold, respectively.

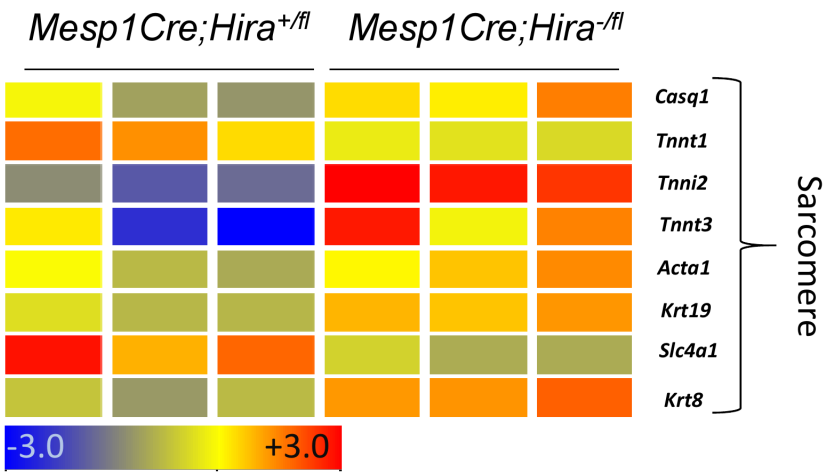

Figure 4-3 The GO analysis grouped certain dysregulated genes under the term “contractile fiber” or “sarcomere”

The heatmap presented here revealed the colour coded fold change of genes grouped under the terms “contractile fiber” and “sarcomere”. A trend in upregulation was observed, aside from *Tnnt1 and Slc4a1* which were downregulated.

4.2) Validation of selected genes by qRT-PCR shows a great reliability of RNAseq

Quantitative real time PCR (qRT-PCR) was carried out to validate candidate genes selected by RNAseq. Genes were selected for their known roles during heart development. Little or no variation of fold change between RNAseq and qRT-PCR data were observed (Figure 4-4).

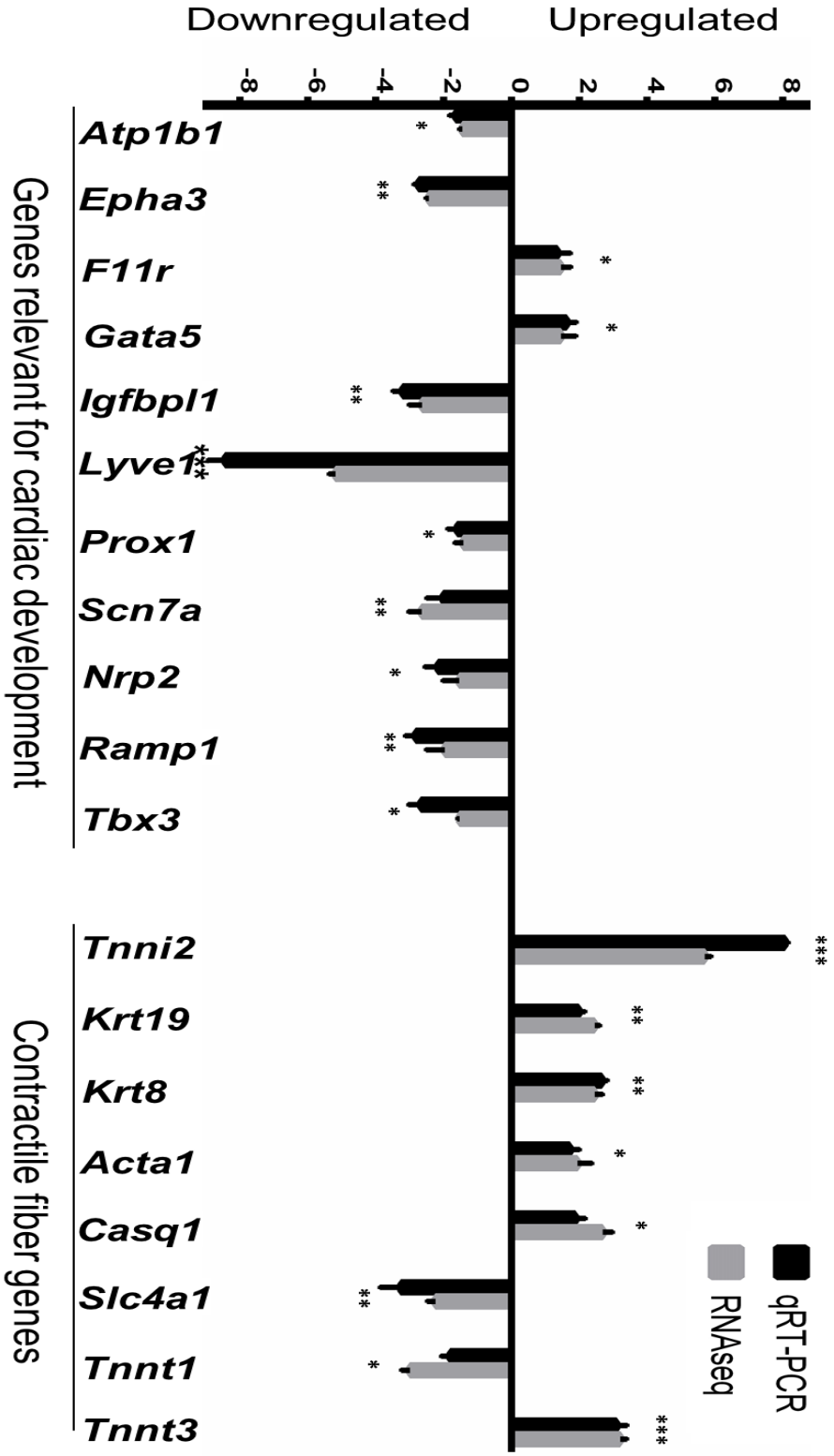

Figure 4-4 Ablation of *Hira* leads to dysregulation of a subset of genes: validation of RNASeq data by qRT-PCR

Selected genes whose expression is up or downregulated in *Mesp1Cre*;*Hira*$^{-/fl}$ compared to *Mesp1Cre*;*Hira*$^{+/fl}$ at E12.5 were validated by QRT-PCR. The x-axis represents the absolute fold change in gene expression in the mutants compared to their WT littermates (n=3) is shown here for both techniques. T-test: $p<0.05$ *, $p<0.01$ **, $p<0.001$ ***. Data are shown as levels of mRNA normalized to *Gapdh* and are representative of three independent experiments. Errors bars represent the standard deviation of technical triplicates. This experiment represents a technological and biological replicate which highlights the reliability of RNAseq technology and validates the genes of interest.

4.3) Expression of most upregulated gene: *Tnni2* and disruption of troponin meshwork

Tnni2 is a fast twitch skeletal muscle gene which was the most upregulated gene in the mutant hearts by both RNA-seq (5.9 fold) and qRT-PCR (7 fold) (Figure 4-4). ISH confirmed Tnni2 overexpression in the mutants (Figure 4-5), suggesting heart contractility could be affected by alteration of sarcomeric components (see discussion p77)

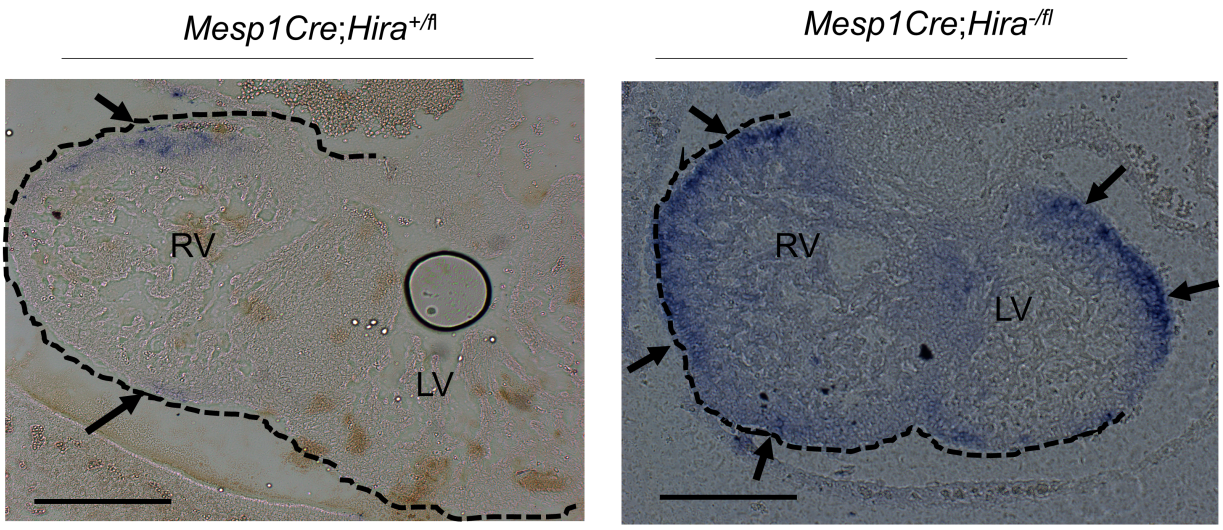

Figure 4-5 *Tnni2* is strongly overexpressed in the heart of *Mesp1Cre;Hira*$^{-/fl}$ embryos

Tnni2 is a fast skeletal type troponin. Here, transverse sections of E12.5 embryonic hearts showed an abnormal strong expression of *Tnni2* mostly in the ventricular wall (arrows) of the heart in *Hira*-conditional mutant hearts compared to the normal expression in the WT. Images are representative of two embryos for each genotype and incubation time were identical *Scale bar: 100µm*

Staining with Troponin C on transverse sections to examine sarcomeric organisation was done in collaboration with Sarah Phelps. It demonstrated a lack of typical parallel organisation of the filament structures in the mutants (Figure 4-6).

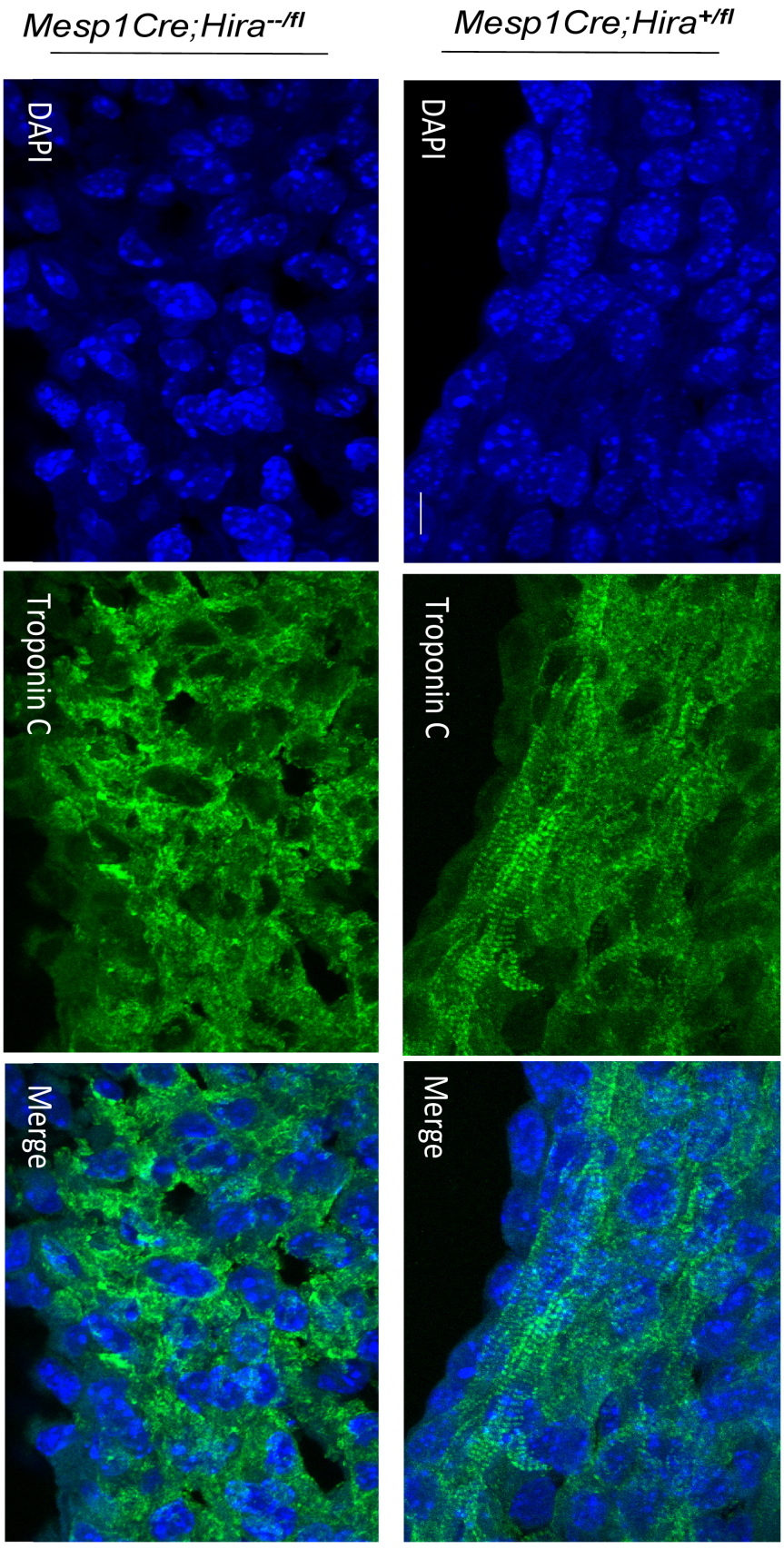

Figure 4-6 Ablation of *Hira* leads to disorganised sarcomeric structure in the heart

Troponins are known to regulate muscle contractility. Here, transverse sections of E12.5 embryonic hearts immunostained with DAPI (nucleus) and Troponin C (sarcomeric structure) show a disorganisation of the contracting meshwork of myofibrils in the absence of HIRA, in the free ventricular wall of the mutants. *Scale bar: 10µm Experiments carried out in collaboration with Dr Sarah Phelps and included with her permission.*

4.4) *Epha3* is expressed in the atrioventricular cushions and is strongly reduced in *Hira*-conditional mutant hearts

The expression of *Epha3*, encoding a receptor tyrosine kinase that is required for EndMT (see p2) in the atrioventricular cushions, was downregulated 2.7 fold in the heart of the mutants compared to their control littermates (Figure 4-4). In agreement, *in situ* hybridization (ISH) revealed that *Epha3* expression was greatly diminished in the cushions and the membranous part of the ventricular septum in the mutants compared to their control littermates (Figure 4-7).

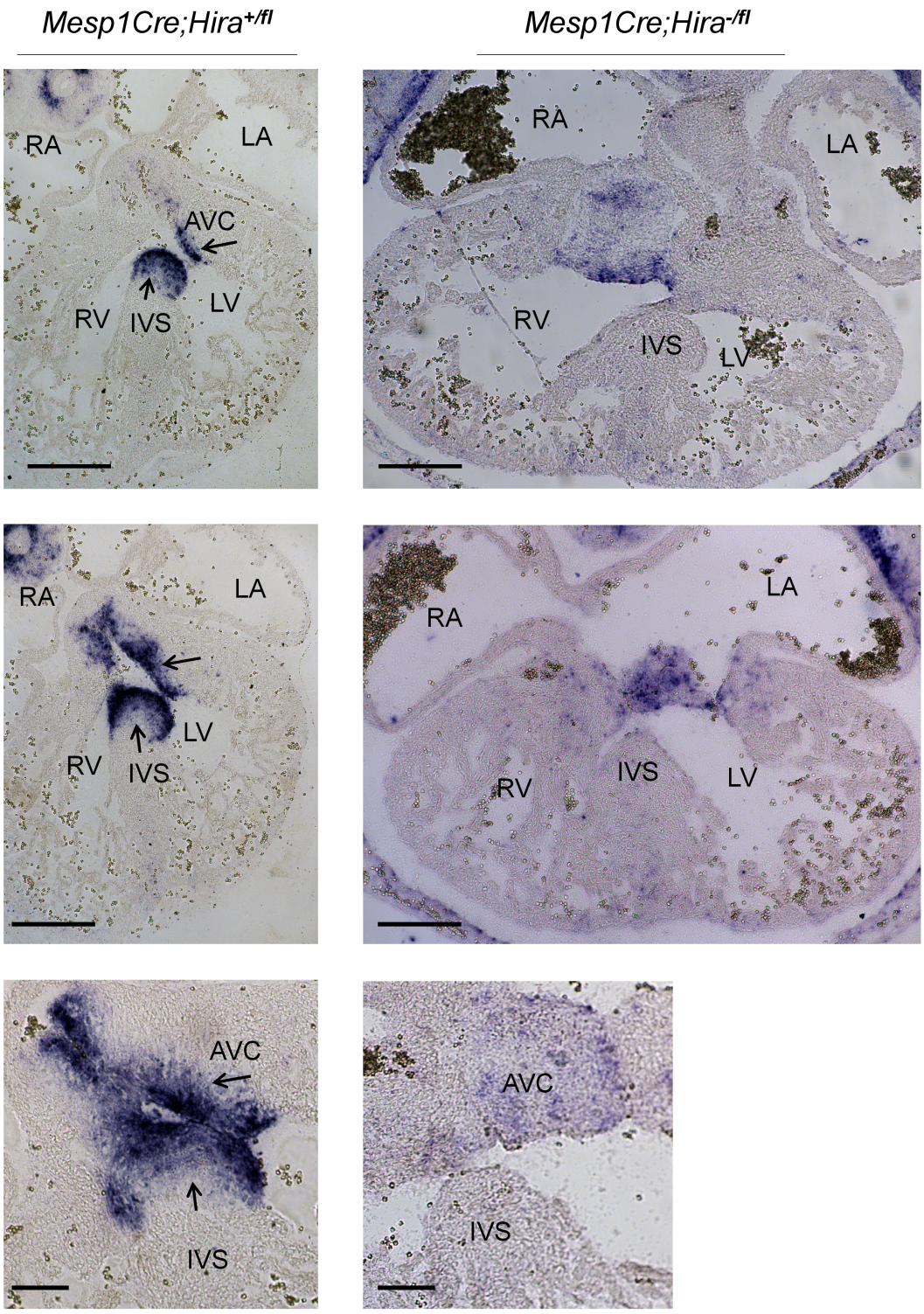

Figure 4-7 Ablation of *Hira* results in the downregulation of *Epha3* in the cardiac cushions

In situ hybridization of *Epha3* on transverse sections of E12.5 embryos with the indicated genotypes show a low expression of *Epha3* in both the membranous portion of the interventricular septum (IVS) and the atrioventricular cushions (AVC) (lower panel) in the mutants. The littermate control have a high expression in those regions (arrows). RV/LV: Right/Left ventricle. RA/LA: Right/Left atrium. Images are representative of two embryos for each genotype and incubation time were identical. *Scale bar: 100µm (top panels) 25 µm (lower panel)*

4.5) Discussion

4.5.1) GO analysis: contractility likely to be affected in *Mesp1Cre*;*Hira*$^{-/fl}$ hearts at E12.5

The ablation of *Hira* in the cardiogenic lineage resulted in the upregulation of *Tnni2* (7 fold) and *Tnnt3* (3.2 fold), genes located close together in both the mouse and human genomes (see next chapter). The encoded proteins are classified as fast skeletal muscle troponins (Ochala, 2008). The troponin complex binds calcium ions, and through its association with actin and tropomyosin is involved in the regulation of striated muscle contraction. It consists of three different subunits, troponin C (TnC), troponin I (TnI) and troponin T (TnT). While various troponins are expressed in the developing heart at E12.5 (Franco et al., 1998), the skeletal troponins have a low expression in cardiac muscle, and upregulation of *Tnnt3* has been associated with reduced cardiac contractility (Huang et al., 2008). In a *Notch1* gain of function mutant, structural defects of the myocardium were attributed to elevated expression of *Tnni2* (Watanabe et al., 2006). The GO analysis revealed several other sarcomeric genes (also under the GO term myofibril) which were dysregulated. *Tnni2, Tnnt3, Casq1, Acta1, Krt8, Krt19* (Stone et al., 2007) were upregulated and the anion exchanger *Slc4a1* and *Tnnt1* were downregulated 3 fold and 2 fold, respectively (Figure 4-3). *Tnnt1* is crucial for cardiac function during embryogenesis up to E16.5 (Manuylov and Tevosian, 2009) and *Slc4a1*$^{-/-}$ neonates suffer from cardiac hypertrophy soon after birth (Alvarez et al., 2007). Immunofluorescence microscopy analysis of the troponin complex demonstrated a disorganised structure of the striated muscles of the myocardium (Figure 4-6). This disruption to the myofibril assembly likely contributes to a diminished efficiency of heart pumping (Risebro et al., 2009). The developing mouse heart starts beating at E8.5. Reduced cardiac output can lead to whole body oedema at E14.5 (Peng et al., 2008). Thus, the haemorrhage and oedema observed at E15.5 could be a consequence of diminished cardiac function secondary to poor maintenance of sarcomeric structure and myofibril disruption.

4.5.2) The role of *Epha3* in the development of cardiac cushions and its potential role in the establishment of a VSD

Epha3 had a diminished expression at E11.5 and E12.5 in *Mesp1Cre;Hira*$^{-/fl}$ hearts (Table 4-1). *Epha3* is expressed in the heart from E10.5 in the atrioventricular cushion and in the mesenchymal cap of the developing septum primum (Stephen et al., 2007). Accordingly, the expression in E12.5 *Mesp1Cre*;*Hira*$^{-/fl}$ was examined in mutant hearts. *Epha3* was downregulated in precisely those regions in the mutants versus the controls (Figure 4-7). Interestingly, *Epha3*-null embryos are perinatal lethals with ASD and cardiac failure, and have earlier atrioventricular cushion defects (Stephen et al., 2007). This is striking in view of the defects seen at E12.5 in *Mesp1Cre;Hira*$^{-/fl}$ mutant hearts (Figure 3-7). As the interventricular

septal defect is at the site of the anticipated embryonic interventricular communication, it maybe that reduced growth of the muscular septum contributes to the abnormality. Furthermore, the ADAM10 membrane metalloprotease has been well characterised during heart development and is required for the EMT process of the atrioventricular cardiac cushions (Zhang et al., 2010). ADAM10 is known for interacting with Eph and Ephrin expressing cells. For instance, it can recognise and regulate the formation of Ephrin-A5/EphA3 complexes (Janes et al., 2005). Epha3, through ADAM10, promotes cleavage of EphrinA5 on the surface of opposing cells (Atapattu et al., 2012, Janes et al., 2005). It is likely that downregulation of *Epha3* perturbs the Eph/Ephrin-mediated cell repulsion and segregation which could contribute to the septal defects in *Hira* mutants.

4.5.3) Other transcriptional changes possibly affecting heart development.

Following the RNAseq at E11.5 and E12.5 of *Mesp1Cre;Hira*$^{-/fl}$ hearts, transcripts were identified which were the most likely responsible for generating the phenotype described in chapter 3. However, 360 dysregulated genes represent a substantial list which cannot be fully discussed within a reasonable text length. The following discussion attempts to describe genes that would be high priorities for further work in the context of HIRA and its role in heart development.

Lyve1 (Lymphatic Vessel Endothelial Hyaluronan Receptor 1) was found to be strongly downregulated (Figure 4-4, 5.1 fold by RNASeq and 8 fold by qRT-PCR at E12.5). *Lyve1* is a marker of the lymphatic system first discovered in 1999 (Banerji et al., 1999) across many organisms (Okuda et al., 2012). The lymphatic system is crucial for fluid regulation. Interestingly, a lymphatic defect often result in substantial oedema (Gauvrit et al., 2014), which was identified in *Mesp1Cre;Hira*$^{fl/-}$ from E13.5. Lymphatic endothelial cells are first detected at E12.5 using markers such as VEGFR-3 (Joukov et al., 1996) and PROX1 (Wigle and Oliver, 1999). The earliest LYVE1 expressing cells occur at the venous pole of the heart (Figure 4-8) around E12. At E12.5, cardiac lymphatic vessels begin to emerge, sprouting from extra-cardiac regions proximal to the OFT (Klotz et al., 2015) and at E13.5, the surface of hearts is covered with LYVE1 expressing cells (Flaht et al., 2012).

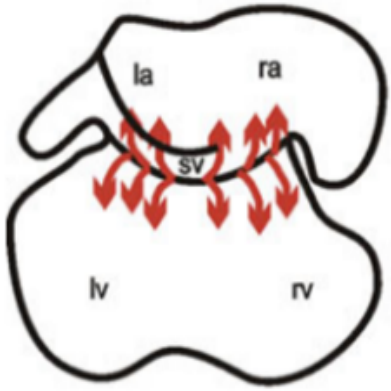

Figure 4-8 Schematic representing the *lyve1* positive strands/tubules/vessels migration pattern

Schematic representing progressive development of *Lyve1* positive strands on the venous pole of the heart. Adapted from (Flaht et al., 2012) la/ra: left/right atrium; lv/rv: left/right ventricle

Although *Lyve1* seemed like a strong candidate gene, it is important to note that fully form lymphatic vessels only begin to grow on the ventricular surface of the dorsal side of the heart from E14.5, and reach the apex by E18.5 (Klotz et al., 2015). In addition, *Lyve1*$^{-/-}$ mice are viable and present no lymphatic phenotype (Luong et al., 2009), which questions the exact role of this gene for the formation of the lymphatic system. On the other hand, *Prox1*$^{-/-}$ mice are embryonic lethal (Wigle and Oliver, 1999). *Prox1* has also been shown to be important for lymphangiogenesis (Wigle and Oliver, 1999), with cells often expressing *Prox1* and *Lyve1* simultaneously (Flaht et al., 2012). *Prox1* was only slightly downregulated (1.4 fold) at E12.5 in *Mesp1Cre;Hira*$^{fl/-}$ hearts, suggesting that lymphatics growth was not greatly affected by *Lyve1* downregulation. Moreover, *Tie2Cre;Hira*$^{fl/-}$ conditional *Hira* mutant, in which *Hira* would also be ablated from in cardiac lymphatics, did not have an embryological phenotype and were only partially affected during their adult life (see p61). This result advocates only a minor role of HIRA in endothelial cells. *Lyve1* downregulation is therefore unlikely to be the main cause of the oedema seen at E15.5 in *Mesp1Cre;Hira*$^{fl/-}$embryos.

Gata5 was not initially part of the dysregulated list of genes at E12.5 since its upregulation was 1.4 fold (Figure 4-4). However, qRT-PCR experiments on additional *Mesp1Cre;Hira*$^{-/fl}$ hearts pointed out a 1.6 fold overexpression, thus placing that gene in the group of significantly upregulated transcripts. Since GATA4, GATA5, and GATA6 share 85% homology of their DNA binding site (Singh et al., 2010), *Gata4*$^{-/-}$ embryos die between E8.5 and E10.5 due to a lack of linear heart tube and failure of ventral morphogenesis (Molkentin et al., 1997), and *Gata4*$^{-/-}$*Gata6*$^{-/-}$ embryos completely lack a heart (Zhao et al., 2008), many

groups have studied *Gata5* during heart formation. In zebrafish, GATA5 directly regulates the cardiac transcription factor *Nkx2.5* (Reiter et al., 1999), and is required for heart development. Although *Gata5* is only expressed in the heart and the lung during embryonic development in the mouse (Morrisey et al., 1997), by itself *Gata5* does not appear crucial for development since $Gata5^{-/-}$ mice are viable (Singh et al., 2010, Molkentin et al., 2000). However, *Gata5,* alongside *Gata4,* regulates the proliferation rate of cardiomyocytes in mice during embryogenesis (Singh et al., 2010). Although $Gata4^{+/-}$ embryos are viable and show no abnormalities, $Gata4^{+/-}$,$Gata5^{-/-}$ compound mutant embryos at E12.5 presented with cardiac defects such as a hypoplastic ventricular compact myocardium and hypoplasia of the endocardial cushions leading to common atrioventricular canal (Singh et al., 2010). By E14.5, these mutants had systemic haemorrhage and body wall oedema, which the authors say is "suggestive of heart failure". It is therefore a possibility for *Gata5* dysregulation to be a contributing factor for the heart defects observed in *Mesp1Cre* conditional *Hira* mutants.

Overall this chapter has described the most relevant differentially expressed genes in the heart of *Mesp1Cre;*$Hira^{fl/-}$ embryos at E11.5 and E12.5. The most upregulated gene, *Tnni2*, along with other dysregulated troponins such as *Tnnt3* were validated by qRT-PCR. Troponin staining revealed myofibrillar disarray in the heart wall, in the same subset of cardiac cells where an overexpression of *Tnni2* detected, which is likely to affect the contraction ability of cardiomyocytes. Of particular interest, *Epha3* which has been associated with the EMT process and atrioventricular cushion formation, was found to be downregulated in the mesenchymal components of the cushions. Taken together, these gene expression changes are likely to be responsible for the VSD and oedema observed at E14.5 and E15.5 in *Mesp1Cre* conditional *Hira* mutants.

To potentially improve on our understanding of HIRA's global gene regulation, the next chapter covers the regions of the genome which have an enrichment of HIRA.

Chapter 5 HIRA ChIP followed by massively parallel DNA sequencing (ChIPseq)

The genome-wide analysis of differential transcription in *Mesp1* conditional mutants at E12.5 was covered in the previous chapter. To investigate the potential role of HIRA in transcriptional regulation through chromatin modification, genome-wide chromatin immunoprecipitation (ChIP) followed by high-throughput DNA sequencing (ChIPseq) was performed on WT hearts at E12.5. This approach might shed light on the dysregulation of certain genes resulting from the ablation of *Hira* in the cardiogenic lineage. Although HIRA has been shown to directly bind naked DNA (Prochasson et al., 2005, Ray-Gallet et al., 2011, Orsi et al., 2013), histone chaperones only bind chromatin transiently (Angelov et al., 2006, Adam et al., 2013). As mentioned in 43, it was therefore necessary to use EGS, a cross-linking agent with arms 8 times longer than traditional formaldehyde (FA) in addition to FA. (Figure 5-1).

	Chemical Formula	Molecular Weight	Spacer Arm (Å)	Useful for Cross-Linking
HCHO	CH_2O	37% (conc.)	2.0	prot/DNA/RNA
DMA	$C_8H_{18}Cl_2N_2O_2$	245.5	8.6	prot/prot
DSS	$C_{16}H_{20}N_2O_8$	368.34	11.4	prot/prot
DSP	$C_{14}H_{16}N_2O_8S_2$	404.42	12.0	prot/prot
EGS	$C_{18}H_{20}N_2O_{12}$	456.36	16.1	prot/prot

Figure 5-1 Cross-Linking Agents

Table representing the molecular weight and respective spacer arm length in angstrom of crosslinking agents. Adapted from (Zeng et al., 2006)

Due to the dual cross-linking (HCHO and EGS), sonication time had to be adapted. 25 rounds of sonication of 1 min were required to sufficiently shear chromatin and obtain fragments small enough to continue with the ChIP. QChIP requires sizes between 500 and 1000bp, whereas smaller fragments are preferred for ChIPseq (~300bp). This was verified by both standard 1% agarose electrophoresis (Figure 5-2) and by bioanalyser (Figure 5-3).

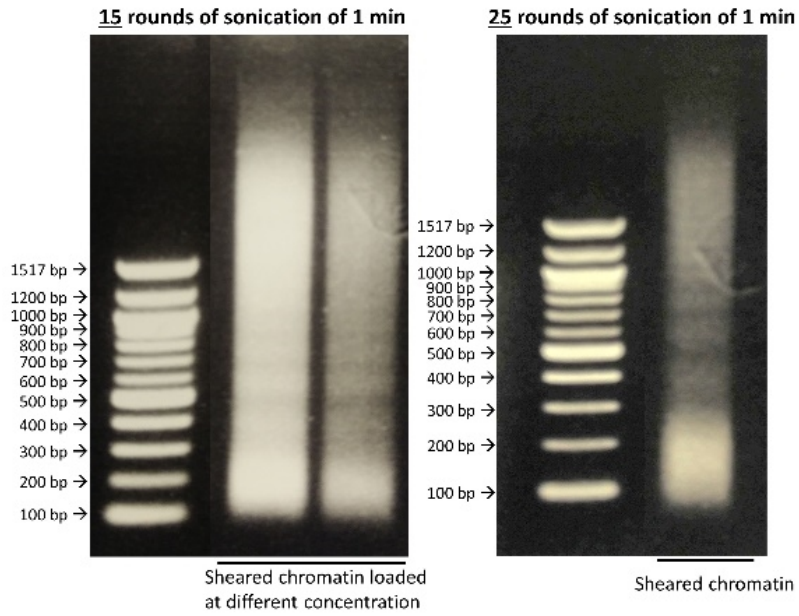

Figure 5-2 Sonication levels of chromatin verified on an 1% agarose gel

Electrophoresis 1% agarose gel displaying sheered chromatin after reverse crosslinking. 25 rounds of replication were required in order to obtain the correct fragment size for ChIPseq.

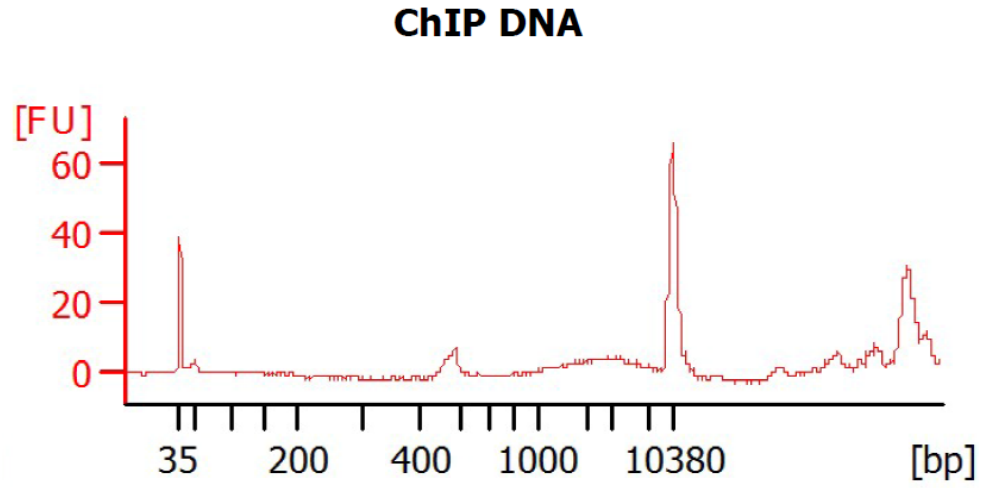

Figure 5-3 High Sensitivity DNA Assay on a Bioanalyser

Analysis of fragment sizes with a bioanalyser. The "bump" here at ~500bp represents the correct fragment size for qChIP.

5.1) ChIP-seq analysis using strand NGS and peak calling

5.1.1) Quality control

ChIP and input chromatin samples were analysed before massive parallel sequencing. The quantity, fragment size and quality of the purified input and ChIP DNA were assessed. The quantity of material was measured with a next generation fluorometer "Qubit® 3.0". The standard nanodrop 1000 would not have been sensitive enough to measure small ChIP DNA. The minimum required concentration for sequencing is 1ng. 0.118*30=**3.54ng** was obtained (Figure 5-4).

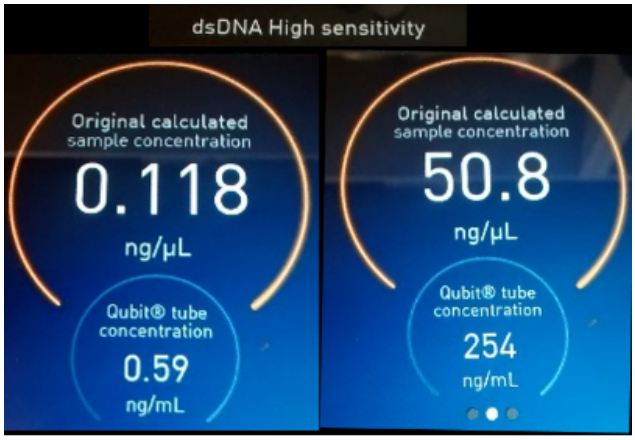

Figure 5-4 ChIP DNA quantified by Qubit® 3.0 Fluorometer

The Qubit fluorometer is designed to accurately quantify very small amount of DNA. The concentration of ChIP DNA and Input DNA are displayed here. 9 µl were used from the ChIP sample to obtain 1ng.

The fragment size was checked by bioanalyser before and after library preparation. The library preparation involved a size selection step for fragments ~200bp +/- 100bp, with the adapters adding a further 120bp (Figure 5-5). It is challenging to decide the sequencing depth (total number of reads) required as it depends on how many sites have been enriched genome wide and the affinity of the antibody used. A maximum sequencing depth of 90million reads was performed. Please see discussion for further analysis.

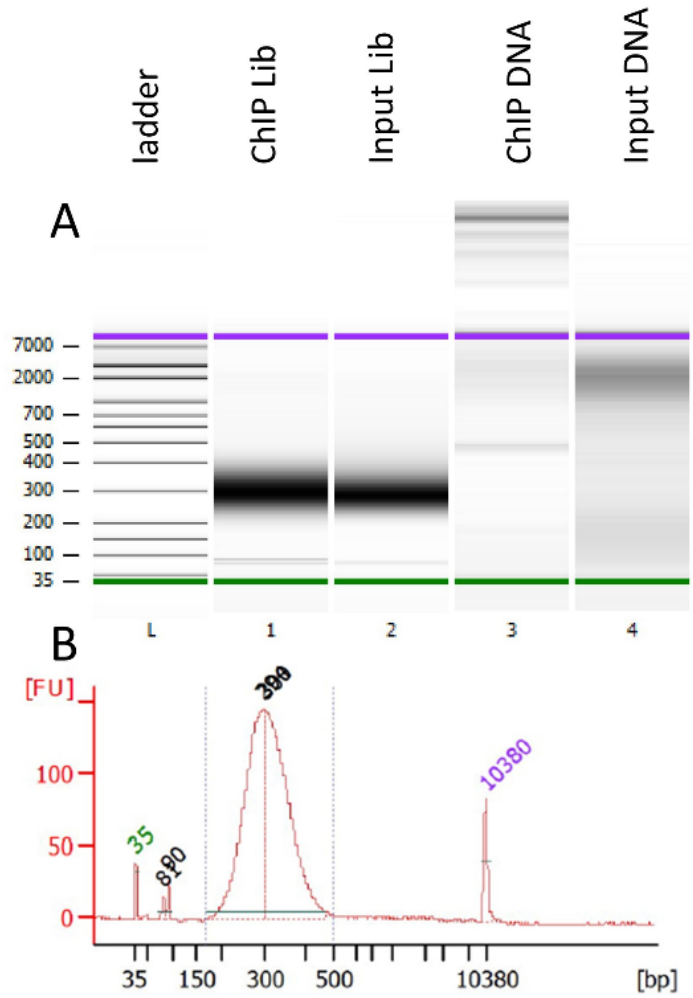

Figure 5-5 ChIP DNA and library bioanalyser trace

Comparison of ChIP DNA and input after and before the library preparation (A), which includes a size selection between 150bp and 500bp (B).

5.1.2) Peak calling

The genome alignment was done to the mouse genome mm10 using bowtie by the UCL genomics group (Mike Hubank group) and the generated .bam files were analysed using the strand NGS software. This software includes different algorithms to detect significant enrichment at given loci. The enriched region detection (ERD) was first used, followed by the better characterised Model-based Analysis of ChIP-Seq (MACS). Figure 5-6 illustrates the region upstream of *Gata5* where both algorithms detected a region bound by HIRA. On the other hand, the putative HIRA enrichment at the *Tbx3* locus was only identified by the ERD method (Figure 5-7).

Figure 5-6 IGV HIRA has a putative binding site at the *Gata5* locus (calculated with the MACS algorithm)

Legend below

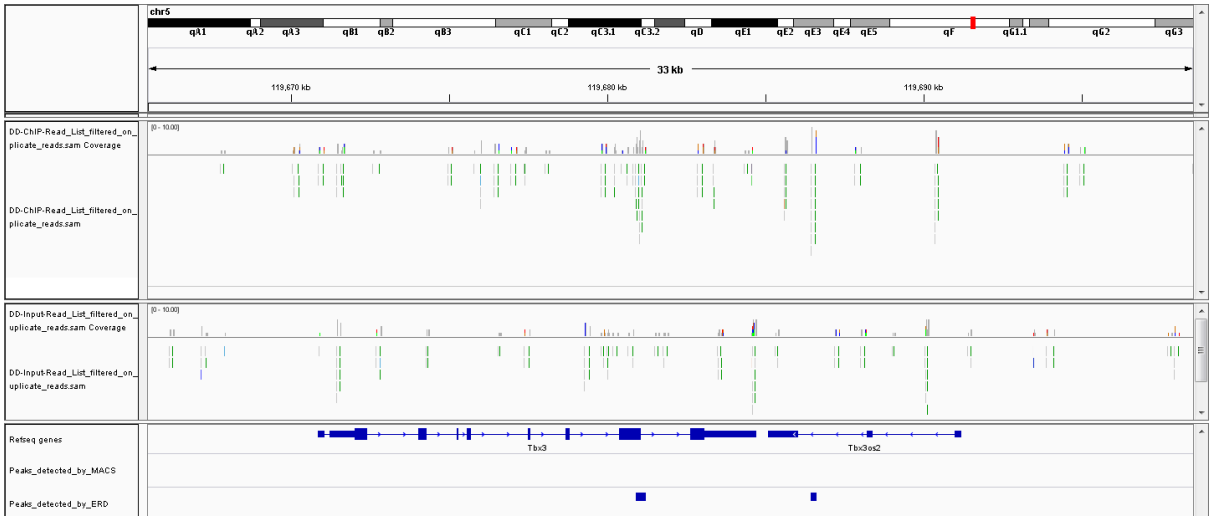

Figure 5-7 HIRA has a putative binding site at the *Tbx3* locus (calculated with the ERD algorithm)

The ChIP track (top) and input track (middle) are represented here. Each grey/green block represents a 43bp read. The lower track represents the reference genome (mm10) and the "peaks" detected by MACS and ERD.

The validation of those loci (*Gata5* and *Tbx3*) by qChIP showed the ERD method to be unreliable, since the *Tbx3* amplification was identical to the intergenic region of chromosome 6 (X6) used as a negative control for specific binding (Figure 5-8). It is possible that the parameters for the ERD algorithm were not correctly defined, however MACS analysis rightfully predicted a ten-fold enrichment of HIRA at the *Gata5* locus compared to the negative control (X6) (Figure 5-8). MACS is the most widespread method to identify read-enriched regions from ChIPseq data and had already been cited more than 300 times in 2012 (Feng et al., 2012).

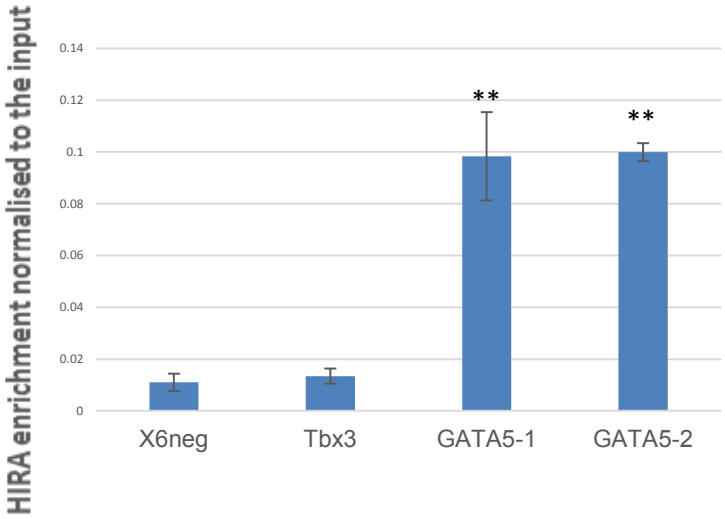

Figure 5-8 HIRA is enriched at the *Gata5* locus but not at the *Tbx3* locus

QChIP shows an enrichment of HIRA upstream of *Gata5*. (validation of the peaks mentioned above). An intergenic region on chromosome 6 was used as a negative control. HIRA does not bind the *Tbx3* locus. Data is normalized to the input (=100) and is representative of 2 independent experiments. Errors bars represent the min/max from technical duplicates. Unpaired t-test: $p<0.01$ **

The genome analysis presented here was carried out following peaks obtained by MACS analysis. It contained the following four steps:

- Remove redundant reads (if not done previously)
- Adjust read position
- Calculate peak enrichment
- Estimate the empirical false discovery rate.

5.1.3) Gene list enriched for HIRA binding in their proximity

The predicted HIRA binding sites obtained by MACS analysis were used to generate a list of genes which had a peak within their gene body and/or 5Kb upstream/downstream of the TSS/TES, respectively. A total of 6625 peaks generated a list of 2515 genes. This method implied that 62% of peaks are distal intergenic and 38% are genic. To further characterise the HIRA ChIPseq enrichment genome-wide, the CEAS tool (Cis-regulatory Element Annotation System) was used which analyses ChIP signals over specific genomic features, such as promoters, gene bodies, exons and 5'/3' untranslated regions (UTR). (Figure 5-9).

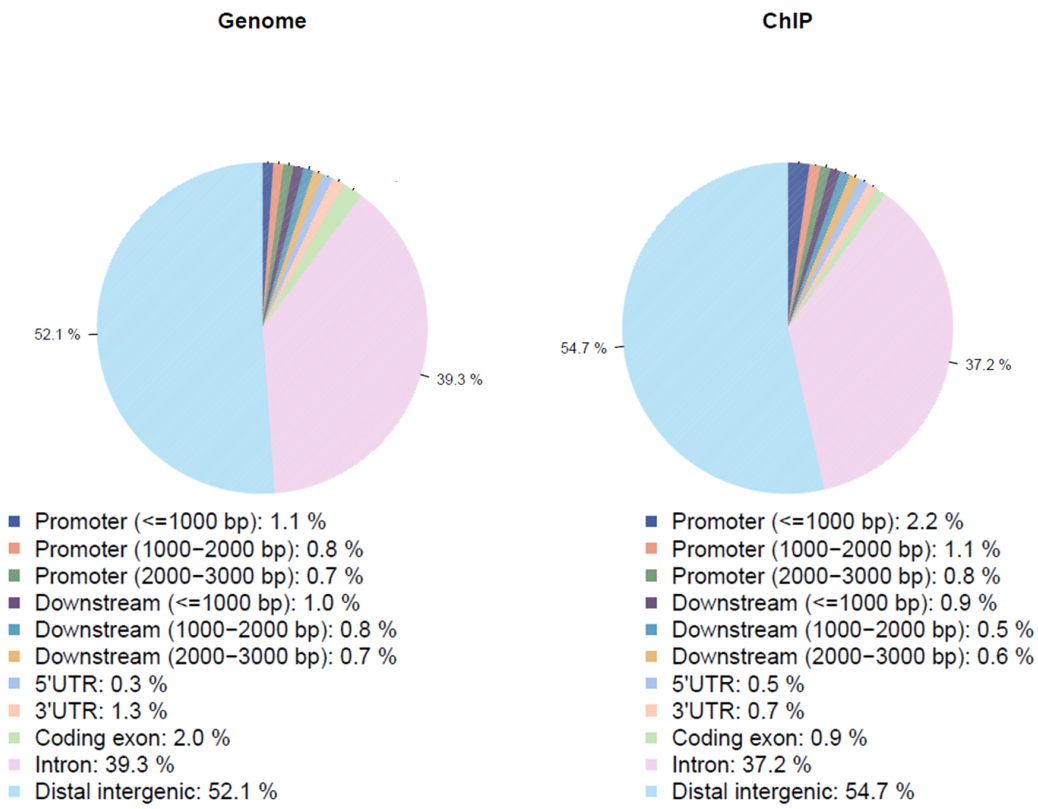

Figure 5-9 CEAS display of HIRA enriched regions spread over the indicated categories
Pie chart generated by CEAS presenting an overview of how ChIP regions are distributed across the genome over important gene features such as promoters, regions upstream/downstream and exons and introns.

With this analysis, only 54.7% of the 6625 peaks were classified as "distal intergenic". The higher proportion of "genic" regions with this method (46% with CEAS compared to 38% with the method described above) was mainly due to certain genes having multiple HIRA peaks (e.g *Epha3*-Figure 5-10).

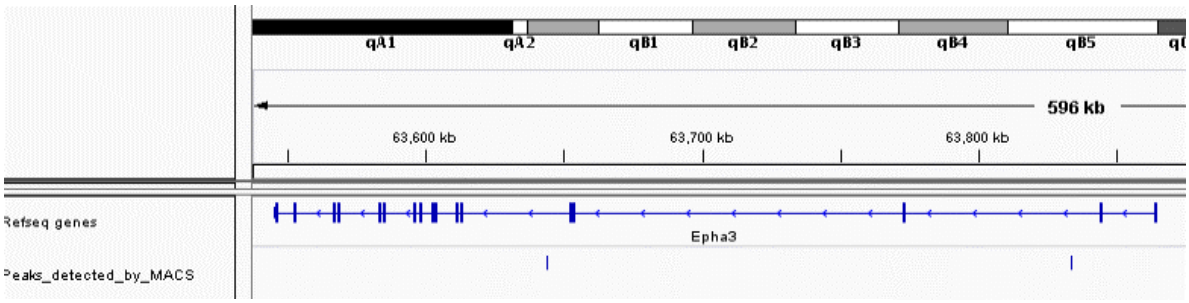

Figure 5-10 IGV screenshot of HIRA binding at the *Epha3* locus

This list of "HIRA enriched genes" was compared to the list of dysregulated genes obtained with the *Mesp1Cre;Hira*$^{fl/-}$ RNAseq dataset (Figure 5-11). A total of 47 genes, out of the 360 genes dysregulated in *Mesp1Cre;Hira*$^{fl/-}$ hearts have regions in their gene body (*Epha3*) or within +/- 5Kb (*Gata5*) with a predicted HIRA binding site(Figure 5-11). A hypergeometric probability test shows that this was not statistically significant (Figure 5-12).

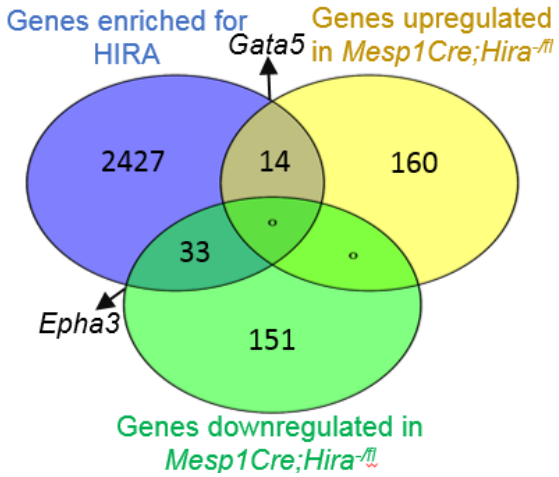

Figure 5-11 Venn diagram displaying the overlap between genes enriched with HIRA and genes significantly dysregulated in Mesp1 conditional *Hira* mutants

Venn diagram displaying the overlap between genes whose expression is dysregulated in E12.5 *Mesp1Cre;Hira*$^{-/fl}$ hearts and genes which are enriched for HIRA, as defined by the presence of a peak in the gene body and/or within 5Kb upstream of the TSS and downstream of TES

$$\mathbb{P}(x; n, a, b) = \frac{n!x!(b-x)!(a-x)!(n+x-a-b)!}{a!b!(n-a)!(n-b)!}$$

Figure 5-12 Equation for the calculation of a hypergeometric probability

Equation for calculation of the probability of having 47 genes (x) in common between two independent groups: 2515 (b, HIRA ChIPseq genes) and 360 (a, RNAseq data) in the mouse genome size which has approximately 22 000 genes (n). The result to this hypergeometric probability is: P(X >= 47) = **0.184**.
(https://www.geneprof.org/GeneProf/tools/hypergeometric.jsp)

However, most HIRA enrichment was situated outside genic regions, which suggested HIRA could have an impact on transcription by acting at distant enhancers, which are often situated over 5Kb away from a gene (Marsman and Horsfield, 2012) (see p96)

5.1.4) HIRA Binding motif

Out of the 6625 peaks obtained from the HIRA ChIPSeq, the binding motif most commonly found using the strand NGS software, with a total of 29,899 matches, was the consensus sequence CTCTCTCT or the reverse complement GAGAGAGA (Figure 5-13) a motif which binds the GAGA factor in *Drosophila melanogaster (van Steensel et al., 2003)*. This GA rich motif (GAGA motif) could be responsible, via other factors, for HIRA recruitment to the chromatin. These 29 899 matches mapped to 45% of peaks, since some peaks contained multiple GAGA motifs (Figure 5-15). Other motifs (see p46) from the Jaspar database were also detected in the 6625 peaks, which highly resemble the GAGA motif (Figure 5-14).

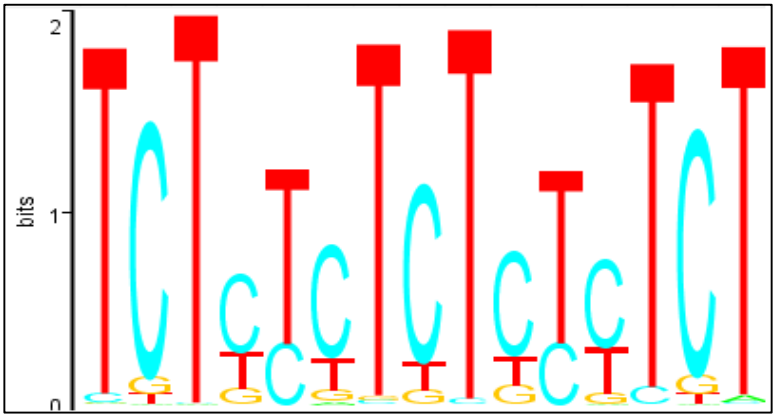

Figure 5-13 Matrix-based nucleotide profile displaying the motif that HIRA binds the most in the HIRA ChIPseq on E12.5 WT hearts

The DNA binding motif most prevalent in the HIRA ChIPseq (29 899 matches), extracted from the JASPAR database. The Y-axis represents how conserved a particular nucleotide is, across the whole genome. Positions that are perfectly conserved contain 2 bits, whilst 1 bit represents the base pairs which occur 50% of the time.

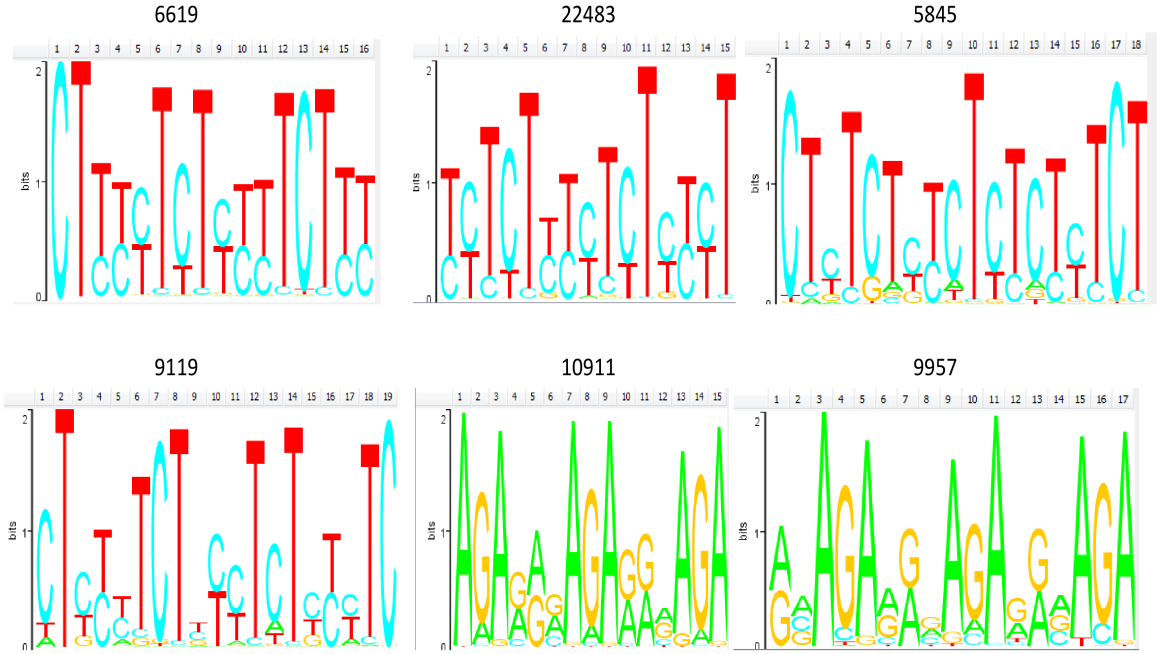

Figure 5-14 Matrix-based nucleotide profiles of HIRA ChIPseq

The DNA binding motifs similar to the GAGA motif are displayed here. The number of instances where the motifs were present in the HIRA ChIPseq's significant peaks are located above each panel.

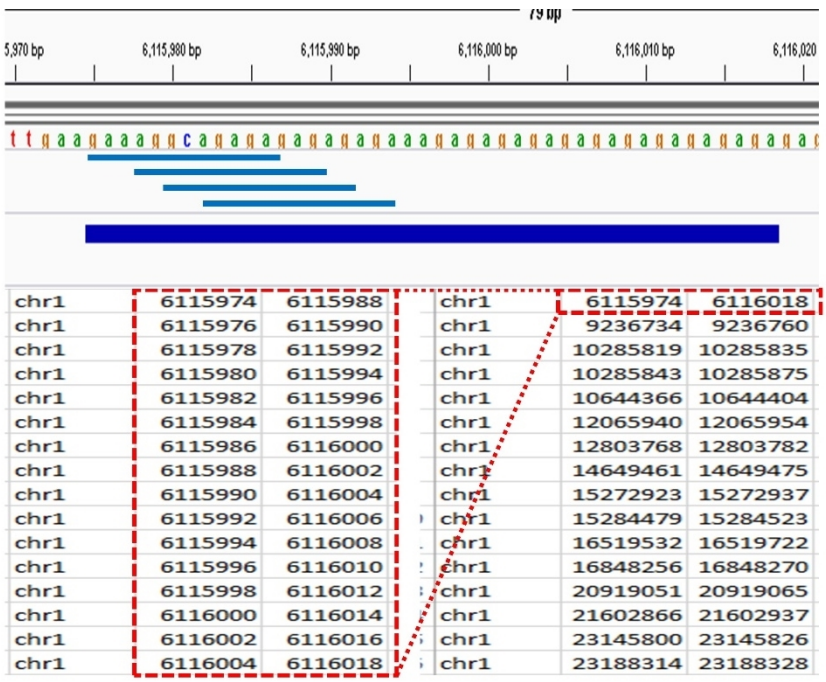

chr1	6115974	6115988	chr1	6115974	6116018
chr1	6115976	6115990	chr1	9236734	9236760
chr1	6115978	6115992	chr1	10285819	10285835
chr1	6115980	6115994	chr1	10285843	10285875
chr1	6115982	6115996	chr1	10644366	10644404
chr1	6115984	6115998	chr1	12065940	12065954
chr1	6115986	6116000	chr1	12803768	12803782
chr1	6115988	6116002	chr1	14649461	14649475
chr1	6115990	6116004	chr1	15272923	15272937
chr1	6115992	6116006	chr1	15284479	15284523
chr1	6115994	6116008	chr1	16519532	16519722
chr1	6115996	6116010	chr1	16848256	16848270
chr1	6115998	6116012	chr1	20919051	20919065
chr1	6116000	6116014	chr1	21602866	21602937
chr1	6116002	6116016	chr1	23145800	23145826
chr1	6116004	6116018	chr1	23188314	23188328

Figure 5-15 Example of multiple GAGA motifs between position 6115974 and 6116018 on chromosome 1

IGV screenshot with overlapping motifs displayed (top panel). Overlapping multiple motifs (horizontal blue bars) had to be clustered into one large region to determine the total number of peaks with a GAGA motif.

As discussed in the fourth chapter, the most upregulated gene from the RNAseq dataset was *Tnni2*. A HIRA peak containing the GAGA motif was detected in proximity of that gene.

5.1.5) HIRA is enriched in the vicinity of the *Tnni2/Tnnt3* loci

A significant peak 17Kb downstream of *Tnni2* and 38Kb upstream of *Tnnt3* was detected (Figure 5-16). This peak will now be referred as the *Tnni2/Lsp1/Tnnt3* (*TLT*) site. The next closed peak is located over 1Mb away.

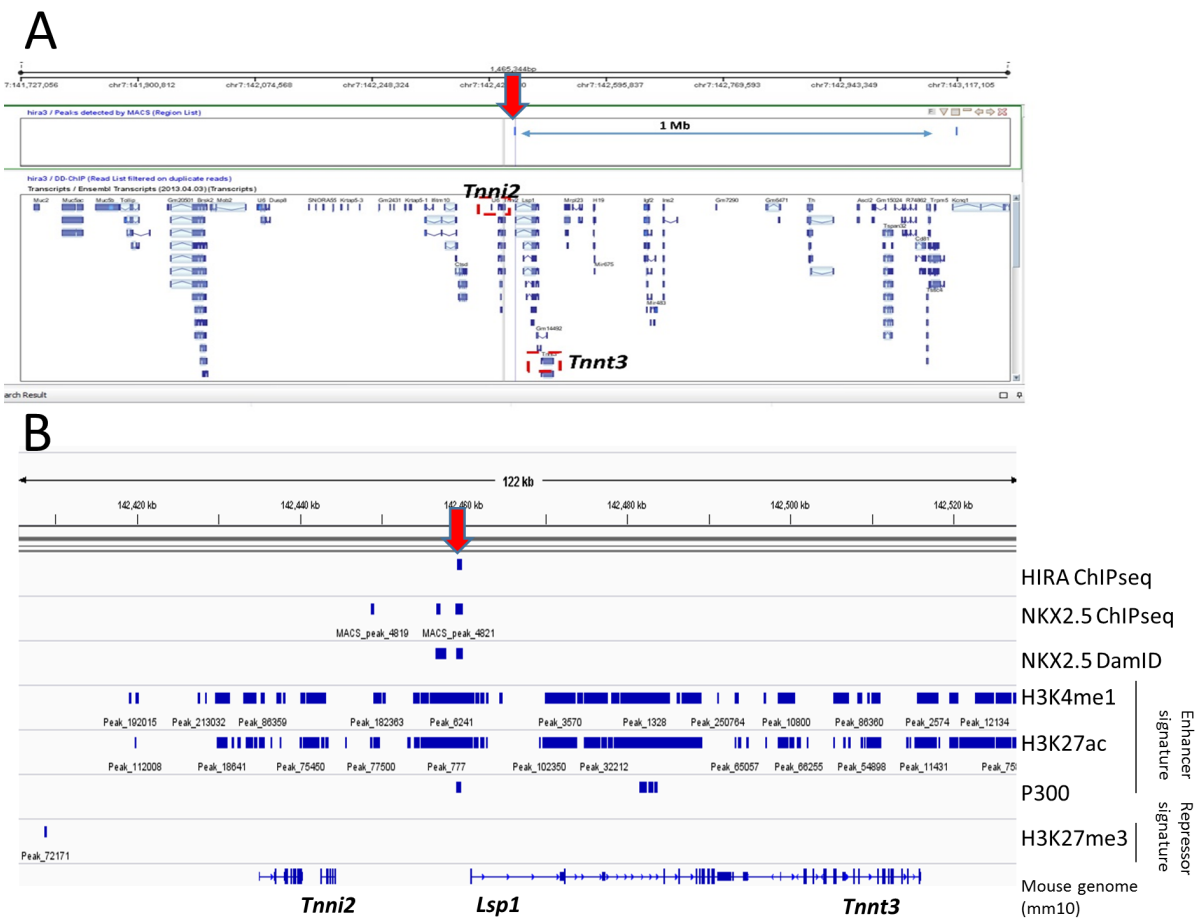

Figure 5-16 IGV profile showing the HIRA enrichment at the *TLT* locus

A. HIRA enrichment at the *TLT* site is situated between *Tnni2* and *Tnnt3* and is highly specific within that region. **B.** The HIRA enrichment overlaps with a NKX2.5 binding site in E11.5 hearts (Dupays et al., 2015) and in HL-1 cells (Bouveret et al., 2015), and enhancer signatures: histone modifications H3K4me1 and H3K27Ac in E13.5 hearts (Shen et al., 2012) and coactivator protein P300 binding in E11.5 hearts (Blow et al., 2010)

The expression of both *Tnni2* and *Tnnt3* was strongly upregulated in our mutant model (see p73). However, no dysregulation of *Lsp1* expression was observed. QChIP validation, in biological replicates, showed an average of 25 fold enrichment at the *TLT* site, compared to an intergenic region on chromosome 6 (Figure 5-17).

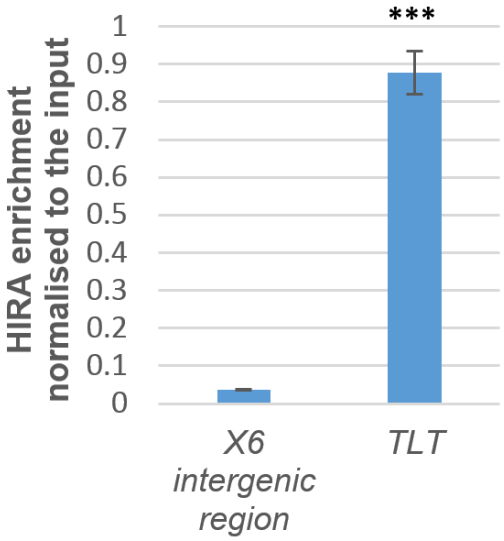

Figure 5-17 QChIP validation of the HIRA enrichment at the *TLT* locus

QChIP validation of the HIRA enrichment at the *TLT* locus. Data is normalized to the input (=100) and is representative of 2 independent experiments. Errors bars represent the min/max from technical duplicates. An intergenic region on chromosome 6 was used as a negative control. Unpaired t-test: $p<0.001$ ***

In addition, this region was of a particular interest for the following reasons: recent research on the role of the transcription factor NKX2.5 during cardiac differentiation revealed that *Tnni2* and *Tnnt3* are strongly upregulated at E11.5/E14.5 in the hearts of embryos with a hypomorphic mutation of *Nkx2.5* and NKX2.5 ChIP experiment in WT E11.5 hearts also revealed a strong enrichment of NKX2.5 at the *TLT* site *(Dupays et al., 2015)*. The authors argue that this site serves as a common enhancer for *Tnni2* and *Tnnt3*, a contention supported by a luciferase assay. Genome wide analysis showed that in general overlap between HIRA and NKX2.5 enrichment is rare (2.98%) (Figure 5-18). In addition, an overlap of 9 genes was found between the set of upregulated genes in *Hira* conditional mutants and the *Nkx2.5* hypomorphic model, including *Tnni2* and *Tnnt3* (Figure 5-18). Moreover, H3K4me1 and H3K27Ac histone modifications in the heart at E11.5 and E13.5, which define putative enhancer elements, were also found to be overlapping at this region (Shen et al., 2012) (downloaded from www.encodeproject.org). H3K27me3, which is regarded as a repressive signal (Kim and Kim, 2012), is not present at the *TLT* site. P300, which defines enhancer regions in the developing heart also binds the *TLT* site (Blow et al., 2010) (Figure 5-16). Out of the 3000 genome wide P300 bound regions, this study indicates that 4.3% (130) candidate regions were selected and validated using transgenic mouse assays. P300 bound regions therefore strongly represent enhancer regions in the developing heart. 80.7% of the regions enriched for both

HIRA and NKX2.5 were found to be in sites coinciding with enhancer chromatin signatures (Figure 5-19).

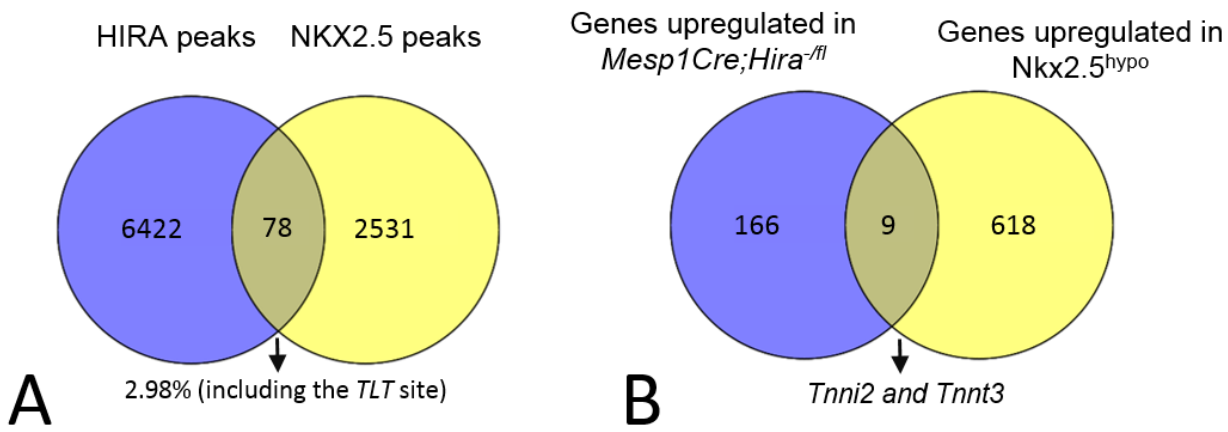

Figure 5-18 Venn diagrams displaying genome wide overlap of HIRA and NKX2.5

A. Venn diagrams representing the overlap between loci associated with HIRA and NKX2.5. **B.** Overlap between the sets of upregulated genes in both mutant models.

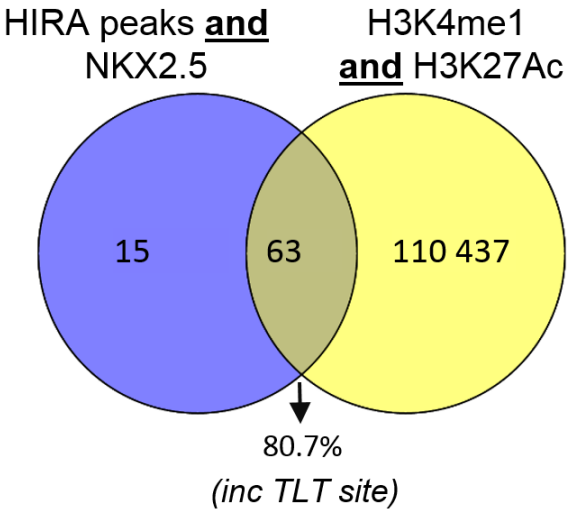

Figure 5-19 Venn diagram displaying HIRA and NKX2.5 enriched regions overlapped with enhancer marks

5.2) HIRA interacts with BRG1 and WHSC1 in the developing heart

HIRA is often part of multiprotein complexes and serves various functions dependent upon the developmental stage and/or tissue it is expressed in. These roles are likely dependent upon the nature of HIRA's interaction partners. Using knowledge of protein interactions outside the cardiovascular system, potential HIRA-partners were investigated *in vivo.*

5.2.1) HIRA interacts with BRG1 but does not interact with HDAC1 and HDAC2 in the heart

BRG1 (Brahma-related gene 1) is the catalytic ATPase subunit of the SWI/SNF chromatin remodelling complexes BAF and PBAF (Ho and Crabtree, 2010, Vradii et al., 2006)

which alter chromatin structure to allow DNA accessibility is known to be important for heart development (see p20). A genetic interaction between ASF1 (part of the HUCA complex) and the Brahma complex has been described previously in the fly (Moshkin et al., 2002). In yeast (*Saccharomyces cerevisiae*), three components of the SWI/SNF chromatin remodelling complex were found to physically Interact with Hir1p and Hir2p, the yeast homologues of HIRA (Dimova et al.). In HeLa cells, ChIPseq experiments investigating known transcription factors and transcription regulators revealed that the HUCA complex and the SWI/SNF ATP dependent chromatin remodeling complex (BRG1, INI1, BAF155 and BAF170) had a significant genome-wide overlap, with BRG1 and HIRA sharing over a third of binding sites across the genome (Pchelintsev et al., 2013a). HIRA has been found to interact with Clr6 (orthologue to human HDAC1) in the yeast (Yamane et al., 2011), to promote global histone deacetylation. In fibroblasts cells (COS7), HDAC1 and HDAC2 were found to form a complex with HIRA which could regulate chromatin assembly/maintenance (Ahmad et al., 2003). The role of HDACs in ESC differentiation and in the heart has been well characterised (see p15). Co-immunoprecipitation of material from WT embryos revealed that HIRA and BRG1 interact, at E12.5 and E14.5 in the heart but no interaction between HIRA and HDAC1/HDAC2 was detected (Figure 5-20). The HIRA antibody used for western blot (WC119) was not always reliably produced which made verifying the HIRA IP challenging.

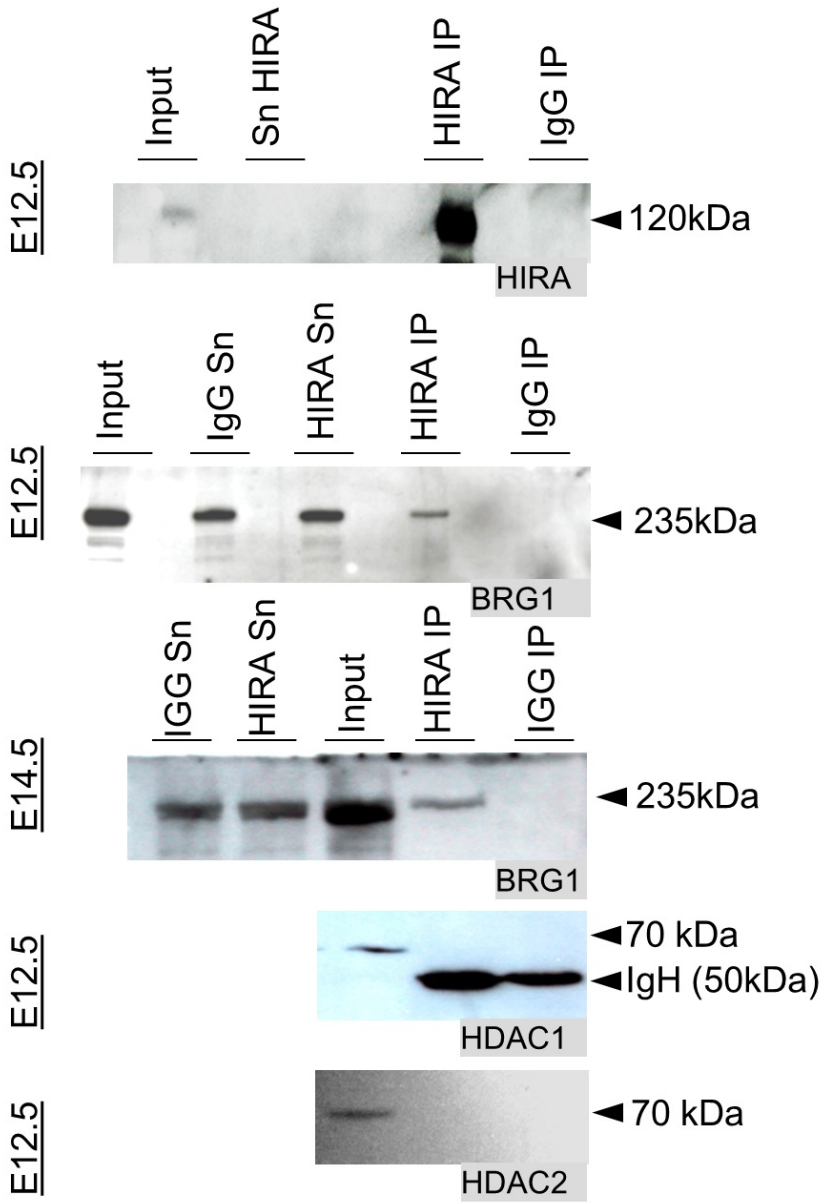

Figure 5-20 HIRA interacts with BRG1 and does not interact with HDAC1/2 in the embryonic heart

Western blotting of immunoprecipitates (HIRA IP) or whole cell protein lysates (input) at E12.5 and E14.5 using WT hearts. An interaction between HIRA and BRG1 was detected in both stages. No interaction between HIRA and HDAC1/2 was detected at E12.5

5.2.2) HIRA interacts with WHSC1

Wolf-Hirschhorn syndrome candidate 1 (WHSC1) is a HMTase known to methylate histone H3 at lysine 36 (H3K36) (Popovic et al., 2014) (see p21). In interferon stimulated mouse embryonic fibroblasts, HIRA has been shown to interact with WHSC1 (Sarai et al., 2013). Interestingly, WHSC1 regulates the function of NKX2.5 in the embryonic heart (Nimura et al., 2009). As described above, NKX2.5 binds the *TLT* site and directly represses *Tnni2/Tnnt3* (Dupays et al., 2015). Therefore, I was decided to test whether the HIRA-WHSC1 interaction took place in hearts. Co-immunoprecipitation revealed that HIRA and WHSC1 interacted *in vivo* at E12.5 and E14.5 in the heart (Figure 5-21).

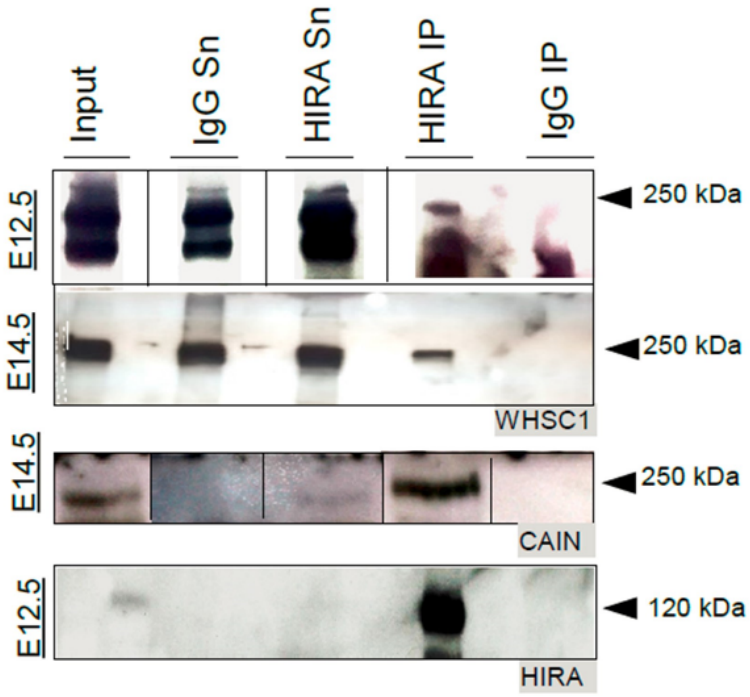

Figure 5-21 HIRA interacts with WHSC1 in the embryonic heart

Western blotting of immunoprecipitates (HIRA IP) or whole cell protein lysates (input) with HIRA at E12.5 and E14.5 using WT hearts. An interaction between HIRA and WHSC1 was detected in both stages. CAIN (CABIN1) is a member of the HUCA complex and served as positive control for HIRA co-IP.

5.3) Discussion

The occupancy of HIRA across the genome at E12.5 in the developing heart revealed that approximately two-thirds of HIRA enriched regions are intergenic and that the most upregulated gene in the absence of HIRA, *Tnni2*, has a HIRA binding site 17Kb downstream. In addition, HIRA interacts with a chromatin remodelling protein (BRG1) and a HMTase (WHSC1) which suggests that HIRA has a specific set of co-regulators during heart development.

5.3.1) Enhancers and H3.3 deposition

Since the overlap between HIRA enriched genes and genes dysregulated in *Mesp1Cre* conditional *Hira* mutants did not reach statistically significant levels (see p88), it is possible that HIRA acts on enhancers situated over 5Kb from the gene body. Enhancers are DNA elements that activate transcription by recruiting tissue-specific transcription factors (TF) and other co-factors required to assemble the pre initiation complex (Kornberg, 2007). Enhancer sequences often contain multiple recognition sequence to allow the binding of TFs (He et al., 2012). However, in the fly, some enhancers can remain neutral when only bound by small level of TFs (Li et al., 2008). Enhancer-bound TFs can bind chromatin modellers which create nucleosome free regions or bend DNA to ultimately render a gene accessible for transcription initiation or elongation (Clapier and Cairns, 2009). A genome-wide characterization of enhancer-promoter interactions in CD4+ T cells revealed that 56% of enhancers were within 50

kb and 44% were further than 50 kb from the gene body (Chepelev et al., 2012). In addition, this study showed that 25% of promoters associate with more than one enhancer. Some enhancers can be very distant from a gene as demonstrated by the 900kb upstream enhancer of *POU3F4* (de Kok et al., 1996). Enhancers can even be located in exons of nearby genes, as demonstrated by H3K4me1, H3K27ac, and P300 (the same marks which were used for the HIRA ChIPseq analysis) which are present in 7% of coding exons in the limb of mouse embryos at E11.5 (Birnbaum et al., 2012). This suggests that chromatin has to loop for this enhancer-promoter interaction to take place. Chromosome conformation capture (3C) involves crosslinking chromatin with formaldehyde in live cells, digesting DNA with restriction enzymes, and then religating DNA strands together before amplifying these new fragments by PCR. A successful amplification using a pair of distal primers (e.g. 40Kb) would indicate a chromatin loop in that region. This technique can provide evidence for interactions between spatially separated regions of chromosomes, and was first used in the context of β-globin genes. In the embryonic brain where erythroid cells are not produced, the globin cluster was found to be linear, as opposed to the liver which produces erythroid cells, where chromatin loops of 40 to 60 kb were detected (Tolhuis et al., 2002). However, looping is not always associated with enhanced gene activity. For example, a higher order chromatin loop around the *Brac1* gene was observed, which promotes promoter and terminator interactions, thereby repressing expression of that gene. Upon oestrogen stimulation of the human breast carcinoma MCF7 cell line, this loop unfolds, followed by increased *Brac1* mRNA levels (Tan-Wong et al., 2008). Similarly, the upregulation of *SAMD4A* following TNF-α stimulation has been linked to the rupture of a "whole-gene" loop across its 221Kb gene body (Larkin et al., 2012). Within this gene, many "subloops" seemed to grow between transcribed regions during transcription. It was shown that the "whole-gene" loop, between the 3' and 5' end of *SAMD4A* is dependent on the transcriptional repressor CTCF (CCCTC-binding factor), which links those chromatin sites together. CTCF, the "master weaver", is responsible for coordinating the structural 3D organisation of genes by forming intra- and inter-chromosome interactions (Phillips and Corces). A 3C experiment could indicate if the *TLT* site does come into proximity of the *Tnni2* or *Tnnt3* promoters and if so, whether this interaction is increased in the hearts of *Mesp1Cre;Hira*$^{fl/-}$ embryos at E12.5.

It is also interesting to note that in ESCs differentiated to cardiomyocytes (Wamstad et al., 2012), the *TLT* locus becomes enriched for the enhancer marks H3K4me1 and H3K27Ac at the differentiated cardiomyocytes stage, compared to undifferentiated ESCs (Figure 5-22), giving further evidence for the enhancer characteristics of the *TLT.*

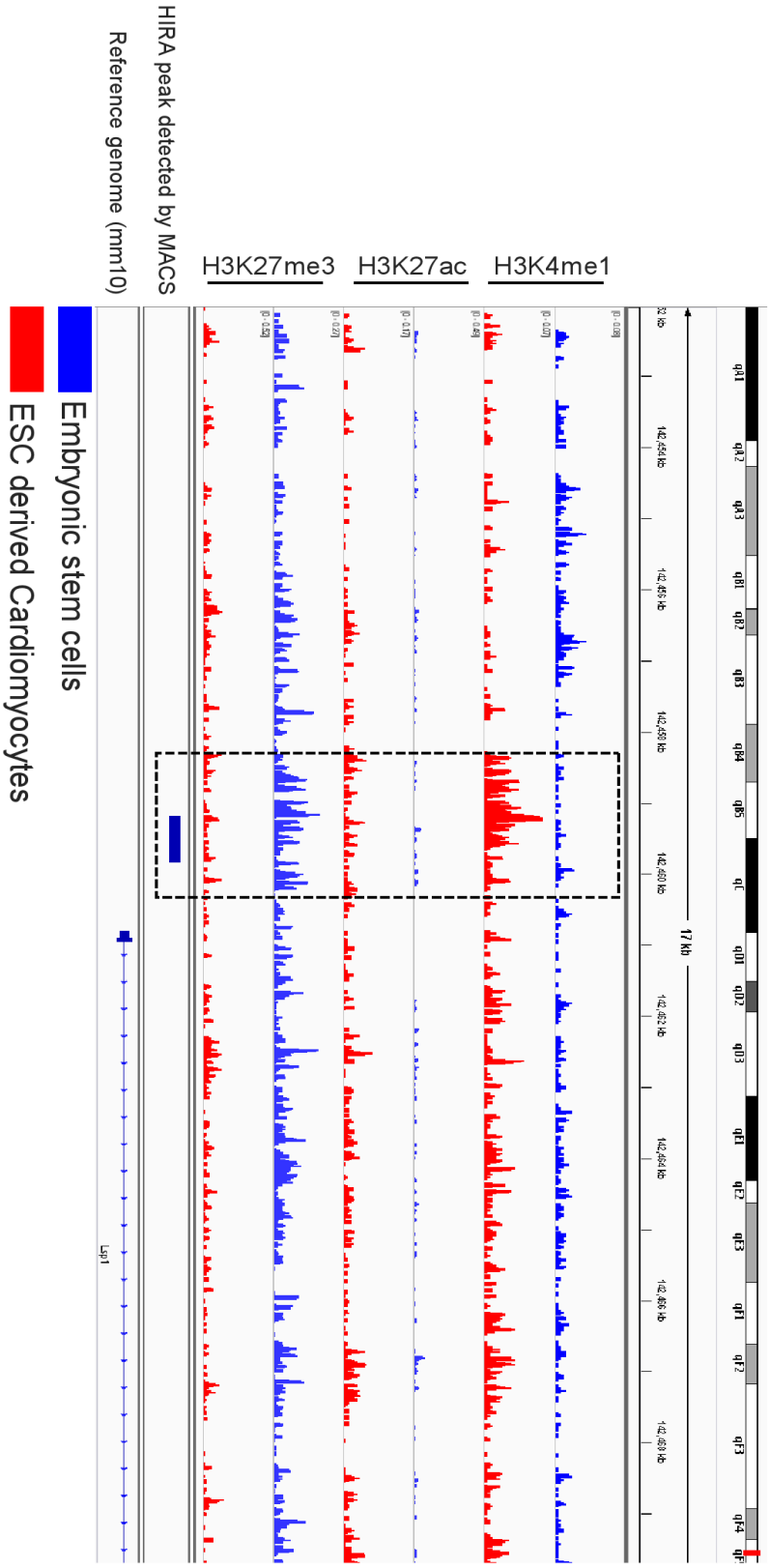

Figure 5-22 Histone enrichments at the *TLT* showing the characteristics of an enhancer in ESC derived cardiomyocytes compared to embryonic stem cells

The enrichment of H3K4me1 and H3K27ac and the lack of repressive H3K27me3 modifications represent a distinct chromatin pattern observed in active enhancers (black box around the *TLT*). The development of this pattern mirrors the upregulation of Tnni2 seen during the differentiation process and supports the association of the *TLT* enhancer with its expression. Histone ChIpseq in ESC derived cardiomyocytes and ESCs were obtained from Wamstad and colleagues (Wamstad et al., 2012) (Gnomex accession numbers 44R and 7R2).

As mentioned in p25, HIRA deposits H3.3 predominantly in genic regions of ESCs, and also at a subset of enhancer and intergenic regions (Goldberg et al., 2010). In parallel with my PhD project, Rasha Saleh has been working with a model of ESCs differentiating over the course of fifteen days towards cardiomyocytes. H3.3 tagged WT and *Hira*

-null ESCs have been used to observe HIRA and H3.3 occupancy by ChIP at various stages of differentiation. A significant enrichment of HIRA (3.5 fold) and H3.3 (7.7 fold) was detected at the *TLT* site at day 15 of differentiation (Figure 5-23). The H3.3 enrichment was quasi absent in *Hira*-null ESCs at day15, suggesting that the deposition of this histone variant is HIRA dependant.

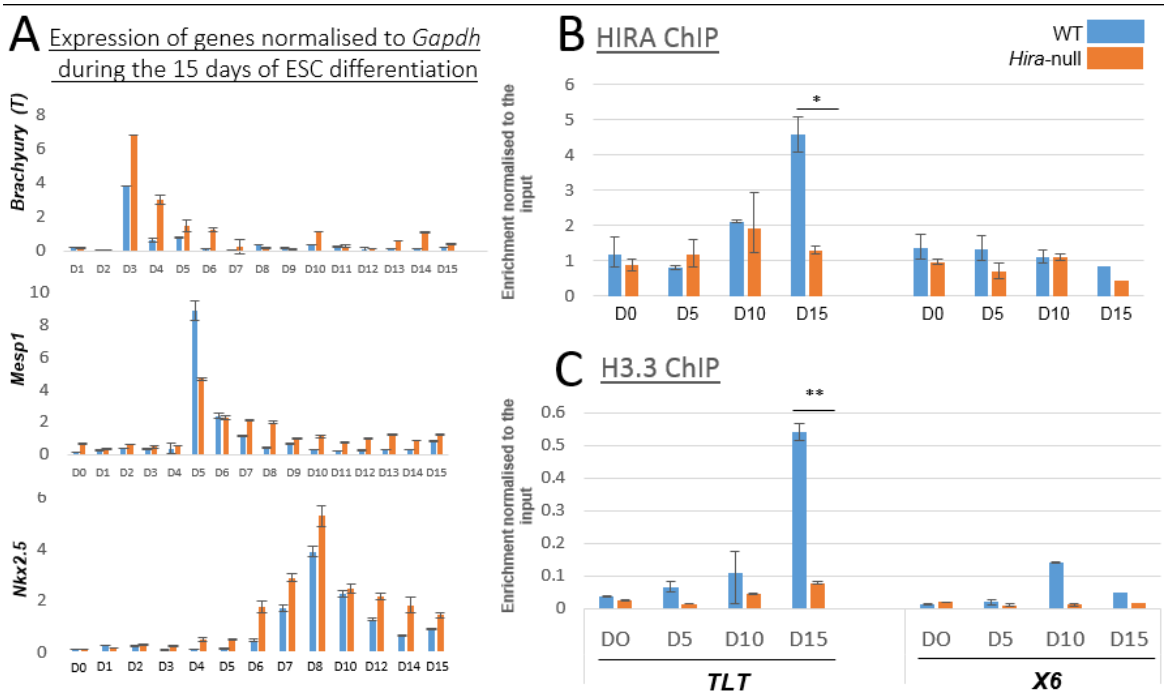

Figure 5-23 HIRA and H3.3 Chip during ESC differentiation

QRT-PCR of *Brachyury (T), Mesp1 and Nkx2.5* over the first 15 days of WT and *Hira*-null ESC differentiation. Data are presented as levels of mRNA normalized to *Gapdh* and are representative of five independent experiments. Errors bars are calculated from the standard deviation of technical triplicates (A). HIRA and H3.3 qChIP on differentiating ESC shows an enrichment of HIRA at the *TLT* site at day 15 (B&C). Unpaired t-test: p<0.05 *, p<0.01 **. E*xperiments carried out by Rasha Saleh and included with her permission.*

H3-H4 tetramers do not normally dissociate during replication dependent nucleosome assembly. However, experiments in HeLa cells revealed that splitting events were occurring in H3.3-H4 tetramers, but not in H3.1-H4 tetramers (Xu et al., 2010). In addition, electron microscopy analysis and sedimentation velocity experiments have shown that H3.3

incorporation perturbs the intramolecular folding of nucleosomal architecture (Chen et al., 2013). Taken together, these results suggests that, at the *TLT* site, H3.3 enriched chromatin adopts a looser and more open structure. Since enhancers often require a combination of TFs to have a significant effect on gene transcription (Spitz and Furlong, 2012), the lack of H3.3 at the *TLT* site could potentially affect the accessibility of NKX2.5 (which has been shown to act as a repressor at this site (Dupays et al., 2015)), and the transcriptional coactivator P300 in *Mesp1Cre;Hira*$^{fl/-}$ embryos by impacting higher ordered chromatin folding.

Further investigation of the 78 sites with a HIRA and NKX2.5 overlap revealed that 63 have enhancer signatures. The list of genes within 50Kb of these 63 regions was compared to the genes significantly dysregulated in *Mesp1Cre;Hira*$^{fl/-}$ embryonic hearts at E12.5. In addition to the previously mentioned *Tnni2* and *Tnnt3*, 3 genes were identified: *Clcnkb*, *Abca4* and *Slc9a3r1*. Similarly to *Tnni2* and *Tnnt3*, all three were upregulated 2.9, 1.72 and 1.53 fold, respectively. Although there are too few loci to draw conclusions, this pattern could imply that HIRA and NKX2.5 co-regulate targets during heart development.

5.3.2) HIRA is enriched at the *Epha3* locus

Two significant sites of enrichment of HIRA were detected within intronic regions of *Epha3 (*Figure 5-10*),* suggesting that HIRA could be involved in transcription activation at this locus. There were no NKX2.5 binding sites by ChIPseq (Dupays et al., 2015) or by DamID (HL-1) (Bouveret et al., 2015) in the vicinity of that gene. *Epha3* expression was not altered in *Nkx2.5* hypomorphs (Dupays et al., 2015). Thus, HIRA might co-localise with different cofactors at this locus. Another possibility is the potential for HIRA enrichment at the gene body to deposit H3.3 and thus directly impact transcription rate, by loosening chromatin, rather than acting on enhancers. 72.5% of genes enriched for HIRA in their gene body only (as opposed to gene body and +/- 5Kb) were found to be downregulated in *Mesp1* conditional mutants (Table 5-1).

Table 5-1 Genes enriched for HIRA in their gene body cross-linked with genes dysregulated in *Mesp1* conditional mutants

Genes dysregulated in *Mesp1* conditional mutants and enriched in HIRA at the gene body	
Upregulated (11)	Downregulated (27)
Abca4	**Adam22**
Cdh4	**Adamtsl2**
Gas2	**Antxr2**
Kbtbd12	**Cacna2d1**
Lmod3	**Cfh**
Padi2	**Col8a1**
Rims2	**Cx3cr1**
Scn8a	**Eln**
Sgip1	**Epha3**
Slc9a3r1	**F13a1**
Tnfrsf1b	**Gatsl2**
	Gfra1
	Grid2
	Il1rap
	Itga8
	Kcnd2
	Kcnd3
	Luzp2
	Masp1
	Ndst4
	Nr3c2
	Pard3b
	Prkar1b
	Reln
	Rgs8
	Ryr3
	Scube2
	Sntb1
	Tnik

In order to test whether HIRA influences chromatin compaction a digestion of chromatin by micrococcal nuclease (MNase) (Yamasaki et al., 2007) could be performed. This enzymatic test digests unprotected DNA and can be used to measure the impact of histone chaperones on chromatin structure (Schneiderman et al., 2012). However, it does not distinguish between histone variants, but rather quantifies nucleosome distribution. In addition, a DNase hypersensitivity assay could test the level of chromatin compaction at a particular sites. This assay is often used as a readout of the accessibility a given region, which could partially reflect a local enrichment of H3.3. An interesting epigenomic profiling experiment is the recently developed "assay for transposase-accessible chromatin using sequencing" (ATAC-seq) which, by directed *in vitro* transposition of sequencing adaptors into native chromatin can identify regions of open chromatin and nucleosome-bound/free regions at specific loci (Buenrostro et al., 2013). Alternatively, the nucleosome turnover rate could be quantified. H3.3 deposition has often been measured in nucleosome turnover studies (Deal et al., 2010), since the RI H3.3 deposition necessitates unwrapping of the DNA around the histone core. Interestingly, in *Drosophila melanogaster,* this replacement occurs prominently in the gene body of transcribed regions of active genes (Mito et al., 2005).

5.3.3) HIRA, FACT and GAGA factor

Many histone chaperones do not directly bind naked DNA (Ray-Gallet et al., 2011). However, experiments in HeLa cells by Almouzni *et al* have shown that 3 members of the HUCA complex (HIRA, UBN1 and CABIN1) can directly bind nucleotides (Ray-Gallet et al., 2011). The same research team stated that in HeLa cells, HIRA-dependent H3.3 enrichment did not have "apparent sequence specificity". In other model systems such as the plant Arabidopsis, HIRA is thought to be recruited to, and repress, the knotted-like homeobox genes via the ASYMMETRIC LEAVES DNA binding proteins, which have loose homology to the MYB family of vertebrate transcription factors (Guo et al., 2008). Surprisingly, the overrepresentation of GA rich motif observed in the HIRA ChIPseq, which might be responsible for HIRA recruitment, was observed in 45% of HIRA binding sites. The core consensus within this site was GAGAGAGA and is equivalent to that first identified in *Drosophila* as the binding site for the GAGA factor, itself a transcriptional regulator (Adkins et al., 2006). In *Drosophila*, H3.3 deposition is directed by the GAGA factor and FACT (facilitates chromatin transcription) (Nakayama et al., 2007). DNAse hypersensitivity assays revealed that this complex can maintain gene expression by protecting certain loci from heterochromatin spreading (Nakayama et al., 2007). Interestingly, the GAGA factor-FACT complex also associates with HIRA and was found to bind DNA in a sequence specific manner (GAGAG cluster) (Nakayama et al., 2007). These proteins were found to be part of a very large complex, including the polybromoassociated Brm (PBAP) remodeling complex, which together direct H3.3 replacement to establish chromatin boundaries at HOX loci (Nakayama et al., 2012). These GAGAG sites also display an increase of H3K4 methylation and a reduction of H3K9 methylation (Nakayama et al., 2007), a combination typical of active chromatin which has been associated with the deposition of H3.3 in Drosophila *(McKittrick et al., 2004).* FACT has been studied in the context of disassembly and re-assembly of chromatin during transcriptional elongation (Belotserkovskaya et al., 2003) but has also been identified as a histone chaperone of H2A/H2B (Kemble et al., 2015). A model has been suggested in which FACT anchors and displaces a H2A-H2B pair, thus allowing PBAP to bind to and displace a H3-H4 tetramer. This process creates accessible nucleosome free regions for the HUCA complex to deposit H3.3 (Figure 5-24).

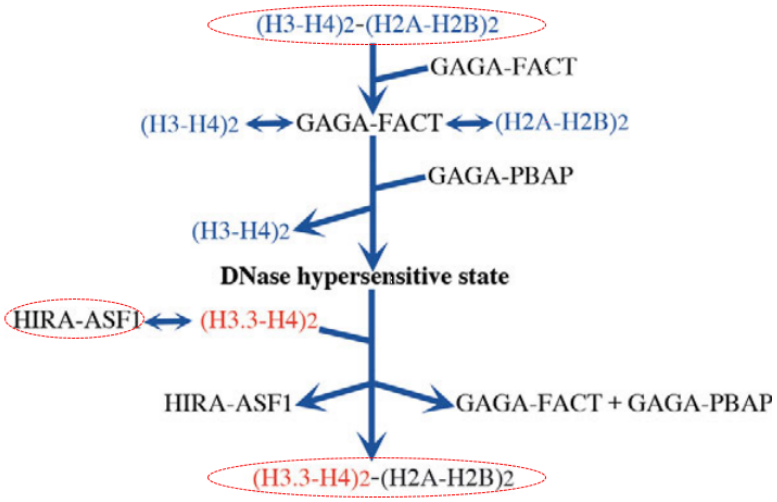

Figure 5-24 H3.3 replacement model involving FACT and the GAGA factor in Drosophila

Schematic model showing how the GAGA factor can recruit FACT and PBAP to a chromatin boundary to create nucleosome free regions which allows the HUCA complex (HIRA-ASF1) to deposit H3.3. Adapted from (Nakayama et al., 2012).

Most of the polycomb group (PcG) and trithorax group (trxG) proteins in Drosophila have vertebrate homologues. However, finding a homologue for the GAGA factor has been challenging. Bioinformatics and antibody cross-reactivity between the fly and humans have identified the POZ-Kruppel-like factor c-Krox/Th-POK, which is encoded by the Z*btb7b* (also Zfp67) gene (Matharu et al., 2010). Th-POK has been linked to CD4/CD8 lymphocyte lineage commitment (He et al., 2005). A more recent strictly *in silico* study has revealed that the mouse homologue of the GAGA factor could be a slightly different gene: *Zbtb3* (*Th-POK*) (Kumar, 2011), a protein that binds to chromatin boundary elements in a muscle cell line, although no *in vivo* studies have been undertaken (Srivastava et al., 2015).

5.3.4) Interaction between HIRA and WHSC1 suggests the formation of a tri-complex at the *TLT* site

As mentioned in p90, HIRA and NKX2.5 at the *TLT* site, both in the HL-1 cardiomyocyte cell line by DamID (Bouveret et al., 2015) and in embryonic hearts at E11.5 by ChIPseq (Dupays et al., 2015). Moreover, in hearts of E11.5 and E14.5 embryos with a hypomorphic allele of *Nkx2.5* there was upregulation of *Tnni2* and *Tnnt3 (Dupays et al., 2015)* mirroring what was observed in *Hira* conditional mutants at E11.5 and E12.5. Interestingly, in the heart development, NKX2.5 interacts with the HMTase WHSC1 to repress the expression of specific genes involved in cardiac morphogenesis (Nimura et al., 2009). Furthermore, work carried out by Rasha Saleh suggests that the HIRA-WHSC1 interaction is specific to fully differentiated cardiomyocytes, since these protein were only found to interact in ESCs after fifteen days of differentiation towards cardiomyocytes (Figure 5-25).

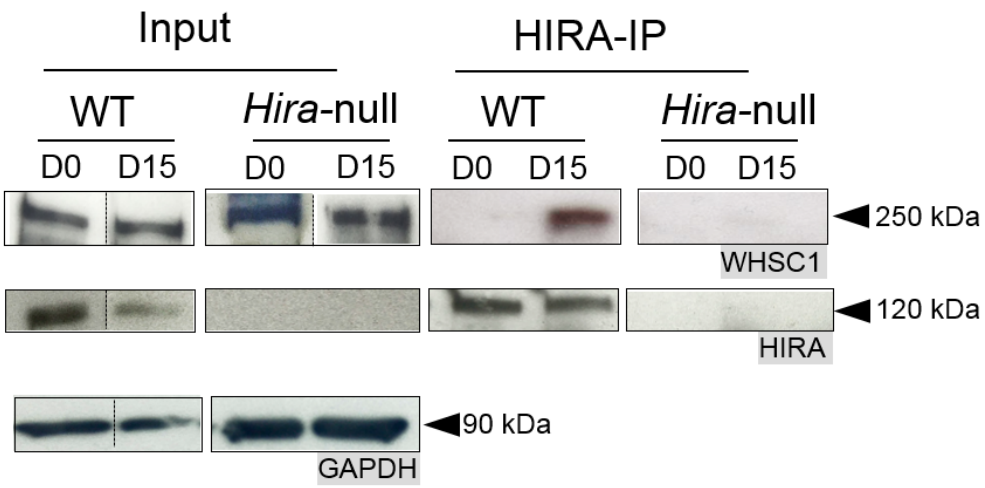

Figure 5-25 HIRA interacts with WHSC1 during ESC differentiation towards cardiomyocytes

Western blotting of immunoprecipitates with HIRA (HIRA IP) or whole cell protein lysate (before immunoprecipitation) from WT and *Hira*-null ESCs on undifferentiated ESCs (D0) and ESCs differentiated towards cardiomyocytes (D15). HIRA was found to interact with WHSC1 at day 15 of differentiation. E*xperiments carried out by Rasha Saleh and included with her permission.*

Remarkably, this HIRA-WHSC1 interaction occurred at the same stage during which an enrichment of HIRA at the *TLT* site was observed (Figure 5-23). This suggests that the formation of a HIRA-WHSC1-NKX2.5 complex which is likely to directly impact transcription during cardiogenesis (see final chapter).

Chapter 6 Overall conclusion and future work

6.1) Final discussion and conclusion

Hira encodes a histone chaperone whose major function is to deposit the variant histone H3.3 within chromatin, and which plays an essential role in regulating chromatin structure stability. HIRA-dependent H3.3 deposition has been linked to important biological processes, such as intellectual disability (Chen et al., 2015), fertilization (Bonnefoy et al., 2007) and response to stress (Chujo et al., 2012a). In my PhD project, the role of HIRA was investigated during the post gastrulation stage of vertebrate development. Conditional mutagenesis was employed to study heart development. The heart is the first organ to fully form during development and presents with complex morphological dynamic changes, which require a tight regulation of numerous genes. The early lethality of *Hira* null embryos was successfully bypassed which was necessary for investigating HIRA's role in the different cardiogenic lineages.

HIRA has been shown here to play an important role in heart development and by extension, in embryonic survival. Cardiogenic mesoderm ablation of *Hira* (*Mesp1Cre)* resulted in cardiac malformations and embryonic lethality. Other conditional *Hira* mutations within the cardiogenic lineages resulted in milder abnormalities or absence of cardiac defects. *Nkx2.5Cre* conditional *Hira* mutants, in which *Hira* was ablated in cardiomyocytes, resulted in embryonic lethality in 89% of cases, 56% of embryos at E15.5 presented with a VSD and 33% with a constriction of the pulmonary trunk. However, the lack of phenotype in the anterior SHF specific *Mef2cCre;Hira*$^{fl/-}$ mutants suggests that *Hira* is required in the FHF and ablation in the SHF has little effect or acts to exacerbate the phenotype of FHF mutants. In addition, *Tie2Cre* and *Wnt1Cre* conditional *Hira* mutants, which tested the requirement of HIRA in the endothelial and neural crest cell populations, respectively, did not show any cardiac abnormalities. A requirement for HIRA in those tissues is not ruled out since *Tie2Cre Hira* conditional mutants suffer from a growth defect postnatally and *Wnt1Cre* conditional *Hira* mutants die at birth. As *Mesp1Cre* is expressed 24h prior to *Nkx2.5Cre* (E6.5 versus E7.5), it is possible that HIRA activity is particularly crucial during the early differentiation steps of multipotent cardiovascular progenitors.

Following ablation of *Hira* in the cardiogenic mesoderm, less than 2% of the genes expressed in the heart at E12.5 were significantly up- or downregulated. HIRA activity is required for correct level of expression of troponins which directly affect cardiac contractility and *Epha3,* a tyrosine kinase receptor critical for the formation of atrioventricular cushions. The deregulation of these genes during cardiogenesis are likely to be responsible for the VSD and the oedema observed at E15.5 in *Mesp1cre* conditional *Hira* mutants. The aberrant

expression of certain genes in the heart is consistent with the previously described association with genes poised for transcriptional activation (Huang and Zhu, 2014, Chen et al., 2013). This data suggests that HIRA modulates chromatin structure which would then affect the accessibility of the transcriptional machinery to regulatory elements.

In order to investigate a potential direct impact of HIRA on transcription, the HIRA genome wide occupancy in the heart was analysed by ChIPseq at E12.5. The heart is constituted of a mixed population of cells, however the majority (65 to 70%) at E18.5 are cardiomyocytes (Banerjee et al., 2007) with the remaining 30% being fibroblasts, endothelial cells, and vascular smooth muscle. The ratio is probably of a similar order at E12.5. HIRA binding sites poorly correlated with altered gene expression. However, the majority of HIRA bound regions were found to be "distal intergenic" and as previously discussed (see p96), there still is an incomplete picture of enhancers across the genome of the animal kingdom (Shlyueva et al., 2014). In an effort to investigate HIRA's potential involvement with known chromatin regulators involved in heart development, a series of co-immunoprecipitation were carried out. BRG1 and WHSC1 were found to interact with HIRA at E12.5 and E14.5. WHSC1 is known to bind NKX2.5, a major cardiac transcription factor (Nimura et al., 2009). NKX2.5 was recently found to bind to the common enhancer of *Tnni2* and *Tnnt3* (*TLT* site) (Dupays et al., 2015). Remarkably, HIRA was also found to bind that exact region by ChIPseq and qChIP. This region was identified as an enhancer by Dupays *et al*, which was further confirmed by the overlapping of H3K4me1/H3K27Ac histone enhancer signatures (Shen et al., 2012) as well as P300, a enhancer binding protein known to regulate genes during cardiac development (Blow et al., 2010) (Figure 5-16). RNAseq analysis revealed that *Tnni2* was the most upregulated gene in *Mesp1Cre;Hira*$^{fl/-}$ embryonic hearts, which suggests a mechanism in which HIRA negatively regulate this gene during cardiogenesis. Work carried out by Rasha Saleh demonstrated that the HIRA enrichment at the *TLT* site is necessary for H3.3 deposition and is specific to differentiated ESCs. A model can be proposed in which HIRA binds to GAGA rich regions, and acts in concert with NKX2.5 and WHSC1 at the *TLT* site to deposit H3.3, thus regulating certain target genes (Figure 6-1).

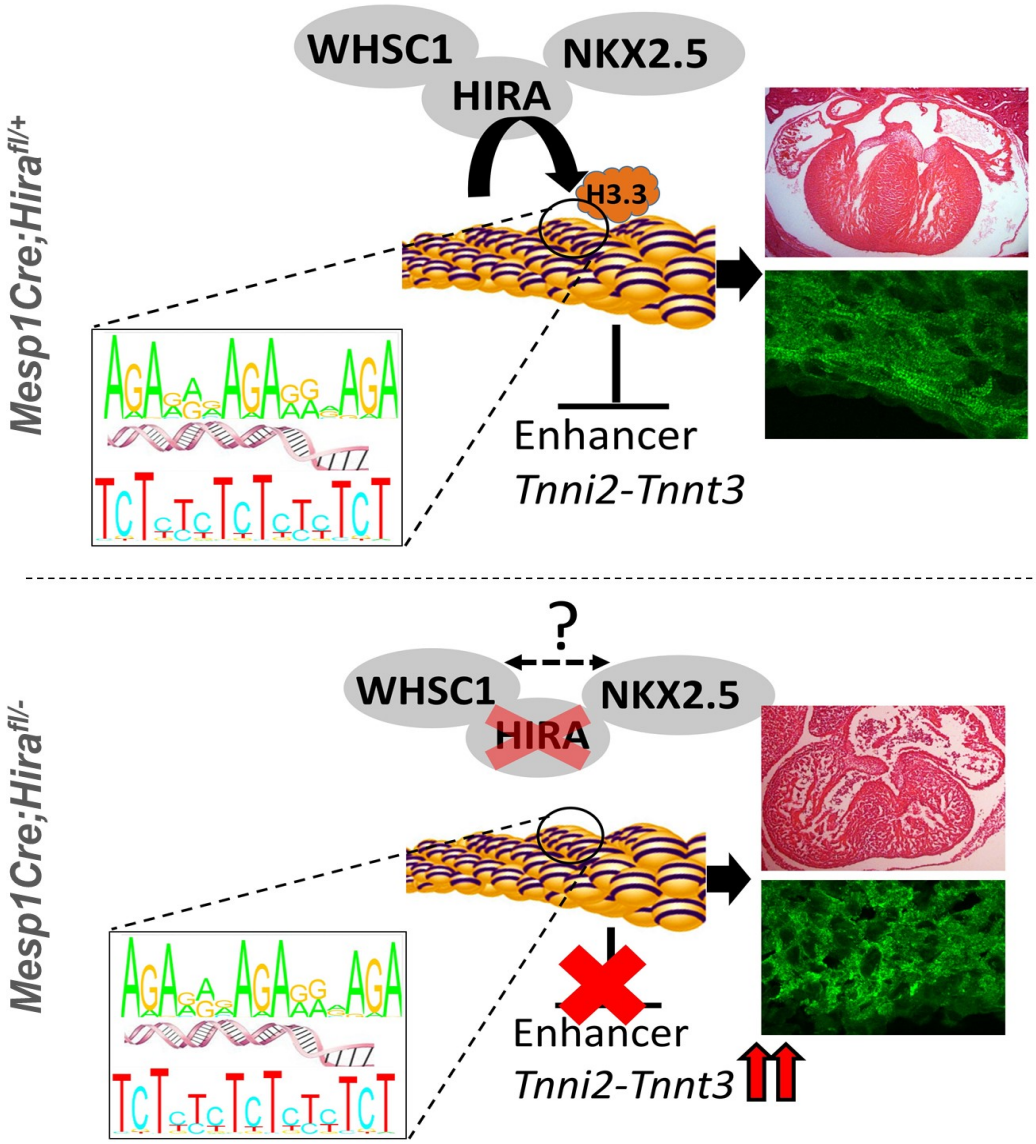

Figure 6-1 Model of regulation of *Tnni2* by HIRA

Model formulated after previously published work (NKX2.5-WHSC1 interaction (Nimura et al., 2009) and repression of *Tnni2* by NKX2.5 (Dupays et al., 2015)), protein interaction analysis and HIRA ChIPseq/qChIP at the *TLT* site in the heart at E12.5 and during ESC differentiation (Rasha Saleh). 45% of HIRA binding sites *in vivo* contained the binding motif represented. The right panels show an H&E staining revealing a VSD at E14.5 (top) and a troponin C staining of the heart wall highlighting the disorganisation of the contracting meshwork of myofibrils (bottom) in the absence of HIRA.

The two HIRA binding sites detected at the *Epha3* locus could indicate a direct regulation of that gene by HIRA. *Epha3* expression was not significantly altered in *Nkx2.5* hypomorphs, nor was there evidence of NKX2.5 binding close to *Epha3* in either the DamID (Bouveret et al., 2015) or NKX2.5 ChIPseq (Dupays et al., 2015). The NKX2.5-WHSC1 complex is thought to repress targets (Nimura et al., 2009), so the absence of NXK2.5 binding sites at *Epha3* is not unexpected. BRG1 has been shown to directly repress *Epha3* in human adrenal carcinoma cell line SW13 (Zhang et al., 2014a), which suggests a possible pathway by which HIRA regulate *Epha3*. The authors revealed that BRG1 associated with the promoter region of

certain BRG1 regulated genes, but no data at the *Epha3* locus was published. Interestingly, *ADAMTS1*, which is regulated by BRG1 (see p20), is required for versican cleavage during the remodelling of the developing endocardial cushions (Kern et al., 2006). However, a study which identified 51,000 BRG1-associated regions across several embryonic tissues at E11.5, showed that this chromatin remodelling protein does not bind at, or around, *Epha3* in the heart (Attanasio et al., 2014).

Conditional ablation of *Hira* has shed some light on the role of HIRA in mesodermal derivatives. There are additional experiments that could prove interesting to better understand the exact requirement and roles of HIRA during cardiovascular development.

6.2) Future work

The data presented in this thesis has described the cardiac defect and transcriptional changes following cardiogenic mesodermal ablation of *Hira.* Identification of HIRA interaction partners in WT hearts suggests that HIRA is part of a large complex, which might affect HIRA's effect on the chromatin. HIRA's genome wide occupancy has shed light on the regulation of *Tnni2/Tnnt3,* and possibly *Epha3*, however, not all genes differentially expressed in *Mesp1Cre;Hira*$^{fl/-}$ hearts could be explained by a proximal (+/- 5Kb) loci with an enrichment of HIRA. There are unanswered questions which could help complete our understanding of the role of HIRA during heart formation. For example, a ChIP analysis of total histone H3 levels could be carried out in WT and *Hira*-null ESCs differentiated towards cardiomyocyte. This would test whether the selective H3.3 deficiency is independent of total H3 incorporation and maintenance.

6.2.1) How are histone modifications affected in the absence of HIRA?

It would be interesting to explore to what extent chromatin binding of WHSC1 and HIRA overlap during different stages of cardiac development, and what signalling mechanisms control their interaction. WHSC1 ChIP by Nimura and colleagues (Nimura et al., 2009) was performed using a FLAG tagged WHSC1 in the mouse, which might explain why my WHSC1 qChIP attempts at the *TLT* site were unsuccessful as there is no antibody available nowadays to ChIP WHSC1. NSD2 ChIP (NSD2 is an alternate name of WHSC1) has been successfully performed in human cells (Ram et al., 2011) using an antibody which may have cross-reactivity in mice. WHSC1 trimethylates H3K36, which, in the yeast, was found to supress the interaction between canonical H3 and histone chaperones (Venkatesh et al., 2012). It is therefore possible that an equilibrium between H3.3 and H3K36me3 takes place in certain actively transcribed genes, which would be disrupted in the absence of HIRA. A H3K36me3 qChIP at the *TLT* site has already been attempted with approximately 10 WT hearts at E12.5 as a pilot experiment, since pooling larger numbers of *Mesp1Cre;Hira*$^{fl/-}$ hearts becomes challenging. Unfortunately,

the resulting signal-to-noise ratio was too low to draw any useful conclusions. Most ChIP protocols require a starting material of 5 million cells and since a heart at E12.5 represents approximately 300,000 cells (Mahalia Page, personal communication), around 16 hearts would be needed to collect sufficient amount of total chromatin. However, new techniques using ultra low input for micrococcal nuclease-based native ChIP (nChIP) have been described (Brind'Amour et al., 2015), which could be applied in the future. An alternative experiment would be H3K36me3 ChIPseq in the ESC model, comparing *Hira* null with WT cells after differentiation towards cardiomyocytes, which would palliate the lack of embryonic material. This model, used by Wamstad and colleagues (Wamstad et al., 2012), presents the drawback of constituting a heterogeneous population of cells, but offers sufficient material to perform ChIPseq at early differentiation stages.

H2A.Z was found to be preferentially associate with H3.3 in ESCs (Yukawa et al., 2014)(see p17). H3.3 knockdown, in the enhancer region, affected H2A.Z deposition at the promoter regions of active genes (Chen et al., 2014), which has often been linked with transcriptional activation (Kumar and Wigge, 2010, Dalvai et al., 2013). This cooperation between the two variants could be disrupted in *Mesp1Cre;Hira*$^{fl/-}$ hearts and a H2A.Z ChIPseq might shed some light on the dynamics of histone variants upon the ablation of *Hira* during heart development.

An important experiment that would strengthen the model presented above would be the identification of a direct interaction between NKX2.5 and HIRA. Co-immunprecipitations have been attempted, which have been unsuccessful due to a poor batches of anti-NKX2.5 antibody (data not shown). An alternative would be a NKX2.5 ChIP at the *TLT* site. Our model predicts a decrease of NKX2.5 binding to the *TLT* in *Mesp1Cre;Hira*$^{fl/}$ hearts compared to WT, which would be consistent with the marked upregulation of *Tnni2/Tnnt3.* Furthermore, it is also possible for the interaction between NKX2.5 and WHSC1 in the heart to be affected in the absence of HIRA. The ESC model mentioned above could be used since co-immunoprecipitation assays require a substantial amount of material. Alternatively, a tandem affinity purification could be used to detect all the proteins binding to NKX2.5, or HIRA. This method involves a double tagging of the protein of interest followed by a two-step purification process and mass spectroscopic analysis (Rohila et al., 2004). A yeast two-hybrid assay could also be done using *Nkx2.5* or *Hira* to construct a bait plasmid. This method has already been used with SMAD1 (Liu et al., 2014a) using a library generated with E9.5 to E11.5 hearts (DeBenedittis et al., 2011). To palliate a possibly weak or transient interaction between HIRA and NKX2.5 and the lack of appropriate antibody, their physical proximity could be assessed. Forster resonance energy transfer (FRET) uses fluorescent tagged proteins and the distance-dependent transfer of energy to investigate molecular interactions *in vivo* (Karpova and

McNally, 2006). A newer method taking advantage of the recently developed superresolution optical imaging techniques, involving bimolecular fluorescence and photoactivated localization (Liu et al., 2014b), could be used in a cardiomyocyte cell line (e.g P19 or HL-1). Finally, crossing *Mesp1Cre;Hira*$^{-/+}$*;Nkx2.5*$^{+/-}$ mice to *Hira*$^{fl/fl}$ mice and observing whether the phenotype worsens with hemizygosity of *Nkx2.5* could be a sign of synergistic relationship between the two proteins.

An additional validation of the direct regulation by HIRA at the *TLT* site could be achieved by an *in vivo* transgenic embryo analysis containing a LacZ (or equivalent) reporter in conjunction with different point mutations using CRISPR-CAS9 (Inui et al., 2014) at the GAGA motif of the *TLT* site. A similar strategy could be used at the *Epha3* putative HIRA binding sites alongside qChIP and qRT-PCR to assess whether HIRA binding is affected and correlates with the expression of that gene.

6.2.2) Which transcriptional changes are the most causative of the phenotype observed in *Mesp1Cre* conditional *Hira* mutants ?

The lack of oedema at E15.5 in *Nkx2.5Cre* conditional mutants contrasts the complete penetrance of this trait observed in the *Mesp1Cre*. This suggests that genes responsible for cardiac contractility (i.e. troponins) are differentially affected. Identifying dysregulated transcripts in *Nkx2.5Cre* conditional mutants (by RNAseq) and comparing them with the *Mesp1Cre* RNAseq dataset could improve our understanding of the roles of *Tnni2/Tnnt3* and *Epha3* in embryonic lethality, since *Nkx2.5*Cre conditional mutants are only partially embryonic lethal.

6.2.3) How is the spatial conformation of the chromatin affected by the ablation of *Hira*?

The regulation of *Tnni2/Tnnt3* via the *TLT* site implies that the chromatin undergoes a particular reorganisation. Co-immunoprecipitation experiments in HeLa cells showed that HIRA interacted with the insulator factor CTCF (Pchelintsev et al., 2013a), which could be interesting to investigate in the developing heart. Moreover, CTCF binding sites overlap with H3.3 deposition in the human genome (Jin et al., 2009, Millau and Gaudreau, 2011). CTCF has also been found to “erase” the H3K27me3 repressive histone mark by triggering H3.3 deposition (Weth et al., 2014). As mentioned in “5.3.1) Enhancers and H3.3 deposition”, a 3C analysis at the *TLT* site could test for 3D proximity between *Tnni2*, the *TLT* site *and Tnnt3* which represent a combined distance of 17Kb + 38Kb= 55Kb. Additional structural property changes of the chromatin in the absence of HIRA at the *TLT* site could be addressed by circular chromosome conformation capture (4C) (Zhao et al., 2006) which can be used to a examine the intra- and/or interchromosomal interactions of a given site, genome wide. Finally, a general effect on chromatin when *Hira* is ablated could be assessed using chromosome conformation capture carbon copy (5C) which detects all contacts between genomic elements (Figure 6-2).

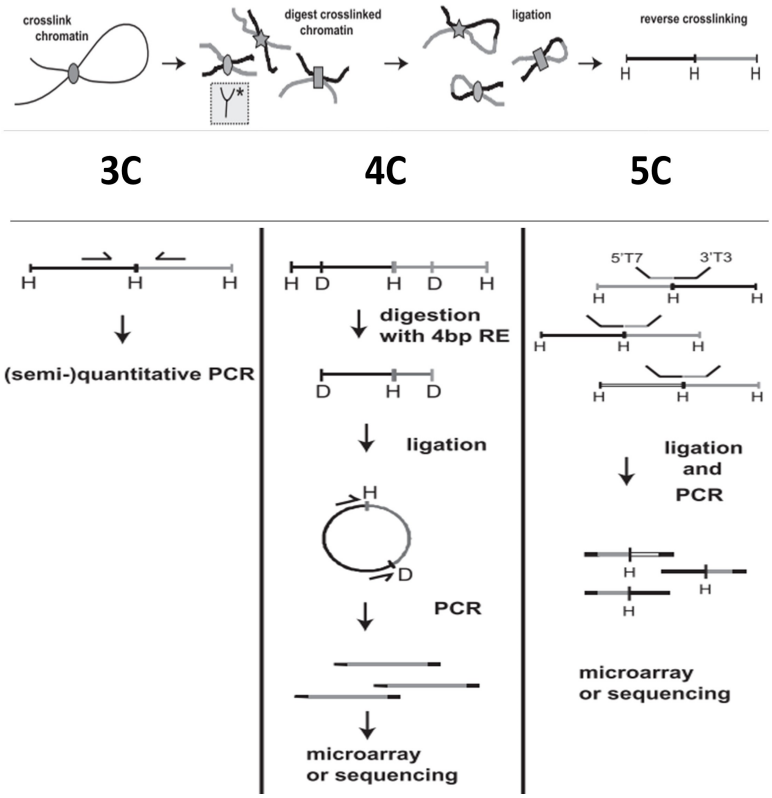

Figure 6-2 Overview of 3C-derived methods

The cross-linking, digestion, and ligation steps are shown on the top. In summary, 3C is "one versus one", 4C is "one versus all" and 5C is "all versus all". Adapted from Laat (2012) (de Wit and de Laat, 2012)

6.2.4) Is the requirement of HIRA specific to the FHF?

In order to validate the specific requirement of HIRA in the FHF, a FHF specific *Cre* driver could be used such as *Hcn4Cre* (hyperpolarization-activated cyclic nucleotide-gated channel 4) (Wu et al., 2014) in conjunction with the *Hira* conditional allele. A phenotype similar to the one observed in *Mesp1Cre* conditional *Hira* mutants in FHF conditional mutants would further support the hypothesis of an autonomous requirement of HIRA in the FHF.

6.2.5) Final remarks and conclusion

Previous work with constitutively *Hira* null embryos suggested a possible role of HIRA past gastrulation (Roberts et al., 2002). HIRA is regarded to have a general role on stress-responsive genes (Chujo et al., 2012b), on chromatin integrity at DNA damage sites (Adam et al., 2013), or on global maintenance of transcriptional silencing in yeast (Anderson et al., 2009), which taken together, suggests that HIRA plays a role in maintaining the integrity of chromatin. The conditional *Hira* mutants presented here, which established the tissue-specific requirements for HIRA, as well as RNAseq and ChIPseq data demonstrated that HIRA has a specific role during heart development. The binding partners of HIRA could have an impact the

on its genome wide occupancy and the deposition of H3.3 or HIRA could impact their recruitment to specific targets. To answer this point, we would need to assess whether their recruitment is affected in the absence of HIRA. Since HIRA binding sites do not correlate strongly with transcriptional changes, it is possible that HIRA serves as a co-regulator of its binding partners. Interestingly, in Drosophila, 5 TFs were found to collectively define cardiac cells. PMad, dTCF, Doc, Pnr, and Tin bound to the same enhancers but without any consistent "motif grammar" (Junion et al.)(2012). This study opened the concept of developmental footprint by TF's occupancy. Similarly in the mouse, the TFs TBX5, NKX2.5 and GATA4 , a T-box-homeo- and zinc finger-domain protein, respectively, were found to regulate certain cardiac enhancers by cooperating across the genome (Luna-Zurita et al.)(2016). The interdependent binding of these heterotypic TFs was shown to regulate gene expression of cardiac progenitors. Individual or double knockouts demonstrated that the cooperation of these TFs was essential to prevent TFs distribution to lineage-inappropriate sites (Luna-Zurita et al.). The ablation of HIRA could have a similar disruptive impact on the genome occupancy of WHSC1 and BRG1 across the genome. Since, *Whsc1* heterozygotes are viable and only partially affected, a synergistic interaction could be tested by crossing *Whsc1*$^{-/+}$ mice to *Hira*$^{+/-}$ mice. The genome wide occupancy of HIRA in the heart has revealed a consensus sequence which likely directs the binding of HIRA to the DNA, in 45% of predicted binding sites. The remaining 55% could be the result of combinatorial interactions between HIRA and other TFs or chromatin remodellers such as WHSC1/BRG1 or possibly CTCF/NKX2.5.

HIRA might therefore have a pleiotropic role, acting both directly on the chromatin by depositing H3.3 and indirectly by interacting with chromatin remodellers or TFs at specific times during development. The latter might explain why certain HIRA binding sites have little or no repercussion on transcriptional activity.

However, the binding of HIRA at the common enhancer of *Tnni2* and *Tnnt3* directly negatively regulate these troponins, which is critical for the formation of contractile myofibers. In addition, HIRA has been implicated in the morphogenesis of atrioventricular endocardial cushions. For the first time, there is evidence for a requirement of HIRA in the cardiovascular lineage.

APPENDIX

The following QR codes can be scanned with a smartphone or tablet using a QR reader app. Otherwise, the links can be pasted onto any browser.

Movie 1: -Transverse OPT reconstructions of *Mesp1Cre;Hira*$^{-/fl}$ E15.5 embryos, travelling from the anterior to the posterior portion of the trunks, with the VSD highlighted.

- 3D reconstruction post OPT scanning of a constricted pulmonary trunk in *Nkx2.5Cre;Hira*$^{-/fl}$ E15.5 embryos.

- beating ESCs when differentiated toward cardiomyocytes

http://tiny.cc/kj3g9x

Movie 2: *Nkx2.5Cre;Hira*$^{fl/-}$: OPT through the heart revealing a VSD

http://tiny.cc/6q3g9x

Movie 3: *Myh6MerCreMer;Hira*$^{fl/+}$ adult heart beating 2 weeks post tamixfen injection, measured using a Visualsonics Vevo 2100 ultrasound system (Echocardiography M-mode recordings)

http://tiny.cc/rxai9x

Genes identified by RNAseq with a marked decreased expression in *Mesp1Cre;Hira*$^{-/fl}$ embryonic hearts at E12.5 compared to their control littermates. The fold change is presented here in absolute value. Test applied: Mann-Whitney unpaired, Benjamini Hochberg FDR, $p \leq 0.05$, $FC \geq 1.5$

EnsemblID	external_gene_id	basic.pval	adj.pval	zscore	Average count *Cre* control	Average count *Hira* mutants	Fold change
UPREGULATED							
ENSMUSG00000000308	Ckmt1	0	0	8.014016	24	203	8.458333
ENSMUSG00000031097	Tnni2	0	0	8.014016	923	5261	5.699892
ENSMUSG00000039099	Wdr93	0	0	8.014016	119.3333333	324	2.715084
ENSMUSG00000040907	Atp1a3	1.11E-16	3.73E-13	8.014016	200.3333333	930.3333333	4.643927
ENSMUSG00000096210	H1f0	5.27E-14	1.11E-10	7.524687	3064	4774	1.558094
ENSMUSG00000022044	Stmn4	1.07E-13	1.79E-10	7.432479	245.6666667	489.6666667	1.993216
ENSMUSG00000020911	Krt19	1.23E-13	1.88E-10	7.413496	989.3333333	1963	1.984164
ENSMUSG00000027500	Stmn2	5.34E-13	6.40E-10	7.216349	113.6666667	395.6666667	3.480938
ENSMUSG00000017723	Wfdc2	7.27E-13	8.09E-10	7.174222	11	78	7.090909
ENSMUSG00000038412	Higd1a	1.18E-12	1.15E-09	7.107568	1601	2483.333333	1.551114
ENSMUSG00000023484	Prph	1.24E-12	1.15E-09	7.101398	8.333333333	61	7.32
ENSMUSG00000049382	Krt8	2.30E-12	2.03E-09	7.015094	285.6666667	762.3333333	2.668611
ENSMUSG00000029121	Crmp1	2.44E-12	2.04E-09	7.006993	346.3333333	690.3333333	1.993263
ENSMUSG00000041361	Myzap	9.96E-12	7.60E-09	6.807153	1297.666667	2000.333333	1.541485
ENSMUSG00000064023	Klk8	1.48E-11	1.06E-08	6.749947	242.6666667	452	1.862637
ENSMUSG00000021613	Hapln1	1.52E-11	1.06E-08	6.746073	2219.666667	3648.666667	1.64379
ENSMUSG00000031451	Gas6	3.68E-11	2.47E-08	6.616502	1977.666667	3358.333333	1.698129
ENSMUSG00000041477	Dcp1b	8.99E-11	5.59E-08	6.483095	152	305	2.006579
ENSMUSG00000032348	Gsta4	1.54E-10	9.21E-08	6.401756	1351.666667	2031	1.502589
ENSMUSG00000070473	Cldn3	2.01E-10	1.13E-07	6.360651	10.33333333	59	5.709677
ENSMUSG00000030871	Ears2	5.40E-10	2.84E-07	6.206929	561	888.6666667	1.584076
ENSMUSG00000019945	0L02Rik	5.68E-10	2.89E-07	6.199008	234.3333333	420.6666667	1.795164
ENSMUSG00000026437	Cdk18	2.54E-09	1.11E-06	5.95912	171.6666667	319	1.858252
ENSMUSG00000021213	Akr1c13	2.85E-09	1.20E-06	5.939898	17	69	4.058824
ENSMUSG00000027611	Procr	3.98E-09	1.63E-06	5.885189	210.6666667	373.6666667	1.773734
ENSMUSG00000006311	Etv2	5.10E-09	1.99E-06	5.843745	9.666666667	85	8.793103
ENSMUSG00000018381	Abi3	5.90E-09	2.23E-06	5.819681	330	568.6666667	1.723232
ENSMUSG00000062785	Kcnc3	8.88E-09	3.24E-06	5.750785	6.333333333	42	6.631579
ENSMUSG00000054793	Cadm4	1.03E-08	3.59E-06	5.726539	60.66666667	143.6666667	2.368132
ENSMUSG00000043664	Tmem221	1.51E-08	5.08E-06	5.660196	0.666666667	21.33333333	32
ENSMUSG00000029762	Akr1b8	1.67E-08	5.49E-06	5.643322	299	488	1.632107
ENSMUSG00000030592	Ryr1	1.73E-08	5.60E-06	5.636739	14.33333333	60	4.186047
ENSMUSG00000034799	Unc13a	4.66E-08	1.37E-05	5.464009	35.33333333	96.33333333	2.726415
ENSMUSG00000042064	Myo3b	5.08E-08	1.43E-05	5.448522	128.6666667	241.6666667	1.878238
ENSMUSG00000000365	Rnf17	5.10E-08	1.43E-05	5.447963	69	152.6666667	2.21256
ENSMUSG00000003355	Fkbp11	7.67E-08	2.08E-05	5.374748	83.66666667	172	2.055777
ENSMUSG00000000811	Txnrd3	9.80E-08	2.60E-05	5.330375	310	490.6666667	1.582796
ENSMUSG00000028943	Espn	1.01E-07	2.60E-05	5.325276	20.66666667	69	3.33871
ENSMUSG00000037161	Mgarp	1.14E-07	2.91E-05	5.302384	171	297.3333333	1.738791
ENSMUSG00000017652	Cd40	1.29E-07	3.20E-05	5.280403	120.3333333	225.3333333	1.872576
ENSMUSG00000021622	Ckmt2	1.30E-07	3.20E-05	5.279269	64.33333333	141.3333333	2.196891
ENSMUSG00000038173	Enpp6	1.61E-07	3.85E-05	5.239973	54	123.3333333	2.283951
ENSMUSG00000020331	Hcn2	5.42E-07	0.000108	5.010993	8	40	5
ENSMUSG00000034891	Sncb	5.86E-07	0.000114	4.995874	4.666666667	31	6.642857
ENSMUSG00000062309	Rpp25	6.19E-07	0.000119	4.985349	126.3333333	226	1.788918
ENSMUSG00000000617	Grm6	6.44E-07	0.000123	4.977683	4.333333333	30	6.923077
ENSMUSG00000020303	Stc2	6.50E-07	0.000123	4.975796	105.3333333	197.6666667	1.876582
ENSMUSG00000043439	A19Rik	6.64E-07	0.000124	4.971724	38	94.33333333	2.482456
ENSMUSG00000036745	Ttll7	7.58E-07	0.000137	4.945907	184.6666667	305.3333333	1.65343
ENSMUSG00000024883	Rin1	7.87E-07	0.00014	4.938613	134	234	1.746269
ENSMUSG00000032202	Rab27a	8.93E-07	0.000155	4.913861	108.6666667	204.6666667	1.883436
ENSMUSG00000045176	M10Rik	1.28E-06	0.00021	4.8433	139	238.6666667	1.717026
ENSMUSG00000024827	Gldc	1.37E-06	0.00022	4.829611	199.6666667	346.6666667	1.736227
ENSMUSG00000039824	Myl6b	1.78E-06	0.000274	4.777147	63.66666667	130.6666667	2.052356
ENSMUSG00000001588	Acap1	1.82E-06	0.000278	4.772559	284.3333333	433	1.52286
ENSMUSG00000072949	Acot1	1.94E-06	0.000293	4.759993	164.6666667	274.3333333	1.665992
ENSMUSG00000031881	Cdh16	2.25E-06	0.000323	4.729476	131.6666667	386	2.931646
ENSMUSG00000050822	Slc29a4	2.29E-06	0.000323	4.726076	48.66666667	107.6666667	2.212329
ENSMUSG00000062380	Tubb3	2.83E-06	0.000393	4.68286	87.66666667	188.6666667	2.152091
ENSMUSG00000038550	Gm129	2.86E-06	0.000393	4.680841	77.66666667	149	1.918455
ENSMUSG00000059213	Ddn	5.02E-06	0.00062	4.563825	7.333333333	34.33333333	4.681818
ENSMUSG00000029032	Arhgef16	5.11E-06	0.000626	4.560385	38.33333333	89	2.321739
ENSMUSG00000026546	Ccdc19	5.20E-06	0.000633	4.556391	37.66666667	88.33333333	2.345133
ENSMUSG00000037386	Rims2	5.87E-06	0.000703	4.531126	19	63	3.315789
ENSMUSG00000019312	Grb7	5.90E-06	0.000703	4.529798	20.66666667	65.33333333	3.16129
ENSMUSG00000023043	Krt18	7.29E-06	0.000844	4.484953	445.3333333	749	1.681886
ENSMUSG00000031461	Myom2	7.41E-06	0.000852	4.481645	45.66666667	99.33333333	2.175182
ENSMUSG00000041605	9C18Rik	7.50E-06	0.000857	4.478896	27	69.33333333	2.567901
ENSMUSG00000004933	Matk	8.32E-06	0.000937	4.456857	23.33333333	64	2.742857
ENSMUSG00000050335	Lgals3	8.80E-06	0.000978	4.444833	27	70	2.592593
ENSMUSG00000046714	Foxc2	9.58E-06	0.001058	4.426532	259	437.6666667	1.689833
ENSMUSG00000021638	Ocln	1.05E-05	0.00115	4.407025	22.66666667	62.33333333	2.75
ENSMUSG00000038811	Gngt2	1.18E-05	0.001234	4.38199	251.6666667	403.3333333	1.602649
ENSMUSG00000045725	Prr15	1.18E-05	0.001234	4.38199	213	325.6666667	1.528951
ENSMUSG00000062044	Lmtk3	1.33E-05	0.00138	4.354781	113.3333333	208.3333333	1.838235

ENSMUSG00000004864	Mapk13	1.50E-05	0.001502	4.328248	47	100	2.12766
ENSMUSG00000030674	Qprt	1.64E-05	0.001622	4.309533	66	126.3333333	1.914141
ENSMUSG00000051367	Six1	1.64E-05	0.001622	4.308723	0.333333333	12.33333333	37
ENSMUSG00000046727	Cystm1	2.04E-05	0.001979	4.260577	150	465.3333333	3.102222
ENSMUSG00000037860	Aim2	2.42E-05	0.002262	4.222134	246.6666667	413.6666667	1.677027
ENSMUSG00000031762	Mt2	2.53E-05	0.002319	4.212285	177	339	1.915254
ENSMUSG00000023033	Scn8a	2.73E-05	0.002489	4.194727	13.66666667	43.66666667	3.195122
ENSMUSG00000029001	Fbxo44	2.81E-05	0.002525	4.18818	147.3333333	328.3333333	2.228507
ENSMUSG00000071553	Cpa2	3.03E-05	0.002676	4.17135	106	240	2.264151
ENSMUSG00000030263	Lrmp	3.60E-05	0.003019	4.132013	53	126.3333333	2.383648
ENSMUSG00000042216	Sgsm1	3.71E-05	0.003101	4.124649	77	143	1.857143
ENSMUSG00000010362	Rdm1	4.28E-05	0.003389	4.091875	376.6666667	601.6666667	1.597345
ENSMUSG00000042724	Map3k9	4.40E-05	0.00345	4.085563	53	104.3333333	1.968553
ENSMUSG00000054612	Mgmt	5.41E-05	0.004145	4.0373	104.3333333	174	1.667732
ENSMUSG00000029522	Pla2g1b	5.75E-05	0.004368	4.022842	1.333333333	15	11.25
ENSMUSG00000028927	Padi2	6.06E-05	0.004562	4.010462	66	131	1.984848
ENSMUSG00000023000	Dhh	6.79E-05	0.004892	3.983562	55	105.3333333	1.915152
ENSMUSG00000021453	Gadd45g	7.06E-05	0.005063	3.974356	340	608.6666667	1.790196
ENSMUSG00000002500	Rpl3l	7.25E-05	0.005135	3.967962	14.33333333	42.66666667	2.976744
ENSMUSG00000041261	Car8	7.56E-05	0.00522	3.958063	268	536	2
ENSMUSG00000000305	Cdh4	8.20E-05	0.005572	3.938566	47.33333333	101	2.133803
ENSMUSG00000039110	Mycbpap	8.53E-05	0.005751	3.929	249	395.3333333	1.587684
ENSMUSG00000022057	Adamdec1	8.69E-05	0.005834	3.924611	23.66666667	58.33333333	2.464789
ENSMUSG00000006731	B4galnt1	9.07E-05	0.006067	3.914212	62.33333333	130	2.085561
ENSMUSG00000096847	Tmem151b	9.80E-05	0.006504	3.895466	93.66666667	156.6666667	1.672598
ENSMUSG00000031738	Irx6	0.0001059	0.006965	3.87666	97.66666667	225	2.303754
ENSMUSG00000074170	Plekhf1	0.0001071	0.006997	3.873917	52.33333333	99.66666667	1.904459
ENSMUSG00000020733	Slc9a3r1	0.0001167	0.00752	3.852957	243.3333333	373.6666667	1.535616
ENSMUSG00000028841	Cnksr1	0.0001357	0.008438	3.815877	44	87.33333333	1.984848
ENSMUSG00000044086	Lmod3	0.00014	0.008578	3.808168	376	637.6666667	1.695922
ENSMUSG00000070000	Fcho1	0.0001422	0.008619	3.80431	52	98	1.884615
ENSMUSG00000050423	Ppp1r3g	0.0001593	0.009319	3.776105	93.66666667	153	1.633452
ENSMUSG00000032011	Thy1	0.0001708	0.009838	3.758698	106	170.3333333	1.606918
ENSMUSG00000070691	Runx3	0.0001711	0.009838	3.758259	3.333333333	22.66666667	6.8
ENSMUSG00000023781	Hes7	0.0001853	0.01037	3.738258	11.33333333	35	3.088235
ENSMUSG00000045348	Nyap1	0.0001935	0.01062	3.727355	146.3333333	221	1.510251
ENSMUSG00000033182	Kbtbd12	0.0002139	0.01144	3.702008	153.3333333	230.6666667	1.504348
ENSMUSG00000025650	Col7a1	0.0002215	0.01178	3.693142	159	292	1.836478
ENSMUSG00000030498	Gas2	0.0002218	0.01178	3.692798	78.33333333	132	1.685106
ENSMUSG00000028599	Tnfrsf1b	0.0002563	0.0132	3.655881	60	125.6666667	2.094444
ENSMUSG00000041120	Nbl1	0.0002571	0.0132	3.655082	129.3333333	197.6666667	1.528351
ENSMUSG00000028125	Abca4	0.0002637	0.0135	3.648574	170.3333333	293.6666667	1.72407
ENSMUSG00000057606	Colq	0.0002725	0.01391	3.64013	137.3333333	224.3333333	1.633495
ENSMUSG00000020785	Camkk1	0.0002905	0.01465	3.623627	57.33333333	102.3333333	1.784884
ENSMUSG00000090394	C07Rik	0.0002985	0.01493	3.616598	115.3333333	179	1.552023
ENSMUSG00000040280	Ndufa4l2	0.0003091	0.01531	3.607552	114.3333333	177.3333333	1.55102
ENSMUSG00000048763	Hoxb3	0.0003367	0.01633	3.585293	51.66666667	94.33333333	1.825806
ENSMUSG00000029403	Cdkl2	0.0003375	0.01633	3.584674	53.66666667	97	1.807453
ENSMUSG00000001494	Sost	0.0003404	0.01633	3.58244	78	228.3333333	2.92735
ENSMUSG00000030428	Ttyh1	0.0003441	0.01643	3.579616	19.66666667	57	2.898305
ENSMUSG00000022487	Gtsf1	0.0003445	0.01643	3.579312	555.3333333	958.3333333	1.72569
ENSMUSG00000025328	Padi3	0.0003519	0.01664	3.573754	37.66666667	94.66666667	2.513274
ENSMUSG00000015090	Ptgds	0.0003605	0.01686	3.56743	11.33333333	38	3.352941
ENSMUSG00000061232	H2-K1	0.0003688	0.01715	3.561459	192.3333333	303	1.57539
ENSMUSG00000048807	Slc35e4	0.0003733	0.01727	3.558274	106.6666667	182	1.70625
ENSMUSG00000054641	Mmrn1	0.0003749	0.01729	3.55715	87.33333333	141.6666667	1.622137
ENSMUSG00000057777	Mab21l2	0.0003833	0.01749	3.551323	59.66666667	105	1.759777
ENSMUSG00000056895	Hist3h2ba	0.000415	0.01838	3.530357	32.66666667	73.33333333	2.244898
ENSMUSG00000059077	Pth	0.0004162	0.01839	3.529593	0	37.66666667	#DIV/0!
ENSMUSG00000036913	Trim67	0.0004308	0.01898	3.520459	32.33333333	66	2.041237
ENSMUSG00000023873	010I14Rik	0.0004619	0.01988	3.501931	27.66666667	61.33333333	2.216867
ENSMUSG00000030350	Prmt8	0.0004659	0.01994	3.499632	15.33333333	45.66666667	2.978261
ENSMUSG00000041556	Fbxo2	0.0004668	0.01994	3.499118	6.666666667	24.66666667	3.7
ENSMUSG00000032680	15Rik	0.0004856	0.02069	3.488576	69.66666667	117.3333333	1.684211
ENSMUSG00000068876	Cgn	0.0005096	0.02139	3.475659	84.66666667	137	1.61811
ENSMUSG00000073530	Pappa2	0.0005326	0.02213	3.463801	18.33333333	48	2.618182
ENSMUSG00000040562	Gstm2	0.000561	0.02292	3.449801	433	654.6666667	1.511932
ENSMUSG00000031972	Acta1	0.0005671	0.01114	2.766222	3379.333333	5831.666667	1.725686
ENSMUSG00000015452	Ager	0.0006068	0.02431	3.428557	93	146.6666667	1.577061
ENSMUSG00000001930	Vwf	0.0006204	0.02468	3.422535	977.6666667	2094	2.141834
ENSMUSG00000022667	Cd200r1	0.0006333	0.02497	3.416937	31.33333333	63.66666667	2.031915
ENSMUSG00000042429	Adora1	0.0006431	0.02519	3.412754	162.6666667	267	1.641393
ENSMUSG00000001025	S100a6	0.0006535	0.02552	3.408379	209.3333333	333.3333333	1.592357
ENSMUSG00000023336	Wfdc1	0.0006818	0.02624	3.396795	35.33333333	69.66666667	1.971698
ENSMUSG00000017713	Tha1	0.0006993	0.02646	3.389853	65.33333333	110	1.683673
ENSMUSG00000028524	Sgip1	0.000702	0.02649	3.388797	16.66666667	42	2.52
ENSMUSG00000040441	Slc26a10	0.0007075	0.02663	3.386656	530.3333333	806	1.519799
ENSMUSG00000087166	L1td1	0.0007163	0.0269	3.383263	7.333333333	28.66666667	3.909091
ENSMUSG00000047197	Gjd3	0.0007501	0.02771	3.37058	11	32	2.909091
ENSMUSG00000023032	Slc4a8	0.0007526	0.02771	3.369664	99.66666667	199	1.996656
ENSMUSG00000061723	Tnnt3	7.53E-04	0.04699	2.194493	275.6666667	420	1.523579
ENSMUSG00000044737	Klk14	0.0007859	0.02838	3.357714	7.333333333	25.66666667	3.5
ENSMUSG00000006216	Clcnkb	0.0007946	0.02853	3.354669	10.33333333	30	2.903226
ENSMUSG00000038453	Srcin1	0.0008108	0.02896	3.349081	8	26.33333333	3.291667
ENSMUSG00000042129	Rassf4	0.0008131	0.02898	3.348296	199	338.6666667	1.701843
ENSMUSG00000033544	Angptl1	0.0008318	0.0294	3.34199	14.66666667	38.66666667	2.636364
ENSMUSG00000037185	Krt80	0.0008409	0.02966	3.338969	209.3333333	381	1.820064
ENSMUSG00000027246	Ell3	0.0008458	0.02977	3.337354	13	35	2.692308

ENSMUSG00000030921	Trim30a	0.0009354	0.03166	3.309269	22.66666667	50	2.205882
ENSMUSG00000000739	Sult5a1	0.0009783	0.0326	3.296694	49	91.33333333	1.863946
ENSMUSG00000074604	Mgst2	0.001021	0.03381	3.284675	6	22	3.666667
ENSMUSG00000075588	Hoxb2	0.001069	0.03512	3.271708	32	73	2.28125
ENSMUSG00000074277	Phldb3	0.001092	0.0356	3.265684	3	16	5.333333
ENSMUSG00000036834	Plch1	0.001114	0.03597	3.260031	26	67.66666667	2.602564
ENSMUSG00000030693	Klk10	0.00119	0.03763	3.241266	0	5.333333333	#DIV/0!
ENSMUSG00000028755	Cda	0.001522	0.04547	3.170456	66.33333333	107.6666667	1.623116
ENSMUSG00000026471	Mr1	0.001559	0.04616	3.163471	96.33333333	157.3333333	1.633218
ENSMUSG00000023064	Sncg	0.001603	0.0473	3.15536	28.33333333	57	2.011765
ENSMUSG00000007122	Casq1	0.004189	0.09098	2.863567	4616.333333	8713.666667	1.887573

DOWNREGULATED

ENSMUSG00000030787	Lyve1	0	0	-8.01402	207.3333333	40	5.183333
ENSMUSG00000026712	Mrc1	6.00E-15	1.68E-11	-7.80405	516	200	2.58
ENSMUSG00000026500	Cox20	2.75E-14	6.60E-11	-7.60942	1257	671	1.873323
ENSMUSG00000036564	Ndrg4	6.58E-14	1.23E-10	-7.4957	3696.333333	2142.333333	1.725377
ENSMUSG00000036006	Fam65b	1.70E-13	2.37E-10	-7.37095	356.3333333	148.3333333	2.402247
ENSMUSG00000032816	Igdcc4	2.18E-13	2.81E-10	-7.33751	790.6666667	404	1.957096
ENSMUSG00000052504	Epha3	7.71E-13	8.09E-10	-7.16615	486.6666667	200.3333333	2.429285
ENSMUSG00000026365	Cfh	4.06E-12	3.25E-09	-6.93507	928.6666667	414	2.243156
ENSMUSG00000040537	Adam22	2.02E-10	1.13E-07	-6.35989	338.6666667	133	2.546366
ENSMUSG00000035551	Igfbpl1	2.80E-10	1.52E-07	-6.3093	542.6666667	206.3333333	2.630048
ENSMUSG00000069515	Lyz1	6.99E-10	3.45E-07	-6.16641	195	79	2.468354
ENSMUSG00000041559	Fmod	1.18E-09	5.65E-07	-6.08321	444	218	2.036697
ENSMUSG00000027971	Ndst4	1.78E-09	8.29E-07	-6.01689	39.33333333	3.666666667	10.72727
ENSMUSG00000038112	AW551984	2.40E-09	1.09E-06	-5.96812	607	322.6666667	1.881198
ENSMUSG00000060913	Trim55	2.58E-09	1.11E-06	-5.95605	5520.666667	3618.666667	1.525608
ENSMUSG00000060882	Kcnd2	9.87E-09	3.53E-06	-5.73293	120	40.66666667	2.95082
ENSMUSG00000042453	Reln	3.87E-08	1.20E-05	-5.49691	288.3333333	144.3333333	1.997691
ENSMUSG00000034810	Scn7a	3.92E-08	1.20E-05	-5.49424	129.6666667	49	2.646259
ENSMUSG00000066113	Adamtsl1	4.41E-08	1.32E-05	-5.47379	286	135.6666667	2.108108
ENSMUSG00000026840	Lamc3	9.97E-08	2.60E-05	-5.32725	107.3333333	37.33333333	2.875
ENSMUSG00000046442	Ppm1e	1.32E-07	3.21E-05	-5.27591	367.6666667	201.3333333	1.826159
ENSMUSG00000033214	Slitrk5	1.70E-07	4.01E-05	-5.23001	576.6666667	274.3333333	2.102066
ENSMUSG00000027931	Npr1	2.49E-07	5.74E-05	-5.15815	440.3333333	238	1.85014
ENSMUSG00000051154	Commd3	2.75E-07	6.24E-05	-5.13996	1480	974.3333333	1.518987
ENSMUSG00000051048	P4ha3	3.51E-07	7.66E-05	-5.09361	429	238.6666667	1.797486
ENSMUSG00000043090	Zfp866	3.97E-07	8.54E-05	-5.07053	533	319	1.670846
ENSMUSG00000034353	Ramp1	4.46E-07	9.47E-05	-5.04837	240.6666667	122.6666667	1.961957
ENSMUSG00000016995	Matn4	4.74E-07	9.95E-05	-5.03659	97.33333333	24.66666667	3.945946
ENSMUSG00000029675	Eln	5.20E-07	0.000106	-5.01882	5324.666667	2640.666667	2.01641
ENSMUSG00000039431	Mtmr7	5.42E-07	0.000108	-5.01074	160.3333333	72.33333333	2.21659
ENSMUSG00000071424	Grid2	5.76E-07	0.000114	-4.99903	28	3	9.333333
ENSMUSG00000041797	Abca9	7.29E-07	0.000134	-4.95355	168.6666667	78	2.162393
ENSMUSG00000026768	Itga8	7.44E-07	0.000136	-4.94943	819.3333333	433.6666667	1.889316
ENSMUSG00000042289	Hsd3b7	8.43E-07	0.000147	-4.92516	332.6666667	186.3333333	1.785331
ENSMUSG00000029338	Antxr2	1.02E-06	0.000173	-4.88832	2604.333333	1594.666667	1.633152
ENSMUSG00000039057	Myo16	1.06E-06	0.000178	-4.88035	177	64.33333333	2.751295
ENSMUSG00000007659	Bcl2l1	1.20E-06	0.000199	-4.8563	717	400.3333333	1.791007
ENSMUSG00000030323	Ift122	1.37E-06	0.00022	-4.82917	943.6666667	614	1.536916
ENSMUSG00000024331	Dsc2	1.39E-06	0.00022	-4.82686	1193.666667	659.3333333	1.810415
ENSMUSG00000000706	Btn1a1	1.39E-06	0.00022	-4.82643	45.33333333	7.666666667	5.913043
ENSMUSG00000039031	Arhgap18	1.44E-06	0.000225	-4.81994	1438.666667	938.3333333	1.533215
ENSMUSG00000027820	Mme	1.67E-06	0.00026	-4.78962	607.3333333	377.6666667	1.60812
ENSMUSG00000028020	Glrb	2.06E-06	0.000308	-4.74794	134.6666667	59.66666667	2.256983
ENSMUSG00000027570	Col9a3	2.13E-06	0.000314	-4.74097	530	237.3333333	2.233146
ENSMUSG00000020524	Gria1	2.13E-06	0.000314	-4.74078	141.3333333	60.66666667	2.32967
ENSMUSG00000028015	Ctso	2.23E-06	0.000322	-4.73174	395.3333333	232	1.704023
ENSMUSG00000020776	Fbf1	2.92E-06	0.000398	-4.67665	1194.333333	799.3333333	1.494162
ENSMUSG00000078670	Fam174b	3.09E-06	0.000417	-4.66494	565.6666667	320	1.767708
ENSMUSG00000022831	Hcls1	3.10E-06	0.000417	-4.66401	164.3333333	78.66666667	2.088983
ENSMUSG00000035829	Ppp1r26	3.15E-06	0.000418	-4.66053	215.3333333	112.3333333	1.916914
ENSMUSG00000038871	Bpgm	3.19E-06	0.000418	-4.65832	1033	504	2.049603
ENSMUSG00000040896	Kcnd3	3.20E-06	0.000418	-4.65787	138.6666667	63.33333333	2.189474
ENSMUSG00000031734	Irx3	3.21E-06	0.000418	-4.6569	303.3333333	171	1.773879
ENSMUSG00000036446	Lum	3.50E-06	0.000445	-4.63912	1436	934.3333333	1.536925
ENSMUSG00000060429	Sntb1	4.71E-06	0.000587	-4.57753	213	113	1.884956
ENSMUSG00000025993	Slc40a1	5.81E-06	0.000702	-4.53304	255.6666667	141.3333333	1.808962
ENSMUSG00000049796	Crh	6.86E-06	0.000811	-4.49808	78	28.66666667	2.72093
ENSMUSG00000025757	Hspa4l	7.16E-06	0.000836	-4.48899	1034	696	1.485632
ENSMUSG00000073940	Hbb-b2	7.81E-06	0.000886	-4.4703	2036	977	2.08393
ENSMUSG00000042604	Kcna4	8.79E-06	0.000978	-4.44505	107.3333333	46.33333333	2.316547
ENSMUSG00000022514	Il1rap	1.08E-05	0.001173	-4.40131	355	198.3333333	1.789916
ENSMUSG00000048814	Lonrf2	1.13E-05	0.001212	-4.39144	126.3333333	58.33333333	2.165714
ENSMUSG00000041836	Ptpre	1.17E-05	0.001234	-4.38329	144.6666667	70.66666667	2.04717
ENSMUSG00000030653	Pde2a	1.23E-05	0.001286	-4.37167	387.3333333	183.3333333	2.112727
ENSMUSG00000001942	Siae	1.34E-05	0.001384	-4.35282	319	170.6666667	1.869141
ENSMUSG00000024899	Papss2	1.45E-05	0.001472	-4.33661	505.6666667	196.6666667	2.571186
ENSMUSG00000059361	Nrsn2	1.47E-05	0.001483	-4.33374	69.33333333	24.66666667	2.810811
ENSMUSG00000025969	Nrp2	1.80E-05	0.001759	-4.28811	641	418.3333333	1.532271
ENSMUSG00000006522	Itih3	2.48E-05	0.0023	-4.21661	191	85.66666667	2.229572
ENSMUSG00000044468	Fam46c	2.50E-05	0.002302	-4.21516	431	144	2.993056
ENSMUSG00000069919	Hba-a1	2.78E-05	0.002511	-4.19061	5061.333333	2899.333333	1.745689
ENSMUSG00000033152	Podxl2	3.02E-05	0.002676	-4.17195	584.6666667	382.3333333	1.529207
ENSMUSG00000026676	Ccdc3	3.31E-05	0.002852	-4.15081	301	158.3333333	1.901053
ENSMUSG00000052187	Hbb-y	3.36E-05	0.002877	-4.14765	44972.33333	22564.66667	1.993042
ENSMUSG00000043943	Naalad2	3.41E-05	0.002889	-4.1444	125.6666667	60.66666667	2.071429

ENSMUSG00000054435	Gimap4	3.89E-05	0.0032	-4.11404	397.3333333	197	2.01692
ENSMUSG00000024620	Pdgfrb	3.96E-05	0.00322	-4.10998	1191.666667	699	1.704816
ENSMUSG00000022488	Nckap1l	4.08E-05	0.003276	-4.10302	230.6666667	124.3333333	1.855228
ENSMUSG00000030098	Grip2	4.15E-05	0.003315	-4.09913	399.6666667	252.6666667	1.581794
ENSMUSG00000044350	Lacc1	5.73E-05	0.004368	-4.02387	363.6666667	229	1.588064
ENSMUSG00000027692	Tnik	6.14E-05	0.004601	-4.0074	466.6666667	305.3333333	1.528384
ENSMUSG00000015944	Gatsl2	6.36E-05	0.004699	-3.99904	278	151.3333333	1.837004
ENSMUSG00000042066	Tmcc2	6.38E-05	0.004699	-3.99822	1021.666667	531.6666667	1.92163
ENSMUSG00000024411	Aqp4	6.66E-05	0.004859	-3.98826	361	212.6666667	1.697492
ENSMUSG00000044338	Aplnr	6.74E-05	0.004892	-3.98539	212	68.33333333	3.102439
ENSMUSG00000031596	Slc7a2	6.77E-05	0.004892	-3.98416	147.3333333	77.66666667	1.896996
ENSMUSG00000039904	Gpr37	7.12E-05	0.00509	-3.97211	42.66666667	12.33333333	3.459459
ENSMUSG00000037709	Fam13a	7.29E-05	0.00514	-3.96675	282.6666667	172	1.643411
ENSMUSG00000006342	Susd2	7.40E-05	0.005175	-3.96314	144.3333333	75.33333333	1.915929
ENSMUSG00000025855	Prkar1b	7.48E-05	0.005188	-3.96054	167	91	1.835165
ENSMUSG00000030681	Mvp	7.61E-05	0.005236	-3.95639	304	186.3333333	1.631485
ENSMUSG00000049107	Ntf3	7.75E-05	0.005286	-3.95216	75.66666667	31.33333333	2.414894
ENSMUSG00000031129	Slc9a9	0.0001109	0.007189	-3.86542	142.3333333	75	1.897778
ENSMUSG00000030513	Pcsk6	0.0001169	0.00752	-3.85254	1056	386.3333333	2.733391
ENSMUSG00000038552	Fndc4	0.0001241	0.007911	-3.83788	533.6666667	359.3333333	1.485158
ENSMUSG00000052336	Cx3cr1	0.0001244	0.007911	-3.83729	143.3333333	76	1.885965
ENSMUSG00000006574	Slc4a1	0.0001309	0.008262	-3.82476	3232	991.3333333	3.260256
ENSMUSG00000015243	Abca1	0.0001375	0.008493	-3.81262	586.3333333	345.6666667	1.696239
ENSMUSG00000033590	Myo5c	0.0001446	0.008701	-3.80016	92.66666667	41.66666667	2.224
ENSMUSG00000069516	Lyz2	0.0001478	0.008786	-3.79474	619.6666667	289.3333333	2.141705
ENSMUSG00000052305	Hbb-b1	0.0001481	0.008786	-3.79423	4395.666667	2255.333333	1.94901
ENSMUSG00000037605	Lphn3	0.0001641	0.009533	-3.7687	316.3333333	177.6666667	1.780488
ENSMUSG00000052430	Bmpr1b	0.0001736	0.009914	-3.75463	73.66666667	31.66666667	2.326316
ENSMUSG00000025889	Snca	0.0001761	0.009988	-3.75104	395	221.3333333	1.784639
ENSMUSG00000036186	Fam69b	0.0001782	0.01007	-3.74807	212.6666667	125	1.701333
ENSMUSG00000021822	Plau	0.0001797	0.01012	-3.74597	225.3333333	121.3333333	1.857143
ENSMUSG00000022887	Masp1	0.0001857	0.01037	-3.73772	337	217.6666667	1.548239
ENSMUSG00000086040	Wipf3	0.0001859	0.01037	-3.73744	562.6666667	359.6666667	1.564411
ENSMUSG00000031618	Nr3c2	0.0001872	0.01041	-3.73569	28.33333333	6.666666667	4.25
ENSMUSG00000025089	Gfra1	0.0001908	0.01054	-3.7309	73.33333333	31.33333333	2.340426
ENSMUSG00000022483	Col2a1	0.0001917	0.01055	-3.72971	3134.666667	1663.333333	1.884569
ENSMUSG00000031543	Ank1	0.0001946	0.01064	-3.72593	692	348.3333333	1.986603
ENSMUSG00000036040	Adamtsl2	0.0002006	0.01089	-3.71826	255	131.6666667	1.936709
ENSMUSG00000030116	Mfap5	0.0002034	0.01098	-3.71476	164.6666667	82	2.00813
ENSMUSG00000041378	Cldn5	0.0002061	0.01109	-3.71142	85.33333333	38.66666667	2.206897
ENSMUSG00000048865	Arhgap30	0.0002135	0.01144	-3.70248	52	19	2.736842
ENSMUSG00000033458	Fan1	0.0002249	0.01186	-3.68927	186.6666667	108.3333333	1.723077
ENSMUSG00000021301	Hecw1	0.0002254	0.01186	-3.6887	44.66666667	15	2.977778
ENSMUSG00000034881	Tbxa2r	0.000229	0.01201	-3.68467	111.6666667	54	2.067901
ENSMUSG00000034059	Ypel4	0.0002499	0.01302	-3.66236	73.33333333	32.33333333	2.268041
ENSMUSG00000028780	Sema3c	0.0002505	0.01302	-3.66175	1115	722	1.544321
ENSMUSG00000020034	Tcp11l2	0.0002526	0.01309	-3.65961	572	366.6666667	1.56
ENSMUSG00000015852	Fcrls	0.0002757	0.01403	-3.63712	127.6666667	64.66666667	1.974227
ENSMUSG00000029671	Wnt16	0.000308	0.0153	-3.60848	57.66666667	23	2.507246
ENSMUSG00000030996	Art1	0.0003361	0.01633	-3.58576	56	22	2.545455
ENSMUSG00000024935	Slc1a1	0.0003495	0.01658	-3.57554	59	16	3.6875
ENSMUSG00000022883	Robo1	0.0003556	0.01672	-3.57102	1456.666667	883	1.649679
ENSMUSG00000063297	Luzp2	0.0003705	0.01718	-3.56025	82.66666667	37.66666667	2.19469
ENSMUSG00000043257	Pigv	0.0003771	0.01731	-3.55561	221	134.6666667	1.641089
ENSMUSG00000055639	Dach1	0.0003864	0.01758	-3.5492	220	134.6666667	1.633663
ENSMUSG00000040253	Gbp7	0.0004008	0.01809	-3.53956	41.33333333	14	2.952381
ENSMUSG00000048582	Gja3	0.0004024	0.01811	-3.5385	39.33333333	12.66666667	3.105263
ENSMUSG00000023216	Epb4.2	0.0004105	0.01829	-3.53324	316.3333333	95.33333333	3.318182
ENSMUSG00000003476	Crhr2	0.000411	0.01829	-3.53292	146.3333333	66	2.217172
ENSMUSG00000040118	Cacna2d1	0.0004579	0.01983	-3.50425	1530.666667	1000.666667	1.529647
ENSMUSG00000057378	Ryr3	0.0004994	0.02117	-3.48108	677	327.6666667	2.066124
ENSMUSG00000074671	Tspyl3	0.0005075	0.02135	-3.47677	102.3333333	52.33333333	1.955414
ENSMUSG00000038264	Sema7a	0.00055	0.02274	-3.45514	47	17.33333333	2.711538
ENSMUSG00000038775	Vill	0.0005603	0.02292	-3.45014	155	89.66666667	1.728625
ENSMUSG00000014361	Mertk	0.0005945	0.02406	-3.43411	306	200.6666667	1.524917
ENSMUSG00000029866	Kel	0.0006574	0.02558	-3.40676	653	193	3.38342
ENSMUSG00000037124	Trim58	0.0006581	0.02558	-3.40646	27.33333333	6	4.555556
ENSMUSG00000009633	G0s2	0.0006642	0.02575	-3.40395	228.6666667	141.3333333	1.617925
ENSMUSG00000053835	H2-T24	0.0006822	0.02624	-3.39663	160.3333333	59	2.717514
ENSMUSG00000020334	Slc22a4	0.0006842	0.02624	-3.39583	47.66666667	13	3.666667
ENSMUSG00000035296	Sgcg	0.000692	0.0264	-3.39273	87.33333333	35.66666667	2.448598
ENSMUSG00000024621	Csf1r	0.0007335	0.02726	-3.37674	562	323	1.739938
ENSMUSG00000027878	Notch2	0.0007518	0.02771	-3.36996	1090.666667	734.6666667	1.484574
ENSMUSG00000026532	Spta1	0.000755	0.02774	-3.36879	864.6666667	287.3333333	3.009281
ENSMUSG00000050211	Pla2g4e	0.0007658	0.02807	-3.36487	62	27.33333333	2.268293
ENSMUSG00000042353	Frem3	0.0007714	0.02809	-3.36286	31	9.333333333	3.321429
ENSMUSG00000044067	Gpr22	0.0007759	0.0282	-3.36125	602.6666667	385.3333333	1.564014
ENSMUSG00000052062	Pard3b	0.0008148	0.02898	-3.34772	317.6666667	211.6666667	1.500787
ENSMUSG00000033114	Slc35d2	0.0008296	0.0294	-3.34273	221.6666667	140.6666667	1.575829
ENSMUSG00000064179	Tnnt1	0.0008493	0.02983	-3.33621	8775.666667	4871.666667	1.801368
ENSMUSG00000047473	Zfp30	0.0008661	0.03016	-3.33076	171.3333333	103	1.66343
ENSMUSG00000051236	Msrb3	0.0008669	0.03016	-3.3305	1596.333333	1065.333333	1.498436
ENSMUSG00000004552	Ctse	0.0008677	0.03016	-3.33024	250.6666667	80.66666667	3.107438
ENSMUSG00000020656	Grhl1	0.0008801	0.03047	-3.32629	429	267.3333333	1.604738
ENSMUSG00000028542	Slc6a9	0.0008989	0.03098	-3.3204	267	158.3333333	1.686316
ENSMUSG00000021068	Nin	0.0009198	0.03145	-3.31397	966.3333333	646.3333333	1.495101
ENSMUSG00000020599	Rgs9	0.0009287	0.0316	-3.31128	93.33333333	45.66666667	2.043796
ENSMUSG00000027338	Prnd	0.0009318	0.0316	-3.31035	78.66666667	30	2.622222

ENSMUSG00000036941	Elac1	0.0009648	0.0324	-3.3006	136.3333333	79	1.725738
ENSMUSG00000033111	406C13Rik	0.0009786	0.0326	-3.29661	317	194	1.634021
ENSMUSG00000043410	Hfm1	0.001023	0.03381	-3.28412	49.33333333	20.33333333	2.42623
ENSMUSG00000026380	Tfcp2l1	0.001054	0.03477	-3.2757	176	107.6666667	1.634675
ENSMUSG00000036353	P2ry12	0.00113	0.03627	-3.25598	35.66666667	12.33333333	2.891892
ENSMUSG00000068196	Col8a1	0.001175	0.03732	-3.24488	149	88.33333333	1.686792
ENSMUSG00000042671	Rgs8	0.001176	0.03732	-3.24464	93.66666667	22	4.257576
ENSMUSG00000069814	D14Rik	0.001199	0.03784	-3.23912	104	41.66666667	2.496
ENSMUSG00000029826	Zc3hav1	0.001211	0.03815	-3.23628	305	178.3333333	1.71028
ENSMUSG00000039109	F13a1	0.001258	0.0394	-3.22539	255.6666667	110.6666667	2.310241
ENSMUSG00000007279	Scube2	0.001262	0.03946	-3.22448	325.3333333	137.3333333	2.368932
ENSMUSG00000032125	Robo4	0.001287	0.04009	-3.21886	208	105	1.980952
ENSMUSG00000038068	Rnf144b	0.001306	0.04053	-3.21466	164.6666667	100.3333333	1.641196
ENSMUSG00000027750	Postn	0.001334	0.04104	-3.20856	9034.666667	5652	1.59849
ENSMUSG00000055912	Tmem150a	0.001407	0.04272	-3.19321	251.3333333	165.3333333	1.520161
ENSMUSG00000029193	Cckar	0.001435	0.04341	-3.18752	21.33333333	5	4.266667
ENSMUSG00000030353	Tead4	0.001481	0.04451	-3.17838	157	96	1.635417
ENSMUSG00000036655	Colec11	0.001482	0.04451	-3.17819	101.6666667	53.66666667	1.89441
ENSMUSG00000020641	Rsad2	0.001551	0.04601	-3.16497	98	36.66666667	2.672727
ENSMUSG00000039899	Fgl2	0.00164	0.04805	-3.1487	612.3333333	390	1.570085
ENSMUSG00000031972	Acta1	0.005671	0.1114	2.766222	3379.333333	5831.666667	0.57948

REFERENCES

ADAM, S., POLO, S. E. & ALMOUZNI, G. 2013. Transcription recovery after DNA damage requires chromatin priming by the H3.3 histone chaperone HIRA. *Cell,* 155**,** 94-106.

ADAM, S., POLO, S. E. & ALMOUZNI, G. 2014. How to restore chromatin structure and function in response to DNA damage – let the chaperones play. *FEBS Journal,* 281**,** 2315-2323.

ADKINS, N. L., HAGERMAN, T. A. & GEORGEL, P. 2006. GAGA protein: a multi-faceted transcription factor. *Biochem Cell Biol,* 84**,** 559-67.

AGALIOTI, T., LOMVARDAS, S., PAREKH, B., YIE, J., MANIATIS, T. & THANOS, D. 2000. Ordered recruitment of chromatin modifying and general transcription factors to the IFN-beta promoter. *Cell,* 103**,** 667-78.

AHMAD, A., TAKAMI, Y. & NAKAYAMA, T. 2003. WD dipeptide motifs and LXXLL motif of chicken HIRA are necessary for transcription repression and the latter motif is essential for interaction with histone deacetylase-2 in vivo. *Biochem Biophys Res Commun,* 312**,** 1266-72.

AHMAD, K. & HENIKOFF, S. 2002. Histone H3 variants specify modes of chromatin assembly. *Proc Natl Acad Sci U S A,* 99 Suppl 4**,** 16477-84.

AHO, S., BUISSON, M., PAJUNEN, T., RYOO, Y. W., GIOT, J. F., GRUFFAT, H., SERGEANT, A. & UITTO, J. 2000. Ubinuclein, a novel nuclear protein interacting with cellular and viral transcription factors. *J Cell Biol,* 148**,** 1165-76.

AIRD, K. M. & ZHANG, R. 2013. Detection of senescence-associated heterochromatin foci (SAHF). *Methods in molecular biology (Clifton, N.J.),* 965**,** 185-196.

ALABERT, C. & GROTH, A. 2012. Chromatin replication and epigenome maintenance. *Nat Rev Mol Cell Biol,* 13**,** 153-167.

ALLFREY, V. G., FAULKNER, R. & MIRSKY, A. E. 1964. ACETYLATION AND METHYLATION OF HISTONES AND THEIR POSSIBLE ROLE IN THE REGULATION OF RNA SYNTHESIS. *Proceedings of the National Academy of Sciences of the United States of America,* 51**,** 786-794.

ALVAREZ, B. V., KIELLER, D. M., QUON, A. L., ROBERTSON, M. & CASEY, J. R. 2007. Cardiac hypertrophy in anion exchanger 1-null mutant mice with severe hemolytic anemia. *Am J Physiol Heart Circ Physiol,* 292**,** H1301-12.

ANDERSON, H. E., WARDLE, J., KORKUT, Ş. V., MURTON, H. E., LÓPEZ-MAURY, L., BÄHLER, J. & WHITEHALL, S. K. 2009. The Fission Yeast HIRA Histone Chaperone Is Required for Promoter Silencing and the Suppression of Cryptic Antisense Transcripts. *Molecular and Cellular Biology,* 29**,** 5158-5167.

ANDERSON, R. H., BROWN, N. A. & MOHUN, T. J. 2015. Insights regarding the normal and abnormal formation of the atrial and ventricular septal structures. *Clinical Anatomy***,** n/a-n/a.

ANDERSON, R. H., SPICER, D. E., BROWN, N. A. & MOHUN, T. J. 2014. The development of septation in the four-chambered heart. *Anat Rec (Hoboken),* 297**,** 1414-29.

ANGELOV, D., BONDARENKO, V. A., ALMAGRO, S., MENONI, H., MONGÉLARD, F., HANS, F., MIETTON, F., STUDITSKY, V. M., HAMICHE, A., DIMITROV, S. & BOUVET, P. 2006. Nucleolin is a histone chaperone with FACT-like activity and assists remodeling of nucleosomes. *The EMBO Journal,* 25**,** 1669-1679.

ANNUNZIATO, A. 2008. DNA Packaging: Nucleosomes and Chromatin. *Nature Education,* 1**,** 26.

ATAPATTU, L., SAHA, N., LLERENA, C., VAIL, M. E., SCOTT, A. M., NIKOLOV, D. B., LACKMANN, M. & JANES, P. W. 2012. Antibodies binding the ADAM10 substrate recognition domain inhibit Eph function. *Journal of Cell Science,* 125**,** 6084-6093.

ATTANASIO, C., NORD, A. S., ZHU, Y., BLOW, M. J., BIDDIE, S. C., MENDENHALL, E. M., DIXON, J., WRIGHT, C., HOSSEINI, R., AKIYAMA, J. A., HOLT, A., PLAJZER-FRICK, I., SHOUKRY, M., AFZAL, V., REN, B., BERNSTEIN, B. E., RUBIN, E. M., VISEL, A. & PENNACCHIO, L. A. 2014. Tissue-specific SMARCA4 binding at active and repressed regulatory elements during embryogenesis. *Genome Res,* 24**,** 920-9.

ATTIEH, Y., GENG, Q.-R., DINARDO, C. D., ZHENG, H., JIA, Y., FANG, Z.-H., GAÑÁN-GÓMEZ, I., YANG, H., WEI, Y., KANTARJIAN, H. & GARCIA-MANERO, G. 2013. Low frequency of H3.3 mutations and upregulated DAXX expression in MDS. *Blood,* 121**,** 4009-4011.

BANASZYNSKI, L. A., WEN, D., DEWELL, S., WHITCOMB, S. J., LIN, M., DIAZ, N., ELSASSER, S. J., CHAPGIER, A., GOLDBERG, A. D., CANAANI, E., RAFII, S., ZHENG, D. & ALLIS, C. D. 2013. Hira-dependent histone H3.3 deposition facilitates PRC2 recruitment at developmental loci in ES cells. *Cell,* 155**,** 107-20.

BANERJEE, I., FUSELER, J. W., PRICE, R. L., BORG, T. K. & BAUDINO, T. A. 2007. Determination of cell types and numbers during cardiac development in the neonatal and adult rat and mouse. *American Journal of Physiology - Heart and Circulatory Physiology,* 293**,** H1883-H1891.

BANERJI, S., NI, J., WANG, S. X., CLASPER, S., SU, J., TAMMI, R., JONES, M. & JACKSON, D. G. 1999. LYVE-1, a new homologue of the CD44 glycoprotein, is a lymph-specific receptor for hyaluronan. *J Cell Biol,* 144**,** 789-801.

BANNISTER, A. J. & KOUZARIDES, T. 2011. Regulation of chromatin by histone modifications. *Cell Res,* 21**,** 381-95.

BANUMATHY, G., SOMAIAH, N., ZHANG, R., TANG, Y., HOFFMANN, J., ANDRAKE, M., CEULEMANS, H., SCHULTZ, D., MARMORSTEIN, R. & ADAMS, P. D. 2009. Human UBN1 is an ortholog of yeast Hpc2p and has an essential role in the HIRA/ASF1a chromatin-remodeling pathway in senescent cells. *Mol Cell Biol,* 29**,** 758-70.

BARNETT, J. V. & DESGROSELLIER, J. S. 2003. Early events in valvulogenesis: a signaling perspective. *Birth Defects Res C Embryo Today,* 69**,** 58-72.

BARRIGA, E. H., TRAINOR, P. A., BRONNER, M. & MAYOR, R. 2015. Animal models for studying neural crest development: is the mouse different? *Development,* 142**,** 1555-60.

BARSKI, A., CUDDAPAH, S., CUI, K., ROH, T. Y., SCHONES, D. E., WANG, Z., WEI, G., CHEPELEV, I. & ZHAO, K. 2007. High-resolution profiling of histone methylations in the human genome. *Cell,* 129**,** 823-37.

BELOTSERKOVSKAYA, R., OH, S., BONDARENKO, V. A., ORPHANIDES, G., STUDITSKY, V. M. & REINBERG, D. 2003. FACT facilitates transcription-dependent nucleosome alteration. *Science,* 301**,** 1090-3.

BERSELL, K., CHOUDHURY, S., MOLLOVA, M., POLIZZOTTI, B. D., GANAPATHY, B., WALSH, S., WADUGU, B., ARAB, S. & KÜHN, B. 2013. Moderate and high amounts of tamoxifen in αMHC-MerCreMer mice induce a DNA damage response, leading to heart failure and death. *Disease Models & Mechanisms,* 6**,** 1459-1469.

BIBEN, C. & HARVEY, R. P. 1997. Homeodomain factor Nkx2-5 controls left/right asymmetric expression of bHLH gene eHand during murine heart development. *Genes Dev,* 11**,** 1357-69.

BIBLE, P. W., KANNO, Y., WEI, L., BROOKS, S. R., O'SHEA, J. J., MORASSO, M. I., LOGANANTHARAJ, R. & SUN, H.-W. 2015. PAPST, a User Friendly and Powerful Java Platform for ChIP-Seq Peak Co-Localization Analysis and Beyond. *PLoS ONE,* 10**,** e0127285.

BIRNBAUM, R. Y., CLOWNEY, E. J., AGAMY, O., KIM, M. J., ZHAO, J., YAMANAKA, T., PAPPALARDO, Z., CLARKE, S. L., WENGER, A. M., NGUYEN, L., GURRIERI, F., EVERMAN, D. B., SCHWARTZ, C. E., BIRK, O. S., BEJERANO, G., LOMVARDAS, S. & AHITUV, N. 2012. Coding exons function as tissue-specific enhancers of nearby genes. *Genome Res,* 22**,** 1059-68.

BLANK, T. A. & BECKER, P. B. 1996. The effect of nucleosome phasing sequences and DNA topology on nucleosome spacing. *J Mol Biol,* 260**,** 1-8.

BLOW, M. J., MCCULLEY, D. J., LI, Z., ZHANG, T., AKIYAMA, J. A., HOLT, A., PLAJZER-FRICK, I., SHOUKRY, M., WRIGHT, C., CHEN, F., AFZAL, V., BRISTOW, J., REN, B., BLACK, B. L., RUBIN, E. M., VISEL, A. & PENNACCHIO, L. A. 2010. ChIP-seq Identification of Weakly Conserved Heart Enhancers. *Nature genetics,* 42**,** 806-810.
BODMER, R. 1993. The gene tinman is required for specification of the heart and visceral muscles in Drosophila. *Development,* 118**,** 719-29.
BONNEFOY, E., ORSI, G. A., COUBLE, P. & LOPPIN, B. 2007. The essential role of Drosophila HIRA for de novo assembly of paternal chromatin at fertilization. *PLoS Genet,* 3**,** 1991-2006.
BORDOLI, L., HÜSSER, S., LÜTHI, U., NETSCH, M., OSMANI, H. & ECKNER, R. 2001. Functional analysis of the p300 acetyltransferase domain: the PHD finger of p300 but not of CBP is dispensable for enzymatic activity. *Nucleic Acids Research,* 29**,** 4462-4471.
BOUVERET, R., WAARDENBERG, A. J., SCHONROCK, N., RAMIALISON, M., DOAN, T., DE JONG, D., BONDUE, A., KAUR, G., MOHAMED, S., FONOUDI, H., CHEN, C. M. & WOUTERS, M. A. 2015. NKX2-5 mutations causative for congenital heart disease retain functionality and are directed to hundreds of targets. 4.
BRAMLAGE, B., KOSCIESSA, U. & DOENECKE, D. 1997. Differential expression of the murine histone genes H3.3A and H3.3B. *Differentiation,* 62**,** 13-20.
BRIEN, G. L., GAMBERO, G., O'CONNELL, D. J., JERMAN, E., TURNER, S. A., EGAN, C. M., DUNNE, E. J., JURGENS, M. C., WYNNE, K., PIAO, L., LOHAN, A. J., FERGUSON, N., SHI, X., SINHA, K. M., LOFTUS, B. J., CAGNEY, G. & BRACKEN, A. P. 2012. Polycomb PHF19 binds H3K36me3 and recruits PRC2 and demethylase NO66 to embryonic stem cell genes during differentiation. *Nat Struct Mol Biol,* 19**,** 1273-81.
BRIND'AMOUR, J., LIU, S., HUDSON, M., CHEN, C., KARIMI, M. M. & LORINCZ, M. C. 2015. Ultra-low-input native ChIP-seq for rare cell populations.
BUCKINGHAM, M., MEILHAC, S. & ZAFFRAN, S. 2005. Building the mammalian heart from two sources of myocardial cells. *Nat Rev Genet,* 6**,** 826-35.
BUENROSTRO, J. D., GIRESI, P. G., ZABA, L. C., CHANG, H. Y. & GREENLEAF, W. J. 2013. Transposition of native chromatin for fast and sensitive epigenomic profiling of open chromatin, DNA-binding proteins and nucleosome position. *Nat Meth,* 10**,** 1213-1218.
CALLIGARIS, S. D., RICCA, M. & CONGET, P. 2013. Cardiac stress test induced by dobutamine and monitored by cardiac catheterization in mice. *J Vis Exp*.
CALMONT, A., IVINS, S., VAN BUEREN, K. L., PAPANGELI, I., KYRIAKOPOULOU, V., ANDREWS, W. D., MARTIN, J. F., MOON, A. M., ILLINGWORTH, E. A., BASSON, M. A. & SCAMBLER, P. J. 2009. Tbx1 controls cardiac neural crest cell migration during arch artery development by regulating Gbx2 expression in the pharyngeal ectoderm. *Development,* 136**,** 3173-83.
CAMBIER, L., PLATE, M., SUCOV, H. M. & PASHMFOROUSH, M. 2014. Nkx2-5 regulates cardiac growth through modulation of Wnt signaling by R-spondin3. *Development,* 141**,** 2959-71.
CARNINCI, P. 2014. Genomics: Mice in the ENCODE spotlight. *Nature,* 515**,** 346-347.
CHEN, P., WANG, Y. & LI, G. 2014. Dynamics of histone variant H3.3 and its coregulation with H2A.Z at enhancers and promoters. *Nucleus,* 5**,** 21-27.
CHEN, P., ZHAO, J., WANG, Y., WANG, M., LONG, H., LIANG, D., HUANG, L., WEN, Z., LI, W., LI, X., FENG, H., ZHAO, H., ZHU, P., LI, M., WANG, Q.-F. & LI, G. 2013. H3.3 actively marks enhancers and primes gene transcription via opening higher-ordered chromatin. *Genes & Development,* 27**,** 2109-2124.
CHEN, W. Y., SHIH, H. T., LIU, K. Y., SHIH, Z. S., CHEN, L. K., TSAI, T. H., CHEN, M. J., LIU, H., TAN, B. C. M., CHEN, C. Y., LEE, H. H., LOPPIN, B., AÏT-AHMED, O. & WU, J. T. 2015. Intellectual disability-associated dBRWD3 regulates gene expression through inhibition of HIRA/YEM-mediated chromatin deposition of histone H3.3. *EMBO reports,* 16**,** 528-538.
CHEPELEV, I., WEI, G., WANGSA, D., TANG, Q. & ZHAO, K. 2012. Characterization of genome-wide enhancer-promoter interactions reveals co-expression of interacting genes and modes of higher order chromatin organization. *Cell Res,* 22**,** 490-503.
CHUJO, M., TARUMOTO, Y., MIYATAKE, K., NISHIDA, E. & ISHIKAWA, F. 2012a. HIRA, a conserved histone chaperone, plays an essential role in low-dose stress response via transcriptional stimulation in fission yeast. *J Biol Chem,* 287**,** 23440-50.
CHUJO, M., TARUMOTO, Y., MIYATAKE, K., NISHIDA, E. & ISHIKAWA, F. 2012b. HIRA, a Conserved Histone Chaperone, Plays an Essential Role in Low-dose Stress Response via Transcriptional Stimulation in Fission Yeast. *The Journal of Biological Chemistry,* 287**,** 23440-23450.
CLAPIER, C. R. & CAIRNS, B. R. 2009. The biology of chromatin remodeling complexes. *Annu Rev Biochem,* 78**,** 273-304.
COLLADO, M. & SERRANO, M. 2010. Senescence in tumours: evidence from mice and humans. *Nat Rev Cancer,* 10**,** 51-7.
COLLAS, P. 2010. The current state of chromatin immunoprecipitation. *Mol Biotechnol,* 45**,** 87-100.
COOPER, M. D., PETERSON, R. D. A. & GOOD, R. A. 1965. A new concept of the cellular basis of immunity. *The Journal of Pediatrics,* 67**,** 907-908.
COWAN, C. A., YOKOYAMA, N., SAXENA, A., CHUMLEY, M. J., SILVANY, R. E., BAKER, L. A., SRIVASTAVA, D. & HENKEMEYER, M. 2004. Ephrin-B2 reverse signaling is required for axon pathfinding and cardiac valve formation but not early vascular development. *Dev Biol,* 271**,** 263-71.
COX, S. G., KIM, H., GARNETT, A. T., MEDEIROS, D. M., AN, W. & CRUMP, J. G. 2012. An essential role of variant histone H3.3 for ectomesenchyme potential of the cranial neural crest. *PLoS Genet,* 8**,** e1002938.
CREYGHTON, M. P., CHENG, A. W., WELSTEAD, G. G., KOOISTRA, T., CAREY, B. W., STEINE, E. J., HANNA, J., LODATO, M. A., FRAMPTON, G. M., SHARP, P. A., BOYER, L. A., YOUNG, R. A. & JAENISCH, R. 2010. Histone H3K27ac separates active from poised enhancers and predicts developmental state. *Proc Natl Acad Sci U S A,* 107**,** 21931-6.
CRUICKSHANKS, H. A., MCBRYAN, T., NELSON, D. M., VANDERKRAATS, N. D., SHAH, P. P., VAN TUYN, J., SINGH RAI, T., BROCK, C., DONAHUE, G., DUNICAN, D. S., DROTAR, M. E., MEEHAN, R. R., EDWARDS, J. R., BERGER, S. L. & ADAMS, P. D. 2013. Senescent cells harbour features of the cancer epigenome. *Nat Cell Biol,* 15**,** 1495-506.
DALVAI, M., BELLUCCI, L., FLEURY, L., LAVIGNE, A. C., MOUTAHIR, F. & BYSTRICKY, K. 2013. H2A.Z-dependent crosstalk between enhancer and promoter regulates cyclin D1 expression. *Oncogene,* 32**,** 4243-51.
DANIEL RICKETTS, M., FREDERICK, B., HOFF, H., TANG, Y., SCHULTZ, D. C., SINGH RAI, T., GRAZIA VIZIOLI, M., ADAMS, P. D. & MARMORSTEIN, R. 2015. Ubinuclein-1 confers histone H3.3-specific-binding by the HIRA histone chaperone complex. *Nat Commun,* 6**,** 7711.
DE BOER, J., ANDRESSOO, J. O., DE WIT, J., HUIJMANS, J., BEEMS, R. B., VAN STEEG, H., WEEDA, G., VAN DER HORST, G. T., VAN LEEUWEN, W., THEMMEN, A. P., MERADJI, M. & HOEIJMAKERS, J. H. 2002. Premature aging in mice deficient in DNA repair and transcription. *Science,* 296**,** 1276-9.
DE KOK, Y. J., VOSSENAAR, E. R., CREMERS, C. W., DAHL, N., LAPORTE, J., HU, L. J., LACOMBE, D., FISCHEL-GHODSIAN, N., FRIEDMAN, R. A., PARNES, L. S., THORPE, P., BITNER-GLINDZICZ, M., PANDER, H. J., HEILBRONNER, H., GRAVELINE, J., DEN DUNNEN, J. T., BRUNNER, H. G., ROPERS, H. H. & CREMERS, F. P. 1996. Identification of a hot

spot for microdeletions in patients with X-linked deafness type 3 (DFN3) 900 kb proximal to the DFN3 gene POU3F4. *Hum Mol Genet,* 5**,** 1229-35.
DE LA CHAPELLE, A., HERVA, R., KOIVISTO, M. & AULA, P. 1981. A deletion in chromosome 22 can cause DiGeorge syndrome. *Hum Genet,* 57**,** 253-6.
DE WIT, E. & DE LAAT, W. 2012. A decade of 3C technologies: insights into nuclear organization. *Genes Dev,* 26**,** 11-24.
DEAL, R. B., HENIKOFF, J. G. & HENIKOFF, S. 2010. Genome-wide kinetics of nucleosome turnover determined by metabolic labeling of histones. *Science,* 328**,** 1161-4.
DEBACQ-CHAINIAUX, F., ERUSALIMSKY, J. D., CAMPISI, J. & TOUSSAINT, O. 2009. Protocols to detect senescence-associated beta-galactosidase (SA-[beta]gal) activity, a biomarker of senescent cells in culture and in vivo. *Nat. Protocols,* 4**,** 1798-1806.
DEBENEDITTIS, P., HARMELINK, C., CHEN, Y., WANG, Q. & JIAO, K. 2011. Characterization of the novel interaction between muskelin and TBX20, a critical cardiogenic transcription factor. *Biochemical and Biophysical Research Communications,* 409**,** 338-343.
DELGADO-OLGUIN, P., HUANG, Y., LI, X., CHRISTODOULOU, D., SEIDMAN, C. E., SEIDMAN, J. G., TARAKHOVSKY, A. & BRUNEAU, B. G. 2012. Epigenetic repression of cardiac progenitor gene expression by Ezh2 is required for postnatal cardiac homeostasis. *Nat Genet,* 44**,** 343-7.
DIMOVA, D., NACKERDIEN, Z., FURGESON, S., EGUCHI, S. & OSLEY, M. A. A Role for Transcriptional Repressors in Targeting the Yeast Swi/Snf Complex. *Molecular Cell,* 4**,** 75-83.
DISTLER, J. H., HIRTH, A., KUROWSKA-STOLARSKA, M., GAY, R. E., GAY, S. & DISTLER, O. 2003. Angiogenic and angiostatic factors in the molecular control of angiogenesis. *Q J Nucl Med,* 47**,** 149-61.
DOVEY, O. M., FOSTER, C. T. & COWLEY, S. M. 2010. Histone deacetylase 1 (HDAC1), but not HDAC2, controls embryonic stem cell differentiation. *Proc Natl Acad Sci U S A,* 107**,** 8242-7.
DUPAYS, L., SHANG, C., WILSON, R., KOTECHA, S., WOOD, S., TOWERS, N. & MOHUN, T. 2015. Sequential Binding of MEIS1 and NKX2-5 on the Popdc2 Gene: A Mechanism for Spatiotemporal Regulation of Enhancers during Cardiogenesis. *Cell Rep,* 13**,** 183-95.
DURANTE, M., BEDFORD, J. S., CHEN, D. J., CONRAD, S., CORNFORTH, M. N., NATARAJAN, A. T., VAN GENT, D. C. & OBE, G. 2013. From DNA damage to chromosome aberrations: joining the break. *Mutat Res,* 756**,** 5-13.
DUTTA, D., RAY, S., HOME, P., SAHA, B., WANG, S., SHEIBANI, N., TAWFIK, O., CHENG, N. & PAUL, S. 2010. Regulation of Angiogenesis by Histone Chaperone HIRA-mediated Incorporation of Lysine 56-acetylated Histone H3.3 at Chromatin Domains of Endothelial Genes. *Journal of Biological Chemistry,* 285**,** 41567-41577.
DYER, L. A. & KIRBY, M. L. 2009. The Role of Secondary Heart Field in Cardiac Development. *Developmental biology,* 336**,** 137-144.
EKLUND, L., BRY, M. & ALITALO, K. 2013. Mouse models for studying angiogenesis and lymphangiogenesis in cancer. *Mol Oncol,* 7**,** 259-82.
ELGIN, S. C. & REUTER, G. 2013. Position-effect variegation, heterochromatin formation, and gene silencing in Drosophila. *Cold Spring Harb Perspect Biol,* 5**,** a017780.
ENGLISH, C. M., ADKINS, M. W., CARSON, J. J., CHURCHILL, M. E. A. & TYLER, J. K. Structural Basis for the Histone Chaperone Activity of Asf1. *Cell,* 127**,** 495-508.
FARRELL, M. J., STADT, H., WALLIS, K. T., SCAMBLER, P., HIXON, R. L., WOLFE, R., LEATHERBURY, L. & KIRBY, M. L. 1999. HIRA, a DiGeorge syndrome candidate gene, is required for cardiac outflow tract septation. *Circ Res,* 84**,** 127-35.
FARRIS, S. D., RUBIO, E. D., MOON, J. J., GOMBERT, W. M., NELSON, B. H. & KRUMM, A. 2005. Transcription-induced chromatin remodeling at the c-myc gene involves the local exchange of histone H2A.Z. *J Biol Chem,* 280**,** 25298-303.
FELSENFELD, G., BOYES, J., CHUNG, J., CLARK, D. & STUDITSKY, V. 1996. Chromatin structure and gene expression. *Proceedings of the National Academy of Sciences of the United States of America,* 93**,** 9384-9388.
FENG, J., LIU, T., QIN, B., ZHANG, Y. & LIU, X. S. 2012. Identifying ChIP-seq enrichment using MACS. *Nature protocols,* 7**,** 10.1038/nprot.2012.101.
FENOUIL, R., CAUCHY, P., KOCH, F., DESCOSTES, N., CABEZA, J. Z., INNOCENTI, C., FERRIER, P., SPICUGLIA, S., GUT, M., GUT, I. & ANDRAU, J. C. 2012. CpG islands and GC content dictate nucleosome depletion in a transcription-independent manner at mammalian promoters. *Genome Res,* 22**,** 2399-408.
FLAHT, A., JANKOWSKA-STEIFER, E., RADOMSKA, D. M., MADEJ, M., GULA, G., KUJAWA, M. & RATAJSKA, A. 2012. Cellular phenotypes and spatio-temporal patterns of lymphatic vessel development in embryonic mouse hearts. *Dev Dyn,* 241**,** 1473-86.
FRANCO, D., LAMERS, W. H. & MOORMAN, A. F. 1998. Patterns of expression in the developing myocardium: towards a morphologically integrated transcriptional model. *Cardiovasc Res,* 38**,** 25-53.
FRIEDEN, L. A., TOWNSEND, T. A., VAUGHT, D. B., DELAUGHTER, D. M., HWANG, Y., BARNETT, J. V. & CHEN, J. 2010. Regulation of heart valve morphogenesis by Eph receptor ligand, ephrin-A1. *Dev Dyn,* 239**,** 3226-34.
FUKS, F., HURD, P. J., WOLF, D., NAN, X., BIRD, A. P. & KOUZARIDES, T. 2003. The methyl-CpG-binding protein MeCP2 links DNA methylation to histone methylation. *J Biol Chem,* 278**,** 4035-40.
FUREY, T. S. 2012. ChIP-seq and beyond: new and improved methodologies to detect and characterize protein-DNA interactions. *Nat Rev Genet,* 13**,** 840-52.
GARCIA-RAMIREZ, M., ROCCHINI, C. & AUSIO, J. 1995. Modulation of chromatin folding by histone acetylation. *J Biol Chem,* 270**,** 17923-8.
GAUVRIT, S., PHILIPPE, J., LESAGE, M., TJWA, M., GODIN, I. & GERMAIN, S. 2014. The role of RNA interference in the developmental separation of blood and lymphatic vasculature. *Vascular Cell,* 6**,** 1-10.
GOLDBERG, A. D., BANASZYNSKI, L. A., NOH, K. M., LEWIS, P. W., ELSAESSER, S. J., STADLER, S., DEWELL, S., LAW, M., GUO, X., LI, X., WEN, D., CHAPGIER, A., DEKELVER, R. C., MILLER, J. C., LEE, Y. L., BOYDSTON, E. A., HOLMES, M. C., GREGORY, P. D., GREALLY, J. M., RAFII, S., YANG, C., SCAMBLER, P. J., GARRICK, D., GIBBONS, R. J., HIGGS, D. R., CRISTEA, I. M., URNOV, F. D., ZHENG, D. & ALLIS, C. D. 2010. Distinct factors control histone variant H3.3 localization at specific genomic regions. *Cell,* 140**,** 678-91.
GORDON, A. M., REGNIER, M. & HOMSHER, E. 2001. Skeletal and cardiac muscle contractile activation: tropomyosin "rocks and rolls". *News Physiol Sci,* 16**,** 49-55.
GROTH, A., CORPET, A., COOK, A. J., ROCHE, D., BARTEK, J., LUKAS, J. & ALMOUZNI, G. 2007. Regulation of replication fork progression through histone supply and demand. *Science,* 318**,** 1928-31.
GUO, M., THOMAS, J., COLLINS, G. & TIMMERMANS, M. C. 2008. Direct repression of KNOX loci by the ASYMMETRIC LEAVES1 complex of Arabidopsis. *Plant Cell,* 20**,** 48-58.
HAIGH, L. S., OWENS, B. B., HELLEWELL, O. S. & INGRAM, V. M. 1982. DNA methylation in chicken alpha-globin gene expression. *Proceedings of the National Academy of Sciences of the United States of America,* 79**,** 5332-5336.
HAKE, S. B., GARCIA, B. A., KAUER, M., BAKER, S. P., SHABANOWITZ, J., HUNT, D. F. & ALLIS, C. D. 2005. Serine 31 phosphorylation of histone variant H3.3 is specific to regions bordering centromeres in metaphase chromosomes. *Proc Natl Acad Sci U S A,* 102**,** 6344-9.

HALFORD, S., WADEY, R., ROBERTS, C., DAW, S. C. M., WHITING, J. A., O'DONNELL, H., DUNHAM, I., BENTLEY, D., LINDSAY, E., BALDINI, A., FRANCIS, F., LEHRACH, H., WILLIAMSON, R., WILSON, D. I., GOODSHIP, J., CROSS, I., BURN, J. & SCAMBLER, P. J. 1993. Isolation of a putative transcriptional regulator from the region of 22q11 deleted in DiGeorge syndrome, Shprintzen syndrome and familial congenital heart disease. *Human Molecular Genetics,* 2**,** 2099-2107.

HALL, C., NELSON, D. M., YE, X., BAKER, K., DECAPRIO, J. A., SEEHOLZER, S., LIPINSKI, M. & ADAMS, P. D. 2001. HIRA, the human homologue of yeast Hir1p and Hir2p, is a novel cyclin-cdk2 substrate whose expression blocks S-phase progression. *Mol Cell Biol,* 21**,** 1854-65.

HALL, I. M., SHANKARANARAYANA, G. D., NOMA, K., AYOUB, N., COHEN, A. & GREWAL, S. I. 2002. Establishment and maintenance of a heterochromatin domain. *Science,* 297**,** 2232-7.

HANG, C. T., YANG, J., HAN, P., CHENG, H. L., SHANG, C., ASHLEY, E., ZHOU, B. & CHANG, C. P. 2010. Chromatin regulation by Brg1 underlies heart muscle development and disease. *Nature,* 466**,** 62-7.

HARDY, S. & ROBERT, F. 2010. Random deposition of histone variants: A cellular mistake or a novel regulatory mechanism? *Epigenetics,* 5**,** 368-72.

HAUBNER, B. J., ADAMOWICZ-BRICE, M., KHADAYATE, S., TIEFENTHALER, V., METZLER, B., AITMAN, T. & PENNINGER, J. M. 2012. Complete cardiac regeneration in a mouse model of myocardial infarction. *Aging (Albany NY),* 4**,** 966-77.

HE, X., DUQUE, T. S. & SINHA, S. 2012. Evolutionary origins of transcription factor binding site clusters. *Mol Biol Evol,* 29**,** 1059-70.

HE, X., HE, X., DAVE, V. P., ZHANG, Y., HUA, X., NICOLAS, E., XU, W., ROE, B. A. & KAPPES, D. J. 2005. The zinc finger transcription factor Th-POK regulates CD4 versus CD8 T-cell lineage commitment. *Nature,* 433**,** 826-33.

HENIKOFF, S. & AHMAD, K. 2005. Assembly of variant histones into chromatin. *Annu Rev Cell Dev Biol,* 21**,** 133-53.

HERRMANN, F., GROß, A., ZHOU, D., KESTLER, H. A. & KÜHL, M. 2012. A Boolean Model of the Cardiac Gene Regulatory Network Determining First and Second Heart Field Identity. *PLoS ONE,* 7**,** e46798.

HILDRETH, V., WEBB, S., BRADSHAW, L., BROWN, N. A., ANDERSON, R. H. & HENDERSON, D. J. 2008. Cells migrating from the neural crest contribute to the innervation of the venous pole of the heart. *Journal of Anatomy,* 212**,** 1-11.

HO, L. & CRABTREE, G. R. 2010. Chromatin remodelling during development. *Nature,* 463**,** 474-484.

HO, L., RONAN, J. L., WU, J., STAAHL, B. T., CHEN, L., KUO, A., LESSARD, J., NESVIZHSKII, A. I., RANISH, J. & CRABTREE, G. R. 2009. An embryonic stem cell chromatin remodeling complex, esBAF, is essential for embryonic stem cell self-renewal and pluripotency. *Proc Natl Acad Sci U S A,* 106**,** 5181-6.

HON, G. C., HAWKINS, R. D. & REN, B. 2009. Predictive chromatin signatures in the mammalian genome. *Hum Mol Genet,* 18**,** R195-201.

HUANG, C. & ZHU, B. 2014. H3.3 turnover: a mechanism to poise chromatin for transcription, or a response to open chromatin? *Bioessays,* 36**,** 579-84.

HUANG, Q. Q., FENG, H. Z., LIU, J., DU, J., STULL, L. B., MORAVEC, C. S., HUANG, X. & JIN, J. P. 2008. Co-expression of skeletal and cardiac troponin T decreases mouse cardiac function. *Am J Physiol Cell Physiol,* 294**,** C213-22.

HUEN, M. S. Y., SY, S. M. H., VAN DEURSEN, J. M. & CHEN, J. 2008. Direct Interaction between SET8 and Proliferating Cell Nuclear Antigen Couples H4-K20 Methylation with DNA Replication. *The Journal of Biological Chemistry,* 283**,** 11073-11077.

INUI, M., MIYADO, M., IGARASHI, M., TAMANO, M., KUBO, A., YAMASHITA, S., ASAHARA, H., FUKAMI, M. & TAKADA, S. 2014. Rapid generation of mouse models with defined point mutations by the CRISPR/Cas9 system. *Scientific Reports,* 4**,** 5396.

JACQUES-FRICKE, B. T., ROFFERS-AGARWAL, J. & GAMMILL, L. S. * Wnt1-cre drives cre expression in premigratory cranial neural crest cells, while Sox10-cre is activated during cranial neural crest migration. *.

JANES, P. W., SAHA, N., BARTON, W. A., KOLEV, M. V., WIMMER-KLEIKAMP, S. H., NIEVERGALL, E., BLOBEL, C. P., HIMANEN, J.-P., LACKMANN, M. & NIKOLOV, D. B. 2005. Adam Meets Eph: An ADAM Substrate Recognition Module Acts as a Molecular Switch for Ephrin Cleavage In trans. *Cell,* 123**,** 291-304.

JANG, H., CHOI, D. E., KIM, H., CHO, E. J. & YOUN, H. D. 2007. Cabin1 represses MEF2 transcriptional activity by association with a methyltransferase, SUV39H1. *J Biol Chem,* 282**,** 11172-9.

JENUWEIN, T. & ALLIS, C. D. 2001. Translating the histone code. *Science,* 293**,** 1074-80.

JIANG, X., ROWITCH, D. H., SORIANO, P., MCMAHON, A. P. & SUCOV, H. M. 2000. Fate of the mammalian cardiac neural crest. *Development,* 127**,** 1607-16.

JIN, B., LI, Y. & ROBERTSON, K. D. 2011. DNA Methylation: Superior or Subordinate in the Epigenetic Hierarchy? *Genes & Cancer,* 2**,** 607-617.

JIN, C., ZANG, C., WEI, G., CUI, K., PENG, W., ZHAO, K. & FELSENFELD, G. 2009. H3.3/H2A.Z double variant-containing nucleosomes mark 'nucleosome-free regions' of active promoters and other regulatory regions. *Nat Genet,* 41**,** 941-5.

JONES, D. T., JAGER, N., KOOL, M., ZICHNER, T., HUTTER, B., SULTAN, M., CHO, Y. J., PUGH, T. J., HOVESTADT, V., STUTZ, A. M., RAUSCH, T., WARNATZ, H. J., RYZHOVA, M., BENDER, S., STURM, D., PLEIER, S., CIN, H., PFAFF, E., SIEBER, L., WITTMANN, A., REMKE, M., WITT, H., HUTTER, S., TZARIDIS, T., WEISCHENFELDT, J., RAEDER, B., AVCI, M., AMSTISLAVSKIY, V., ZAPATKA, M., WEBER, U. D., WANG, Q., LASITSCHKA, B., BARTHOLOMAE, C. C., SCHMIDT, M., VON KALLE, C., AST, V., LAWERENZ, C., EILS, J., KABBE, R., BENES, V., VAN SLUIS, P., KOSTER, J., VOLCKMANN, R., SHIH, D., BETTS, M. J., RUSSELL, R. B., COCO, S., TONINI, G. P., SCHULLER, U., HANS, V., GRAF, N., KIM, Y. J., MONORANU, C., ROGGENDORF, W., UNTERBERG, A., HEROLD-MENDE, C., MILDE, T., KULOZIK, A. E., VON DEIMLING, A., WITT, O., MAASS, E., ROSSLER, J., EBINGER, M., SCHUHMANN, M. U., FRUHWALD, M. C., HASSELBLATT, M., JABADO, N., RUTKOWSKI, S., VON BUEREN, A. O., WILLIAMSON, D., CLIFFORD, S. C., MCCABE, M. G., COLLINS, V. P., WOLF, S., WIEMANN, S., LEHRACH, H., BRORS, B., SCHEURLEN, W., FELSBERG, J., REIFENBERGER, G., NORTHCOTT, P. A., TAYLOR, M. D., MEYERSON, M., POMEROY, S. L., YASPO, M. L., KORBEL, J. O., KORSHUNOV, A., EILS, R., PFISTER, S. M. & LICHTER, P. 2012. Dissecting the genomic complexity underlying medulloblastoma. *Nature,* 488**,** 100-5.

JOUKOV, V., PAJUSOLA, K., KAIPAINEN, A., CHILOV, D., LAHTINEN, I., KUKK, E., SAKSELA, O., KALKKINEN, N. & ALITALO, K. 1996. A novel vascular endothelial growth factor, VEGF-C, is a ligand for the Flt4 (VEGFR-3) and KDR (VEGFR-2) receptor tyrosine kinases. *Embo j,* 15**,** 290-98.

JUNION, G., SPIVAKOV, M., GIRARDOT, C., BRAUN, M., GUSTAFSON, E. H., BIRNEY, E. & FURLONG, EILEEN E. M. A Transcription Factor Collective Defines Cardiac Cell Fate and Reflects Lineage History. *Cell,* 148**,** 473-486.

KALLAPPAGOUDAR, S., YADAV, R. K., LOWE, B. R. & PARTRIDGE, J. F. 2015. Histone H3 mutations—a special role for H3.3 in tumorigenesis? *Chromosoma,* 124**,** 177-189.

KAMAKAKA, R. T. & BIGGINS, S. 2005. Histone variants: deviants? *Genes Dev,* 19**,** 295-310.

KANG, S. H., SEOK, Y. M., SONG, M. J., LEE, H. A., KURZ, T. & KIM, I. 2015. Histone deacetylase inhibition attenuates cardiac hypertrophy and fibrosis through acetylation of mineralocorticoid receptor in spontaneously hypertensive rats. *Mol Pharmacol,* 87**,** 782-91.

KAPLAN, N., HUGHES, T. R., LIEB, J. D., WIDOM, J. & SEGAL, E. 2010. Contribution of histone sequence preferences to nucleosome organization: proposed definitions and methodology. *Genome Biol,* 11**,** 140.
KARPOVA, T. & MCNALLY, J. G. 2006. Detecting protein-protein interactions with CFP-YFP FRET by acceptor photobleaching. *Curr Protoc Cytom,* Chapter 12**,** Unit12.7.
KASAHARA, H., BARTUNKOVA, S., SCHINKE, M., TANAKA, M. & IZUMO, S. 1998. Cardiac and extracardiac expression of Csx/Nkx2.5 homeodomain protein. *Circ Res,* 82**,** 936-46.
KEMBLE, D. J., MCCULLOUGH, L. L., WHITBY, F. G., FORMOSA, T. & HILL, C. P. 2015. FACT Disrupts Nucleosome Structure by Binding H2A-H2B with Conserved Peptide Motifs. *Mol Cell,* 60**,** 294-306.
KERN, C. B., TWAL, W. O., MJAATVEDT, C. H., FAIREY, S. E., TOOLE, B. P., IRUELA-ARISPE, M. L. & ARGRAVES, W. S. 2006. Proteolytic Cleavage of Versican During Cardiac Cushion Morphogenesis. *Developmental dynamics : an official publication of the American Association of Anatomists,* 235**,** 2238-2247.
KIM, J. & KIM, H. 2012. Recruitment and biological consequences of histone modification of H3K27me3 and H3K9me3. *Ilar j,* 53**,** 232-9.
KIRBY, M. L. & WALDO, K. L. 1995. Neural crest and cardiovascular patterning. *Circ Res,* 77**,** 211-5.
KIRSCH, I. R., GREEN, E. D., YONESCU, R., STRAUSBERG, R., CARTER, N., BENTLEY, D., LEVERSHA, M. A., DUNHAM, I., BRADEN, V. V., HILGENFELD, E., SCHULER, G., LASH, A. E., SHEN, G. L., MARTELLI, M., KUEHL, W. M., KLAUSNER, R. D. & RIED, T. 2000. A systematic, high-resolution linkage of the cytogenetic and physical maps of the human genome. *Nat Genet,* 24**,** 339-40.
KISANUKI, Y. Y., HAMMER, R. E., MIYAZAKI, J., WILLIAMS, S. C., RICHARDSON, J. A. & YANAGISAWA, M. 2001. Tie2-Cre transgenic mice: a new model for endothelial cell-lineage analysis in vivo. *Dev Biol,* 230**,** 230-42.
KLOTZ, L., NORMAN, S., VIEIRA, J. M., MASTERS, M., ROHLING, M., DUBÉ, K. N., BOLLINI, S., MATSUZAKI, F., CARR, C. A. & RILEY, P. R. 2015. Cardiac lymphatics are heterogeneous in origin and respond to injury. *Nature,* 522**,** 62-67.
KORNBERG, R. D. 2007. The molecular basis of eukaryotic transcription. *Proceedings of the National Academy of Sciences of the United States of America,* 104**,** 12955-12961.
KOVACIC, J. C., MERCADER, N., TORRES, M., BOEHM, M. & FUSTER, V. 2012. Epithelial-to-mesenchymal and endothelial-to-mesenchymal transition: from cardiovascular development to disease. *Circulation,* 125**,** 1795-808.
KROCK, B. L., SKULI, N. & SIMON, M. C. 2011. Hypoxia-Induced Angiogenesis: Good and Evil. *Genes & Cancer,* 2**,** 1117-1133.
KUMAR, S. 2011. Remote homologue identification of Drosophila GAGA factor in mouse. *Bioinformation,* 7**,** 29-32.
KUMAR, S. V. & WIGGE, P. A. 2010. H2A.Z-containing nucleosomes mediate the thermosensory response in Arabidopsis. *Cell,* 140**,** 136-47.
LAMOUR, V., LECLUSE, Y., DESMAZE, C., SPECTOR, M., BODESCOT, M., AURIAS, A., OSLEY, M. A. & LIPINSKI, M. 1995. A human homolog of the S. cerevisiae HIR1 and HIR2 transcriptional repressors cloned from the DiGeorge syndrome critical region. *Hum Mol Genet,* 4**,** 791-9.
LANGE, M., KAYNAK, B., FORSTER, U. B., TONJES, M., FISCHER, J. J., GRIMM, C., SCHLESINGER, J., JUST, S., DUNKEL, I., KRUEGER, T., MEBUS, S., LEHRACH, H., LURZ, R., GOBOM, J., ROTTBAUER, W., ABDELILAH-SEYFRIED, S. & SPERLING, S. 2008. Regulation of muscle development by DPF3, a novel histone acetylation and methylation reader of the BAF chromatin remodeling complex. *Genes Dev,* 22**,** 2370-84.
LARKIN, J. D., COOK, P. R. & PAPANTONIS, A. 2012. Dynamic reconfiguration of long human genes during one transcription cycle. *Mol Cell Biol,* 32**,** 2738-47.
LE, S., DAVIS, C., KONOPKA, J. B. & STERNGLANZ, R. 1997. Two new S-phase-specific genes from Saccharomyces cerevisiae. *Yeast,* 13**,** 1029-42.
LEE, Y. F., NIMURA, K., LO, W. N., SAGA, K. & KANEDA, Y. 2014. Histone H3 lysine 36 methyltransferase Whsc1 promotes the association of Runx2 and p300 in the activation of bone-related genes. *PLoS One,* 9**,** e106661.
LEHMAN, W., CRAIG, R. & VIBERT, P. 1994. Ca(2+)-induced tropomyosin movement in Limulus thin filaments revealed by three-dimensional reconstruction. *Nature,* 368**,** 65-7.
LESCROART, F., CHABAB, S., LIN, X., RULANDS, S., PAULISSEN, C., RODOLOSSE, A., AUER, H., ACHOURI, Y., DUBOIS, C., BONDUE, A., SIMONS, B. D. & BLANPAIN, C. 2014. Early lineage restriction in temporally distinct populations of Mesp1 progenitors during mammalian heart development. *Nat Cell Biol,* 16**,** 829-40.
LI, X. Y., MACARTHUR, S., BOURGON, R., NIX, D., POLLARD, D. A., IYER, V. N., HECHMER, A., SIMIRENKO, L., STAPLETON, M., LUENGO HENDRIKS, C. L., CHU, H. C., OGAWA, N., INWOOD, W., SEMENTCHENKO, V., BEATON, A., WEISZMANN, R., CELNIKER, S. E., KNOWLES, D. W., GINGERAS, T., SPEED, T. P., EISEN, M. B. & BIGGIN, M. D. 2008. Transcription factors bind thousands of active and inactive regions in the Drosophila blastoderm. *PLoS Biol,* 6**,** e27.
LICKERT, H., TAKEUCHI, J. K., VON BOTH, I., WALLS, J. R., MCAULIFFE, F., ADAMSON, S. L., HENKELMAN, R. M., WRANA, J. L., ROSSANT, J. & BRUNEAU, B. G. 2004. Baf60c is essential for function of BAF chromatin remodelling complexes in heart development. *Nature,* 432**,** 107-12.
LIN, C.-J., LIN, C.-Y., CHEN, C.-H., ZHOU, B. & CHANG, C.-P. 2012. Partitioning the heart: mechanisms of cardiac septation and valve development. *Development,* 139**,** 3277-3299.
LIN, C. J., CONTI, M. & RAMALHO-SANTOS, M. 2013. Histone variant H3.3 maintains a decondensed chromatin state essential for mouse preimplantation development. *Development,* 140**,** 3624-34.
LIN, C. J., KOH, F. M., WONG, P., CONTI, M. & RAMALHO-SANTOS, M. 2014. Hira-mediated H3.3 incorporation is required for DNA replication and ribosomal RNA transcription in the mouse zygote. *Dev Cell,* 30**,** 268-79.
LIN, Q., SCHWARZ, J., BUCANA, C. & OLSON, E. N. 1997. Control of Mouse Cardiac Morphogenesis and Myogenesis by Transcription Factor MEF2C. *Science (New York, N.Y.),* 276**,** 1404-1407.
LINDSAY, E. A., BOTTA, A., JURECIC, V., CARATTINI-RIVERA, S., CHEAH, Y. C., ROSENBLATT, H. M., BRADLEY, A. & BALDINI, A. 1999. Congenital heart disease in mice deficient for the DiGeorge syndrome region. *Nature,* 401**,** 379-83.
LINDSAY, E. A., VITELLI, F., SU, H., MORISHIMA, M., HUYNH, T., PRAMPARO, T., JURECIC, V., OGUNRINU, G., SUTHERLAND, H. F., SCAMBLER, P. J., BRADLEY, A. & BALDINI, A. 2001. Tbx1 haploinsufficieny in the DiGeorge syndrome region causes aortic arch defects in mice. *Nature,* 410**,** 97-101.
LIU, Y., HARMELINK, C., PENG, Y., CHEN, Y., WANG, Q. & JIAO, K. 2014a. CHD7 interacts with BMP R-SMADs to epigenetically regulate cardiogenesis in mice. *Hum Mol Genet,* 23**,** 2145-56.
LIU, Z., XING, D., SU, Q. P., ZHU, Y., ZHANG, J., KONG, X., XUE, B., WANG, S., SUN, H., TAO, Y. & SUN, Y. 2014b. Super-resolution imaging and tracking of protein–protein interactions in sub-diffraction cellular space. *Nat Commun,* 5.
LLEVADOT, R., MARQUES, G., PRITCHARD, M., ESTIVILL, X., FERRUS, A. & SCAMBLER, P. 1998. Cloning, chromosome mapping and expression analysis of the HIRA gene from Drosophila melanogaster. *Biochem Biophys Res Commun,* 249**,** 486-91.
LOPPIN, B., BONNEFOY, E., ANSELME, C., LAURENCON, A., KARR, T. L. & COUBLE, P. 2005. The histone H3.3 chaperone HIRA is essential for chromatin assembly in the male pronucleus. *Nature,* 437**,** 1386-90.
LOPPIN, B., DOCQUIER, M., BONNETON, F. & COUBLE, P. 2000. The maternal effect mutation sesame affects the formation of the male pronucleus in Drosophila melanogaster. *Dev Biol,* 222**,** 392-404.

LORAIN, S., QUIVY, J. P., MONIER-GAVELLE, F., SCAMPS, C., LECLUSE, Y., ALMOUZNI, G. & LIPINSKI, M. 1998. Core histones and HIRIP3, a novel histone-binding protein, directly interact with WD repeat protein HIRA. *Mol Cell Biol,* 18**,** 5546-56.

LOVE, C., SUN, Z., JIMA, D., LI, G., ZHANG, J., MILES, R., RICHARDS, K. L., DUNPHY, C. H., CHOI, W. W., SRIVASTAVA, G., LUGAR, P. L., RIZZIERI, D. A., LAGOO, A. S., BERNAL-MIZRACHI, L., MANN, K. P., FLOWERS, C. R., NARESH, K. N., EVENS, A. M., CHADBURN, A., GORDON, L. I., CZADER, M. B., GILL, J. I., HSI, E. D., GREENOUGH, A., MOFFITT, A. B., MCKINNEY, M., BANERJEE, A., GRUBOR, V., LEVY, S., DUNSON, D. B. & DAVE, S. S. 2012. The genetic landscape of mutations in Burkitt lymphoma. *Nat Genet,* 44**,** 1321-5.

LUGER, K., MADER, A. W., RICHMOND, R. K., SARGENT, D. F. & RICHMOND, T. J. 1997. Crystal structure of the nucleosome core particle at 2.8 A resolution. *Nature,* 389**,** 251-60.

LUNA-ZURITA, L., STIRNIMANN, CHRISTIAN U., GLATT, S., KAYNAK, BOGAC L., THOMAS, S., BAUDIN, F., SAMEE, MD ABUL H., HE, D., SMALL, ERIC M., MILEIKOVSKY, M., NAGY, A., HOLLOWAY, ALISHA K., POLLARD, KATHERINE S., MÜLLER, CHRISTOPH W. & BRUNEAU, BENOIT G. Complex Interdependence Regulates Heterotypic Transcription Factor Distribution and Coordinates Cardiogenesis. *Cell.*

LUND, J., ROE, B., CHEN, F., BUDARF, M., GALILI, N., RIBLET, R., MILLER, R. D., EMANUEL, B. S. & REEVES, R. H. 1999. Sequence-ready physical map of the mouse chromosome 16 region with conserved synteny to the human velocardiofacial syndrome region on 22q11.2. *Mamm Genome,* 10**,** 438-43.

LUONG, M. X., TAM, J., LIN, Q., HAGENDOORN, J., MOORE, K. J., PADERA, T. P., SEED, B., FUKUMURA, D., KUCHERLAPATI, R. & JAIN, R. K. 2009. Lack of lymphatic vessel phenotype in LYVE-1/CD44 double knockout mice. *J Cell Physiol,* 219**,** 430-7.

MA, Q., ZHOU, B. & PU, W. T. 2008. Reassessment of Isl1 and Nkx2-5 cardiac fate maps using a Gata4-based reporter of Cre activity. *Developmental Biology,* 323**,** 98-104.

MAGNAGHI, P., ROBERTS, C., LORAIN, S., LIPINSKI, M. & SCAMBLER, P. J. 1998. HIRA, a mammalian homologue of Saccharomyces cerevisiae transcriptional co-repressors, interacts with Pax3. *Nat Genet,* 20**,** 74-7.

MANSOOR, F. & ALI, R. 2007. Characterization of chromatin modified with reactive oxygen species: Recognition by autoantibodies in cancer. *Clinical Biochemistry,* 40**,** 928-935.

MANUYLOV, N. L. & TEVOSIAN, S. G. 2009. Cardiac Expression of Tnnt1 Requires the GATA4-FOG2 Transcription Complex. *TheScientificWorldJOURNAL,* 9.

MARSMAN, J. & HORSFIELD, J. A. 2012. Long distance relationships: Enhancer–promoter communication and dynamic gene transcription. *Biochimica et Biophysica Acta (BBA) - Gene Regulatory Mechanisms,* 1819**,** 1217-1227.

MARTIN, C. & ZHANG, Y. 2007. Mechanisms of epigenetic inheritance. *Current Opinion in Cell Biology,* 19**,** 266-272.

MASUMOTO, H., HAWKE, D., KOBAYASHI, R. & VERREAULT, A. 2005. A role for cell-cycle-regulated histone H3 lysine 56 acetylation in the DNA damage response. *Nature,* 436**,** 294-298.

MATHARU, N. K., HUSSAIN, T., SANKARANARAYANAN, R. & MISHRA, R. K. 2010. Vertebrate Homologue of Drosophila GAGA Factor. *Journal of Molecular Biology,* 400**,** 434-447.

MAZE, I., NOH, K. M., SOSHNEV, A. A. & ALLIS, C. D. 2014. Every amino acid matters: essential contributions of histone variants to mammalian development and disease. *Nat Rev Genet,* 15**,** 259-71.

MCELHINNEY, D. B., GEIGER, E., BLINDER, J., WOODROW BENSON, D. & GOLDMUNTZ, E. 2003. NKX2.5 mutations in patients with congenital heart disease. *Journal of the American College of Cardiology,* 42**,** 1650-1655.

MCKITTRICK, E., GAFKEN, P. R., AHMAD, K. & HENIKOFF, S. 2004. Histone H3.3 is enriched in covalent modifications associated with active chromatin. *Proc Natl Acad Sci U S A,* 101**,** 1525-30.

MCLEOD, M. J. 1980. Differential staining of cartilage and bone in whole mouse fetuses by alcian blue and alizarin red S. *Teratology,* 22**,** 299-301.

MCMAHON, A. P. & BRADLEY, A. 1990. The Wnt-1 (int-1) proto-oncogene is required for development of a large region of the mouse brain. *Cell,* 62**,** 1073-85.

MEILHAC, S. M., ESNER, M., KELLY, R. G., NICOLAS, J. F. & BUCKINGHAM, M. E. 2004. The clonal origin of myocardial cells in different regions of the embryonic mouse heart. *Dev Cell,* 6**,** 685-98.

MESHORER, E., YELLAJOSHULA, D., GEORGE, E., SCAMBLER, P. J., BROWN, D. T. & MISTELI, T. 2006. Hyperdynamic plasticity of chromatin proteins in pluripotent embryonic stem cells. *Dev Cell,* 10**,** 105-16.

MICHAELOVSKY, E., FRISCH, A., CARMEL, M., PATYA, M., ZARCHI, O., GREEN, T., BASEL-VANAGAITE, L., WEIZMAN, A. & GOTHELF, D. 2012. Genotype-phenotype correlation in 22q11.2 deletion syndrome. *BMC Med Genet,* 13**,** 122.

MIKKELSEN, T. S., KU, M., JAFFE, D. B., ISSAC, B., LIEBERMAN, E., GIANNOUKOS, G., ALVAREZ, P., BROCKMAN, W., KIM, T. K., KOCHE, R. P., LEE, W., MENDENHALL, E., O'DONOVAN, A., PRESSER, A., RUSS, C., XIE, X., MEISSNER, A., WERNIG, M., JAENISCH, R., NUSBAUM, C., LANDER, E. S. & BERNSTEIN, B. E. 2007. Genome-wide maps of chromatin state in pluripotent and lineage-committed cells. *Nature,* 448**,** 553-60.

MILLAU, J. F. & GAUDREAU, L. 2011. CTCF, cohesin, and histone variants: connecting the genome. *Biochem Cell Biol,* 89**,** 505-13.

MILUTINOVIC, S., ZHUANG, Q. & SZYF, M. 2002. Proliferating cell nuclear antigen associates with histone deacetylase activity, integrating DNA replication and chromatin modification. *J Biol Chem,* 277**,** 20974-8.

MITO, Y., HENIKOFF, J. G. & HENIKOFF, S. 2005. Genome-scale profiling of histone H3.3 replacement patterns. *Nat Genet,* 37**,** 1090-7.

MOLDOVAN, G.-L., PFANDER, B. & JENTSCH, S. PCNA, the Maestro of the Replication Fork. *Cell,* 129**,** 665-679.

MOLKENTIN, J. D., LIN, Q., DUNCAN, S. A. & OLSON, E. N. 1997. Requirement of the transcription factor GATA4 for heart tube formation and ventral morphogenesis. *Genes Dev,* 11**,** 1061-72.

MOLKENTIN, J. D., TYMITZ, K. M., RICHARDSON, J. A. & OLSON, E. N. 2000. Abnormalities of the genitourinary tract in female mice lacking GATA5. *Mol Cell Biol,* 20**,** 5256-60.

MOORMAN, A., WEBB, S., BROWN, N. A., LAMERS, W. & ANDERSON, R. H. 2003. DEVELOPMENT OF THE HEART: (1) FORMATION OF THE CARDIAC CHAMBERS AND ARTERIAL TRUNKS. *Heart,* 89**,** 806-814.

MOORMAN, A. F. & CHRISTOFFELS, V. M. 2003. Cardiac chamber formation: development, genes, and evolution. *Physiol Rev,* 83**,** 1223-67.

MORRISEY, E. E., IP, H. S., TANG, Z., LU, M. M. & PARMACEK, M. S. 1997. GATA-5: a transcriptional activator expressed in a novel temporally and spatially-restricted pattern during embryonic development. *Dev Biol,* 183**,** 21-36.

MOSES, K. A., DEMAYO, F., BRAUN, R. M., REECY, J. L. & SCHWARTZ, R. J. 2001. Embryonic expression of an Nkx2-5/Cre gene using ROSA26 reporter mice. *Genesis,* 31**,** 176-80.

MOSHKIN, Y. M., ARMSTRONG, J. A., MAEDA, R. K., TAMKUN, J. W., VERRIJZER, P., KENNISON, J. A. & KARCH, F. 2002. Histone chaperone ASF1 cooperates with the Brahma chromatin-remodelling machinery. *Genes Dev,* 16**,** 2621-6.

NAGY, A., GERTSENSTEIN, M., VINTERSTEN, K. & BEHRINGER, R. 2009. Alcian Blue Staining of the Mouse Fetal Cartilaginous Skeleton. *Cold Spring Harbor Protocols,* 2009**,** pdb.prot5169.

NAKAMURA, T., COLBERT, M. C. & ROBBINS, J. 2006. Neural crest cells retain multipotential characteristics in the developing valves and label the cardiac conduction system. *Circ Res,* 98**,** 1547-54.

NAKAYAMA, T., NISHIOKA, K., DONG, Y. X., SHIMOJIMA, T. & HIROSE, S. 2007. Drosophila GAGA factor directs histone H3.3 replacement that prevents the heterochromatin spreading. *Genes Dev,* 21**,** 552-61.
NAKAYAMA, T., SHIMOJIMA, T. & HIROSE, S. 2012. The PBAP remodeling complex is required for histone H3.3 replacement at chromatin boundaries and for boundary functions. *Development,* 139**,** 4582-90.
NEPH, S., VIERSTRA, J., STERGACHIS, A. B., REYNOLDS, A. P., HAUGEN, E., VERNOT, B., THURMAN, R. E., JOHN, S., SANDSTROM, R., JOHNSON, A. K., MAURANO, M. T., HUMBERT, R., RYNES, E., WANG, H., VONG, S., LEE, K., BATES, D., DIEGEL, M., ROACH, V., DUNN, D., NERI, J., SCHAFER, A., HANSEN, R. S., KUTYAVIN, T., GISTE, E., WEAVER, M., CANFIELD, T., SABO, P., ZHANG, M., BALASUNDARAM, G., BYRON, R., MACCOSS, M. J., AKEY, J. M., BENDER, M. A., GROUDINE, M., KAUL, R. & STAMATOYANNOPOULOS, J. A. 2012. An expansive human regulatory lexicon encoded in transcription factor footprints. *Nature,* 489**,** 83-90.
NG, R. K. & GURDON, J. B. 2008. Epigenetic memory of an active gene state depends on histone H3.3 incorporation into chromatin in the absence of transcription. *Nat Cell Biol,* 10**,** 102-9.
NIMURA, K., URA, K., SHIRATORI, H., IKAWA, M., OKABE, M., SCHWARTZ, R. J. & KANEDA, Y. 2009. A histone H3 lysine 36 trimethyltransferase links Nkx2-5 to Wolf-Hirschhorn syndrome. *Nature,* 460**,** 287-91.
OCHALA, J. 2008. Thin filament proteins mutations associated with skeletal myopathies: defective regulation of muscle contraction. *J Mol Med (Berl),* 86**,** 1197-204.
OKANO, M., BELL, D. W., HABER, D. A. & LI, E. 1999. DNA methyltransferases Dnmt3a and Dnmt3b are essential for de novo methylation and mammalian development. *Cell,* 99**,** 247-57.
OKUDA, K. S., ASTIN, J. W., MISA, J. P., FLORES, M. V., CROSIER, K. E. & CROSIER, P. S. 2012. lyve1 expression reveals novel lymphatic vessels and new mechanisms for lymphatic vessel development in zebrafish. *Development,* 139**,** 2381-91.
OLD, R. W. & WOODLAND, H. R. 1984. Histone genes: not so simple after all. *Cell,* 38**,** 624-6.
OOI, J. Y., TUANO, N. K., RAFEHI, H., GAO, X. M., ZIEMANN, M., DU, X. J. & EL-OSTA, A. 2015. HDAC inhibition attenuates cardiac hypertrophy by acetylation and deacetylation of target genes. *Epigenetics,* 10**,** 418-30.
ORSI, G. A., ALGAZEERY, A., MEYER, R. E., CAPRI, M., SAPEY-TRIOMPHE, L. M., HORARD, B., GRUFFAT, H., COUBLE, P., AÏT-AHMED, O. & LOPPIN, B. 2013. <italic>Drosophila</italic> Yemanuclein and HIRA Cooperate for <italic>De Novo</italic> Assembly of H3.3-Containing Nucleosomes in the Male Pronucleus. *PLoS Genet,* 9**,** e1003285.
OSLEY, M. A. 1991. The regulation of histone synthesis in the cell cycle. *Annu Rev Biochem,* 60**,** 827-61.
PAFFETT-LUGASSY, N., SINGH, R., NEVIS, K. R., GUNER-ATAMAN, B., O'LOUGHLIN, E., JAHANGIRI, L., HARVEY, R. P., BURNS, C. G. & BURNS, C. E. 2013. Heart field origin of great vessel precursors relies on nkx2.5-mediated vasculogenesis. *Nat Cell Biol,* 15**,** 1362-1369.
PARK, P. J. 2009. ChIP-seq: advantages and challenges of a maturing technology. *Nat Rev Genet,* 10**,** 669-80.
PAYLOR, R., GLASER, B., MUPO, A., ATALIOTIS, P., SPENCER, C., SOBOTKA, A., SPARKS, C., CHOI, C. H., OGHALAI, J., CURRAN, S., MURPHY, K. C., MONKS, S., WILLIAMS, N., O'DONOVAN, M. C., OWEN, M. J., SCAMBLER, P. J. & LINDSAY, E. 2006. Tbx1 haploinsufficiency is linked to behavioral disorders in mice and humans: implications for 22q11 deletion syndrome. *Proc Natl Acad Sci U S A,* 103**,** 7729-34.
PAYNE, S., BURNEY, M. J., MCCUE, K., POPAL, N., DAVIDSON, S. M., ANDERSON, R. H. & SCAMBLER, P. J. 2015. A critical role for the chromatin remodeller CHD7 in anterior mesoderm during cardiovascular development. *Dev Biol*.
PCHELINTSEV, N. A., MCBRYAN, T., RAI, T. S., VAN TUYN, J., RAY-GALLET, D., ALMOUZNI, G. & ADAMS, P. D. 2013a. Placing the HIRA histone chaperone complex in the chromatin landscape. *Cell reports,* 3**,** 1012-1019.
PCHELINTSEV, N. A., MCBRYAN, T., RAI, T. S., VAN TUYN, J., RAY-GALLET, D., ALMOUZNI, G. & ADAMS, P. D. 2013b. Placing the HIRA histone chaperone complex in the chromatin landscape. *Cell Rep,* 3**,** 1012-9.
PENG, X., WU, X., DRUSO, J. E., WEI, H., PARK, A. Y., KRAUS, M. S., ALCARAZ, A., CHEN, J., CHIEN, S., CERIONE, R. A. & GUAN, J. L. 2008. Cardiac developmental defects and eccentric right ventricular hypertrophy in cardiomyocyte focal adhesion kinase (FAK) conditional knockout mice. *Proc Natl Acad Sci U S A,* 105**,** 6638-43.
PERANTONI, A. O., TIMOFEEVA, O., NAILLAT, F., RICHMAN, C., PAJNI-UNDERWOOD, S., WILSON, C., VAINIO, S., DOVE, L. F. & LEWANDOSKI, M. 2005. Inactivation of FGF8 in early mesoderm reveals an essential role in kidney development. *Development,* 132**,** 3859-71.
PERSON, A. D., KLEWER, S. E. & RUNYAN, R. B. 2005. Cell biology of cardiac cushion development. *Int Rev Cytol,* 243**,** 287-335.
PHILLIPS, J. E. & CORCES, V. G. CTCF: Master Weaver of the Genome. *Cell,* 137**,** 1194-1211.
PLEIN, A., CALMONT, A., FANTIN, A., DENTI, L., ANDERSON, N. A., SCAMBLER, P. J. & RUHRBERG, C. 2015. Neural crest–derived SEMA3C activates endothelial NRP1 for cardiac outflow tract septation. *The Journal of Clinical Investigation,* 125**,** 2661-2676.
POOT, R. A., BOZHENOK, L., VAN DEN BERG, D. L., STEFFENSEN, S., FERREIRA, F., GRIMALDI, M., GILBERT, N., FERREIRA, J. & VARGA-WEISZ, P. D. 2004. The Williams syndrome transcription factor interacts with PCNA to target chromatin remodelling by ISWI to replication foci. *Nat Cell Biol,* 6**,** 1236-44.
POPOVIC, R., MARTINEZ-GARCIA, E., GIANNOPOULOU, E. G., ZHANG, Q., ZHANG, Q., EZPONDA, T., SHAH, M. Y., ZHENG, Y., WILL, C. M., SMALL, E. C., HUA, Y., BULIC, M., JIANG, Y., CARRARA, M., CALOGERO, R. A., KATH, W. L., KELLEHER, N. L., WANG, J. P., ELEMENTO, O. & LICHT, J. D. 2014. Histone methyltransferase MMSET/NSD2 alters EZH2 binding and reprograms the myeloma epigenome through global and focal changes in H3K36 and H3K27 methylation. *PLoS Genet,* 10**,** e1004566.
PORTAL-NUNEZ, S., LOZANO, D. & ESBRIT, P. 2012. Role of angiogenesis on bone formation. *Histol Histopathol,* 27**,** 559-66.
PRICE, BRENDAN D. & D'ANDREA, ALAN D. Chromatin Remodeling at DNA Double-Strand Breaks. *Cell,* 152**,** 1344-1354.
PROBST, A. V., DUNLEAVY, E. & ALMOUZNI, G. 2009. Epigenetic inheritance during the cell cycle. *Nat Rev Mol Cell Biol,* 10**,** 192-206.
PROCHASSON, P., FLORENS, L., SWANSON, S. K., WASHBURN, M. P. & WORKMAN, J. L. 2005. The HIR corepressor complex binds to nucleosomes generating a distinct protein/DNA complex resistant to remodeling by SWI/SNF. *Genes & Development,* 19**,** 2534-2539.
QUIVY, J.-P., GERARD, A., COOK, A. J. L., ROCHE, D. & ALMOUZNI, G. 2008. The HP1-p150/CAF-1 interaction is required for pericentric heterochromatin replication and S-phase progression in mouse cells. *Nat Struct Mol Biol,* 15**,** 972-979.
RAI, T. S., COLE, J. J., NELSON, D. M., DIKOVSKAYA, D., FALLER, W. J., VIZIOLI, M. G., HEWITT, R. N., ANANNYA, O., MCBRYAN, T., MANOHARAN, I., VAN TUYN, J., MORRICE, N., PCHELINTSEV, N. A., IVANOV, A., BROCK, C., DROTAR, M. E., NIXON, C., CLARK, W., SANSOM, O. J., ANDERSON, K. I., KING, A., BLYTH, K. & ADAMS, P. D. 2014. HIRA orchestrates a dynamic chromatin landscape in senescence and is required for suppression of neoplasia. *Genes & Development,* 28**,** 2712-2725.
RAI, T. S., PURI, A., MCBRYAN, T., HOFFMAN, J., TANG, Y., PCHELINTSEV, N. A., VAN TUYN, J., MARMORSTEIN, R., SCHULTZ, D. C. & ADAMS, P. D. 2011. Human CABIN1 is a functional member of the human HIRA/UBN1/ASF1a histone H3.3 chaperone complex. *Mol Cell Biol,* 31**,** 4107-18.

RAM, O., GOREN, A., AMIT, I., SHORESH, N., YOSEF, N., ERNST, J., KELLIS, M., GYMREK, M., ISSNER, R., COYNE, M., DURHAM, T., ZHANG, X., DONAGHEY, J., EPSTEIN, CHARLES B., REGEV, A. & BERNSTEIN, BRADLEY E. 2011. Combinatorial Patterning of Chromatin Regulators Uncovered by Genome-wide Location Analysis in Human Cells. *Cell,* 147**,** 1628-1639.

RAMSBOTTOM, S. A., SHARMA, V., RHEE, H. J., ELEY, L., PHILLIPS, H. M., RIGBY, H. F., DEAN, C., CHAUDHRY, B. & HENDERSON, D. J. 2014. Vangl2-regulated polarisation of second heart field-derived cells is required for outflow tract lengthening during cardiac development. *PLoS Genet,* 10**,** e1004871.

RANGASAMY, D., BERVEN, L., RIDGWAY, P. & TREMETHICK, D. J. 2003. Pericentric heterochromatin becomes enriched with H2A.Z during early mammalian development. *Embo j,* 22**,** 1599-607.

RAUCH, A., ZINK, S., ZWEIER, C., THIEL, C., KOCH, A., RAUCH, R., LASCORZ, J., HUFFMEIER, U., WEYAND, M., SINGER, H. & HOFBECK, M. 2005. Systematic assessment of atypical deletions reveals genotype–phenotype correlation in 22q11.2. *Journal of Medical Genetics,* 42**,** 871-876.

RAY-GALLET, D., QUIVY, J.-P., SCAMPS, C., MARTINI, E. M. D., LIPINSKI, M. & ALMOUZNI, G. 2002. HIRA Is Critical for a Nucleosome Assembly Pathway Independent of DNA Synthesis. *Molecular Cell,* 9**,** 1091-1100.

RAY-GALLET, D., WOOLFE, A., VASSIAS, I., PELLENTZ, C., LACOSTE, N., PURI, A., SCHULTZ, D. C., PCHELINTSEV, N. A., ADAMS, P. D., JANSEN, L. E. & ALMOUZNI, G. 2011. Dynamics of histone H3 deposition in vivo reveal a nucleosome gap-filling mechanism for H3.3 to maintain chromatin integrity. *Mol Cell,* 44**,** 928-41.

REA, S., EISENHABER, F., O'CARROLL, D., STRAHL, B. D., SUN, Z. W., SCHMID, M., OPRAVIL, S., MECHTLER, K., PONTING, C. P., ALLIS, C. D. & JENUWEIN, T. 2000. Regulation of chromatin structure by site-specific histone H3 methyltransferases. *Nature,* 406**,** 593-9.

REITER, J. F., ALEXANDER, J., RODAWAY, A., YELON, D., PATIENT, R., HOLDER, N. & STAINIER, D. Y. 1999. Gata5 is required for the development of the heart and endoderm in zebrafish. *Genes Dev,* 13**,** 2983-95.

RESTIVO, A., SARKOZY, A., DIGILIO, M. C., DALLAPICCOLA, B. & MARINO, B. 2006. 22q11 deletion syndrome: a review of some developmental biology aspects of the cardiovascular system. *J Cardiovasc Med (Hagerstown),* 7**,** 77-85.

RISEBRO, C. A., SEARLES, R. G., MELVILLE, A. A., EHLER, E., JINA, N., SHAH, S., PALLAS, J., HUBANK, M., DILLARD, M., HARVEY, N. L., SCHWARTZ, R. J., CHIEN, K. R., OLIVER, G. & RILEY, P. R. 2009. Prox1 maintains muscle structure and growth in the developing heart. *Development,* 136**,** 495-505.

ROBERTS, C., SUTHERLAND, H. F., FARMER, H., KIMBER, W., HALFORD, S., CAREY, A., BRICKMAN, J. M., WYNSHAW-BORIS, A. & SCAMBLER, P. J. 2002. Targeted mutagenesis of the Hira gene results in gastrulation defects and patterning abnormalities of mesoendodermal derivatives prior to early embryonic lethality. *Mol Cell Biol,* 22**,** 2318-28.

ROGGE, G. A. & WOOD, M. A. 2013. The role of histone acetylation in cocaine-induced neural plasticity and behavior. *Neuropsychopharmacology,* 38**,** 94-110.

ROHILA, J. S., CHEN, M., CERNY, R. & FROMM, M. E. 2004. Improved tandem affinity purification tag and methods for isolation of protein heterocomplexes from plants. *Plant J,* 38**,** 172-81.

SAGA, Y., KITAJIMA, S. & MIYAGAWA-TOMITA, S. 2000. Mesp1 expression is the earliest sign of cardiovascular development. *Trends Cardiovasc Med,* 10**,** 345-52.

SAGA, Y., MIYAGAWA-TOMITA, S., TAKAGI, A., KITAJIMA, S., MIYAZAKI, J. & INOUE, T. 1999. MesP1 is expressed in the heart precursor cells and required for the formation of a single heart tube. *Development,* 126**,** 3437-47.

SAKAI, A., SCHWARTZ, B. E., GOLDSTEIN, S. & AHMAD, K. 2009. Transcriptional and developmental functions of the H3.3 histone variant in Drosophila. *Curr Biol,* 19**,** 1816-20.

SANTENARD, A., ZIEGLER-BIRLING, C., KOCH, M., TORA, L., BANNISTER, A. J. & TORRES-PADILLA, M. E. 2010. Heterochromatin formation in the mouse embryo requires critical residues of the histone variant H3.3. *Nat Cell Biol,* 12**,** 853-62.

SARAI, N., NIMURA, K., TAMURA, T., KANNO, T., PATEL, M. C., HEIGHTMAN, T. D., URA, K. & OZATO, K. 2013. WHSC1 links transcription elongation to HIRA-mediated histone H3.3 deposition. *Embo j,* 32**,** 2392-406.

SCAMBLER, P. J. 2000. The 22q11 deletion syndromes. *Human Molecular Genetics,* 9**,** 2421-2426.

SCHLAEGER, T. M., BARTUNKOVA, S., LAWITTS, J. A., TEICHMANN, G., RISAU, W., DEUTSCH, U. & SATO, T. N. 1997. Uniform vascular-endothelial-cell-specific gene expression in both embryonic and adult transgenic mice. *Proc Natl Acad Sci U S A,* 94**,** 3058-63.

SCHNEIDERMAN, J. I., ORSI, G. A., HUGHES, K. T., LOPPIN, B. & AHMAD, K. 2012. Nucleosome-depleted chromatin gaps recruit assembly factors for the H3.3 histone variant. *Proceedings of the National Academy of Sciences of the United States of America,* 109**,** 19721-19726.

SCHONES, D. E. & ZHAO, K. 2008. Genome-wide approaches to studying chromatin modifications. *Nat Rev Genet,* 9**,** 179-91.

SCHWARTZENTRUBER, J., KORSHUNOV, A., LIU, X. Y., JONES, D. T., PFAFF, E., JACOB, K., STURM, D., FONTEBASSO, A. M., QUANG, D. A., TONJES, M., HOVESTADT, V., ALBRECHT, S., KOOL, M., NANTEL, A., KONERMANN, C., LINDROTH, A., JAGER, N., RAUSCH, T., RYZHOVA, M., KORBEL, J. O., HIELSCHER, T., HAUSER, P., GARAMI, M., KLEKNER, A., BOGNAR, L., EBINGER, M., SCHUHMANN, M. U., SCHEURLEN, W., PEKRUN, A., FRUHWALD, M. C., ROGGENDORF, W., KRAMM, C., DURKEN, M., ATKINSON, J., LEPAGE, P., MONTPETIT, A., ZAKRZEWSKA, M., ZAKRZEWSKI, K., LIBERSKI, P. P., DONG, Z., SIEGEL, P., KULOZIK, A. E., ZAPATKA, M., GUHA, A., MALKIN, D., FELSBERG, J., REIFENBERGER, G., VON DEIMLING, A., ICHIMURA, K., COLLINS, V. P., WITT, H., MILDE, T., WITT, O., ZHANG, C., CASTELO-BRANCO, P., LICHTER, P., FAURY, D., TABORI, U., PLASS, C., MAJEWSKI, J., PFISTER, S. M. & JABADO, N. 2012. Driver mutations in histone H3.3 and chromatin remodelling genes in paediatric glioblastoma. *Nature,* 482**,** 226-31.

SEGAL, E., FONDUFE-MITTENDORF, Y., CHEN, L., THASTROM, A., FIELD, Y., MOORE, I. K., WANG, J. P. & WIDOM, J. 2006. A genomic code for nucleosome positioning. *Nature,* 442**,** 772-8.

SERBEDZIJA, G. N., BRONNER-FRASER, M. & FRASER, S. E. 1992. Vital dye analysis of cranial neural crest cell migration in the mouse embryo. *Development,* 116**,** 297-307.

SHARPE, J., AHLGREN, U., PERRY, P., HILL, B., ROSS, A., HECKSHER-SORENSEN, J., BALDOCK, R. & DAVIDSON, D. 2002. Optical projection tomography as a tool for 3D microscopy and gene expression studies. *Science,* 296**,** 541-5.

SHEN, Y., YUE, F., MCCLEARY, D. F., YE, Z., EDSALL, L., KUAN, S., WAGNER, U., DIXON, J., LEE, L., LOBANENKOV, V. V. & REN, B. 2012. A map of the cis-regulatory sequences in the mouse genome. *Nature,* 488**,** 116-20.

SHERWOOD, P. W., TSANG, S. V. & OSLEY, M. A. 1993. Characterization of HIR1 and HIR2, two genes required for regulation of histone gene transcription in Saccharomyces cerevisiae. *Mol Cell Biol,* 13**,** 28-38.

SHLYUEVA, D., STAMPFEL, G. & STARK, A. 2014. Transcriptional enhancers: from properties to genome-wide predictions. *Nat Rev Genet,* 15**,** 272-286.

SHPRINTZEN, R. J. 2008. Velo-Cardio-Facial Syndrome: 30 Years of Study. *Developmental disabilities research reviews,* 14**,** 3-10.

SIEDNER, S., KRUGER, M., SCHROETER, M., METZLER, D., ROELL, W., FLEISCHMANN, B. K., HESCHELER, J., PFITZER, G. & STEHLE, R. 2003. Developmental changes in contractility and sarcomeric proteins from the early embryonic to the adult stage in the mouse heart. *J Physiol,* 548**,** 493-505.

SIMS, R. J., 3RD & REINBERG, D. 2006. Histone H3 Lys 4 methylation: caught in a bind? *Genes Dev,* 20**,** 2779-86.
SINGH, M. K., LI, Y., LI, S., COBB, R. M., ZHOU, D., LU, M. M., EPSTEIN, J. A., MORRISEY, E. E. & GRUBER, P. J. 2010. Gata4 and Gata5 Cooperatively Regulate Cardiac Myocyte Proliferation in Mice. *The Journal of Biological Chemistry,* 285**,** 1765-1772.
SMITH, Z. D. & MEISSNER, A. 2013. DNA methylation: roles in mammalian development. *Nat Rev Genet,* 14**,** 204-20.
SOHAL, D. S., NGHIEM, M., CRACKOWER, M. A., WITT, S. A., KIMBALL, T. R., TYMITZ, K. M., PENNINGER, J. M. & MOLKENTIN, J. D. 2001. Temporally regulated and tissue-specific gene manipulations in the adult and embryonic heart using a tamoxifen-inducible Cre protein. *Circ Res,* 89**,** 20-5.
SONG, T. Y., YANG, J. H., PARK, J. Y., SONG, Y., HAN, J. W., YOUN, H. D. & CHO, E. J. 2012. The role of histone chaperones in osteoblastic differentiation of C2C12 myoblasts. *Biochem Biophys Res Commun,* 423**,** 726-32.
SPECTOR, M. S., RAFF, A., DESILVA, H., LEE, K. & OSLEY, M. A. 1997. Hir1p and Hir2p function as transcriptional corepressors to regulate histone gene transcription in the Saccharomyces cerevisiae cell cycle. *Mol Cell Biol,* 17**,** 545-52.
SPITZ, F. & FURLONG, E. E. 2012. Transcription factors: from enhancer binding to developmental control. *Nat Rev Genet,* 13**,** 613-26.
SRIVASTAVA, S., DHAWAN, J. & MISHRA, R. K. 2015. Epigenetic mechanisms and boundaries in the regulation of mammalian Hox clusters. *Mech Dev*.
STACHON, A. C., BASKIN, B., SMITH, A. C., SHUGAR, A., CYTRYNBAUM, C., FISHMAN, L., MENDOZA-LONDONO, R., KLATT, R., TEEBI, A., RAY, P. N. & WEKSBERG, R. 2007. Molecular diagnosis of 22q11.2 deletion and duplication by multiplex ligation dependent probe amplification. *Am J Med Genet A,* 143a**,** 2924-30.
STANKUNAS, K., HANG, C. T., TSUN, Z. Y., CHEN, H., LEE, N. V., WU, J. I., SHANG, C., BAYLE, J. H., SHOU, W., IRUELA-ARISPE, M. L. & CHANG, C. P. 2008. Endocardial Brg1 represses ADAMTS1 to maintain the microenvironment for myocardial morphogenesis. *Dev Cell,* 14**,** 298-311.
STASEVICH, T. J., HAYASHI-TAKANAKA, Y., SATO, Y., MAEHARA, K., OHKAWA, Y., SAKATA-SOGAWA, K., TOKUNAGA, M., NAGASE, T., NOZAKI, N., MCNALLY, J. G. & KIMURA, H. 2014. Regulation of RNA polymerase II activation by histone acetylation in single living cells. *Nature,* 516**,** 272-5.
STEPHEN, L. J., FAWKES, A. L., VERHOEVE, A., LEMKE, G. & BROWN, A. 2007. A critical role for the EphA3 receptor tyrosine kinase in heart development. *Dev Biol,* 302**,** 66-79.
STERGACHIS, A. B., NEPH, S., SANDSTROM, R., HAUGEN, E., REYNOLDS, A. P., ZHANG, M., BYRON, R., CANFIELD, T., STELHING-SUN, S., LEE, K., THURMAN, R. E., VONG, S., BATES, D., NERI, F., DIEGEL, M., GISTE, E., DUNN, D., VIERSTRA, J., HANSEN, R. S., JOHNSON, A. K., SABO, P. J., WILKEN, M. S., REH, T. A., TREUTING, P. M., KAUL, R., GROUDINE, M., BENDER, M. A., BORENSTEIN, E. & STAMATOYANNOPOULOS, J. A. 2014. Conservation of trans-acting circuitry during mammalian regulatory evolution. *Nature,* 515**,** 365-370.
STEWART, M. D., LI, J. & WONG, J. 2005. Relationship between histone H3 lysine 9 methylation, transcription repression, and heterochromatin protein 1 recruitment. *Mol Cell Biol,* 25**,** 2525-38.
STONE, M. R., O'NEILL, A., LOVERING, R. M., STRONG, J., RESNECK, W. G., REED, P. W., TOIVOLA, D. M., URSITTI, J. A., OMARY, M. B. & BLOCH, R. J. 2007. Absence of keratin 19 in mice causes skeletal myopathy with mitochondrial and sarcolemmal reorganization. *J Cell Sci,* 120**,** 3999-4008.
STRAUSS, M., ARRECHEDERA, H., ARGUELLO, C., AYESTA, C., ALVAREZ, M. & ANSELMI, G. 1987. Mesenchymal tissue of the interventricular septum. Structural and ultrastructural study. *Anat Embryol (Berl),* 176**,** 231-7.
STRUHL, K. 1999. Fundamentally different logic of gene regulation in eukaryotes and prokaryotes. *Cell,* 98**,** 1-4.
SZENKER, E., LACOSTE, N. & ALMOUZNI, G. 2012. A developmental requirement for HIRA-dependent H3.3 deposition revealed at gastrulation in Xenopus. *Cell Rep,* 1**,** 730-40.
SZENKER, E., RAY-GALLET, D. & ALMOUZNI, G. 2011. The double face of the histone variant H3.3. *Cell Research,* 21**,** 421-434.
TAGAMI, H., RAY-GALLET, D., ALMOUZNI, G. & NAKATANI, Y. 2004. Histone H3.1 and H3.3 Complexes Mediate Nucleosome Assembly Pathways Dependent or Independent of DNA Synthesis. *Cell,* 116**,** 51-61.
TAKEUCHI, J. K. & BRUNEAU, B. G. 2009. Directed transdifferentiation of mouse mesoderm to heart tissue by defined factors. *Nature,* 459**,** 708-11.
TAKEUCHI, J. K., LOU, X., ALEXANDER, J. M., SUGIZAKI, H., DELGADO-OLGUIN, P., HOLLOWAY, A. K., MORI, A. D., WYLIE, J. N., MUNSON, C., ZHU, Y., ZHOU, Y.-Q., YEH, R.-F., HENKELMAN, R. M., HARVEY, R. P., METZGER, D., CHAMBON, P., STAINIER, D. Y. R., POLLARD, K. S., SCOTT, I. C. & BRUNEAU, B. G. 2011. Chromatin remodelling complex dosage modulates transcription factor function in heart development. *Nat Commun,* 2**,** 187.
TALBERT, P. B. & HENIKOFF, S. 2010. Histone variants--ancient wrap artists of the epigenome. *Nat Rev Mol Cell Biol,* 11**,** 264-75.
TAN-WONG, S. M., FRENCH, J. D., PROUDFOOT, N. J. & BROWN, M. A. 2008. Dynamic interactions between the promoter and terminator regions of the mammalian BRCA1 gene. *Proc Natl Acad Sci U S A,* 105**,** 5160-5.
TOLHUIS, B., PALSTRA, R. J., SPLINTER, E., GROSVELD, F. & DE LAAT, W. 2002. Looping and interaction between hypersensitive sites in the active beta-globin locus. *Mol Cell,* 10**,** 1453-65.
TRAINOR, P. A. 2010. Craniofacial Birth Defects: The Role of Neural Crest Cells in the Etiology and Pathogenesis of Treacher Collins Syndrome and the Potential for Prevention. *American journal of medical genetics. Part A,* 0**,** 2984-2994.
TRIFONOV, E. N. 2011. Cracking the chromatin code: precise rule of nucleosome positioning. *Phys Life Rev,* 8**,** 39-50.
TSCHIERSCH, B., HOFMANN, A., KRAUSS, V., DORN, R., KORGE, G. & REUTER, G. 1994. The protein encoded by the Drosophila position-effect variegation suppressor gene Su(var)3-9 combines domains of antagonistic regulators of homeotic gene complexes. *Embo j,* 13**,** 3822-31.
TYLER, J. K., ADAMS, C. R., CHEN, S. R., KOBAYASHI, R., KAMAKAKA, R. T. & KADONAGA, J. T. 1999. The RCAF complex mediates chromatin assembly during DNA replication and repair. *Nature,* 402**,** 555-60.
UDUGAMA, M., CHANG, F. T., CHAN, F. L., TANG, M. C., PICKETT, H. A., MCGHIE, J. D., MAYNE, L., COLLAS, P., MANN, J. R. & WONG, L. H. 2015. Histone variant H3.3 provides the heterochromatic H3 lysine 9 tri-methylation mark at telomeres. *Nucleic Acids Res*.
VAN DEN HOFF, M. J., MOORMAN, A. F., RUIJTER, J. M., LAMERS, W. H., BENNINGTON, R. W., MARKWALD, R. R. & WESSELS, A. 1999. Myocardialization of the cardiac outflow tract. *Dev Biol,* 212**,** 477-90.
VAN HOLDE, K. E., SAHASRABUDDHE, C. G. & SHAW, B. R. 1974. A model for particulate structure in chromatin. *Nucleic Acids Research,* 1**,** 1579-1586.
VAN STEENSEL, B., DELROW, J. & BUSSEMAKER, H. J. 2003. Genomewide analysis of Drosophila GAGA factor target genes reveals context-dependent DNA binding. *Proc Natl Acad Sci U S A,* 100**,** 2580-5.
VENKATESH, S., SMOLLE, M., LI, H., GOGOL, M. M., SAINT, M., KUMAR, S., NATARAJAN, K. & WORKMAN, J. L. 2012. Set2 methylation of histone H3 lysine 36 suppresses histone exchange on transcribed genes. *Nature,* 489**,** 452-5.
VERZI, M. P., MCCULLEY, D. J., DE VAL, S., DODOU, E. & BLACK, B. L. 2005. The right ventricle, outflow tract, and ventricular septum comprise a restricted expression domain within the secondary/anterior heart field. *Dev Biol,* 287**,** 134-45.
VINCENT, S. D. & BUCKINGHAM, M. E. 2010. How to make a heart: the origin and regulation of cardiac progenitor cells. *Curr Top Dev Biol,* 90**,** 1-41.

VINCENTZ, J. W., BARNES, R. M., FIRULLI, B. A., CONWAY, S. J. & FIRULLI, A. B. 2008. Cooperative interaction of Nkx2.5 and Mef2c transcription factors during heart development. *Developmental dynamics : an official publication of the American Association of Anatomists,* 237**,** 3809-3819.

VOON, H. P., HUGHES, J. R., RODE, C., DE LA ROSA-VELAZQUEZ, I. A., JENUWEIN, T., FEIL, R., HIGGS, D. R. & GIBBONS, R. J. 2015. ATRX Plays a Key Role in Maintaining Silencing at Interstitial Heterochromatic Loci and Imprinted Genes. *Cell Rep,* 11**,** 405-18.

VRADII, D., WAGNER, S., DOAN, D. N., NICKERSON, J. A., MONTECINO, M., LIAN, J. B., STEIN, J. L., VAN WIJNEN, A. J., IMBALZANO, A. N. & STEIN, G. S. 2006. Brg1, the ATPase subunit of the SWI/SNF chromatin remodeling complex, is required for myeloid differentiation to granulocytes. *J Cell Physiol,* 206**,** 112-8.

WAMSTAD, J. A., ALEXANDER, J. M., TRUTY, R. M., SHRIKUMAR, A., LI, F., EILERTSON, K. E., DING, H., WYLIE, J. N., PICO, A. R., CAPRA, J. A., ERWIN, G., KATTMAN, S. J., KELLER, G. M., SRIVASTAVA, D., LEVINE, S. S., POLLARD, K. S., HOLLOWAY, A. K., BOYER, L. A. & BRUNEAU, B. G. 2012. Dynamic and Coordinated Epigenetic Regulation of Developmental Transitions in the Cardiac Lineage. *Cell,* 151**,** 206-220.

WANG, X., ZHANG, J., CAO, Y., DIAO, L., WANG, H., MA, X., MA, D. & HUANG, G. 2014. [Sequence analyses of HIRA gene 3'UTR region and related microRNA]. *Zhonghua Yi Xue Za Zhi,* 94**,** 1223-6.

WATANABE, Y., KOKUBO, H., MIYAGAWA-TOMITA, S., ENDO, M., IGARASHI, K., AISAKI, K., KANNO, J. & SAGA, Y. 2006. Activation of Notch1 signaling in cardiogenic mesoderm induces abnormal heart morphogenesis in mouse. *Development,* 133**,** 1625-34.

WEBB, S., QAYYUM, S. R., ANDERSON, R. H., LAMERS, W. H. & RICHARDSON, M. K. 2003. Septation and separation within the outflow tract of the developing heart. *Journal of Anatomy,* 202**,** 327-342.

WETH, O., PAPROTKA, C., GÜNTHER, K., SCHULTE, A., BAIERL, M., LEERS, J., GALJART, N. & RENKAWITZ, R. 2014. CTCF induces histone variant incorporation, erases the H3K27me3 histone mark and opens chromatin. *Nucleic Acids Research,* 42**,** 11941-11951.

WIDOM, J. 2001. Role of DNA sequence in nucleosome stability and dynamics. *Q Rev Biophys,* 34**,** 269-324.

WIGLE, J. T. & OLIVER, G. 1999. Prox1 function is required for the development of the murine lymphatic system. *Cell,* 98**,** 769-78.

WONG, L. H., REN, H., WILLIAMS, E., MCGHIE, J., AHN, S., SIM, M., TAM, A., EARLE, E., ANDERSON, M. A., MANN, J. & CHOO, K. H. A. 2009. Histone H3.3 incorporation provides a unique and functionally essential telomeric chromatin in embryonic stem cells. *Genome Research,* 19**,** 404-414.

WU, M., PENG, S. & ZHAO, Y. 2014. Inducible gene deletion in the entire cardiac conduction system using Hcn4-CreERT2 BAC transgenic mice. *Genesis,* 52**,** 134-40.

WYSOCKA, J., SWIGUT, T., MILNE, T. A., DOU, Y., ZHANG, X., BURLINGAME, A. L., ROEDER, R. G., BRIVANLOU, A. H. & ALLIS, C. D. 2005. WDR5 associates with histone H3 methylated at K4 and is essential for H3 K4 methylation and vertebrate development. *Cell,* 121**,** 859-72.

XIAO, B., JING, C., WILSON, J. R., WALKER, P. A., VASISHT, N., KELLY, G., HOWELL, S., TAYLOR, I. A., BLACKBURN, G. M. & GAMBLIN, S. J. 2003. Structure and catalytic mechanism of the human histone methyltransferase SET7/9. *Nature,* 421**,** 652-6.

XU, M., LONG, C., CHEN, X., HUANG, C., CHEN, S. & ZHU, B. 2010. Partitioning of Histone H3-H4 Tetramers During DNA Replication–Dependent Chromatin Assembly. *Science,* 328**,** 94-98.

YAMANE, K., MIZUGUCHI, T., CUI, B., ZOFALL, M., NOMA, K. & GREWAL, S. I. 2011. Asf1/HIRA facilitate global histone deacetylation and associate with HP1 to promote nucleosome occupancy at heterochromatic loci. *Mol Cell,* 41**,** 56-66.

YAMASAKI, T., MURATA, T., JIN, C., KATO, K., NOGUCHI, M., NAKADE, K., PAN, J., NAGATA, K. & YOKOYAMA, K. 2007. Assays of nucleosome assembly and the inhibition of histone acetyltransferase activity. (11) Digestion of chromatin; and (12) Purification and characterization of DNA after digestion of chromatin.

YANG, J. H., SONG, Y., SEOL, J. H., PARK, J. Y., YANG, Y. J., HAN, J. W., YOUN, H. D. & CHO, E. J. 2011. Myogenic transcriptional activation of MyoD mediated by replication-independent histone deposition. *Proc Natl Acad Sci U S A,* 108**,** 85-90.

YANG, X., LI, L., LIANG, J., SHI, L., YANG, J., YI, X., ZHANG, D., HAN, X., YU, N. & SHANG, Y. 2013. Histone Acetyltransferase 1 Promotes Homologous Recombination in DNA Repair by Facilitating Histone Turnover. *The Journal of Biological Chemistry,* 288**,** 18271-18282.

YANG, X. J. & SETO, E. 2007. HATs and HDACs: from structure, function and regulation to novel strategies for therapy and prevention. *Oncogene,* 26**,** 5310-8.

YAO, T. P., OH, S. P., FUCHS, M., ZHOU, N. D., CH'NG, L. E., NEWSOME, D., BRONSON, R. T., LI, E., LIVINGSTON, D. M. & ECKNER, R. 1998. Gene dosage-dependent embryonic development and proliferation defects in mice lacking the transcriptional integrator p300. *Cell,* 93**,** 361-72.

YOSHIDA, T., VIVATBUTSIRI, P., MORRISS-KAY, G., SAGA, Y. & ISEKI, S. 2008. Cell lineage in mammalian craniofacial mesenchyme. *Mechanisms of Development,* 125**,** 797-808.

YU, E. Y., STEINBERG-NEIFACH, O., DANDJINOU, A. T., KANG, F., MORRISON, A. J., SHEN, X. & LUE, N. F. 2007. Regulation of telomere structure and functions by subunits of the INO80 chromatin remodeling complex. *Mol Cell Biol,* 27**,** 5639-49.

YUKAWA, M., AKIYAMA, T., FRANKE, V., MISE, N., ISAGAWA, T., SUZUKI, Y., SUZUKI, M. G., VLAHOVICEK, K., ABE, K., ABURATANI, H. & AOKI, F. 2014. Genome-wide analysis of the chromatin composition of histone H2A and H3 variants in mouse embryonic stem cells. *PLoS One,* 9**,** e92689.

ZAFFRAN, S., KELLY, R. G., MEILHAC, S. M., BUCKINGHAM, M. E. & BROWN, N. A. 2004. Right ventricular myocardium derives from the anterior heart field. *Circ Res,* 95**,** 261-8.

ZAFFRAN, S., ROBRINI, N. & BERTRAND, N. 2014. Retinoids and Cardiac Development. *Journal of Developmental Biology,* 2**,** 50.

ZENG, P. Y., VAKOC, C. R., CHEN, Z. C., BLOBEL, G. A. & BERGER, S. L. 2006. In vivo dual cross-linking for identification of indirect DNA-associated proteins by chromatin immunoprecipitation. *Biotechniques,* 41**,** 694, 696, 698.

ZHANG, C., TIAN, L., CHI, C., WU, X., YANG, X., HAN, M., XU, T., ZHUANG, Y. & DENG, K. 2010. Adam10 is essential for early embryonic cardiovascular development. *Dev Dyn,* 239**,** 2594-602.

ZHANG, L., NEMZOW, L., CHEN, H., HU, J. J. & GONG, F. 2014a. Whole Genome Expression Profiling Shows that BRG1 Transcriptionally Regulates UV Inducible Genes and Other Novel Targets in Human Cells. *PLoS ONE,* 9**,** e105764.

ZHANG, L., NOMURA-KITABAYASHI, A., SULTANA, N., CAI, W., CAI, X., MOON, A. M. & CAI, C.-L. 2014b. Mesodermal Nkx2.5 is necessary and sufficient for early second heart field development. *Developmental Biology,* 390**,** 68-79.

ZHANG, R., POUSTOVOITOV, M. V., YE, X., SANTOS, H. A., CHEN, W., DAGANZO, S. M., ERZBERGER, J. P., SEREBRIISKII, I. G., CANUTESCU, A. A., DUNBRACK, R. L., PEHRSON, J. R., BERGER, J. M., KAUFMAN, P. D. & ADAMS, P. D. 2005. Formation of MacroH2A-containing senescence-associated heterochromatin foci and senescence driven by ASF1a and HIRA. *Dev Cell,* 8**,** 19-30.

ZHANG, X., YANG, Z., KHAN, S. I., HORTON, J. R., TAMARU, H., SELKER, E. U. & CHENG, X. 2003. Structural basis for the product specificity of histone lysine methyltransferases. *Mol Cell,* 12**,** 177-85.

ZHANG, Z. G., ZHANG, L., JIANG, Q. & CHOPP, M. 2002. Bone marrow-derived endothelial progenitor cells participate in cerebral neovascularization after focal cerebral ischemia in the adult mouse. *Circ Res,* 90**,** 284-8.

ZHAO, R., WATT, A. J., BATTLE, M. A., LI, J., BONDOW, B. J. & DUNCAN, S. A. 2008. Loss of both GATA4 and GATA6 blocks cardiac myocyte differentiation and results in acardia in mice. *Developmental Biology,* 317**,** 614-619.

ZHAO, Z., TAVOOSIDANA, G., SJOLINDER, M., GONDOR, A., MARIANO, P., WANG, S., KANDURI, C., LEZCANO, M., SANDHU, K. S., SINGH, U., PANT, V., TIWARI, V., KURUKUTI, S. & OHLSSON, R. 2006. Circular chromosome conformation capture (4C) uncovers extensive networks of epigenetically regulated intra- and interchromosomal interactions. *Nat Genet,* 38**,** 1341-7.

ZWEIER, C., STICHT, H., AYDIN-YAYLAGÜL, I., CAMPBELL, C. E. & RAUCH, A. 2007. Human TBX1 Missense Mutations Cause Gain of Function Resulting in the Same Phenotype as 22q11.2 Deletions. *The American Journal of Human Genetics,* 80**,** 510-517.